

LARGE SCALE LABORATORY TESTING OF GEOSYNTHETICS IN ROADWAY APPLICATIONS

FHWA/MT-21-001/9564-602

Final Report

prepared for
THE STATE OF MONTANA
DEPARTMENT OF TRANSPORTATION

in cooperation with
THE U.S. DEPARTMENT OF TRANSPORTATION
FEDERAL HIGHWAY ADMINISTRATION

March 2021
Revised April 2021

prepared by
Steve Perkins, Ph.D., P.E. Eli Cuelho

Montana State University TRI Environmental
Bozeman, MT Manhattan, MT



RESEARCH PROGRAMS



You are free to copy, distribute, display, and perform the work; make derivative works; make commercial use of the work under the condition that you give the original author and sponsor credit. For any reuse or distribution, you must make clear to others the license terms of this work. Any of these conditions can be waived if you get permission from the sponsor. Your fair use and other rights are in no way affected by the above.

Large-Scale Laboratory Testing of Geosynthetics in Roadway Applications

Final Report

Prepared by

Steve Perkins

Department of Civil Engineering &

Western Transportation Institute

College of Engineering

Montana State University – Bozeman

&

Eli Cueho

TRI Environmental

Prepared for the

MONTANA DEPARTMENT OF TRANSPORTATION

in cooperation with the

U.S. DEPARTMENT OF TRANSPORTATION

FEDERAL HIGHWAY ADMINISTRATION

March, 2021

TECHNICAL REPORT DOCUMENTATION PAGE

1. Report No. FHWA/MT-21-003/9564-602		2. Government Accession No.		3. Recipient's Catalog No.	
4. Title and Subtitle Large-Scale Laboratory Testing of Geosynthetics in Roadway Applications				5. Report Date March 2021	
				6. Performing Organization Code MSU Index No. 4W7117	
7. Author Steve Perkins, Ph.D., P.E. and Eli Cuelho [Revised]				8. Performing Organization Report No. Not applicable	
9. Performing Organization Name and Address Department of Civil Engineering & Western Transportation Institute College of Engineering Montana State University – Bozeman Bozeman, MT 59717				10. Work Unit No.	
				11. Contract or Grant No. Project No. 9564-602	
12. Sponsoring Agency Name and Address Research Programs, Montana Department of Transportation (SPR) http://dx.doi.org/10.13039/100009209 2701 Prospect Avenue, PO Box 201001, Helena, MT 59620-1001				13. Type of Report and Period Covered Final Report (2/2018 – 3/2021)	
				14. Sponsoring Agency Code 5401	
15. Supplementary Notes Conducted in cooperation with the U.S. Department of Transportation, Federal Highway Administration. This report can be found at https://www.mdt.mt.gov/research/projects/geotech/lab_testing.shtml DOI: https://doi.org/10.21949/1518310 Recommended Citation: Steve Perkins, Ph.D., P.E. and Eli Cuelho [Revised]. Large-Scale Laboratory Testing of Geosynthetics in Roadway Applications. United States. Montana Department of Transportation. Western Transportation Institute – Montana State University. https://doi.org/10.21949/1518310					
16. Abstract This project studied the performance of geotextile-reinforced test sections when compared to an unreinforced case to assess benefit in terms of an extension of the life of the pavement. A single test track was constructed in an indoor test facility and contained two test sections with a reinforcement geotextile (woven and non-woven) while the third section was unreinforced. The test sections constructed had a nominal section of 3.4 inch of hot mix asphalt and 13.3 inch of base course aggregate on a clay subgrade with a constructed CBR of 3.5. The test sections were trafficked by a full-scale accelerated pavement tester with approximately 1 million traffic passes applied. The raw rutting results showed the unreinforced test section to perform better than the two sections with a geotextile. An analysis of the data showed that the three test sections performed similarly in terms of rutting performance for the conditions present in this study. The spreadsheet design model developed previously for MDT by the PI using reasonable input parameters predicted little reinforcement benefit for these conditions. This model showed moderate reinforcement benefit for weaker subgrade conditions that might be present in typical Montana roadways during seasonally wetter periods. This study did not quantify the separation benefit of the geotextiles, which are a recognized benefit applicable to most roadways in the state. A cost analysis showed the cost of the woven and non-woven geotextiles was approximately 13 and 6.5 % of the total roadway material cost, respectively. The benefit associated with this cost lies in the geotextile's function as a separator, which may reduce the cost of rehabilitation and reconstruction operations and to ensure the structural performance of the pavement during seasonal periods where the subgrade may become wet and weak.					
17. Key Words Pavement Design, Highways, Pavement Performance Subgrade Stabilization, Geotextiles, Geosynthetics, Reinforcement, Separation, Base Course, Performance Field Test, Test Sections, Montana			18. Distribution Statement No restrictions. This document is available through the National Technical Information Service, Springfield, VA 22161. Enter any other agency mandated distribution statements. Remove NTIS statement if it does not apply.		
19. Security Classif. (of this report) Unclassified		20. Security Classif. (of this page) Unclassified		21. No. of Pages 218	
				22. Price	

Disclaimer Statement

This document is disseminated under the sponsorship of the Montana Department of Transportation (MDT) and the United States Department of Transportation (USDOT) in the interest of information exchange. The State of Montana and the United States assume no liability for the use or misuse of its contents.

The contents of this document reflect the views of the authors, who are solely responsible for the facts and accuracy of the data presented herein. The contents do not necessarily reflect the views or official policies of MDT or the USDOT.

The State of Montana and the United States do not endorse products of manufacturers.

This document does not constitute a standard, specification, policy or regulation.

Alternative Format Statement

MDT attempts to provide accommodations for any known disability that may interfere with a person participating in any service, program, or activity of the Department. Alternative accessible formats of this information will be provided upon request. For further information, call 406/444.7693, TTY 800/335.7592, or Montana Relay at 711.

Acknowledgements

The companies TenCate Mirafi and Propex are acknowledged for their cooperation in providing geosynthetic materials for the test sections. TRI Environmental is acknowledged for their support as a subcontractor responsible for construction, loading and monitoring of the test sections.

Table of Contents

List of Tables	ix
List of Figures	xi
1 Introduction.....	1
2 Literature Review.....	3
2.1 Previous Literature Reviews	3
2.2 Test Sections	5
2.3 Analytical Modeling.....	22
2.4 Design Methods.....	26
2.5 NCHRP 01-50	44
2.6 Summary and Relationship to this Project	47
3 Accelerated Pavement Test Facility.....	49
4 Test Section Materials.....	51
4.1 Hot-Mix Asphalt	51
4.2 Base Course Aggregate	53
4.3 Subgrade.....	54
4.4 Geotextiles.....	58
5 Test Section Construction	60
5.1 Quality Control Testing Plan	60
5.2 Subgrade Construction	62
5.2.1 Vane shear strength.....	65
5.2.2 Moisture content	66
5.2.3 CBR strength.....	67
5.2.4 Dynamic stiffness.....	67
5.2.5 Strength (DCP).....	68
5.2.6 Unit weight.....	69
5.3 Instrumentation.....	69
5.4 Geosynthetics	72
5.5 Base Course Aggregate	73
5.5.1 Moisture Content	75

5.5.2	Dynamic Stiffness	75
5.5.3	Strength (DCP).....	75
5.5.4	Unit Weight.....	76
5.6	Asphalt	77
6	Test Section Trafficking and Data Collection	80
6.1	Surface Rut Measurement Results	80
6.2	Base Course and Subgrade Deflection Measurement Results	83
7	Post Trafficking Forensic Evaluation	89
7.1	Asphalt	89
7.2	Base Course Aggregate	90
7.3	Subgrade.....	90
7.4	Topographic Profiles and Photos	92
7.5	Geosynthetics	96
8	Analysis of Results	99
8.1	Evaluation of Representative Subgrade CBR Strength.....	99
8.2	Comparison of Results to Literature	99
8.3	Analysis of Rutting Response	100
8.4	Evaluation of Spreadsheet Model	108
9	Geotextile Costs and Benefits.....	111
10	Conclusion	112
11	References.....	113
12	Appendix A: HMA Material Testing Data Sheets	118
13	Appendix B: Base Aggregate Material Testing Data Sheets	140
14	Appendix C: Subgrade Material Testing Data Sheets	150
15	Appendix D: Geotextile Material Testing Data Sheets.....	155
16	Appendix E: Horizontal Layout of Construction QC Measurement Locations.....	158
17	Appendix F: Survey Elevation Measurement Layout of Construction QC	162
18	Appendix G: Position and Layout of Displacement Sensors within Each Test Section.....	164
19	Appendix H: Discussion of Base Course Layer Properties During First Construction.....	168
20	Appendix I: Transverse rut profiles for each test section as a function of traffic.....	172

21	Appendix J: Transverse rut profiles of all test sections and measurement lines at all wheel passes	176
22	Appendix K: Post-Trafficking Dynamic Modulus Test Results for Asphalt Cores	186
23	Appendix L: Selected Photos of Forensic Investigations	189

List of Tables

Table 2-1: Test section performance from studies in Berg et al. (2000).	4
Table 2-2: Variables that influence the effect of reinforcement (after Berg et al. 2000).	5
Table 2-3: Test section location and load type of studies since 2000.....	9
Table 2-4: Test section layers and properties of sections since 2000.	10
Table 2-5: Geosynthetic reinforcement products used in test sections since 2000.....	12
Table 2-6: Test section performance of sections since 2000.	13
Table 2-7: Instrumentation and/or measurement parameter for test sections since 2000.....	15
Table 2-8: Major findings from studies since 2000.	16
Table 2-9: Studies involving location of geogrid.	21
Table 2-10: Experimental and software predicted LCR values for BX and TX geogrids.....	32
Table 2-11: Input parameters for Perkins and Edens (2003) model.	36
Table 2-12: Test section experimental and Perkins and Edens (2003) model predictions of LCR.	39
Table 4-1: Material properties of Hot-Mix samples obtained from Montana.	51
Table 4-2: Material properties of Montana mixes for dynamic modulus tests.	52
Table 4-3: Material properties of Surface C HMA used for test sections.	52
Table 4-4: Material properties of crushed base course aggregate.....	54
Table 4-5: Material properties of subgrade.....	55
Table 4-6: Material properties of geotextiles.....	59
Table 5-1: Subgrade QC measurements in each test section during construction.....	61
Table 5-2: Base course QC measurements in each test section during construction.....	61
Table 5-3: Average vane shear strengths for the compacted subgrade.....	66
Table 5-4: Average moisture content for the compacted subgrade.	66
Table 5-5: Average CBR strength for the compacted subgrade.	67
Table 5-6: Average dynamic stiffness of the compacted subgrade.	68
Table 5-7: Average moisture content of the compacted base course.....	75
Table 5-8: Average dynamic stiffness of the compacted base course.	75
Table 5-9: Average dry unit weights of the compacted base course.	76
Table 5-10: Average density of the compacted asphalt layer from nuclear density tests.....	79
Table 7-1: Summary of post-trafficking asphalt density.	89
Table 7-2: Results of washed sieve analysis on extracted samples from the base course.	90

Table 7-3: Post-trafficking subgrade average moisture content.	91
Table 8-1: HMA average thickness and standard deviation.	102
Table 8-2: Base course average thickness and standard deviation.	102
Table 8-3: Subgrade vane shear strength standard deviation.....	103
Table 8-4: Subgrade in-field CBR strength standard deviation.....	103
Table 8-5: Subgrade dynamic stiffness standard deviation.	103
Table 8-6: Subgrade average DCP and standard deviation.	104
Table 8-7: Base course dynamic stiffness standard deviation.	104
Table 8-8: Base course average DCP and standard deviation.	104
Table 8-9: Subgrade composite average resilient modulus and standard deviation.	105
Table 8-10: Base course composite average a_2 and standard deviation.	105
Table 8-11: Parameters used in AASHTO pavement design equation and predicted ESALs....	106
Table 8-12: Parameters from statistical analysis.	107
Table 8-13: Parameters used in spreadsheet model to produce TBR=1.	109
Table 8-14: Table 4-1 from Berg et al. (2000) providing guidelines for geotextile reinforcement of paved roads.	110
Table 9-1: Typical unit pay item costs for typical MDT roadway projects.....	111
Table 19-1: Average moisture content of the compacted base course for the first construction..	168
Table 19-2: Average dynamic stiffness of the compacted base course for the first construction..	168
Table 19-3: Average dry unit weights of the compacted base course for the first construction...	169

List of Figures

Figure 2-1: LCR versus subgrade CBR for all studies.	18
Figure 2-2: LCR versus pavement structural number for all studies.	19
Figure 2-3: LCR versus base thickness for all studies.	20
Figure 2-4: LCR versus subgrade CBR for studies using BX1200.	20
Figure 2-5: LCR versus pavement structural number for studies using BX1200.	21
Figure 2-6: LCR versus subgrade CBR for Tenax MS220.	28
Figure 2-7: Geosynthetic Structural Coefficient (GSC) versus subgrade CBR for BXG12.	29
Figure 2-8: LCR versus subgrade CBR for TX5.	31
Figure 2-9: Test section and Tensar (2014) software LCR values for TX5 and TX7.	33
Figure 2-10: Test section and Tensar (2014) software LCR values for BX1100 and BX1200.	33
Figure 2-11: Effect of pavement structural number on LCR from Perkins and Edens (2003) model.	37
Figure 2-12: Effect of subgrade CBR on LCR from Perkins and Edens (2003) model.	37
Figure 2-13: Test section experimental and Perkins and Edens (2003) model predictions of LCR, all 19 studies.	41
Figure 2-14: Test section experimental and Perkins and Edens (2003) model predictions of LCR, 15 of 19 studies.	41
Figure 2-15: Test section experimental and Perkins and Edens (2003) model predictions of LCR, 7 studies from 2007 to present.	42
Figure 2-16: Flow chart of response model modules.	44
Figure 3-1: Accelerated test facility concrete lined trench.	49
Figure 3-2: Accelerated pavement test device.	50
Figure 4-1: Dynamic complex modulus versus load frequency at a test temperature of 20°C for 3 MT mixes.	53
Figure 4-2: Laboratory and in-field CBR results for subgrade.	56
Figure 4-3: Compaction of subgrade into wooden boxes.	57
Figure 4-4: CBR versus elapsed time from wooden box tests.	57
Figure 4-5: Vane shear strength versus CBR for all subgrade tests.	58
Figure 5-1: Survey measurement technique during construction.	62
Figure 5-2: Spread and tracked subgrade prior to compaction.	63
Figure 5-3: Compacting the subgrade.	64

Figure 5-4: Leveling the final surface of the subgrade.	64
Figure 5-5: Finished surface of the subgrade.....	65
Figure 5-6: Subgrade DCP results as a function of depth.....	69
Figure 5-7: Cross-section of LVDT installation in the subgrade and base course.	70
Figure 5-8: Installing LVDT anchor.	71
Figure 5-9: LVDT sensor prior to installation.	71
Figure 5-10: Position of the measurement point with respect to the subgrade surface.	72
Figure 5-11: Cross-sectional view of constructed test sections.....	72
Figure 5-12: Installed geosynthetics.	73
Figure 5-13: Gravel screeded to uniform depth.....	74
Figure 5-14: Final compacted surface of the base course.....	74
Figure 5-15: Base Course DCP results as a function of depth.....	76
Figure 5-16: Placement of hot-mix asphalt.....	77
Figure 5-17: Compaction of hot-mix asphalt using smooth drum roller.	78
Figure 5-18: Compaction of hot-mix asphalt pneumatic roller.	78
Figure 6-1: Test section surface temperature versus time.	80
Figure 6-2: Rut measurement locations within each test section.....	81
Figure 6-3: Longitudinal rut responses for all test sections.....	82
Figure 6-4: Transverse rut profile progression in the Control test section, south measurement line.....	82
Figure 6-5: Transverse rut profiles of all test sections and measurement lines at 903,438 wheel passes.	83
Figure 6-6: Displacement response of Control subgrade sensors.....	84
Figure 6-7: Displacement response of RS280i subgrade sensors.	84
Figure 6-8: Displacement response of Geotex801 subgrade sensors.....	85
Figure 6-9: Displacement response of Control base course sensors.....	85
Figure 6-10: Displacement response of RS280i base course sensors.	86
Figure 6-11: Displacement response of Geotex801 base course sensors.	86
Figure 6-12: Average displacement response of all subgrade sensors.	87
Figure 6-13: Average displacement response of all base course sensors.	87
Figure 6-14: Average strain response in the base course for all test sections.....	88
Figure 7-1: Post-trafficking subgrade DCP results as a function of depth.	91
Figure 7-2: Post-trafficking surface profiles of the Control test section.	92

Figure 7-3: Post-trafficking profile photo of north face of Control trench wall.	93
Figure 7-4: Post-trafficking surface profiles of the RS280i test section.	93
Figure 7-5: Post-trafficking profile photo of north face of RS280i trench wall.	94
Figure 7-6: Post-trafficking surface profiles of the Geotex 801 test section.	94
Figure 7-7: Post-trafficking profile photo of north face of Geotex 801 trench wall.	95
Figure 7-8: Post-trafficking full profile photo of Geotex 801 test section.	96
Figure 7-9: Photo of extracted RS280i geotextile.	97
Figure 7-10: Close-up photo of extracted RS280i geotextile.	97
Figure 7-11: Photo of extracted Geotex 801 geotextile.	98
Figure 7-12: Close-up photo of extracted Geotex 801 geotextile.	98
Figure 8-1: Longitudinal rut responses showing data scatter.	101
Figure 19-1: Longitudinal rut response from first construction.	170
Figure 19-2: Average vertical strain in the base layer from first construction.	170

1 Introduction

The availability and quality of base course aggregates is becoming limited in many states, requiring departments of transportation to be even more innovative and efficient with their roadway designs. These limitations and requirements are even more acute in areas where low-volume roads are more prevalent, budgets are shrinking, user expectations are increasing and commodities are under high demand.

In Montana, gravel sources are becoming difficult to find and difficult to permit in densely populated areas. The Bakken oil development has previously placed additional strain on aggregate sources in the Glendive district. There are areas in Eastern Montana where aggregates are hauled a significant distance. The Billings and Great Falls districts have areas where aggregate prices are relatively high because of lack of available sources.

Geosynthetics are routinely used in transportation applications to facilitate construction, improve stability and enhance longevity. Geosynthetic reinforcement is used to reduce the amount of gravel used in the construction of roadways and/or to extend the life of roadways. An extended service life of the roadway will reduce impacts from maintenance and construction operations on road users and surrounding businesses. Extending the pavement service life will lengthen the construction interval between major rehabilitation projects. This will cause fewer disruptions to traffic and thereby enhance route safety. The benefits and outcomes discussed above serve the core concepts in Montana Department of Transportation's (MDT) mission statement, namely quality, safety, cost effectiveness and sensitivity to the environment. Eastern Montana contains many miles of low volume roads and is experiencing tremendous infrastructure challenges due primarily to oil and gas development and increasing demands from the agricultural industry. These roads are in areas where gravel is scarce and contain design conditions for which data on the benefits of geosynthetic reinforcement is missing.

The MDT has sponsored several projects conducted by the Western Transportation Institute at Montana State University (WTI/MSU) related to geosynthetic reinforcement of paved roadways. These projects include efforts to provide experimental evidence of performance of geosynthetic reinforced paved roads by the construction of test sections (Perkins, 1999, 2002) and those designed to provide design models for reinforced roads (Perkins 2001a,b, and Perkins et al. 2004). Test section work performed in the two studies noted above along with other studies reported in the literature was summarized by Berg et al. (2000) and more recently by Perkins (2016). The two projects involving the construction of test sections used two types of pavement test facilities, namely a large concrete box to which a stationary cyclic load was applied to a circular plate and a heavy vehicle simulator involving a load applied to a dual wheel assembly rolled across the pavement. These projects and the design models that were developed are discussed in more detail in Section 2.

Based on the work of these previous studies and their in-house experience, MDT believes that geosynthetics can be used responsibly to provide cost-savings on upcoming highway construction projects in the state. Typical construction projects currently under consideration have; however, design conditions that differ from those contained in previous studies. This project provides MDT with experimental evidence of performance for these typical projects to proceed with future designs and answers the following questions:

- Do standard stabilization geotextiles used commonly as a construction expedient provide structural benefit to the pavement as seen by an increase in the number of traffic passes carried to reach a certain rut depth?
- What is the structural benefit of reinforcement geosynthetics for a pavement cross section having an asphalt and base course thickness moderately greater than those incorporated into previous studies?

The main objective of this project is to characterize the performance of geosynthetic-reinforced test sections when compared to an unreinforced case to assess benefit in terms of an extension of the life of the pavement. This objective was achieved through the construction of a single test track containing three test sections, a detailed analysis and synthesis of the results and the evaluation of an analytical design tool previously developed for MDT and to be used by pavement engineers to design geosynthetic-reinforced pavements.

2 Literature Review

The purpose of this literature review is to provide: 1) An understanding of previous studies providing experimental documentation of the benefit of geosynthetics used for reinforcement of the base course layer of flexible pavements with an emphasis on studies where geotextiles were used for reinforcement and 2) The basis for the spreadsheet design model previously developed by the PI and provided as a version update as part of this project.

The material presented in this chapter shows that the majority of studies conducted used geogrids as the reinforcement geosynthetic. While the present study is focused on reinforcement geotextiles, a review of all studies is appropriate as the spreadsheet design model was developed by using results from studies incorporating both geogrids and geotextiles. The spreadsheet design model is used in this project to examine the results obtained and to predict reinforcement benefit for a weaker subgrade condition to provide recommendations for a range of subgrade conditions. The validity of this model is further established in this chapter by comparison of the model to the results of studies that have been conducted since the model was originally developed. A comprehensive review of studies involving both geotextiles and geogrids is therefore provided in this chapter.

2.1 Previous Literature Reviews

The project Principal Investigator (PI) performed an extensive literature review on this topic in the late 1990's (Perkins and Ismeik, 1997a, 1997b). This literature review was used in the development of a practice-oriented document (Berg et al., 2000) commissioned by the Geosynthetic Manufacturer's Association (GMA). The document contained a synthesis of research performed up to the year 2000 and has become known as the GMA White Paper II (GMA-WPII).

The review illustrated the value added to flexible pavements by using geosynthetic reinforcement. The review showed the benefits of geosynthetic reinforcement, the conditions where reinforcement is beneficial, geosynthetic properties that are most influential and the mechanisms responsible for reinforcement. Conclusions from the review were used to evaluate existing design procedures, to comment on potential cost benefits and to develop application specifications.

Nineteen studies published between 1987 and 1999 were included in the review. Information on the following variables was tabulated for each study:

- Type of pavement test facility and loading arrangement.
- Thickness, material types and properties of pavement layers used in the test sections.
- The geosynthetic type and location.
- Value added benefit expressed in terms of Traffic Benefit Ratio (TBR), Base Course Reduction Ratio (BCR) and/or Layer Coefficient Ratio (LCR).

Table 2-1 provides a summary of test conditions and results from pertinent studies summarized in Berg et al. (2000). The geosynthetics from Amoco are the only geotextile included in these studies.

Table 2-1: Test section performance from studies in Berg et al. (2000).

Author	Section Number	Layer thickness (mm)		Subgrade CBR	Structural number	Geosynthetic / Location ¹	TBR	BCR	LCR
		AC	Base						
Al-Qadi et al. (1997)	1	90	100	7.0	1.97	Amoco 2002 - B	1.60	-	1.08
	2					BX1200 - B	1.40	-	1.06
Collin et al. (1996)	1	50	180	1.9	1.78	BX1100 - B	2.00	-	1.13
	2		300		2.44		3.30	-	1.22
	3		180		1.78	BX1200 - B	2.00	-	1.13
	4		300		2.44		10.00	-	1.46
Haas et al. (1988)	1	100	200	8.0	2.68	BX1100 - B	3.30	-	1.22
	2	75		3.5	2.28		3.00	-	1.20
	3		1.0	2.28	1.80		-	1.10	
	4		300	0.5	2.83		1.00	-	1.00
	5		200	3.5	2.28		-	50.0	2.00
Kinney et al. (1998)	1	61	240	2.5	2.28	BX1200 - B	2.00	-	1.12
	2		355		2.92		3.40	-	1.22
Perkins (1999)	1	75	300	1.5	2.83	Amoco 2006 - B	8.50	-	1.42
	2				2.83	BX1100 - B	17.00	-	1.58
	3				2.83	BX1100 - 2/3	56.00	-	1.88
	4				2.83	BX1200 - B	45.00	-	1.82
Perkins and Cortez (2005)	1	75	300	1.5	2.83	Amoco 2006 - B	9.00	-	1.43
	2				2.83	BX1100 - B	10.00	-	1.46
	3				2.83	BX1200 - B	31.50	-	1.73
Webster (1993)	1	50	350	3.0	2.72	BX1100 - B	2.70	-	1.18
	2		450		3.27	BX1200 - B	1.30	-	1.04
	3		350		2.72	BX1200 - M	2.20	-	1.14
	4		300		2.44	BX1200 - B	3.10	-	1.21
	5		350	2.72	4.70		-	1.29	
	6		250	8.0	2.17		6.70	-	1.37
	7		150		1.61		22.00	-	1.69
	8		250		2.17		-	40.0	1.67
	9		350	3.0	2.72	FORTRAC 35/20-20	1.10	-	1.01
	10				2.72	Miragrid 5T	1.00	-	1.00
	11				2.72	Tenax LBO 201 SAMP	1.00	-	1.00
	12				2.72	Conweb GB-3022	1.60	-	1.08

¹B-Bottom of base layer, M-Middle of base layer, 2/3- Two thirds below top of base layer

The information tabulated in the GMA-WPII was used to develop general guidelines for conditions where reinforcement appears to provide most benefit. The main findings are summarized in Table 2-2. This information was also used to provide a qualitative review of reinforcement application potential for paved permanent roads, where this review was specific to geotextiles, geogrids or geotextile-geogrid composites.

The GMA-WPII provided a recommended practice for the use of reinforcement geosynthetics in paved roads. The principal elements related to design involve choosing a design cross-section for a typical pavement without reinforcement and modifying this cross-section or design life with one of the two benefit ratios (TBR or BCR). The benefit ratios could be estimated by comparing conditions of the design in question to those from test sections summarized in the GMA-WPII. Alternatively, benefit values could be obtained by constructing test sections for the particular conditions of interest. An appendix was provided as a guideline for the construction of comparison test sections.

Table 2-2: Variables that influence the effect of reinforcement (after Berg et al. 2000).

Pavement Component	Variable	Condition where reinforcement appears to provide most benefit
Geosynthetic	Low strain modulus	Higher modulus improves performance
	Location	Bottom of thin bases (≤ 300 mm), middle of thick bases (> 300 mm)
	Geogrid aperture	$> D_{50}$ of adjacent base
	Aperture stiffness	Rigid
Subgrade	Strength	CBR < 8
Base	Thickness	≤ 250 mm for moderate loads
	Gradation	Well-graded
	Angularity	Angular
HMA	Thickness	75 mm

2.2 Test Sections

Since the year 2000, an additional 12 studies involving the construction of test sections and the documentation of reinforcement benefit have been identified. Table 2-3 provides details on the type of facility and load details for each study. Table 2-4 gives details on the thickness, pavement layer material types, subgrade strength, geosynthetic type and approximate structural number of each test section constructed. The layer thickness listed corresponds to the control section to which the reinforced section is compared. In these 12 studies, 39 individual test sections have been identified. Table 2-5 lists the geosynthetic products used in these studies, the structure of the geosynthetic, the aperture size if the geosynthetic is a geogrid and the secant modulus at 2 % strain. The three Mirafi products are the only geotextiles included in these studies. Table 2-6 provides values of benefit in terms of TBR, BCR and LCR (Layer Coefficient Ratio) for each of the test sections and includes the main variables that influence performance. If TBR or BCR was

determined in the study, LCR is then determined from these values. LCR is directly calculated from BCR by Equation 1. If TBR is provided, LCR is determined by using the AASHTO 1993 flexible pavement design equation to evaluate the increased base layer coefficient to give the increased ESALs corresponding to the experimental TBR value. When using the AASHTO 1993 design equation, the following parameters were assumed: Reliability = 80 %, Standard Deviation = 0.45, Initial Serviceability = 4.2, Terminal Serviceability = 2.5. Table 2-7 provides details on any instrumentation used in the test sections. Table 2-8 summarizes major findings for each of the studies.

$$LCR = \frac{1}{1-BCR/100} \quad (1)$$

Several of the studies presented above contain features and results that warrant further discussion. The study by Aran (2006) involved a relatively strong cross-section (SN = 4.1 for the control and 3.47 for the reinforced section) on a relatively strong subgrade (CBR=7.7 to 8.5). During the monitoring period from 1987 to 2005, the sections showed little rutting or cracking. FWD tests and pavement condition surveys showed the sections to be performing similarly. The lack of distress in either section is not conclusive evidence that the reinforcement was responsible for the equivalent performance. Equivalency may have been due to strong cross-sections resting on a strong subgrade for which little distress would be expected. In the absence of strain instrumentation on the reinforcement, it is not possible to show whether the reinforcement was mobilized to provide a reinforcement function. These considerations raise some questions regarding whether the geosynthetic provided any performance benefits for a relatively strong pavement cross-section resting on a relatively strong subgrade.

The study of Ghafoori and Sharbaf (2016) involved test sections on a strong subgrade (CBR=10). Strain gauge instrumentation was placed on the geogrids. Negligible strain was measured in the tests conducted indicating the geogrids were not mobilized during traffic loading, which implies they did not perform a reinforcing function. Stress cells; however, showed a significant decrease in vertical stress in the top of the subgrade for the reinforced sections with the order of reduction corresponding to the order of rutting performance. Without mobilization of the geogrids, it is difficult to attribute the stress reduction observed and the improved rutting performance to the reinforcement. The results in Ghafoori and Sharbaf (2016) also appear to conflict with an earlier paper (Ghafoori and Sharbaf, 2015), which reported results from a control section and a reinforced section with a base thickness of 406 mm. The rutting results reported showed the sections to perform nearly identically and different from results contained in the 2016 report. The authors were asked to comment on the potential discrepancy but did not respond.

Hanandeh et al. (2016) showed comparatively low TBR values for the test section conditions examined. In addition to the reinforcement geosynthetic, a non-woven geotextile was placed between the base and subgrade in all sections, including the control section. This material may

have provided a baseline level of reinforcement that made the distinction between sections having additional reinforcement products less noticeable.

Robinson et al. (2018) reported results from two reinforced sections on a subgrade with a CBR of 5.9 with a relatively thin pavement cross section. The two reinforced sections contained less HMA and base aggregate as compared to the control. The two reinforced test sections were constructed approximately two years later than the control test section. HMA source materials and volumetric measurements from gyratory compaction pucks indicate good consistency between the two sets of test sections constructed two years apart. Physical and mechanical properties of constructed HMA in the test sections were not reported. Constructed physical properties and in-place CBR appear to be similar for the base aggregate and subgrade materials for the two sets of test sections.

The sections were loaded to 811,200 ESALs. The sections reached permanent surface deformations of approximately 5.16 and 4.75 mm for the two reinforced sections and 7.4 mm for the control section. Permanent surface deformation is a change in elevation under the wheel path. Rut values of 7.95 and 6.68 for the two reinforced sections and 16.26 for the control were reported, where rut is the maximum vertical distance between the high and low points of the HMA surface. The paper states that little to no deformation took place in the subgrade of the test sections. Photographs of excavated cross-sections confirms this statement. These photographs also show little permanent vertical deformation in the base aggregate layer and seem to show that the majority of surface permanent deformation is due to deformation in the HMA layer. These photographs also seem to show that the larger rut value reported for the control section is due to shoving and upheaval in the HMA layer. The paper did not report observed values of permanent deformation in the base aggregate layer. Instrumentation was not included in the study to measure strain in the geogrids to see if they were mobilized.

The paper reports effective base layer structural coefficients for each section that would be needed to reach the terminal ESAL value reported above. The values of LCR shown in Table 2-6 correspond to the ratio of the effective base layer structural coefficient of each reinforced section to the control section. This approach assumes the reinforced test sections with a reduced cross-section performed the same as the control section, which is considered conservative since the reinforced test sections were performing better than the control section up to the terminal level of loading.

The paper concludes that the benefit expressed by the LCR values shown in Table 2-6 is due to the reinforcement. This conclusion is questionable given the observation that rutting occurred mainly in the HMA layer. The relatively small level of permanent surface deformation at the termination of loading makes it questionable whether these results pertain to long term pavement performance. Lastly, the order of improvement of the two test sections does not follow the order of increase in the geogrid stiffness, further indicating that the reinforcement was not responsible for the improvement observed.

Finally, the study of Tang et al. (2008) involved scaled loading and test section layer thickness and is most likely not representative of field conditions or comparable to results of other studies that did not involve scaling.

In addition to the studies summarized in this section, Helstrom et al. (2007) constructed test sections along a state route in Maine to investigate geogrids for reinforcement and geocomposites for drainage. The sections contained 150 mm of HMA and two different sets of sections with a base thickness of 300 mm and 600 mm. Mechanical properties of the subgrade were not reported; however, the subgrade was described as very poor, highly frost susceptible, having an SPT blow count as low as 7 and a natural water content approaching its liquid limit. Local bearing failures along the route were previously reported. One type of geogrid reinforcement (Tensar BX1200) was used. The geogrid was placed at the bottom and in the middle of different sections for both base thickness values. Instrumentation was included to monitor strain in the geogrid and pore water pressure in the base and subgrade soils. FWD tests were periodically performed. The sections were constructed in the summer of 2002. Monitoring of the sections continued until May 2005.

Based on the strains induced in the geogrid over the monitoring period, the study concluded that the sections with 300 mm of base developed what was considered close to the lower limit of strain to show that the reinforcement was mobilized and that benefit was derived from the geogrid. For the sections with 600 mm of base, insufficient strain was developed in the geogrid to conclude that the reinforcement was mobilized. FWD tests, while generally not considered to be the best means to assess reinforcement benefit, supported the observations above. The structural number for the sections with 300 mm and 600 mm of base is approximately 4.0 and 5.7, indicating that reinforcement benefit is low to negligible for sections of this thickness even when a weak subgrade is present. Monitoring of rutting and cracking was not reported in this study.

Table 2-3: Test section location and load type of studies since 2000.

Author	Facility type	Facility dimensions (m)	Test section length (m)	Load type	Applied cyclic pressure (kPa)	Applied cyclic load (kN)	Load frequency (Hz) or wheel speed (km/hr)
Abu-Farsakh and Chen (2011)	Indoor test box	2 (length) x 2 (width) x 7 (height)	NA	Stationary circular plate, 305 mm diameter	550	40	0.77
Aran (2006)	Public roadways	3.6 lane width	128 – 600	Random traffic	Random	Random	Random
Ghafoori and Sharbaf (2016)	Indoor test tank	1.8 (diameter) x 2.1 (height)	NA	Stationary circular plate, 305 mm diameter	550	40	0.77
Hanandeh et al. (2016)	Outdoor test track	4 m lane width	24	Dual wheel, single axle	NR	44, 54 and 64	16.8
Henry et al. (2009)	Indoor test track	3.2	7.9	Dual wheel, single axle	690	48.9	12.9
Jersey et al. (2012)	Outdoor covered test track	2.4	15.2	Dual wheel, single axle and dual wheel tandem axle	607	44.5 and 89	NR
Kwon (2007)	Outdoor test track	3.2	7.6	Dual wheel, single axle	689	44.5	8 and 16
Robinson et al. (2018)	Outdoor covered test track	3 (width)	15.0	Dual wheel, tandem axle	827	88.9	NR
Saghebfar et al. (2016)	Indoor test track	4.9 width	3.05	Dual wheel, single axle	620	80	11.3
Sharp (2005)	Public roadway	3.6 lane width	274 - 1915	Random traffic	Random	Random	Random
Tang et al. (2008)	Indoor test pit	0.56 width	1.37	Single wheel	621	2.7	9.9
Valero et al. (2014)	Outdoor test oval	4.6 width	30.5	Two axle truck, super single tires	690	80	NR

NA - Not Applicable

NR - Not Reported

Table 2-4: Test section layers and properties of sections since 2000.

	Section Number	Layer thickness (mm)		Layer material types			Structural number
Author		AC	Base	Base	Subgrade type (CBR)	Geosynthetic / Location ¹	
Abu-Farsakh and Chen (2011)	1	51	305	GW	CL (1)	BX1100 - B	1.84
	2					BX1200 - B	
	3					TX160 - B	
	4					TX160 - M	
	5					TX170 - B	
	6					TX170 – M	
	7					TX170 – 1/3	
Aran (2006)	1	108	254	GW	NR (8.5)	NR	3.47
Ghafoori and Sharbaf (2016)	1	76	305	GP-GM	SC-SM (10)	BX1100 - B	2.86
	2		406				3.42
	3		305			TX130 - B	2.86
	4		406				3.42
Hanandeh et al. (2016)	1	76	457	GW	CH (1.1)	TX150 - B	2.94
	2					TX150 - D	
	3					RS580i - B	
	4		254				2.26
Henry et al. (2009)	1	150	300	GP-GM	ML (5.2)		4.31
	2	100	300				3.43
	3	150	600				4.31
	4	100	600				3.43
Jersey et al. (2012)	1	43	203	GP-GM	CH (3)	TX 140 - B	1.8
Kwon (2007)	1	76	203	SP-SM	CL-ML (2.5)	BX1100 - B	2.15
	2		CL-ML (3.5)		BX1200 - B		
	3					305	2.48
	4					457	2.97

Robinson et al. (2018)	1	81	148	GW-GM	CH (5.9)	TX-1 - B	2.22
	2	82	150			TX-2 - B	2.24
Saghebfar et al. (2016)	1	152	305	GP	CH (5)	RS280i - B	3.00
	2					RS380i - B	
Sharp (2005)	1	121	432	GW	NR (5.3)	BX1100 - B	4.28
Tang et al. (2008)	1	38	66	Crushed Stone	SW-SM (1.5)	Grid B - B	0.96
	2					Grid C - B	
	3					Grid D - B	
Valero et al. (2014)	1	51	203	Crushed Stone	CH (3)	E'Grid 1616 - B	1.38
	2					E'Grid 2020 - B	
	3					E'Grid 3030 - B	
	4					TX5 - B	
	5					TX7 - B	
	6					RX1200 - B	

¹B-Bottom of base layer, D-Two layers, M-Middle of base layer, 1/3-One third below top of base layer

NA - Not Applicable

NR - Not Reported

Table 2-5: Geosynthetic reinforcement products used in test sections since 2000.

Manufacturer Brand Name	Manufacturer	Structure	Aperture size XMD/MD (mm)	2 % Secant modulus (kN/m)	
				XMD	MD
E'Grid 1616	BOSTD New Grids	Geogrid Biaxial Punched Sheet Drawn	40/40	475	450
E'Grid 2020			40/40	565	535
E'Grid 3030			40/40	880	810
RX1200			37/25	980	390
RS280i	Mirafi	Geotextile Woven	NA	450	350
RS380i				750	450
RS580i				1313	350
BX1100	Tensar	Geogrid Biaxial Punched Sheet Drawn	25/33	330	205
BX1200			25/33	450	300
TX130		Geogrid Triangular	33/33 ¹	200 ²	
TX140			40/40 ¹	225 ²	
TX150			40/40 ¹	270 ²	
TX160			40/40 ¹	300 ²	
TX170			40/40 ¹	480 ²	
TX5			40/40 ¹	370	NR
TX7			40/40 ¹	455	NR
TX-1			40/40 ¹	270 ²	
TX-2			33/33 ¹	225 ²	
Grid B	NR	Geogrid Biaxial Woven	NR	750	740
Grid C		Geogrid Biaxial Extruded		780	490
Grid D		Geogrid Biaxial Woven		560	515

¹Longitudinal/diagonal measurements of triangular aperture²Radial stiffness at 0.5% strain, kN/m

NA - Not Applicable

NR - Not Reported

Table 2-6: Test section performance of sections since 2000.

	Section Number	Layer thickness (mm)		Subgrade CBR	Structural number	Geosynthetic / Location ¹	TBR	BCR	LCR
Author		AC	Base						
Abu-Farsakh and Chen (2011)	1	51	305	1.0	1.84	BX1100 - B	2.1	-	1.13
	2					BX1200 - B	3.5	-	1.24
	3					TX160 - B	3.8	-	1.25
	4					TX160 - M	3.0	-	1.20
	5					TX170 - B	4.6	-	1.29
	6					TX170 – M	3.5	-	1.24
	7					TX170 – 1/3	7.2	-	1.39
Aran (2006)	1	108	254	8.5	3.47	NR - B	-	-	1.31
Ghafoori and Sharbaf (2016)	1	76	305	10.0	2.86	BX1100 - B	1.85	-	1.11
	2		406		3.42	BX1100 – M	2.78	-	1.18
	3		305		2.86	TX130 - B	3.00	-	1.20
	4		406		3.42	TX130 - M	8.5	-	1.40
Hanandeh et al. (2016)	1	76	457	1.1	2.94	TX150 - B	1.34	-	1.05
	2					TX150 - D	1.59	-	1.08
	3		254		2.26	RS580i - B	1.94	-	1.12
	4						-	<< 44	<<1.79
Henry et al. (2009)	1	150	300	5.2	4.31	BX1200 - B	0.63		< 1
	2	100	300		3.43		1.33	-	1.05
	3	150	600		5.96		0.82	-	< 1
	4	100	600		5.08		1.47	-	1.06
Jersey et al. (2012)	1	43	203	3.0	1.8	TX 140 - B	12.3	-	1.53
Kwon (2007)	1	76	203	2.5	2.15	BX1100 - B	1.95	-	1.12
	2					BX1200 - B	2.42	-	1.16
	3		305	3.5	2.48		2.68	-	1.18
	4		457		2.97	BX1200 - M	1.73	-	1.10
Robinson et al. (2018)	1	81	148	5.9	2.22	TX-1 - B	-	-	1.70
	2	82	150		2.24	TX-2 - B	-	-	1.65

Saghebfar et al. (2016)	1	152	305	5.0	3.00	RS280i	1.38	50	1.05
	2					RS380i	1.88	-	1.11
Sharp (2005)	1	121	432	5.3	4.28	BX1100 - M	-	35.3	1.55
Tang et al. (2008)	1	38	66	1.5	0.96	Grid B - B	2.9	-	1.25
	2					Grid C - B	24.0	-	1.84
	3					Grid D - B	3.6	-	1.30
Valero et al. (2014)	1	51	203	3.0	1.38	E'Grid 1616 - B	-	24.8	1.33
	2					E'Grid 2020 - B	-	29.6	1.42
	3					E'Grid 3030 - B	-	35.1	1.54
	4					TX5 - B	-	13.0	1.15
	5					TX7 - B	-	13.0	1.15
	6					RX1200 - B	-	30.1	1.43

¹B-Bottom of base layer, D-Two layers, M-Middle of base layer

NA - Not Applicable

NR - Not Reported

Table 2-7: Instrumentation and/or measurement parameter for test sections since 2000.

Author	Surface of test section	Asphalt concrete	Base aggregate	Geosynthetic	Subgrade
Abu-Farsakh and Chen (2011)	Rut depth	None	None	Strain	Vertical stress, strain, pore water pressure
Aran (2006)	None	None	None	None	None
Ghafoori and Sharbaf (2016)	Rut depth	None	None	Strain	Vertical stress
Hanandeh et al. (2016)	Rut depth	None	Vertical deformation	None	Vertical stress, vertical deformation, pore water pressure
Henry et al. (2009)	Rut depth	Strain, temperature	Stress, strain, moisture content	Strain	Stress, strain, moisture content
Jersey et al. (2012)	Rut depth	None	None	None	None
Kwon (2007)	Rut depth	Horizontal strain, temperature	Vertical and radial deformation, temperature	None	Vertical stress and deformation, moisture content, pore water pressure, temperature
Robinson et al. (2018)	Rut depth	None	None	None	None
Saghebfar et al. (2016)	Rut depth	Longitudinal strain, temperature	None	Horizontal strain	Vertical stress
Sharp (2005)	Rut depth, FWD, pavement smoothness	None	None	None	None
Tang et al. (2008)	Rut depth	None	None	None	None
Valero et al. (2014)	Rut depth	None	None	None	None

Table 2-8: Major findings from studies since 2000.

Author	Performance criteria	Geosynthetic type	Geosynthetic location and layering	Base course layer equivalency	Other observations
Abu-Farsakh and Chen (2011)	Rutting	Performance increased with geogrid stiffness. For comparative stiffness, a triangular geogrid performed 9 % better than a biaxial geogrid.	Locating the geogrid at the upper 1/3 position in the base layer resulted in substantially increased benefit. Locating the geogrid in the middle of the base layer resulted in poorer performance as compared to the bottom.		Permanent strain in the geogrids was as much as 0.5 %. Reinforcement reduced vertical stress and strain in the top of the subgrade. Applying a tack coat to the geogrid resulted in a 71 % increase in performance.
Aran (2006)	Crack and pavement condition surveys				The control section and a reinforced section with less HMA appeared to perform similarly. Very little distress was seen in either section. Results from the study were believed to be inconclusive.
Ghafoori and Sharbaf (2016)	Rutting	Triangular geogrid performed better than a biaxial geogrid.			TBR values are high for the strong subgrade used. Vertical stress on subgrade was shown to be substantially lower in reinforced sections. Negligible strain was measured in the geogrids.
Hanandeh et al. (2016)	Rutting	Woven geotextile performed better than two layers of triangular geogrid.	Two layers of triangular geogrid performed better than one layer at bottom.	Woven geotextile in reduced base section performed poorly.	TBR values were comparatively low. A non-woven was placed between the base and subgrade in all sections. This material may have provided reinforcement that made sections more equivalent.
Henry et al. (2009)	Rutting				Negligible benefit was seen for the thick sections and strong subgrade used.
Jersey et al. (2012)	Rutting				

Kwon (2007)	Rutting	Stiffer biaxial geogrids offer better performance.	Optimal location is at the bottom of thin base layers and at the 1/3 position for thick base layers. Two layers in thick base layers is beneficial.		
Robinson et al. (2018)	Rutting, impulse stiffness modulus, base damage index.				LCR values are comparatively high for the strength of the subgrade.
Saghebfar et al. (2016)	Rutting	Strain developed rapidly and leveled off at values between 0.15 and 0.2%.		Woven geotextile in reduced base section performed well.	Rutting results produced relatively low TBR values but a high BCR value for one product. Vertical stress on subgrade was lower for better performing sections.
Sharp (2005)	Rutting, FWD, pavement smoothness.				The reinforced reduced base section performed equal to the control section in terms of rutting, but worse in terms of FWD back-calculated modulus, pavement condition surveys and IRI.
Tang et al. (2008)	Rutting	Stiff biaxial geogrids performed better than flexible geogrids.			Layer thickness and wheel load were scaled. Results may not be directly comparable to other studies using non-scaled variables.
Valero et al. (2014)	Rutting	The biaxial geogrids generally performed better than the triangular geogrids.			The biaxial geogrid sections had two sections for each product. Significant scatter was seen between the two sections. The triangular geogrid sections had only one section for each product.

To validate and/or update the general guidelines given in Berg et al. (2000) and summarized in Table 2-1, the results of test sections summarized in Table 2-2 and Table 2-6 are synthesized in the figures below. Figure 2-1 provides a plot of LCR versus subgrade CBR for all test sections listed in Table 2-2 and Table 2-6. While there is appreciable scatter in the results, due in part to different geosynthetics and section thickness, an overall trend of decreasing benefit with increasing subgrade strength is observed. The four points at a CBR of 10 are from the study by Ghafoori and Sharbaf (2016). The point at CBR of 8.5 was from the study by Aran (2006). These studies, as discussed previously, have some uncertainty. The four studies corresponding to the data points at a CBR of 8.0 have modest values of structural number ranging from 1.6 to 2.7 and may suggest some benefit for thin sections on stronger subgrades. The three points with the largest LCR values are from the study by Webster (1993) where a pavement load over three times the typical value for highway applications was used, suggesting that performance improvement due to reinforcement for thin sections on strong subgrades may be realized only for abnormally heavy pavement loads.

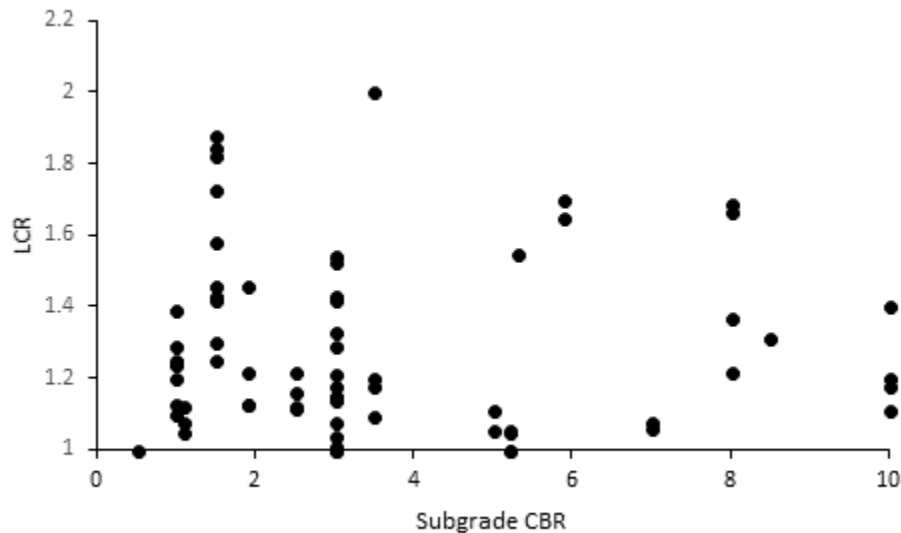


Figure 2-1: LCR versus subgrade CBR for all studies.

Figure 2-2 and Figure 2-3 show plots of LCR versus pavement structural number and base thickness for all test sections. These results show a trend of decreasing LCR with increasing SN and base thickness. Benefit is negligible for $SN \geq 4$ and base thickness ≥ 450 mm.

The trends discussed above are seen more clearly by plotting results for a single type of geosynthetic. The geogrid BX1200 was used most frequently in the studies reported. Plots of LCR versus subgrade CBR and pavement structural number are shown in Figure 2-4 and Figure 2-5. In

Figure 2-4, the three points for CBR of 8 are from the study by Webster (1993) and correspond to relatively thin sections. These sections were also loaded with a very heavy wheel load of 130 kN and are subject to the possible limitation discussed above.

Four of the studies listed in Table 2-2 and Table 2-6 involved comparative test sections with a geogrid placed at the bottom of the base versus a section where the same geogrid was placed within the base. The effect of geogrid location is expressed by a percentage difference in LCR when the geogrid is placed within the base as compared to when it was at the bottom of the base. The results (Table 2-9) show that locating the geogrid at various points within the base can result in both improved and worse performance. The number of results is insufficient to draw clear conclusions on the variables of most importance with regard to geogrid location. The modest level of improvement of most results along with the potential for worse performance suggests that placing the geogrid at the bottom of the base is a safe and reasonable approach until more detailed studies are conducted.

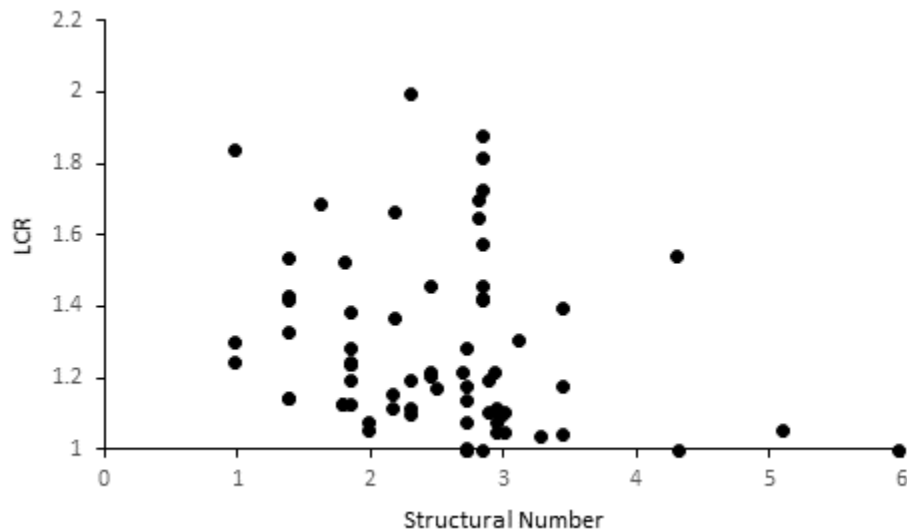


Figure 2-2: LCR versus pavement structural number for all studies.

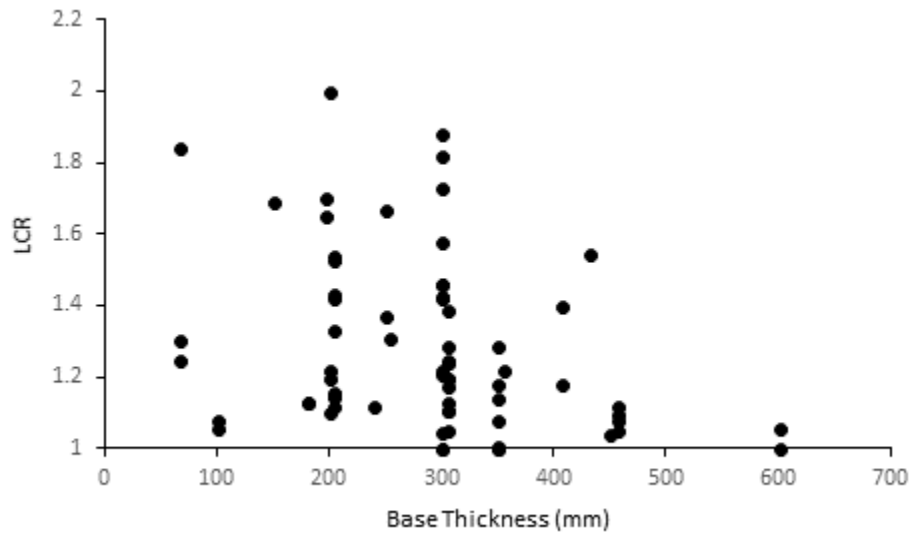


Figure 2-3: LCR versus base thickness for all studies.

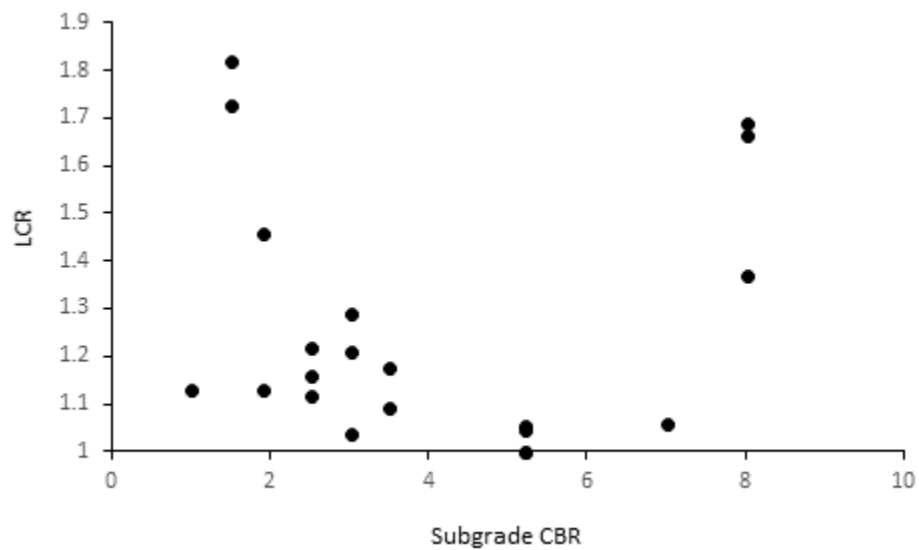


Figure 2-4: LCR versus subgrade CBR for studies using BX1200.

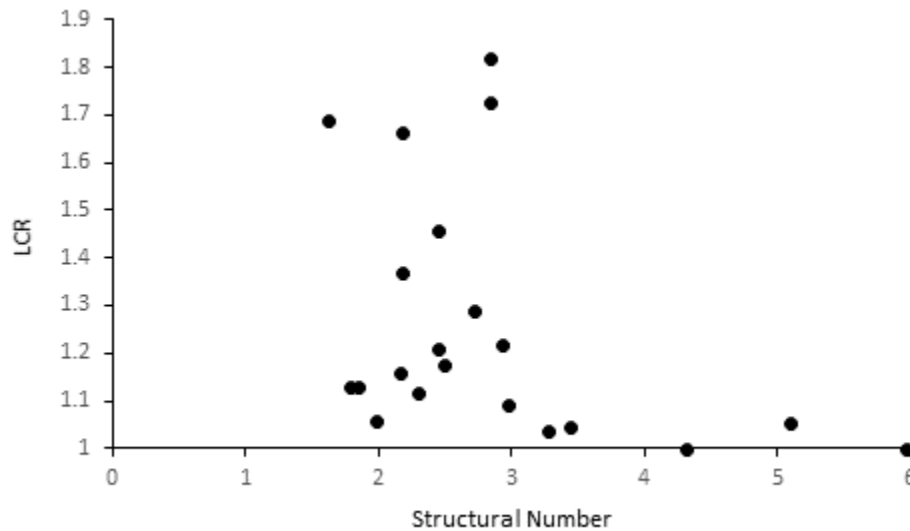


Figure 2-5: LCR versus pavement structural number for studies using BX1200.

Table 2-9: Studies involving location of geogrid.

Study	Thickness (mm)		Subgrade CBR	Geogrid/ Location	LCR % Change
	HMA	Base			
Abu-Farsakh and Chen (2011)	51	305	1.0	TX160-M	-4.0
				TX170-M	-3.9
				TX170-1/3	7.8
Hanandeh et al. (2016)	76	457	1.1	TX150-D	2.9
Perkins (1999)	75	300	1.5	BX1100-2/3	19.0
Webster (1993)	50	350	3.0	BX1200-M	-11.6

The majority of the studies that used two or more geogrids of the same type but with different tensile stiffness values showed that performance increased with increasing stiffness. It is generally accepted that tensile stiffness is the most important mechanical property of geosynthetics for base reinforcement applications. Three studies involved a comparison of biaxial and triangular geogrids. Abu-Farsakh and Chen (2011) and Ghafoori and Sharbaf (2016) showed better performance with triangular versus biaxial geogrids of similar stiffness. Valero et al. (2014); however, showed the opposite. Hanandeh et al. (2016) showed better performance with a woven geotextile in comparison to a triangular geogrid. Five studies involved the use of a woven geotextile. In general, these studies appear to produce lower values of LCR in comparison to test sections with geogrids for similar pavement cross-section and subgrade conditions.

In summary, the additional test sections constructed since the year 2000 tend to support the conclusions made by Berg et al. (2000) and are summarized in Table 2-1. An exception to this is that some evidence suggests that stronger subgrades with thin pavement cross-sections may benefit from reinforcement. The upper limit for subgrade strength for typical highway applications after which reinforcement benefit is negligible still appears to be a CBR of 8. The majority of test sections show that reinforcement benefit becomes negligible after a structural number of 4 or a base thickness of 450 mm is reached. Studies involving examination of placement position of the geogrid within the base show this is an important variable; however, the limited data available makes it difficult to make general conclusions. The number of sections involving the use of geotextiles is limited and has produced varying levels of observed benefit. This conclusion supports the need for the research undertaken in this project to show benefit values for geotextiles commonly used by MDT for typical project pavement conditions.

2.3 Analytical Modeling

Perkins and Ismeik (1997b) provided a summary of studies having an analytical component. The majority of these studies used the finite element method as the analysis platform. Seven studies conducted during the period of 1989 to 1996 were identified and discussed. Since that time, 8 additional studies have been identified. These additional studies are briefly described below.

Kwon et al. (2005a, 2005b) developed a finite element-based model for geosynthetic reinforcement. Their approach employs anisotropic stress-dependent stiffness models for the granular base and subgrade and a membrane for the reinforcement. The reinforcement membrane element is characterized by in-plane isotropic elastic properties and by interface shear and normal elastic stiffnesses. The soil properties and tensile modulus of the geosynthetic properties are determined from laboratory tests, although the geosynthetic tensile modulus is determined from standard monotonic tension tests that do not account for the small-strain cyclic loads in reinforced pavements; the shear and normal stiffnesses at the soil-geosynthetic interfaces are assumed. The influence of residual horizontal confinement stresses is included in the stress-dependent soil stiffness models (Kwon et al., 2008). Some model validation was performed using a set of field results from the University of Illinois ATREL test facility (Kwon, 2007; Kwon et al., 2009). Validation consisted of comparisons of resilient pavement response under increasing wheel loads as predicted by the finite element model against measured responses from field instrumentation. The compaction-induced residual horizontal confining stresses were estimated from forensic DCP testing conducted after failure of the sections; the method for making these estimates was not detailed. Additional model calibration based on observed field responses included dividing the granular base and subgrade into sublayers to account for the effect of intermixing of base and subgrade on the soil properties and so that different distributions of residual horizontal stresses

could be applied within each sublayer. The comparisons of predicted to measured residual responses after making these calibrations were judged good. No comparisons between predicted and measured rutting response are reported.

The distinct element method (DEM) is an alternate modeling tool. Konietzky et al. (2004) and Kwon et al. (2008) used a DEM to model geogrid pullout tests and to simulate lateral confinement developed during compaction and traffic loading. Using a DEM model, a vertical consolidation pressure representing a compaction load was applied to a column of aggregate containing a geogrid layer. The horizontal stresses in the aggregate after the consolidation pressure was removed were found to be approximately twice as large as when no geogrid was present. The application of shear load between the geogrid and the aggregate also produced additional locked-in horizontal stresses. These types of DEM studies have provided some numerical confirmation of experimental results as well as insights into the mechanism of lateral restraint. These results have added qualitative support to the mechanistic-empirical design methods proposed by Perkins et al. (2004) (discussed in more detail below) that rely upon the mechanism of lateral restraint. However, additional fundamental research is needed to relate the confinement predicted from the simple geometry of the DEM to confinement that occurs in full-scale pavements. The complexity of DEM, particularly in the 3D formulation required for analyzing the geogrid problem and the long run times associated with the computations limit its near-term use to basic research and do not make it suitable for the development of mechanistic-empirical design methods.

Perkins (1999) demonstrated via carefully instrumented test sections the mechanism of lateral confinement accompanying base reinforcement. This mechanism provided a basis for a finite element based mechanistic-empirical (ME) model for geosynthetic reinforced pavements (Perkins, 2001). The ME model contains a response model consisting of a three-dimensional finite element model with elasto-plastic constitutive models for most of the pavement layers. The response model describes stress and strain response parameters for geosynthetic-reinforced flexible pavement systems where the geosynthetic is placed at the bottom of the unbound aggregate layer. The finite element model contains membrane elements and an anisotropic linear-elastic material model for the geosynthetic inclusion. Membrane elements carry stress in tension while having no bending stiffness.

Principal response parameters extracted from the finite element model include vertical strain in the top of the subgrade and bulk stress in the unbound base aggregate layer. These response parameters are used in empirical damage models for the prediction of long-term pavement performance and the definition of reinforcement benefit. Reinforcement benefit is defined in terms of an extension of service life of the pavement, a reduction in aggregate thickness for equivalent service life, or a

combination of the two. The damage models were calibrated from reinforced and unreinforced pavement test sections. The model was shown to provide general descriptions of reinforcement mechanisms that are consistent with those previously observed in instrumented pavement test sections.

The ME model was used in a parametric study to generate regression equations describing reinforcement benefit in terms of variables relating to pavement geometry, subgrade strength and geosynthetic properties. The resulting design model therefore consists of a series of regression equations used to predict reinforcement benefit for a given set of pavement design conditions. A Microsoft Excel spreadsheet program was developed to contain these regression equations and serves as a simple design tool for estimating TBR or BCR. This program was updated to a current version of Excel as part of this research project.

Perkins et al. (2004) developed a more sophisticated ME model that was designed to be compatible with the Level 1 MEPDG being developed at that time. Level 1 MEPDG models use finite-element based mechanistic structural response models with stress-dependent material models and material specific damage models for rutting and fatigue cracking. The Perkins et al. (2004) model demonstrates pavement performance improvements similar to those seen in laboratory and full-scale pavement test sections.

The Perkins et al. (2004) model contains methods that account for the development of lateral confinement during compaction and traffic loading. Perkins et al. (2005) demonstrated the necessity of these methods by evaluating a series of mechanistic-empirical models with and without these methods. The study showed that without these methods, very little performance improvement was predicted. Studies that do not incorporate special techniques for modeling lateral confinement implicitly, such as Kwon et al. (2009), have had to elevate values of base course resilient modulus by explicitly applying an arbitrary lateral confinement pressure to show an effect on resilient response. These studies have typically validated models by comparing predicted resilient response to measurements from test sections and have not incorporated damage models for rutting to allow for a comparison of rutting performance.

Saad et al. (2006) carried out a series of finite element simulations using a three-dimensional model where a tire load of 40 kN was applied over a rectangular area. The asphalt concrete was modeled with an isotropic linear elastic model, the base with a Drucker-Prager isotropic elastic-plastic model, the subgrade with the CAM-Clay model and the geosynthetic with an isotropic linear elastic model. Full bonding between the geosynthetic and the surrounding materials was assumed.

A parametric study was conducted with the model where the variables were 1) a base thickness of 152 and 305 mm, 2) a low and high modulus and friction angle base, 3) a weak and strong

subgrade, and 4) the geosynthetic located at the asphalt concrete – base interface, the lower third of the base and the base – subgrade interface.

The vertical deformation, the maximum tensile strain in the bottom of the asphalt concrete and the maximum compressive strain in the top of the subgrade were evaluated for each analysis. The largest reduction of tensile strain in the bottom of the asphalt concrete layer was observed when the geosynthetic was placed at the asphalt concrete – base interface and is nearly independent of the base thickness and subgrade strength. The largest reduction in surface deformation and compressive strain in the top of the subgrade was observed for a thin base and when the geosynthetic was placed in the lower third of the base layer. Accompanying experimental results were not available to validate the findings from the model.

Clapp (2007) developed a three-dimensional finite element model for relatively thick flexible pavement sections. The model was calibrated against test sections performed by Henry et al. (2009). Calibration involved comparing computed and measured strains in unreinforced pavement cross-sections. For reinforced sections, permanent deformation models for the base aggregate were modified to include the horizontal confining strains produced by the reinforcement during compaction and traffic loading. The model was used in a parametric study to examine the influence of HMA modulus, base aggregate modulus, subgrade modulus, HMA thickness and geogrid location. Findings from the study tended to support earlier studies that showed greater performance improvement with lower HMA thickness and lower subgrade modulus.

Abu-Farsakh and Nazzal (2009) and Nazzal et al. (2010) developed a mechanistic (finite element model) using plasticity material models for the base and subgrade layers, which showed promise for purely mechanistic-based modeling. The model describes the behavior of base materials under unsaturated field condition (due to matric suction). The model was used to perform an extensive finite element parametric study to evaluate and identify the effect of different geogrid properties and subgrade strength/stiffness on the long-term performance of geogrid-reinforced base pavement sections under traffic loading.

Moayedi et al. (2009) used a two-dimensional axisymmetric finite element model to examine the importance of location of the geosynthetic reinforcement within the base layer. The geosynthetic was placed at the HMA – base interface, at the base – subbase interface and at the subbase – subgrade interface. The results showed the vertical surface deformation was reduced from 1.16 mm for a model with no reinforcement to a value of 0.0019 mm for models with reinforcement. The models showed essentially no difference with reinforcement location. The paper provided insufficient detail to understand how the model showed such a dramatic reduction of vertical deformation with reinforcement. The paper did not provide any guidance on how the model

responses should be related to long-term performance. Accompanying experimental results were not available to validate the findings from the model.

Kim and Lee (2013) developed a three-dimensional finite element model to examine pavement response measures of reinforced pavements. The model used an isotropic linear elastic model for the asphalt concrete, isotropic nonlinear elastic models for the base and subgrade and an orthotropic linear elastic model for the reinforcement. A uniform pressure of 550 kPa was applied over a circular area with a radius of 152.4 mm. Sections with an asphalt thickness of 38 and 76 mm and with a base thickness of 152 and 304 mm were examined. Two sets of subgrade properties representing a weak and a strong subgrade were examined. The model showed that reinforcement reduced the vertical deformation of the pavement layers and reduced the vertical strain in the top of the subgrade. These effects were more significant for the case of the weaker subgrade as compared to the stronger subgrade and for thinner pavement sections as compared to thicker sections.

An NCHRP project (Luo et al., 2017) was recently completed that contains elements of material testing, large-scale pavement testing, analytical modeling and design development. Given the comprehensive nature of this study, it is described separately in Section 2.5.

Most of the finite element based analytical models discussed in this section tend to employ simplistic modeling components, particularly for the reinforcement. Many of these models have been used to show the mechanical response of reinforced pavements. Some have been compared to instrumented test sections to evaluate their suitability. Most models discussed above have not extended the mechanical model by either an additional mechanical component or an empirical component to provide a predictive model for long term pavement performance, where performance is described in terms of rutting and cracking. Most models, therefore, are not currently suitable for reinforced pavement design.

2.4 Design Methods

AASHTO (2013) provides a standard practice for geosynthetic reinforcement of the aggregate base course of flexible pavement structures. The standard practice evolved from recommendations given in the GMA WPII (Berg et al., 2000), is entirely empirical and relies upon the results of studies involving comparative test sections where reinforcement benefit, defined in terms of TBR or BCR, has been documented. The standard practice recommends that designers choose a study that has design conditions as close to the pavement being designed. These conditions include the thickness of the pavement cross-section, the strength and stiffness of the subgrade and the specific geosynthetic. An unreinforced pavement design is performed to establish the thickness of the section for the project conditions. The TBR or BCR identified as appropriate to the project

conditions is then used to modify either the design life of the pavement or to modify the thickness of the base course aggregate.

Three proprietary empirical design methods developed by manufacturers for specific geosynthetic products have been identified. These methods use improved structural base layer coefficients (LCR) within the context of the AASHTO '93 Pavement Design Guide (AASHTO, 1993). References for these methods are Tenax (2001), TenCate (2010) and Tensar (2014).

Tenax (2001) was developed based on the AASHTO '93 pavement design equation and uses a Layer Coefficient Ratio (LCR) to modify the structural contribution of the base when reinforcement is added. LCR has a value greater than or equal to one and is used in Equation 2 to modify the structural number (SN) for use in the AASHTO' 93 pavement design equation. Equation 2 can be used to calculate the required thickness of the asphalt layer (D_1) or the base layer (D_2).

$$SN = D_1 a_1 + D_2 a_2 m_2 LCR + D_3 a_3 m_3 \quad (2)$$

In Equation 2, a_1 , a_2 and a_3 are the layer coefficients for the asphalt concrete, base aggregate and subbase layers, respectively, D_3 is the subbase thickness, if present and m_2 and m_3 are the drainage coefficients for the base aggregate and subbase layers. All layer thickness are in units of inches.

LCR was determined from test sections for a particular multilayer polypropylene extruded biaxial geogrid. Test sections were constructed in a pavement test box where a cyclic load was applied to a stationary plate (Cancelli et al. 1996). In these test sections, a fine sand subgrade was used. A subgrade with a CBR ranging from 1 to 18 was produced for different test sections by placing the sand at different dry densities. Placement of loose sand to produce low values of subgrade CBR results primarily in volumetric compaction when subject to traffic loads, which is considerably different from an undrained shear distortion pattern of deformation typical of weak soft subgrades.

Results from this study produced a design chart for LCR (Figure 2-6), which was expressed as a function of subgrade CBR. The results indicated an LCR of over 1.4 for subgrade CBR values greater than 8.

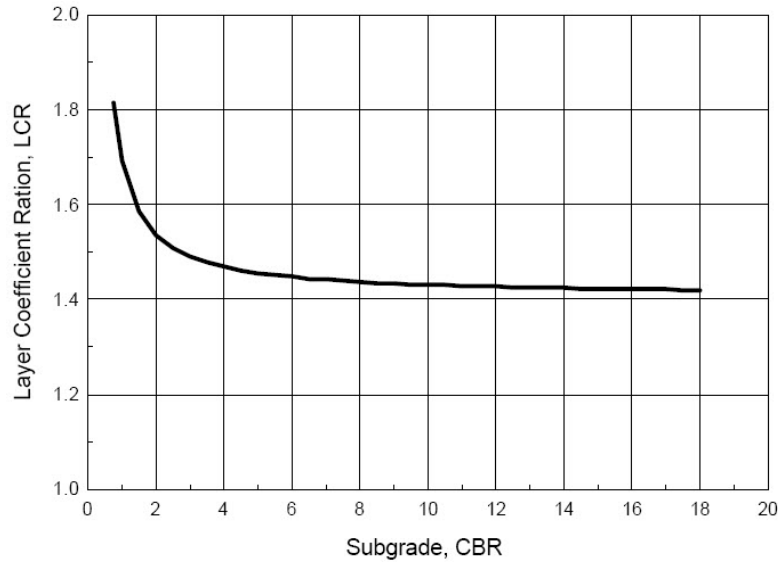


Figure 2-6: LCR versus subgrade CBR for Tenax MS220.

Subsequent test sections were constructed in an outdoor test track and subjected to truck traffic (Cancelli and Montanelli, 1999). A clay subgrade was used in the outdoor test track and placed at a CBR ranging from 1 to 8. Results from this study were analyzed by Berg et al. (2000) and for the subgrade at a CBR of 8 a TBR of 1.6 was obtained. This produces an LCR considerably below 1.4 and is in conflict with the data presented in the design curve.

TenCate (2010) was originally developed for reinforced pavements within the context of the 1972 AASHTO pavement design equation (Pearce, 1981). The approach is similar to that used in Tenax (2001) in that the AASHTO equation for structural number is modified by adding a term (M) to the structural contribution of the base course aggregate containing a geosynthetic (Equation 3). The design method was advanced for two woven polypropylene geotextiles. Values of M were given as a function of the CBR value of the subgrade and the design traffic for the roadway. Values of M ranged between 1.08 and 1.22. While reference was made to the use of theoretical behavior models for structural analysis (Thompson and Radd, 1979) and consideration for geosynthetics used for both separation benefits and confining effects, the basis for the M values used in the design method was not provided.

$$SN = D_1 a_1 + D_2 a_2 m_2 M \quad (3)$$

The method was recently updated and expressed within the context of the AASHTO '93 design equation for structural number. The parameter M was replaced by a Geosynthetic Structural Coefficient (GSC). Values of base course reduction (BCR) factors were provided for four

polypropylene woven geotextiles and two coated polyester woven biaxial geogrids as a function of the CBR of the subgrade. Values of BCR ranged from 3.7 to 60.9 % for CBR values ranging from 20 to 0.5 with varying BCR values for each geosynthetic within that CBR range. The basis for these values was not provided. It can be shown that a relationship between BCR and LCR, which is the same as between BCR and GSC is given by Equation 4. For the BCR values listed above, GSC values ranging from 1.04 to 2.56 are obtained. For the Mirafi geogrid BXG12, values of *GSC* from the *BCR* values provided by TenCate (2010) are shown in Figure 2-7.

$$GSC = LCR = \frac{1}{1-BCR} \quad (4)$$

The Tensar (2014) design method for reinforcement of paved roads was originally developed for extruded polypropylene biaxial geogrids (Tensar, 1996). That method relied upon the use of Traffic Benefit Ratio (TBR). Results from tests sections by Collin et al. (1996) were used to express TBR as a function of the thickness of the base course and the allowable rut for the roadway. Results from other studies (Haas et al., 1988, Barksdale et al., 1989 and Webster, 1993) were used as support for the TBR values used from Collin et al. (1996). Design curves were provided for two extruded polypropylene biaxial geogrids, namely BX1100 and BX1200. TBR values as a function of subgrade strength were not provided.

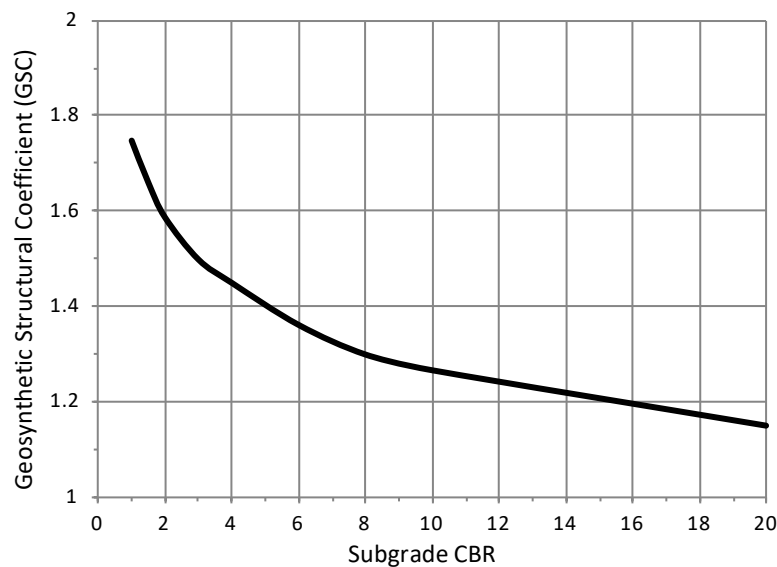


Figure 2-7: Geosynthetic Structural Coefficient (GSC) versus subgrade CBR for BXG12.

TBR was used to extend the performance period of the pavement by direct use of the definition of TBR or to reduce the base thickness for an equivalent performance period as the unreinforced pavement. The latter was accomplished within the context of the AASHTO '93 pavement design equations by solving for the structural benefit of the base giving a particular TBR and using this benefit to reduce the base thickness to yield the same traffic level as the unreinforced pavement.

This approach has been updated for use with a new extruded polypropylene triangularly configured geogrid. Tensar (2014) describes how the structural layer coefficient, as used in the AASHTO '93 pavement design equation, for an aggregate base is modified for the geogrid and how it is dependent on the thickness of the asphalt concrete layer and the subgrade strength. The improvement factors for a given set of pavement design conditions are calculated from regression equations supported by various experimental studies involving the evaluation of laboratory-scale and full-scale test sections. The improvement factors are calculated within a licensed program (Tensar, 2014). The design method can be used for pavements with an asphalt thickness as great as 250 mm; however, the method warns that empirical evidence for reinforcement benefit is available only up to asphalt thickness of 200 mm. The current software allows triangular geogrids TX5 and TX7, and biaxial geogrids Type 1 (BX1100) and Type 2 (BX1200) to be analyzed.

The improvement in the structural layer coefficient for various pavement design conditions was calibrated from several experimental studies; however, only one study was documented and referenced. Jersey and Tingle (2010) showed results for a geogrid for a pavement with 50 mm of asphalt concrete and 200 mm of aggregate base on a subgrade with a CBR of 3. Other supporting studies are reported to be documented in internal reports.

The Tensar licensed program was used to evaluate LCR values for an unreinforced pavement cross section consisting of 75 mm of asphalt concrete and 300 mm of aggregate base and for a subgrade having a CBR ranging from 0.5 to 20. The cross section was analyzed for the product TX5. The program was used to evaluate BCR by decreasing the reinforced base thickness until a number of traffic passes equivalent to the unreinforced section was obtained. Equation 4 was then used to calculate LCR, with the results shown in Figure 2-8. Values of LCR ranging from 1.76 to 1.04 were obtained.

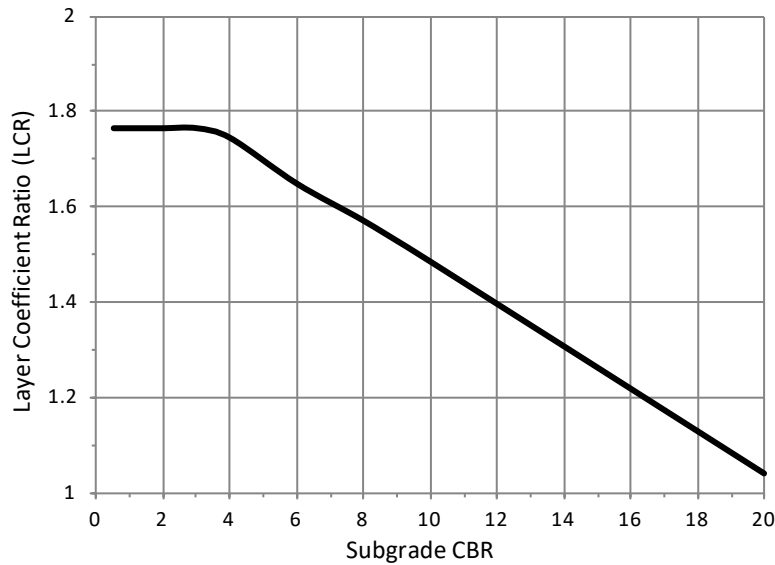


Figure 2-8: LCR versus subgrade CBR for TX5.

Tensar (2014) software was also used to evaluate LCR for test sections listed in Table 2-2 and Table 2-6. Test sections with TX5 (150), TX7 (170), BX1100 and BX1200 where the geogrid was placed at the bottom of the base were analyzed. In the software, the AASHTO '93 pavement design parameters were set equal to the following: Reliability = 80 %, Standard Deviation = 0.45, Initial Serviceability = 4.2, Terminal Serviceability = 2.5. Subgrade resilient modulus in units of psi was calculated from Equation 5. The subgrade stabilization module was not used.

$$M_R = 2555 \text{ CBR}^{0.65} \quad (5)$$

Table 2-10 lists the test sections that were analyzed and shows the experimental and Tensar (2014) software predictions of LCR. All test sections analyzed correspond to situations where a single layer of geogrid was placed at the bottom of the base. Figure 2-9 and Figure 2-10 plot test section and software LCR values for the TX and BX geogrids, respectively. These results show that the software overpredicts the reinforcement performance for the available test sections with TX 5 and TX7 geogrids. The software predictions for the BX geogrids are generally better; however, there is an overall tendency for overprediction of performance.

Table 2-10: Experimental and software predicted LCR values for BX and TX geogrids.

	Section Number	Layer thickness (mm)		Subgrade CBR	Geosynthetic	LCR ¹		
Author		AC	Base			E	S	
Abu-Farsakh and Chen (2011)	1	51	305	1.0	BX1100	1.13	2.79	
	2				BX1200	1.24	3.45	
	5				TX170	1.29	2.25	
Ghafoori (2016)	1	76	305	10.0	BX1100	1.11	1.19	
Hanandeh (2016)	1	76	457	1.1	TX150	1.05	1.57	
Henry et al. (2009)	1	150	300	5.2	BX1200	< 1	1.60	
	2	100	300			1.10	1.60	
Kwon (2007)	1	76	203	2.5	BX1100	1.12	2.98	
	2		305	3.5	BX1200	1.16	3.57	
	3					1.18	3.56	
	4		457		1.10	2.98		
Robinson (2018)	1	81	148	5.9	TX-150	1.70	2.29	
Valero et al. (2014)	4	51	203	3.0	TX5	1.15	2.33	
	5				TX7	1.15	2.55	
Al-Qadi et al. (1997)	2	90	100	7.0	BX1200	1.06	2.06	
Collin et al. (1996)	1	50	180	1.9	BX1100	1.13	1.71	
	2		300			1.22	1.25	
	3		180		BX1200	1.13	2.09	
	4		300			1.46	1.63	
Haas et al. (1988)	1	100	200	8.0	BX1100	1.22	1.49	
	2	75		3.5		1.20	1.54	
	3			1.0		1.10	1.56	
	4		300	0.5		1.00	1.25	
	5		200	3.5		2.00	1.55	
Kinney et al. (1998)	1	61	240	2.5	BX1200	1.12	1.90	
	2		355			1.22	1.52	
Perkins (1999)	2	75	300	1.5	BX1100	1.58	1.25	
	4				BX1200	1.82	1.63	
Perkins and Cortez (2005)	2	75	300	1.5	BX1100	1.46	1.25	
	3				BX1200	1.73	1.63	
Webster (1993)	1	50	350	3.0	BX1100	1.18	1.16	
	2		450	3.0	BX1200	1.04	1.34	
	4		300	3.0		1.21	1.63	
	5		350	3.0		1.29	1.55	
	6		250	8.0		1.37	1.76	
	7		150	8.0		1.69	2.05	
	8		250	8.0		1.67	1.76	

¹E: Test section experiment; S: Tensar (2014) software

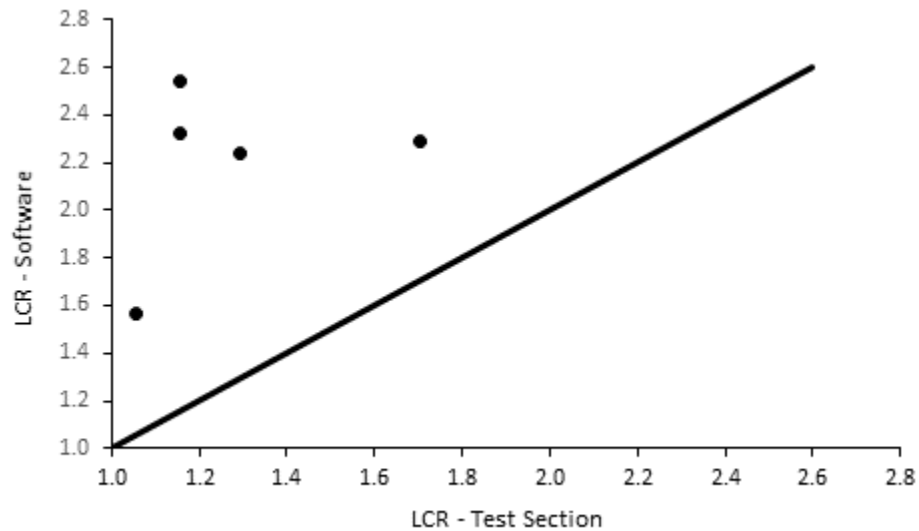
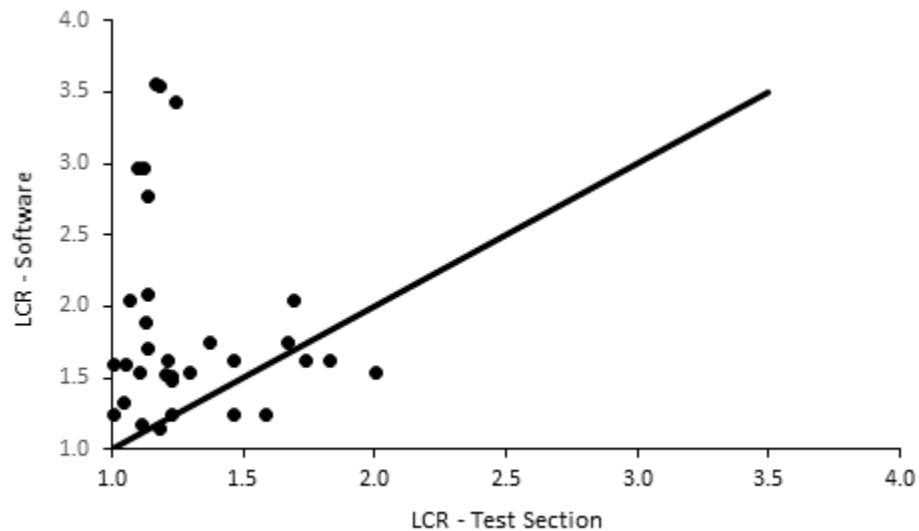


Figure 2-9: Test section and Tensar (2014) software LCR values for TX5 and TX7.



predictions. The review did not tabulate specific test section conditions and performance improvement measures and did not directly compare these performance improvement measures to corresponding predictions from the design software.

The three manufacturer's design methods reviewed predict an increase of benefit as the subgrade CBR decreases. The three methods predict different levels of benefit, which is partly due to each method being for a particular geosynthetic and partly due to each method being calibrated from different experimental studies. Tensar (2014) appears to limit the reinforcement benefit below a subgrade CBR of 3 whereas the other two methods show this benefit to continue to increase.

There are three principal limitations associated with these methods. The first involves the level of documentation associated with establishing the basis for the benefit values used in the methods. As discussed previously in this section, TenCate (2010) and Tensar (2014) do not provide adequate public documentation to allow the designer to judge the basis for the benefit values reported. Tenax (2001) provides sufficient documentation; however, the use of an unrealistic subgrade and the lack of consistency with field test sections raises some questions concerning the appropriateness of the benefit values reported.

A second limitation of Tenax (2001) and TenCate (2010) is the suggestion that a single benefit curve for a given geosynthetic product that is a function of the subgrade strength or modulus but is not dependent on other pavement configuration variables. As discussed previously, reinforcement benefit is known to depend on the thickness of the asphalt concrete, base aggregate and subbase, if present, the structural quality of these materials and the placement position of the geosynthetic within the base layer (Berg et al., 2000). Tensar (2014) accounts for layer thickness; however, the basis for this accounting could not be established.

The third limitation with these methods concerns the relatively high values of benefit predicted for subgrade strengths approaching and exceeding a CBR of 8. In general, most studies presented in this review show diminishing benefit for subgrade strength approaching a CBR of 8. At the time of the Berg et al. (2000) report, this led to a recommendation of a subgrade with a CBR of 8 being the typical limit for expected reinforcement benefit. Some recent data suggests certain limiting conditions where reinforcement benefit might be realized for pavements supported by subgrades with a CBR approaching or exceeding a value of 8.

A generic design model was developed by Perkins and Edens (2003) and is based on a project reported by Perkins (2001a,b). The design model has as its basis a mechanistic-empirical design program that was developed as part of the project. The mechanistic model consists of a three-dimensional (3-D) finite element model matching the nominal conditions for the pavement test facility described in Perkins (1999). This facility consisted of a 2 m by 2 m by 1.5 m deep

reinforced concrete box in which the roadway cross section was constructed and loaded by 40 kN applied cyclically at a period of 1.5 seconds to a 304 mm diameter steel plate resting on a waffled rubber pad in turn resting on the asphalt concrete surface. A 3-D model was used to account for the potential influence of the box's square corners and for the geosynthetic inclusion that has direction dependent material properties.

The mechanistic model used elasto-plastic constitutive models for the majority of the pavement layers. A bounding surface plasticity model was used to account for the positive effect of aggregate confinement on the increase in stiffness and strength of the base course aggregate. An orthotropic linear-elastic model was used for the geosynthetic. Anisotropy was included to account for differences in elastic modulus between machine and cross-machine directions and allowed for specification of the in-plane shear modulus and in-plane Poisson's ratio.

The principal response parameters extracted from the finite element model include vertical strain in the top of the subgrade and bulk stress in the unbound base aggregate layer. These response parameters were used in empirical damage models for the prediction of long-term pavement performance and the definition of reinforcement benefit. Reinforcement benefit is defined in terms of an extension of service life of the pavement, a reduction in aggregate thickness for equivalent service life, or a combination of the two. The damage models were calibrated from reinforced and unreinforced pavement test sections using several types of geosynthetics. The model was shown to provide general descriptions of reinforcement mechanisms that are consistent with those previously observed in instrumented pavement test sections.

The mechanistic-empirical model was used in a parametric study to generate regression equations describing reinforcement benefit in terms of variables relating to pavement geometry, subgrade strength and geosynthetic properties. These parameters included asphalt concrete and unbound aggregate thickness, quality of these materials, subgrade strength and geosynthetic elastic properties. A total of 465 pavement design cases were analyzed. The model therefore consists of a series of regression equations used to predict reinforcement benefit for a given set of pavement design conditions. These regression equations have been coded into an Excel Spreadsheet with a simple user interface.

The Perkins and Edens (2003) model requires the input properties shown in Table 2-11. The input values shown in this table are selected to provide predictions that could be compared to the manufacturer's methods discussed above. Quality of the asphalt concrete and base aggregate materials is defined in terms of layer coefficients defined in the AASHTO '93 method. The tensile stiffness of the geosynthetic is defined by a modulus at 2 % axial strain. Differences in modulus between the two principal directions of the geosynthetic are accounted for by the modulus ratio.

The parametric study performed to originally develop the model was conducted by including geosynthetics having different classes of interaction properties and in-plane mechanical behavior as defined by an in-plane Poisson's ratio and an in-plane shear modulus.

A range of pavement cross sections and subgrade strengths were used in the model, as noted in Table 2-11. The model produces a value of BCR, which is used in Equation 4 to determine LCR. For a pavement with a subgrade CBR of 2.0, the base course thickness was varied between 150 to 1000 mm to produce a range of values of structural number (SN). For each pavement cross section, the model was used to predict BCR, with corresponding LCR values shown against SN in Figure 2-11. The results show LCR to decrease with increasing base layer thickness and structural number. Reinforcement benefit becomes insignificant beyond a SN of approximately 5.

Table 2-11: Input parameters for Perkins and Edens (2003) model.

Property	Value
Asphalt concrete thickness, D_1 (mm)	75
Asphalt concrete layer coefficient, a_1	0.40
Base thickness, D_2 (mm)	Variable (150 – 1000)
Base layer coefficient, a_2	0.14
Base layer drainage coefficient, m_2	1.0
Subgrade CBR	Variable (0.5 – 8.0)
Geosynthetic modulus, GSM-2% (kN/m)	1140
Geosynthetic modulus ratio, GMR	0.995
Reduction factor for interface shear	1.0
Reduction for Poisson's ratio	Checked
Reduction for shear modulus	Unchecked

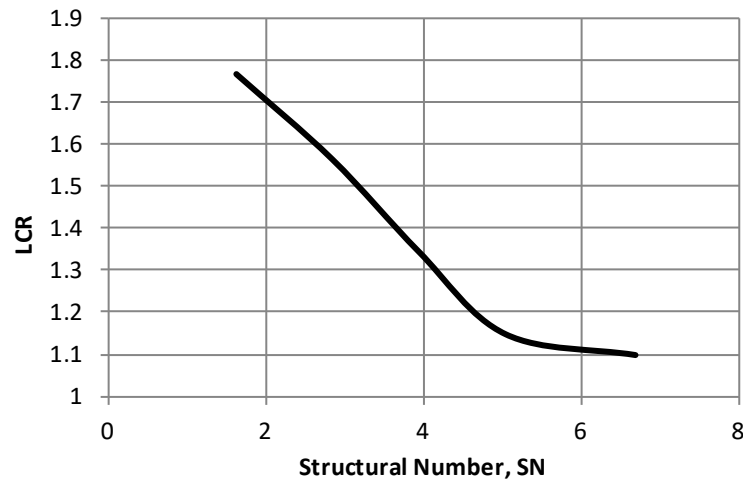


Figure 2-11: Effect of pavement structural number on LCR from Perkins and Edens (2003) model.

For a pavement with a base course thickness of 300 mm, the pavement subgrade CBR strength was varied between 0.5 and 8. The model was used to evaluate the BCR for each case with the resulting LCR shown against subgrade CBR in Figure 2-12. The results show that LCR decreases with increasing subgrade CBR. The results in Figure 2-11 and Figure 2-12 show the ability of this model to account for two key components known to influence the benefit derived from geosynthetic reinforcement and match general trends in experimental data seen in Figure 2-2 and Figure 2-3.

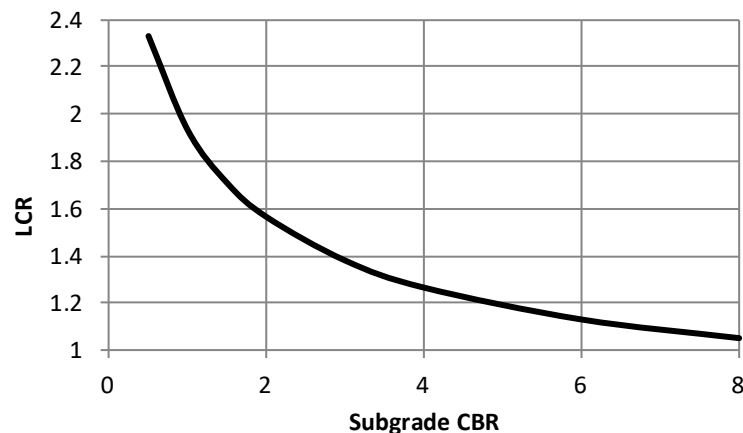


Figure 2-12: Effect of subgrade CBR on LCR from Perkins and Edens (2003) model.

The Perkins and Edens (2003) model was used to predict LCR for the test sections summarized in Table 2-2 and Table 2-6. Model predictions are made only for test sections where the geosynthetic was placed at the bottom of the base as the model was formulated only for that condition. Results from these predictions are tabulated in Table 2-12. LCR results from test sections and model predictions for all test sections listed in Table 2-12 are plotted in Figure 2-13. This figure shows appreciable scatter, as was evidenced in the comparison of test section LCR values to Tensar (2014) software predictions for TX and BX geogrids (Figure 2-9 and Figure 2-10). While showing appreciable scatter, the Perkins and Edens (2003) model is seen to be more representative of the available results and more conservative. Several studies contained conditions that created some questions about the results. Figure 2-14 shows results with values from Ghafoori and Sharbaf (2016), Robinson et al. (2018), Tang et al. (2008) and Webster (1993) removed. Questions concerning the first three studies were discussed previously. Results from Webster (1993) were removed because of the heavy load that was used in this study and how it may skew results to this condition, which is not representative of typical highway loading. Elimination of these results reduces the amount of scatter, particularly for those studies producing high values of LCR from test sections as compared to model predictions. Finally, Figure 2-15 shows results from studies since the year 2007 for which no questions concerning the studies existed. Model predictions for these studies is generally very good.

Table 2-12: Test section experimental and Perkins and Edens (2003) model predictions of LCR.

	Section	Layer thickness (mm)		Subgrade CBR	Geosynthetic / Location ¹	LCR ²	
Author	Number	AC	Base			E	M
Abu-Farsakh and Chen (2011)	1	51	305	1.0	BX1100 - B	1.13	1.40
	2				BX1200 - B	1.24	1.45
	3				TX160 - B	1.25	1.30
	4				TX160 - M	1.20	
	5				TX170 - B	1.29	1.36
	6				TX170 – M	1.24	
	7				TX170 – 1/3	1.39	
Aran (2006)	1	108	254	8.5	NR - B	1.31	
Ghafoori and Sharbaf (2016)	1	76	305	10.0	BX1100 - B	1.11	1.01
	2		406		BX1100 – M	1.18	1.01
	3		305		TX130 - B	1.20	1.00
	4		406		TX130 - M	1.40	1.00
Hanandeh et al. (2016)	1	76	457	1.1	TX150 - B	1.05	1.17
	2				TX150 - D	1.08	
	3				RS580i - B	1.12	1.25
	4		254			1.79	
Henry et al. (2009)	1	150	300	5.2	BX1200 - B	0.93	1.02
	2	100	300			1.05	1.05
	3	150	600			0.97	1.00
	4	100	600			1.06	1.02
Jersey et al. (2012)	1	43	203	3.0	TX 140 - B	1.53	1.04
Kwon (2007)	1	76	203	2.5	BX1100 - B	1.12	1.15
	2				BX1200 - B	1.16	1.18
	3		305	3.5		1.18	1.12
	4		457		BX1200 - M	1.10	1.11
Robinson et al. (2018)	1	81	148	5.9	TX-1 - B	1.70	1.00
	2	82	150		TX-2 - B	1.65	1.00
Saghebfar et al. (2016)	1	152	305	5.0	RS280i	1.05	1.00
	2				RS380i	1.11	1.00
Sharp (2005)	1	121	432	5.3	BX1100 - M	1.55	
Tang et al. (2008)	1	38	66	1.5	Grid B - B	1.25	1.38
	2				Grid C - B	1.84	1.50
	3				Grid D - B	1.30	1.35

Valero et al. (2014)	1	51	203	3.0	E'Grid 1616 - B	1.33	1.36
	2				E'Grid 2020 - B	1.42	1.38
	3				E'Grid 3030 - B	1.54	1.42
	4				TX5 - B	1.15	1.13
	5				TX7 - B	1.15	1.20
	6				RX1200 - B	1.43	1.34
Al-Qadi et al. (1997)	1	90	100	7.0	Amoco 2002 - B	1.08	1.00
	2				BX1200 - B	1.06	1.03
Collin et al. (1996)	1	50	180	1.9	BX1100 - B	1.13	1.25
	2		300			1.22	1.23
	3		180		BX1200 - B	1.13	1.29
	4		300			1.46	1.27
Haas et al. (1988)	1	100	200	8.0	BX1100 - B	1.22	1.01
	2	75		3.5		1.20	1.11
	3			1.0		1.10	1.35
	4			0.5		1.00	1.51
	5			200		3.5	2.00
Kinney et al. (1998)	1	61	240	2.5	BX1200 - B	1.12	1.20
	2		355			1.22	1.19
Perkins (1999)	1	75	300	1.5	Amoco 2006 - B	1.42	1.13
	2				BX1100 - B	1.58	1.24
	3				BX1100 - 2/3	1.88	
	4				BX1200 - B	1.82	1.29
Perkins and Cortez (2005)	1	75	300	1.5	Amoco 2006 - B	1.43	1.13
	2				BX1100 - B	1.46	1.24
	3				BX1200 - B	1.73	1.29
Webster (1993)	1	50	350	3.0	BX1100 - B	1.18	1.14
	2		450		BX1200 - B	1.04	1.16
	3		350		BX1200 - M	1.14	
	4		300		BX1200 - B	1.21	1.17
	5		350	1.29		1.17	
	6		250	1.37		1.03	
	7		150	1.69		1.02	
	8		250		1.67	1.04	

¹B-Bottom of base layer, M-Middle of base layer, 1/3- One third below top of base layer, 2/3- Two thirds below top of base layer

²E-Test section experiment; M-Model prediction

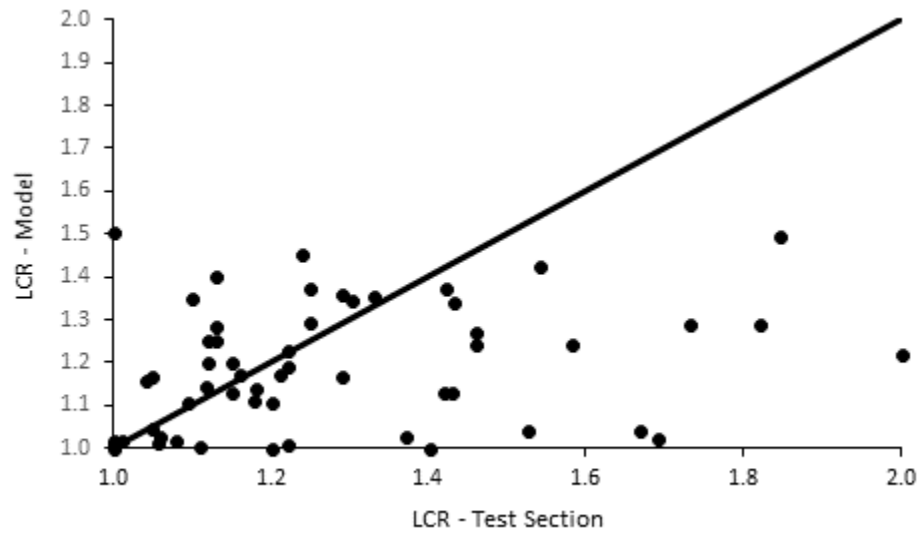


Figure 2-13: Test section experimental and Perkins and Edens (2003) model predictions of LCR, all 19 studies.

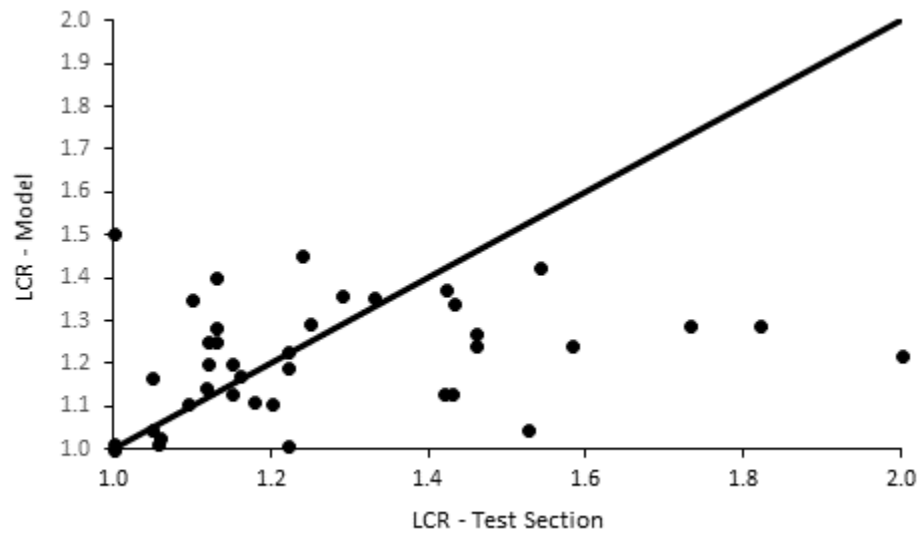


Figure 2-14: Test section experimental and Perkins and Edens (2003) model predictions of LCR, 15 of 19 studies.

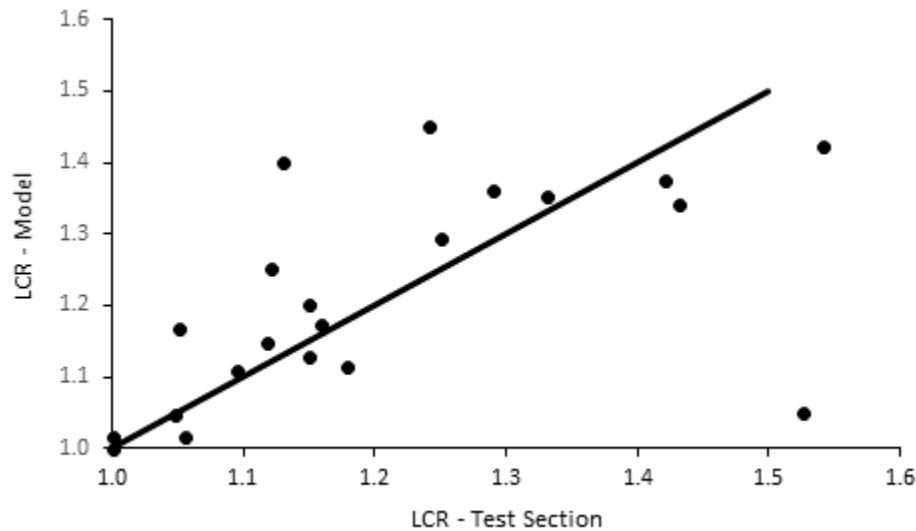


Figure 2-15: Test section experimental and Perkins and Edens (2003) model predictions of LCR, 7 studies from 2007 to present.

Perkins et al. (2004) developed a fully mechanistic-empirical model for reinforced pavements. The model uses features for the conventional pavement layers from NCHRP Project 1-37a (NCHRP, 2004), which was the project that resulted in the current AASHTO mechanistic-empirical pavement design guide. These features include material and damage models for the bound (asphalt concrete) and unbound (base and subgrade) layers and a finite element response model for the pavement cross-section. The model was developed to be compatible with models expected for use in the AASHTO mechanistic-empirical pavement design guide. The properties used in the material and damage models were determined by conducting corresponding laboratory tests on these materials from previously constructed test sections (Perkins, 1999, 2002).

The finite element response model was a two-dimensional axisymmetric model. A uniform pressure of 550 kPa was applied over a circular area having a radius of 152 mm on top of the asphalt surface for pavement load. The reinforcement sheet was modeled by the direct inclusion of structural 2-node membrane elements with contact surfaces between the membrane and surrounding solid elements.

Material and damage models for rutting for the traditional pavement layers were consistent with those used in NCHRP 1-37a. For the reinforcement, the finite element response model requires the use of a single isotropic elastic modulus. This property is determined from a method described by Perkins and Eiksund (2005) involving the elastic tensile modulus in the machine and cross-

machine directions (ASTM, 2010), in-plane Poisson's ratio from biaxial tests and an in-plane shear modulus from aperture stability modulus tests.

The upper and lower surfaces of the reinforcement were set up to be contact surfaces. Shear interaction along each contact surface was described in terms of a Coulomb friction model having pertinent material properties of coefficient of friction and an elastic slip parameter. The elastic slip parameter describes the interface shear stiffness or modulus, which was evaluated from cyclic pullout tests (ASTM 2009b).

Previous work (Perkins et al. 2005) showed that modeling the elastic response of a reinforced pavement simply using the components described above does not sufficiently account for the beneficial influence of the reinforcement on pavement response. It is commonly accepted that geosynthetic base reinforcement results from confinement and restraint of the aggregate adjacent to the reinforcement, which has recently been demonstrated experimentally (White et al. 2011). To account for this, response model modules were developed that simulate certain construction and traffic loading effects that the reinforcement has on the pavement system. The non-linear elastic material model used for the base aggregate and subgrade imposes certain limitations in rigorously modeling the effects of the reinforcement. This relatively simple constitutive model is insufficient for exactly describing the full sequential process of construction followed by the application of many repetitions of vehicular traffic. Since the material model for the base aggregate shows improved performance through an increased elastic modulus arising from an increase in mean stress, the response model modules have been developed to yield an increase in aggregate confinement during compaction and traffic loading.

The response model modules include a model describing effects during compaction and three response models used in succession and in an iterative manner to describe the effects of reinforcement during traffic loading.

Figure 2-16 provides a flow chart of these response models. The compaction model is used to describe the increase of aggregate confinement taking place as compaction causes aggregate to move laterally and be confined by interaction with the reinforcement.

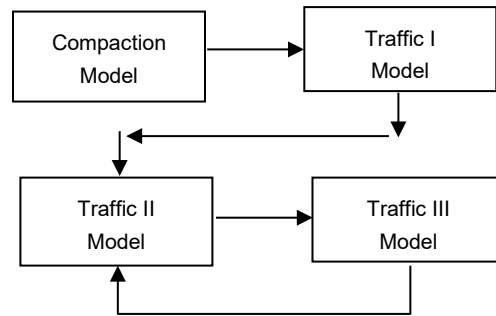


Figure 2-16: Flow chart of response model modules

Lateral confinement of the aggregate base layer also develops during vehicular loading of the roadway. Additional lateral confinement is due to the development of interface shear stresses between the aggregate and the reinforcement, which in turn transfers load to the reinforcement. As a cycle of traffic load is applied, there is both a transient or cyclic shear stress and a residual shear stress that exists when the traffic load is removed. The residual interface shear stress continues to grow as repeated traffic loads are applied, meaning that the lateral confinement of the aggregate base layer becomes greater with increasing traffic load repetitions. The Traffic I response model module is used to provide data for the transient interface shear stress distribution between the reinforcement and the surrounding materials. The Traffic II and III models are used repeatedly for successively increasing periods of life of the pavement to describe pavement response as reinforcement continues to contribute to an increase in confinement as traffic level increases.

The mechanistic-empirical design model by Perkins et al. (2004) involves relatively complex software and analysis methods. It is suitable as a design tool only if it was programmed into a pavement design software package with properly constructed user interfaces.

2.5 NCHRP 01-50

The objective of this research project (Luo et al., 2017) was to develop a methodology for quantifying the influence of geosynthetics on pavement performance for use in pavement design and analysis. The project was intended to have the methodology developed be consistent with a mechanistic-empirical pavement design framework to facilitate incorporation into the AASHTOWare Pavement ME Design software. The project focused on the use of geosynthetics in unbound base/subbase layers or as a base/subgrade interface layer for both flexible and rigid pavements. Components associated only with flexible pavements are discussed in this review.

The project was divided into six tasks: (a) full-scale laboratory testing of typical flexible pavement sections in an instrumented large-scale tank (LST); (b) laboratory triaxial testing of different base

courses with geosynthetics at different locations within the test samples; (c) finite element computations to match the results of the LST tests; (d) use of the same finite element program to develop full factorial sets of pavement data to construct an Artificial Neural Network (ANN) model of the critical strains and stresses in pavements; (e) generation of a new model of permanent deformation to predict pavement performance; and (f) comparison of the predicted performance of pavements with and without geosynthetics embedded in the unbound base courses.

The LST tests used two geosynthetics, a geogrid and a geotextile. The flexible pavement sections used 6 inches of HMA and 6 and 10 inches of base aggregate. The geosynthetic was placed at the bottom of the 6-inch sections and in the middle of the 10 inch sections. Loading of these sections involved dynamic and static loading. For dynamic loading tests, load levels of 9, 12 and 16 kips were applied at 80, 100 and 150 cycles, respectively. The sections were not loaded by sufficient load cycles to produce appreciable rutting on the pavement.

Test sections contained instrumentation to measure vertical and horizontal stress, strain on the geosynthetic, lateral deformation on and adjacent to the geosynthetic, tensile strain at the bottom of the HMA and vertical surface deformation. Results showed higher tensile strain at the bottom of the HMA layer for geogrid and geotextile reinforced sections with the geogrid section being the highest. Displacement on the geogrid and geotextile as compared to similar points in control sections showed the effectiveness of both geosynthetics in reducing lateral spreading. It was not clear what type of load had been placed when these observations were made.

Laboratory triaxial testing was performed on two different base courses with geosynthetics at different locations within the test samples. One base course was the base used in LST tests. Geogrid and geotextile samples were placed in 3 different locations within the sample. The effect of the geosynthetic on the anisotropic resilient modulus properties and permanent deformation was examined. Results showed that the geogrid increased the vertical resilient modulus by 10 to 20 % while the geotextile resulted in a 10 % reduction to a 10 % increase in modulus. The horizontal resilient modulus increased by 10 to 26 % for the geogrid and by 17 to 57 % for the geotextile. The study also concluded that the size sample used (6-inch diameter by 6 inch in height) produced different and more favorable results as compared to other studies where a 6 inch diameter by 12 inch in height samples were used. This implies that the test is dependent on specimen geometry and makes its application for determining basic engineering properties of a composite geosynthetic-aggregate material questionable.

Repeated load triaxial tests were also performed to examine permanent deformation properties of reinforced aggregate specimens. Tests were performed at different levels of confining stress and deviatoric stress. Permanent axial strain was reduced by as much as 36 % for larger values of

deviatoric stress when the reinforcement was placed in the middle of the specimen. Placement of the reinforcement in other locations in the sample resulted in less reduction of permanent strain.

Predictive equations for horizontal and vertical modulus and permanent vertical deformation of the base aggregate considering an increase in confinement due to the reinforcement were developed. The model assumes a zone of influence corresponding to 3 inches above and below the geosynthetic. A difference in radial strain between the aggregate and the geosynthetic is accounted for by an analytical factor. A restoring radial force on the aggregate due to shear interaction with the geosynthetic is used to determine an increase in lateral confinement. This restoring force is a function of the stiffness of the geosynthetic and its Poisson's ratio. The increase in confinement is then used to determine a modified vertical and horizontal modulus of the aggregate. Presumably, a pavement resting on a weaker subgrade experiences greater radial strain producing a greater restoring force and a more pronounced increase in modulus, but this was not explained in the report.

A permanent deformation damage model was developed to match the data collected from the repeated load triaxial tests. The model was calibrated for both unreinforced and reinforced specimens and when the reinforcement was placed in different positions. These models were presumably used in rutting models for the pavement cross-sections analyzed, although these details were not clear from the report. As described above, an influence zone of 3 inches above and below the geosynthetic was used to describe the effect of confinement on resilient modulus. It is not clear from the report whether the permanent deformation properties for a reinforced base were also used for material within the same zone of influence. The report also claims that this influence zone is negligible when the reinforcement is at the bottom of the base. Many test sections; however, have been constructed with the reinforcement at the bottom of the base and shown very favorable performance improvements. It is not clear how the results of this study are able to predict performance for this condition.

A two-dimensional axisymmetric finite element model was developed to match the stress, strain and displacement results seen from the LST tests. The model incorporated anisotropy, stress-dependency and plasticity zones. Triaxial test results were used to select anisotropy ratios and permanent deformation.

Material models were a viscoelastic model for the HMA, a cross-anisotropic stress-dependent nonlinear elastic model for the aggregate and an isotropic linear elastic model for the subgrade. Dynamic modulus tests on the HMA were used to express HMA modulus as a function of load frequency. Resilient modulus tests were used to determine parameters for the aggregate model. The elastic modulus of the subgrade was determined from correlations to CBR. Standard tests

ASTM 4595 and 6637 were used to provide tensile modulus for the geosynthetic while the pullout test (ASTM 6706) was used to provide interface properties.

For reinforced cross-sections, a membrane element with contact surfaces was used for the geosynthetic inclusion. Vertical and horizontal modulus in a zone surrounding the reinforcement were modified by the approach described above. Responses (surface deflection, vertical stress vs depth in aggregate and subgrade layer, and tensile strain bottom of HMA) from the finite element model were compared to the LST tests with good agreement generally shown. It was not clear from the report which load (static, dynamic and load magnitude) was used.

The finite element program described above was used to develop full factorial sets of pavement data to construct Artificial Neural Network (ANN) models for the critical strains and stresses in pavements. Outcome of the ANN models are critical response parameters that are then fed into the AASHTO ME-PDG to predict performance.

Variables in the ANN models included thickness of HMA and base aggregate, modulus of HMA, base and subgrade, anisotropic ratio of base, geosynthetic stiffness and geosynthetic location. Output responses included critical stress and strain measures. These measures were then used in the AASHTO ME-PDG design program to predict rutting, fatigue cracking and roughness. The permanent deformation model developed in this project was used for the base and subgrade layers.

Data from the Long Term Pavement Performance (LTPP) program and the Texas Pavement Management Information System (PMIS) for in-service pavement sections having geosynthetics in or at the bottom of unbound bases was used to compare to predictions from the overall approach described above. There were five sections in each of the two programs that were identified and analyzed. Rutting, fatigue cracking and roughness predictions were compared to the data from the sections in the two programs. Predictions were also made of identical sections without the geosynthetic; however, data from the field sections were not available for comparison. In general, the predictions of rutting, fatigue cracking and roughness compared well to the field sections and improvement, particularly with respect to rutting, was predicted for sections containing reinforcement. The project did not attempt to predict pavement performance for the test sections available from literature and as summarized in this report.

Implementation of the results of this project needs to be done within the context of the AASHTO MEPDG. It is not clear where this implementation work stands.

2.6 Summary and Relationship to this Project

This literature review revisited studies conducted prior to the year 2000 that were summarized by Perkins and Ismeik (1997a,b) and were the basis of the practice-oriented document by Berg et al.

(2000). Research involving the construction of test sections since the year 2000 were summarized and discussed. The results from all available test sections support previously established trends of decreasing pavement performance benefit from geosynthetic reinforcement as subgrade strength and stiffness increases and as the pavement section thickness increases. The upper limit for subgrade strength for typical highway applications after which reinforcement benefit is negligible appears to be a CBR of 8 and is consistent with earlier recommendations given in Berg et al. (2000). The majority of test sections show that reinforcement benefit becomes negligible after a structural number of 4 or a base thickness of 450 mm is reached. Studies involving examination of placement position of the geogrid within the base show this is an important variable; however, the limited data available makes it difficult to make general conclusions. The number of sections involving the use of geotextiles is limited and has produced varying levels of observed benefit.

Currently available design methods include the empirical AASHTO (2013) standard of practice, several proprietary methods from specific manufacturers and two methods developed by Perkins and Edens (2003) and Perkins et al. (2004). The AASHTO (2013) standard of practice requires identifying test sections having conditions close to the project conditions of interest and limits its application for a broad range of design conditions. A close examination of manufacturers methods and a comparison to available test section results indicates they tend to overestimate reinforcement benefit. The method of Perkins and Edens (2003) appears to produce reasonable values of benefit (TBR and BCR) when compared to all available test section results. The benefit values resulting from this method are most suitable for use in existing empirical design methods for flexible pavements, such as the AASHTO 1993 PDG.

The recently completed NCHRP project 01-50 (Luo et al., 2017) appears to be compatible with the AASHTO ME-PDG. A partial validation of this method was performed in the NCHRP project by comparing predictions from the method to LTPP test sections containing geosynthetics. Further validation of this method appears to be needed.

The work being performed in this project fills a gap existing in our knowledge of geosynthetics for base reinforcement. The use of geotextiles for reinforcement in pavement sections with a moderate cross-section and a moderate level of subgrade strength has not been adequately examined and will provide useful information to MDT for future projects.

3 Accelerated Pavement Test Facility

Testing took place within a test facility operated by TRI Environmental located in Greenville, SC. The test sections were constructed in a concrete-lined trench having the dimensions shown in Figure 3-1. The trench features a 15-foot long ramp at one end to provide access to equipment during construction. The opposite end of the trench is bound by a vertical wall; however, it was designed with a narrow extension that is 3 feet wide and 5 feet long to allow the loading wheel to travel past the end of the test sections during trafficking.



Figure 3-1: Accelerated test facility concrete lined trench.

Trafficking of the test sections was done using a full-scale accelerated pavement tester (APT) shown in Figure 3-2. Wheel loads were applied through a dual-wheel assembly equipped with 315/80 R 22.5 HSU2 tires rated for high load carrying capacity. The transverse width of the dual tire footprint was 22 in. The vertical force applied to the wheel carriage was approximately 9000 lb with the tires inflated to a tire pressure of 90 psi, where this tire pressure is typical of highway freight traffic. The test sections were trafficked bi-directionally along the centerline of the test section. A climate control system was built to control the temperature of the test area during trafficking and is displayed in Figure 3-2. This system consisted of two manifolds, positioned on either side of the traffic lane, to distribute cold or warm air over the surface of the area being

trafficked. Three air conditioner/heater units were attached to each manifold and were controlled by a thermostat. The temperature-controlled air blew across the exposed asphalt surface to cool or heat it depending on the temperature inside the lab.



Figure 3-2: Accelerated pavement test device.

4 Test Section Materials

4.1 Hot-Mix Asphalt

The hot-mix asphalt (HMA) layer for the test sections was constructed using a mixture from Greenville, SC. Prior to the selection of this material, tests were performed on HMA materials from Montana in order to compare a mixture from South Carolina. Samples of HMA were obtained from three separate Montana project sources that were considered representative of mixes in the state. The basic properties of the Montana mixes are listed in Table 4-1.

Table 4-1: Material properties of Hot-Mix samples obtained from Montana.

Property	Montana Project Sources		
	Ashland	Bridger Canyon	Great Falls
PG Grade	64-28	64-28	64-28
Asphalt content (%)	5.09	5.30	5.36
Rice specific gravity (G_{mm})	2.46	2.44	2.42
Bulk specific gravity (G_{mb})	2.36	2.39	2.35
Air void content (%)	3.99	2.46	3.00
VMA	13.7	13.8	13.8
VFA	71	82	79

Bulk materials from the three Montana mixes shown in Table 4-1 were sent to the National Center for Asphalt Technology (NCAT) for dynamic modulus testing. Bulk material was re-heated and compacted to a target air voids content of 7 +/- 0.5 %. Three samples for each mix were prepared and tested. Table 4-2 provides volumetric data for the specimens compacted at NCAT for dynamic modulus testing. Dynamic modulus testing uses 3 to 4 frequencies of loading and three test temperatures. The complex modulus (E^*) is determined for each combination of load frequency and temperature. Figure 4-1 shows values of E^* from these tests for the test temperature of 20°C. Full results from these tests are given in Appendix A.

At the beginning of the project, two mixes from the Greenville, SC area were identified as potential matches to Montana mixes and were tested accordingly. At the time the test sections were ready for the HMA layer to be placed, these two mixes were not available and was not scheduled to be produced for any upcoming projects. An alternative mix was selected and is described as a Surface C asphalt, according to the South Carolina DOT mix design. It was purchased from a hot-mix plant (Rogers Group – Greer, SC) near the TRI Environmental laboratory. Properties of the mix were determined by the QC lab at the hot-mix plant during the morning that the paving was done. These properties are summarized in Table 4-3 with full results provided in Appendix A. Hamburg wheel

tracking tests were not performed on this mix due to the unavailability of test equipment at MDT at this time. Hamburg wheel tracking tests were performed; however, on the two trial SC mixes mentioned above and readily passed MDT's standards.

Table 4-2: Material properties of Montana mixes for dynamic modulus tests.

Mix ID	Sample	Air Voids, %	P _b	G _{mm}	G _{mb}	VMA	VFA
Ashland	1	7.3	5.1	2.45	2.28	16.7	56.2
Ashland	2	7.4	5.1	2.45	2.27	16.8	55.8
Ashland	3	7.1	5.1	2.45	2.28	16.5	56.9
Bridger Canyon	1	7.2	5.3	2.44	2.26	17.7	59.4
Bridger Canyon	2	7.4	5.3	2.44	2.26	17.9	58.7
Bridger Canyon	3	7.5	5.3	2.44	2.26	18.0	58.4
Great Falls	1	6.7	5.4	2.42	2.26	17.1	60.8
Great Falls	2	6.5	5.4	2.42	2.26	16.9	61.5
Great Falls	3	7.4	5.4	2.42	2.24	17.7	58.2

Table 4-3: Material properties of Surface C HMA used for test sections.

Property	Surface C
PG Grade	64-22
Asphalt content (%)	5.55
Rice specific gravity (G _{mm})	2.45
Bulk specific gravity (G _{mb})	2.34
Air void content (%)	4.35
VMA	16.9

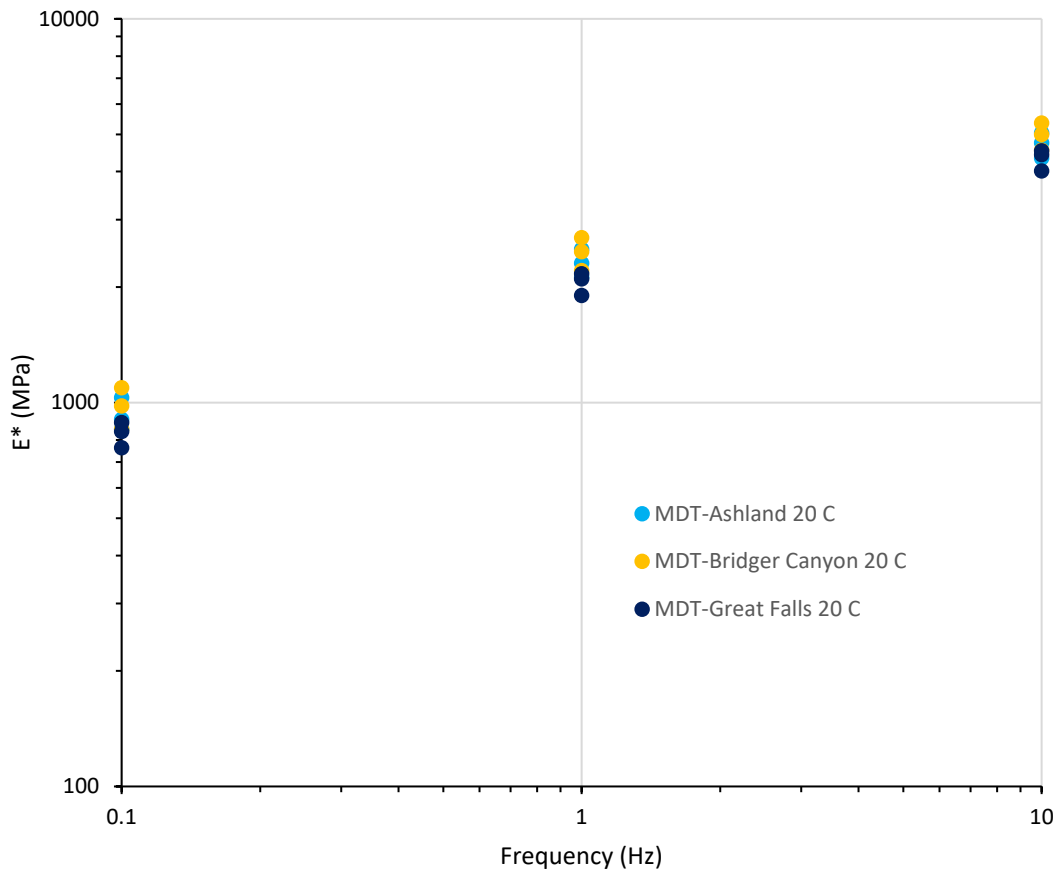


Figure 4-1: Dynamic complex modulus versus load frequency at a test temperature of 20°C for 3 MT mixes.

4.2 Base Course Aggregate

The crushed base course for this project was selected by MDT and meets their specifications for Type 7A aggregate. The material was obtained from the Brewer Pit near Forsyth, MT. It was classified as poorly-graded sand (SP) according to the USCS classification system and A-1-a according to the AASHTO soil classification system and has 47.6 % retained on the number 4 sieve. Other relevant properties of the base course are listed in Table 4-4. Data sheets from the tests performed are given in Appendix B.

Table 4-4: Material properties of crushed base course aggregate.

Property	Value
Specific gravity of fine mat'ls	2.65
Specific gravity of course mat'ls	2.63
Fractured face content (1+)	65%
% passing #200 sieve	4.6%
Maximum dry unit weight [‡]	136.7 lb/ft ³
Optimum moisture content [‡]	7.7%
CBR @ 95% Modified Proctor dry unit weight	100%
R-value at 2.07 MPa (300 psi) exudation pressure	72.5
L.A. Abrasion loss	18%
Micro-Deval loss	5.5%

[‡] determined using Modified Proctor method (ASTM D1557)

4.3 Subgrade

A subgrade soil was mutually selected by members of the MDT technical panel and the research staff at MSU and TRI. The material was obtained from a mine near the laboratory facilities in Greenville, SC. It was classified as lean clay (CL) according to the USCS classification system and A-6 according to the AASHTO soil classification system. Other relevant properties of the subgrade are listed in Table 4-5. Details of the Atterberg limits, particle size analysis, Proctor compaction analysis results and R-value test results for the subgrade are provided in Appendix C. A variety of laboratory tests and experiments were performed on the subgrade to characterize its strength properties. CBR, vane shear and moisture content were the primary measures in these experiments. Laboratory CBR tests (ASTM D1883) were performed on samples compacted using 25 blows per layer on samples prepared at moisture contents ranging from about 20 to 35%. The results of these tests are shown in Figure 4-2 and are labeled as Lab CBR. Field CBR tests were performed on subgrade specimens prepared in four wooden boxes measuring 4 feet square and 5.5 inches thick. These boxes were lined with plastic and subgrade was prepared at four different moisture contents (approximately 22, 25, 27 and 30%) and compacted into the boxes using a jumping-jack compactor (Figure 4-3). Field CBR, vane shear strength and moisture content were measured at 6 hours, 6 days and 41 days after compaction. Three in-field CBR tests, 18 vane shear tests and three moisture contents were taken at each time interval. The tests corresponding to the 6 hour interval are shown in in Figure 4-2 and are labeled as Box Field CBR. Field CBR tests were

also performed during the compaction of the subgrade in the test sections. These results are presented in Section 5.2 and are included in Figure 4-2 as MDT Test Section Field CBR. As described later in this report, the HMA and base course layers were reconstructed after initially loading the test sections. Additional measurements on the top of the subgrade were taken during reconstruction. The values included in Figure 4-2 are from the first construction. TRI has performed subsequent work in the facility after the MDT sections were completed. Field CBR tests performed during compaction of the subgrade in these subsequent test sections are included in Figure 4-2 as Additional Test Section Field CBR.

Table 4-5: Material properties of subgrade.

Property	Value
Liquid Limit	40%
Plastic Limit	25%
Plasticity Index	15%
% passing #200 sieve	75.5%
Maximum dry unit weight [†]	102.1 lb/ft ³
Optimum moisture content [†]	18.6%
Maximum dry unit weight [‡]	111.8 lb/ft ³
Optimum moisture content [‡]	17.0%
R-value at 2.07 MPa (300 psi) exudation pressure	23.5

[†] determined using Standard Proctor method (ASTM D698)

[‡] determined using Modified Proctor method (ASTM D1557)

Based on these results from these four series of tests, it is seen that the lab and field CBR tests yield comparable correlations to vane shear strength. These tests indicate that to achieve a target CBR of 2.5 %, the subgrade should be prepared to a moisture content of around 28 % and produce a vane shear strength around 98 kPa.

The tests performed on the subgrade prepared in the four wooden boxes was used to assess strength gain with time. Figure 4-4 shows the average in-field CBR measurement in each box at the three elapsed time intervals of 6 hours, 6 days and 41 days. The results from the three boxes with initial moisture contents of 25, 27 and 30 % are presented and show an increase of in-field CBR with elapsed time. The moisture content of the subgrade in these three boxes decreased by 0.6 to 0.9 % and is partly responsible for this strength gain. The relationship between moisture content and CBR in Figure 4-2 indicates the increase in CBR would be 0.7 to 1 % for a decrease in moisture

content of 0.6 and 0.9 %, respectively. This accounts for 50 to 100 % of the CBR strength gain seen in Figure 4-4. For those results showing a strength gain not fully accounted for by a decrease in moisture content, the additional gain is believed to be due to a thixotropic effect known to occur in clay soils.

Data from the wooden box tests was added to Figure 4-2 to assess the impact of elapsed time and thixotropy on the relationship between vane shear strength and CBR. Figure 4-5 shows that this relationship shifts to the right with elapsed time. Examination of the data shows that in-field CBR measurements increase at a faster rate with time as compared to vane shear strength measurements. These observations are used later in this report to assess the representative CBR of the subgrade at the time of trafficking.

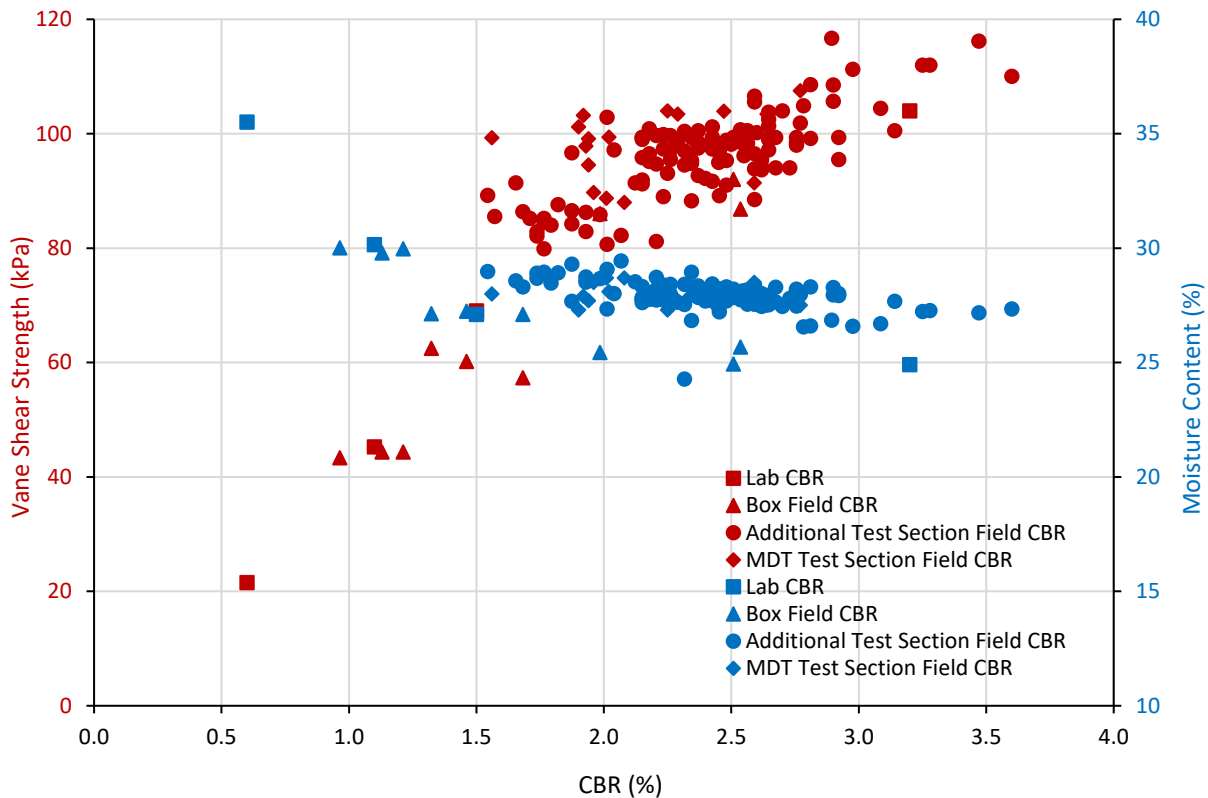


Figure 4-2: Laboratory and in-field CBR results for subgrade.



Figure 4-3: Compaction of subgrade into wooden boxes.

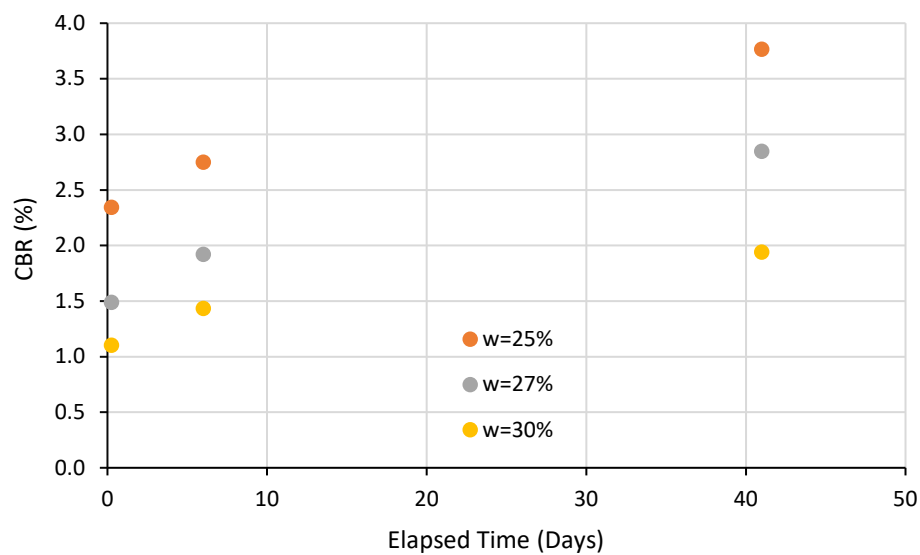


Figure 4-4: CBR versus elapsed time from wooden box tests.

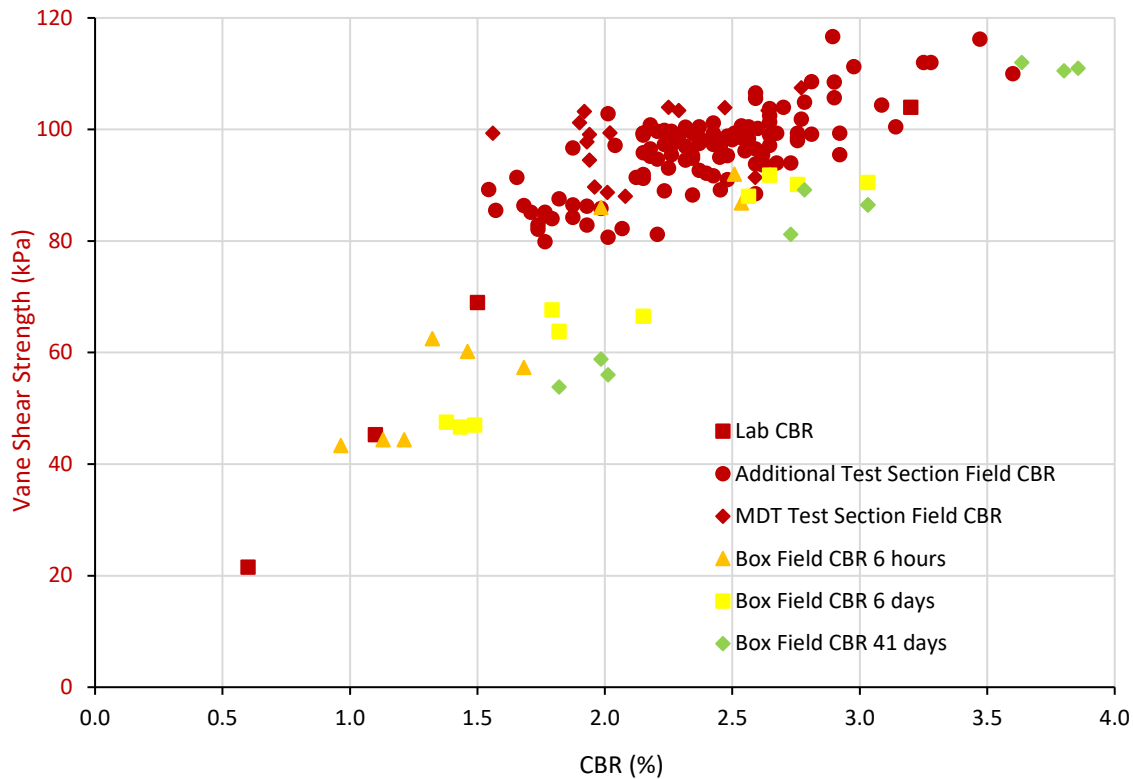


Figure 4-5: Vane shear strength versus CBR for all subgrade tests.

4.4 Geotextiles

A woven geotextile (TenCate RS280i) and a non-woven geotextile (Propex Geotex 801) were selected by MDT as the two geosynthetics for this testing. A roll of each material was obtained directly from the manufacturers of these products. Wide-width tensile tests (ASTM D4595) were run on both materials and grab tensile tests (ASTM D4632) were run on the non-woven geotextile. The results of these tests are summarized in Table 4-6 and the full laboratory reports for these tests are in Appendix D.

Table 4-6: Material properties of geotextiles.

Test	Property	RS280i	Geotex 801
Wide-Width Tension (ASTM D4595)	MD strength @ 2% strain (kN/m)	13.9	0.52
	XMD strength @ 2% strain (kN/m)	15.5	0.43
	MD strength @ 5% strain (kN/m)	31.0	1.25
	XMD strength @ 5% strain (kN/m)	32.0	1.00
	MD strength @ 10% strain (kN/m)	58.8	2.35
	XMD strength @ 10% strain (kN/m)	49.2	2.01
	MD Ultimate strength (kN/m)	65.8	14.8
	XMD Ultimate strength (kN/m)	50.5	18.1
Grab Tensile (ASTM D4632)	MD tensile strength (kN/m)	NA	0.97
	XMD tensile strength (kN/m)	NA	0.99

5 Test Section Construction

The test sections were constructed using the subgrade, base course, geosynthetics and asphalt materials described in the previous section. Instrumentation was installed in the subgrade and base course layers. Quality control testing and quality assurance of the layers constructed was carried out for all layers. An overview of the quality control plan, construction and instrumentation is documented below. The description of construction follows the order in which the materials were placed.

5.1 Quality Control Testing Plan

Several measurements were made on each layer during construction to provide quality control. Measurements were made using the methods and devices listed below.

- Elevation and thickness – surveys
- In-situ shear strength of the subgrade– hand-held vane shear
- In-situ moisture content – oven
- Dynamic stiffness – lightweight deflectometer (LWD)
- Strength – dynamic cone penetrometer (DCP) and in-field CBR
- Density – sand cone and nuclear densometer

Most of the QC measurements were concentrated in the center region of the test sections and within the anticipated wheel path. A list of the measurements made within each test section on the subgrade and base course are outlined in Table 5-1 and Table 5-2, respectively. Each of the three test sections were delineated into six 2-foot wide longitudinal segments (labeled A through F) to position the measurements made during construction. A plan view of the measurement locations within each test section and for each material type is provided in Appendix E. The only measurement made on the asphalt during construction was density using a nuclear densometer. Cores were taken of this layer during the forensic investigation following traffic loading. During construction, three density measurements were made on the asphalt in each of the sub-sections (A-F) for a total of 18 measurements per test section.

Table 5-1: Subgrade QC measurements in each test section during construction.

Measurement Type	Layer	Measurements per Layer	Measurement Locations
In-situ shear strength	All	24	A, B, C, D, E, F
Moisture content	All	12	A, B, C, D, E, F
Bearing strength (CBR)	All	2	Variable
Dynamic stiffness (LWD)	4, 5, 6	6	A, B, C, D, E, F
Strength (DCP)	Final	6	A, B, C, D, E, F
Unit weight (sand cone)	Final	4	B-C, D-E

Table 5-2: Base course QC measurements in each test section during construction.

Measurement Type	Layer	Measurements per Layer	Measurement Locations
Moisture content	All	3	B, C-D, E
Dynamic stiffness (LWD)	All	6	A, B, C, D, E, F
Strength (DCP)	Final	6	A, B, C, D, E, F
Unit weight (sand cone)	Final	2	B-C, D-E
Unit weight (nuclear densometer)	Final	2	B-C, D-E

Eighteen survey measurements were made in each test section after each layer was constructed. The vertical position of these measurements is provided in Appendix F. Elevations were taken by measuring down from a stiff steel member that spanned the concrete trench (Figure 5-1).



Figure 5-1: Survey measurement technique during construction.

5.2 Subgrade Construction

The clay subgrade was built in six layers each approximately 6 inches deep. The process began by mixing the subgrade using a skid-steer tractor and adding water to bring it to the target moisture content and shear strength associated with a bearing strength of 2.5% CBR. Periodic measures of moisture content and vane shear strength were taken during the mixing process to ensure uniformity. Once the subgrade had reached the target strength and moisture content, a skid-steer tractor was used to deposit, spread and track the prepared clay in the concrete-lined trench (Figure 5-2). Using this method, it took approximately three batches of clay to make one 6-inch layer across the entire the test area. The clay was kept covered with plastic to maintain its moisture content when not in use. Compaction of the subgrade was accomplished using a 54-inch smooth drum vibrating compactor (Hamm, Model H 5i), as shown in Figure 5-3. The sixth and final layer of the subgrade was leveled by hand to a tolerance of ± 0.20 inches (Figure 5-4). A small double smooth drum roller was used to smooth and finish the final top surface of the subgrade, which is shown in Figure 5-5.

As discussed in Section 5.5, the HMA and base course layer were reconstructed after an initial series of traffic passes. The subgrade was not reconstructed. A small amount of the top of the subgrade was removed during the second construction to expose material unaffected by the first

construction base course placement. As constructed properties of the subgrade given in the sections below are mainly from the first construction. Any values arising from the second construction are defined in the following sections.



Figure 5-2: Spread and tracked subgrade prior to compaction.



Figure 5-3: Compacting the subgrade.



Figure 5-4: Leveling the final surface of the subgrade.



Figure 5-5: Finished surface of the subgrade.

5.2.1 Vane shear strength

Average vane shear strengths for each compacted layer of subgrade are summarized in Table 5-3 for each test section. Averages for individual layers are based on 24 measurements per test section. The values listed for layer 6 were taken immediately before the placement of base for the second construction. The higher values are due to thixotropic effects due to the elapsed time since the material was originally placed and a decrease in moisture content. The composite average is calculated using the layer average values and weighting the layer value by an influence value determined from a stress distribution solution from the theory of elasticity. This process gives greater weight to the upper layers of the subgrade. Due to the proximity of the concrete wall associated with the end of the trench, measurements nearest the wall (first four vane shear strength measurements within sub-section A) within Test Section 1 were not used.

Table 5-3: Average vane shear strengths for the compacted subgrade.

Layer [†]	Average Vane Shear Strength (kPa)		
	Test Section 1	Test Section 2	Test Section 3
Composite	117.2	112.1	113.9
6	147.1	138.4	141.8
5	97.8	91.4	94.5
4	103.9	99.4	99.2
3	103.4	107.5	104.0
2	103.4	99.5	103.2
1	88.7	89.7	88.0

[†] Layer 1 is at the bottom of the subgrade and Layer 6 is at the top.

5.2.2 Moisture content

Average moisture content results for each compacted layer of subgrade are summarized in Table 5-4 for each test section. Averages for individual layers are based on 12 measurements per test section. The values listed for layer 6 were taken immediately before the placement of base for the second construction. The composite average is calculated using the layer average values and weighting the layer value by an influence value determined from a stress distribution solution from the theory of elasticity. This process gives greater weight to the upper layers of the subgrade. Due to the proximity of the concrete wall associated with the end of the trench, measurements nearest the wall (first two measurements within sub-section A) within Test Section 1 were not used in the average.

Table 5-4: Average moisture content for the compacted subgrade.

Layer [†]	Average Moisture Content (%)		
	Test Section 1	Test Section 2	Test Section 3
Composite	27.3	27.3	27.3
6	25.9	25.9	25.8
5	28.6	28.5	28.6
4	27.6	28.1	27.9
3	27.5	27.5	27.3
2	27.7	27.8	27.9
1	28.7	28.5	28.7

[†] Layer 1 is at the bottom of the subgrade and Layer 6 is at the top.

5.2.3 CBR strength

In-field CBR tests were conducted in substantial accordance with ASTM D4429 using the minimum recommended surcharge of 30 lb. Two tests were conducted on each subgrade layer within each test section. The exact locations of these tests varied from layer to layer but were generally concentrated toward the center of each test section. The average CBR strengths are reported in Table 5-5. All values in this table are from tests performed during the first construction. The composite average is calculated using the layer average values and weighting the layer value by an influence value determined from a stress distribution solution from the theory of elasticity. This process gives greater weight to the upper layers of the subgrade.

Table 5-5: Average CBR strength for the compacted subgrade.

Layer [†]	Average CBR (%)		
	Test Section 1	Test Section 2	Test Section 3
Composite	2.11	2.22	1.90
6	1.90	1.94	1.56
5	1.93	2.59	1.94
4	2.47	2.02	2.34
3	2.64	2.77	2.25
2	2.29	2.33	1.92
1	2.01	1.96	2.08

[†] Layer 1 is at the bottom of the subgrade and Layer 6 is at the top.

5.2.4 Dynamic stiffness

A Zorn ZFG 3000 Light Weight Deflectometer (LWD) was used to measure the dynamic stiffness of the last three layers of subgrade. Six LWD measurements were made in each test section. The LWD has a 1 foot diameter plate, 22 pound drop weight and calculates stiffness by measuring the acceleration as the drop weight impacts the load plate resting on top of the soil. The average results of the LWD tests are summarized in Table 5-6. The values listed for layer 6 were taken immediately before the placement of base for the second construction. The composite average is calculated using the layer average values and weighting the layer value by an influence value determined from a stress distribution solution from the theory of elasticity. This process gives greater weight to the upper layers of the subgrade. The measurements from Test Section 1, sub-sections A and B were not used in the results due to the proximity of the concrete end wall.

Table 5-6: Average dynamic stiffness of the compacted subgrade.

Layer [†]	Average Dynamic Stiffness (MN/mm ²)		
	Test Section 1	Test Section 2	Test Section 3
Composite	6.14	5.42	5.57
6	6.73	5.74	6.09
5	5.05	4.56	4.64
4	6.36	5.95	5.71

[†] Layer 4 is near the center of the subgrade layer and Layer 6 is at the top.

5.2.5 Strength (DCP)

A Kessler Dual Mass Dynamic Cone Penetrometer (DCP) with magnetic ruler and a 10.1 pound hammer was used to evaluate the strength of the subgrade after it had been fully constructed. Six tests were conducted in each test section, the results of which are shown in Figure 5-6 in terms of CBR. The tests were performed immediately before the placement of base for the second construction. Comparison of these results to those from the first construction shows a modest gain in strength namely in the depth range of 3 to 12 inches. On the average, the strength increase was 5 to 8 % greater from the first to second construction.

The bearing strength of the subgrade was calculated as a function of depth using Equation 6 developed by Kleyn (1975). As before, the measurements from Test Section 1, sub-section A were not used in the results. Average strengths based on the DCP tests were as follows: Test Section 1 CBR = 2.27%, Test Section 2 CBR = 2.27% and Test Section 3 CBR = 2.24%.

$$CBR = \frac{292}{(mm/blow)^{1.12}} \quad (6)$$

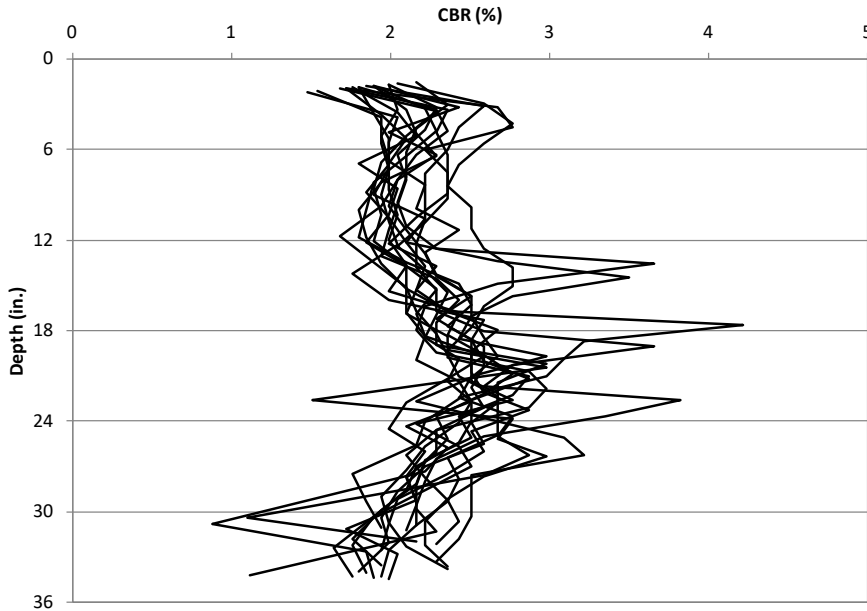


Figure 5-6: Subgrade DCP results as a function of depth.

5.2.6 Unit weight

In-place dry unit weight of the final layer of subgrade was measured using the sand cone method (ASTM D1556). Four measurements were made within each test section. The average dry unit weights for each test section were as follows: Test Section 1 = 96.3 lb/ft³, Test Section 2 = 93.4 lb/ft³ and Test Section 3 = 92.3 lb/ft³. These measurements were made immediately prior to placement of base aggregate for the second construction.

5.3 Instrumentation

Linear variable differential transducers (LVDTs) were installed to measure the displacement of subgrade and base course surfaces during trafficking. Three sensors were installed in the subgrade and three sensors were installed in the base course, as shown in the illustrations in Appendix G for each test section. The position of these measurements was designed to capture vertical movements caused by the load wheels during trafficking.

The first step during the installation process was to excavate a hole in the vicinity of the measurement point to allow each sensor to be inserted into the ground. The size of the access holes was kept as small as possible to minimize disturbance of the soil in the anticipated wheel path. All the soil that was extracted from each hole was temporarily stored in a sealed bucket so that it could be replaced once the sensor was in place. The datum for each displacement measurement was the bottom of the concrete trench, as illustrated in Figure 5-7. This was accomplished by driving a

steel rod through the subgrade until it reached the trench floor (see Figure 5-8). A small piece of $\frac{3}{4}$ in. thick plastic was placed on the floor prior to constructing the subgrade in the area where each of the metal anchors was to be located. A small nail was welded to the bottom of the steel rod so that when driven it would penetrate the plastic and keep the anchor from floating upward during construction and trafficking.

The bodies of the LVDTs were attached to the anchors using two u-bolts that extended through a metal plate welded to the top of the anchor. Each LVDT was outfitted with a sealed mechanism that extended the core of the LVDT to a round plate that would be positioned at the point of measurement (top of subgrade or base course layers). This extension mechanism was designed to keep the soil from jamming the LVDT as it allowed free movement of the LVDT core throughout the duration of the test. A photo of a typical LVDT setup is shown in Figure 5-9 prior to installation. The body of the LVDT was positioned on the anchor plate so that the vertical alignment of the plate at the end of the LVDT was level with the surface of the subgrade or base course, as shown in Figure 5-10.

Sealed data cables extended from the bottoms of the LVDTs and through protective tubes outside of the trench. These wires were attached to the data acquisition system through individual signal conditioners.

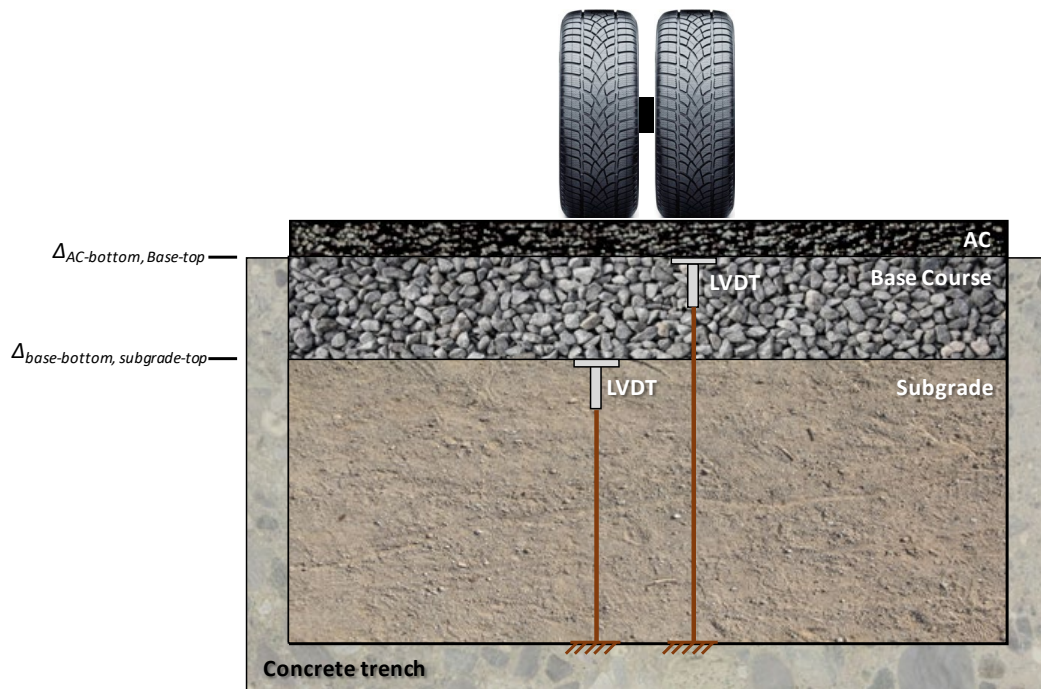


Figure 5-7: Cross-section of LVDT installation in the subgrade and base course.



Figure 5-8: Installing LVDT anchor.



Figure 5-9: LVDT sensor prior to installation.



Figure 5-10: Position of the measurement point with respect to the subgrade surface.

5.4 Geosynthetics

TenCate RS280i and Propex Geotex 801 were the two geotextile products used in this testing program. A roll of each material was obtained from the manufacturers. Pieces of each material were cut to 11 ft. wide to match the width of the concrete trench. Each test section was 12 ft. long. Test Section 1 was the Control (no geosynthetic), Test Section 2 was reinforced with TenCate RS280i and Test Section 3 was reinforced with Propex Geotex 801. A cross-sectional illustration of the test section layout is shown in Figure 5-11. The geotextile materials between Test Sections 2 and 3 overlapped one another by 1 ft. (6 in. within each test section). The geotextiles were pulled taut to remove any wrinkles – no stakes or pins were used to hold the materials in place. A photo of the installed geosynthetics is shown in Figure 5-12.

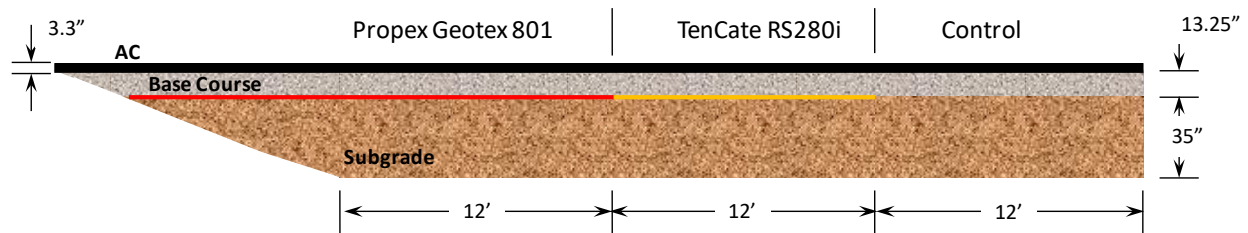


Figure 5-11: Cross-sectional view of constructed test sections.



Figure 5-12: Installed geosynthetics.

5.5 Base Course Aggregate

The base aggregate was shipped from Montana in 3000 lb. super sacks and stored on site until construction of the base course. Preparation of the base aggregate began by unloading three to four bags onto the lab floor, mixing with a skid-steer tractor and adding water until it reached the target moisture content. The aggregate was deposited on the test area without driving on it and spread across the test sections by hand. The test sections were originally constructed by preparing the base course to a moisture content ranging from 6.4 to 8.2 %. HMA was also placed on this first construction and traffic loading occurred thereafter. The test sections were seen to rut more rapidly than expected. The reason for this observation was believed to be due to too high of a moisture content of the base leading to lower stiffness values. Trafficking was stopped and the HMA layer and the base course layer were removed and reconstructed. The base course layer in the second construction was placed at a lower moisture content to correct the problem discovered in the first construction. The material contained in the body of this report pertains to the second construction. Additional details of the first construction are provided in Appendix H where this data is examined to provide lessons learned concerning base course layer preparation in the field.

The base course for the second construction was constructed in three layers, each of which was screeded to a uniform depth prior to compaction (Figure 5-13). Compaction was accomplished using a 48-inch double drum smooth vibrating compactor to create a smooth, flat surface on the final lift (Figure 5-14). Each of the layers was tested and then allowed to air dry prior to compacting the subsequent layer. The final average thickness of the base course layer was 13.29 ± 0.20 inches.



Figure 5-13: Gravel screeded to uniform depth.



Figure 5-14: Final compacted surface of the base course.

5.5.1 Moisture Content

Optimum moisture content of the base course aggregate was 7.7% based on the Modified Proctor results. The base aggregate was prepared to a moisture content of 1 to 2 percent below optimum to yield better compaction. Average moisture contents taken immediately after compaction for each of the test sections and layers are summarized in Table 5-7.

Table 5-7: Average moisture content of the compacted base course.

Layer [†]	Average Moisture Content (%)		
	Test Section 1	Test Section 2	Test Section 3
3	5.9	5.8	6.4
2	6.4	6.3	7.0
1	6.6	6.4	6.5

[†] Layer 1 is the bottom base layer and Layer 3 is the top layer.

5.5.2 Dynamic Stiffness

Six measures of dynamic stiffness were made within each test section within the anticipated rut path using the Zorn ZFG 3000 Light Weight Deflectometer (LWD). The measurements in sub-section 1A were not used in the average calculations because of the proximity of the end wall. Average dynamic stiffnesses for each layer within each test section are summarized in Table 5-8

Table 5-8: Average dynamic stiffness of the compacted base course.

Layer [†]	Average Dynamic Stiffness (MN/mm ²)		
	Test Section 1	Test Section 2	Test Section 3
3	123.63	115.54	122.42
2	24.25	19.63	23.77
1	19.40	15.98	17.85

[†] Layer 1 is the bottom base layer and Layer 3 is the top layer.

5.5.3 Strength (DCP)

Six DCP measurements were taken within each test section using the dual mass DCP device (drop hammer weight of 17.6 lb.) on the finished surface of the base course. These measurements were taken outside of the wheel path to keep from damaging the geosynthetics in the wheel track area. The results from these tests are shown in the plot in Figure 5-15. The bearing strength (in terms of CBR) as a function of depth was calculated using Equation 6 developed by Kleyn (1975). The measurements from Test Section 1, sub-section A were not used in the results. Average CBR strengths were calculated using values between about 2 and 10 inches of depth to avoid areas near the top and bottom of the compacted layer. The average strengths were as follows: Test Section 1 CBR = 72.4%, Test Section 2 CBR = 73.9% and Test Section 3 CBR = 73.8%.

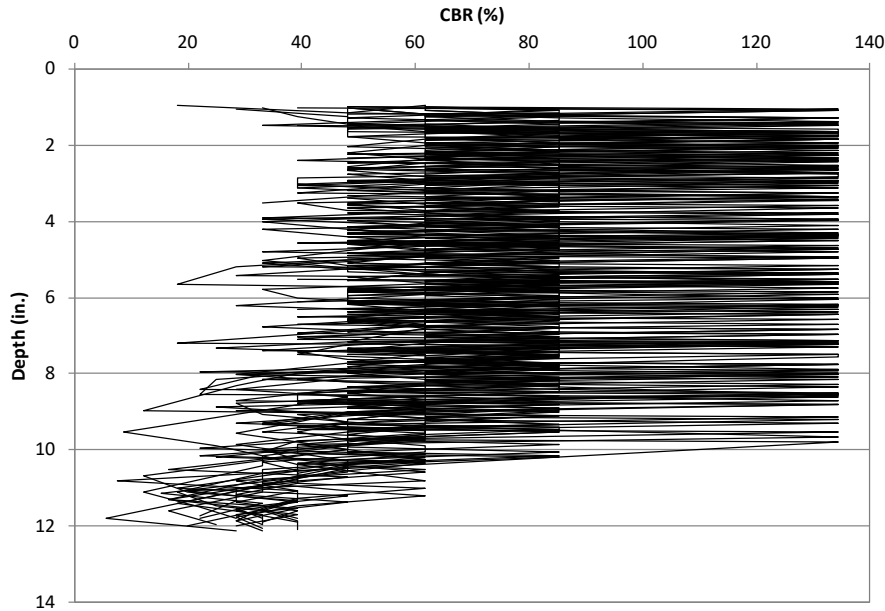


Figure 5-15: Base Course DCP results as a function of depth.

5.5.4 Unit Weight

In-place dry unit weight of each layer of compacted base course was measured using the sand cone method (four measurements per test section). A nuclear density gauge was also used to measure the unit weight of the final layer (eight measurements per test section). Nuclear density measurements were made at a probe depth of 8 inches. The average dry unit weights for each test section are summarized in Table 5-9. The full report for the nuclear density tests is provided in Appendix B.

Table 5-9: Average dry unit weights of the compacted base course.

Layer [†]	Average Dry Unit Weight (lb/ft ³) and Percent Compaction Based on Modified Proctor		
	Test Section 1	Test Section 2	Test Section 3
3 (nuclear)	137.5 (100.6%)	136.9 (100.1%)	137.7 (100.7%)
3 (sand cone)	137.7 (100.7%)	138.7 (101.5%)	137.5 (100.6%)
2	137.7 (100.7%)	137.9 (100.9%)	136.5 (99.9%)
1	136.0 (99.5%)	135.5 (99.1%)	137.4 (100.5%)

[†] Layer 1 is the bottom base layer and Layer 3 is the top layer.

5.6 Asphalt

Surface C asphalt, according to the South Carolina DOT mix design, was purchased from a hot-mix plant (Rogers Group – Greer, SC) near the TRI Environmental laboratory. Properties of the mix were determined by the QC lab at the hot-mix plant during the morning that the test track was paved. These properties are summarized in Appendix A. The asphalt was placed in a single lift that had an average thickness of 3.37 ± 0.13 in. It was placed using a full-size paving machine (Figure 5-16) and compacted using a tandem roller (Figure 5-17) and pneumatic roller (Figure 5-18).



Figure 5-16: Placement of hot-mix asphalt.



Figure 5-17: Compaction of hot-mix asphalt using smooth drum roller.



Figure 5-18: Compaction of hot-mix asphalt pneumatic roller.

Density measurements were made during construction using a nuclear density gauge to ensure adequate compaction. After compaction was complete, 36 measurements of density were made in each test section to fully evaluate the density of the asphalt mat (two measurements were made at each position shown in the illustration in Appendix E). The average density within each test section and the percent compaction compared to the maximum density of 152.9 lb/ft³ are shown in Table 5-10. Individual nuclear density test results are provided in Appendix A. Cores were taken from each test section after trafficking was completed and used to determine density and to conduct dynamic modulus tests. Density values from cores were greater than those listed in Table 5-10. The results of these tests are discussed in section 7.1 and are used in section 8 to examine the influence of material variability on test section performance. Results of dynamic modulus tests show little difference in modulus between the three test sections.

Table 5-10: Average density of the compacted asphalt layer from nuclear density tests.

Nuclear Density	Average Density and Percent Compaction		
	Test Section 1	Test Section 2	Test Section 3
Density (lb/ft ³)	137.8	139.4	140.8
Percent Compaction (%)	90.1	91.2	92.1

6 Test Section Trafficking and Data Collection

Performance of the three test sections was evaluated by trafficking the test sections using the full-scale accelerated pavement tester described in Section 3 and measuring surface rut progression over time. A total of 903,438 traffic passes were applied to the pavement over a period of 107 days.

The climate control system described in Section 3 was able to depress or increase the temperature of the test sections by about 5 °F from the ambient temperature of the building. Figure 6-1 shows a record of the pavement test section surface temperature versus wheel passes for the duration of loading. The data gaps seen in Figure 6-1 are due to periods when the data logger malfunctioned and data was not collected. An overall average temperature during testing was 73 °F.

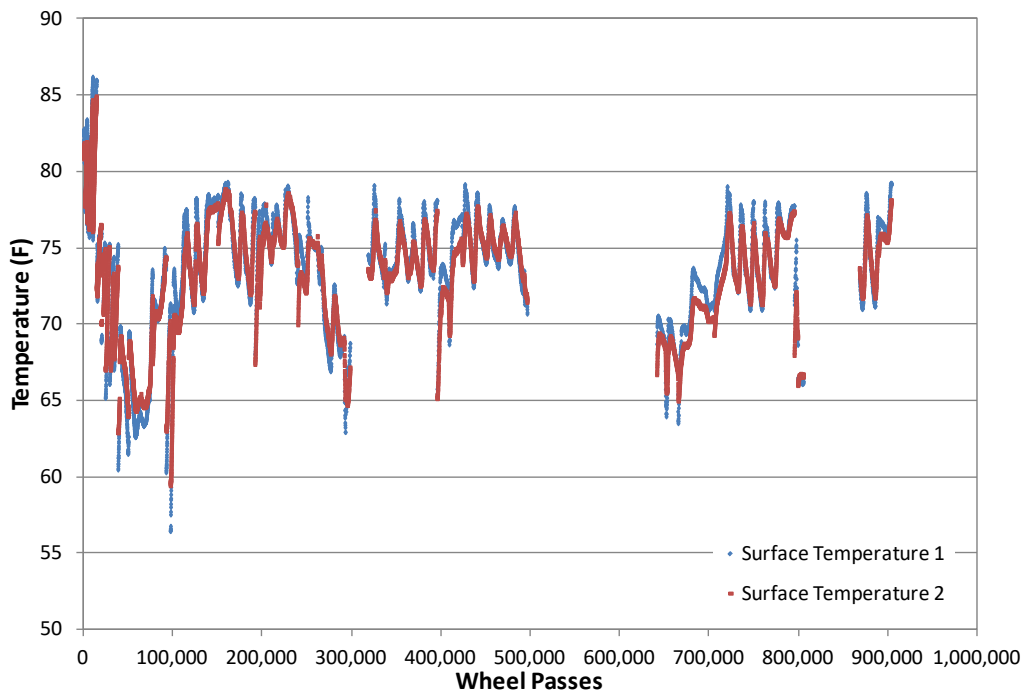


Figure 6-1: Test section surface temperature versus time.

6.1 Surface Rut Measurement Results

Longitudinal rut measurements were made at 6-inch intervals within the two wheel paths made by the dual wheel assembly, for a total of 22 measurements within each test section. Measurements were concentrated on the center 5-foot portion of the test section to avoid potential influence from the end wall and transitions between adjacent test sections. Two rut profiles were also taken perpendicular to traffic in each test section by making vertical measurements every 3 inches across

the entire width of the pavement (4 feet on either side of the centerline). The position of these measurements in each test section is illustrated in Figure 6-2. Longitudinal and transverse measurements were made in all three test sections at the following 19 traffic counts: 0, 500, 1500, 3500, 6000, 10,000, 20,000, 30,000, 40,000, 76,934, 124,998, 200,444, 249,998, 297,890, 399,316, 495,992, 599,992, 804,954 and 903,438.

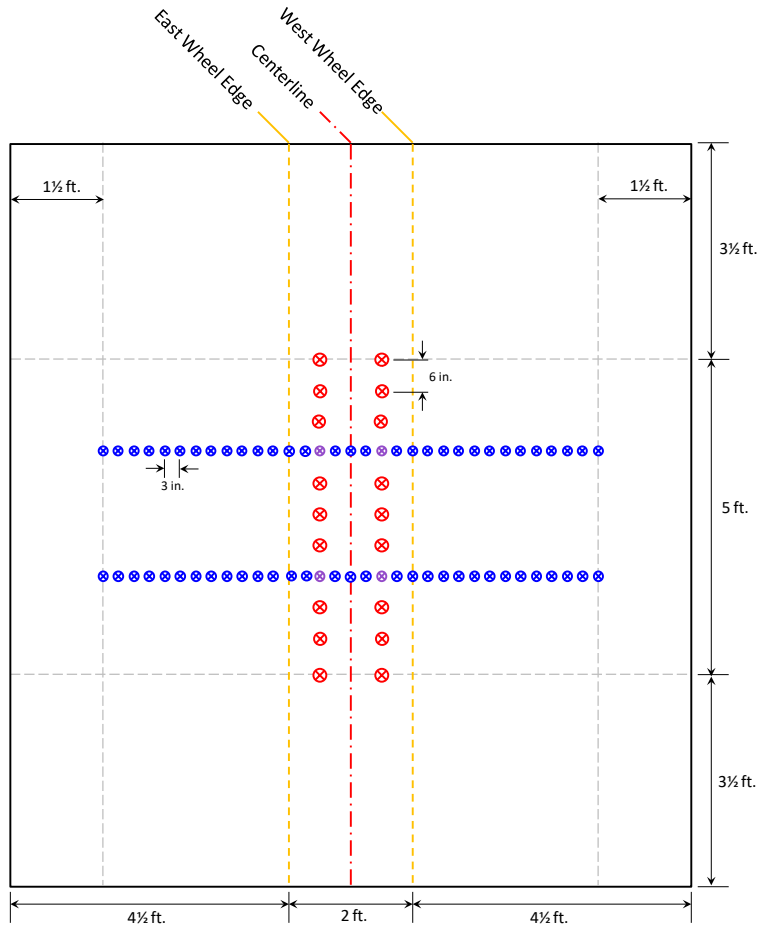


Figure 6-2: Rut measurement locations within each test section.

The 22 rut measurements made in the longitudinal direction were averaged together to create a single value for each test section at each level of traffic. These values were plotted with respect to traffic level, as shown in Figure 6-3. Measurements made in the transverse direction can be presented as a rut profile for each location within each test section as a function of increasing traffic, as shown in the example in Figure 6-4 for the Control test section. The remaining transverse plots as a function of increasing wheel passes are shown in Appendix I. Alternatively, rut profiles can also be presented for all the test sections at a particular traffic count, as presented in Figure 6-5 for 903,438 wheel passes. Plots for all traffic levels are presented in Appendix J.

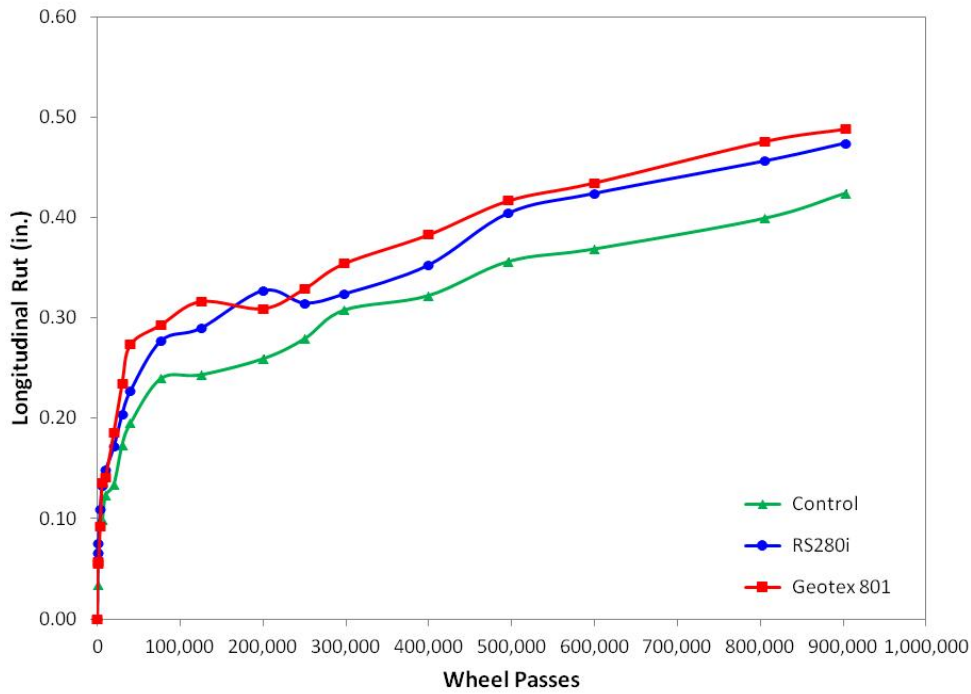


Figure 6-3: Longitudinal rut responses for all test sections.

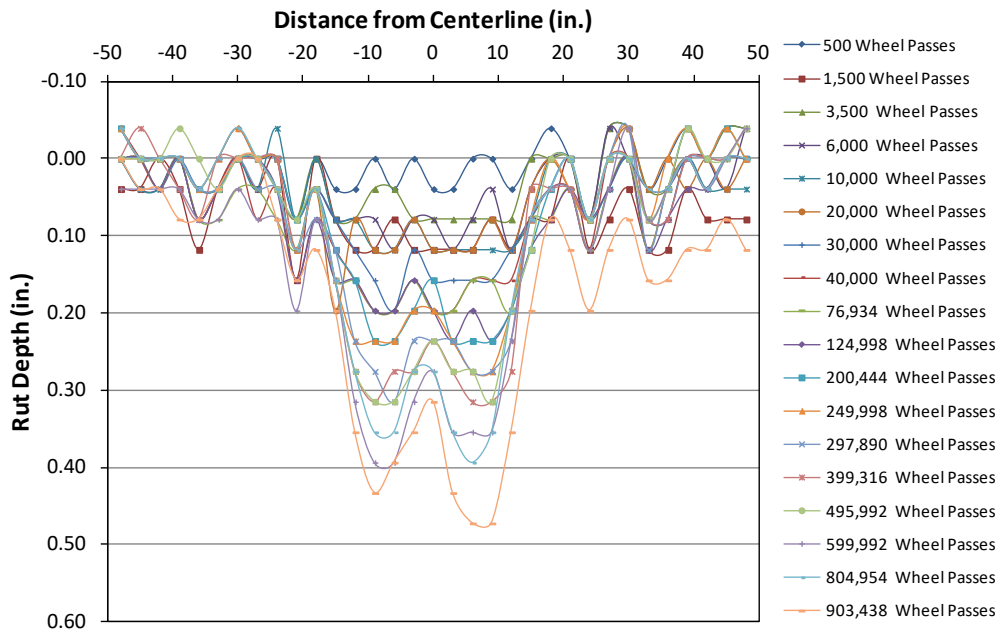


Figure 6-4: Transverse rut profile progression in the Control test section, south measurement line.

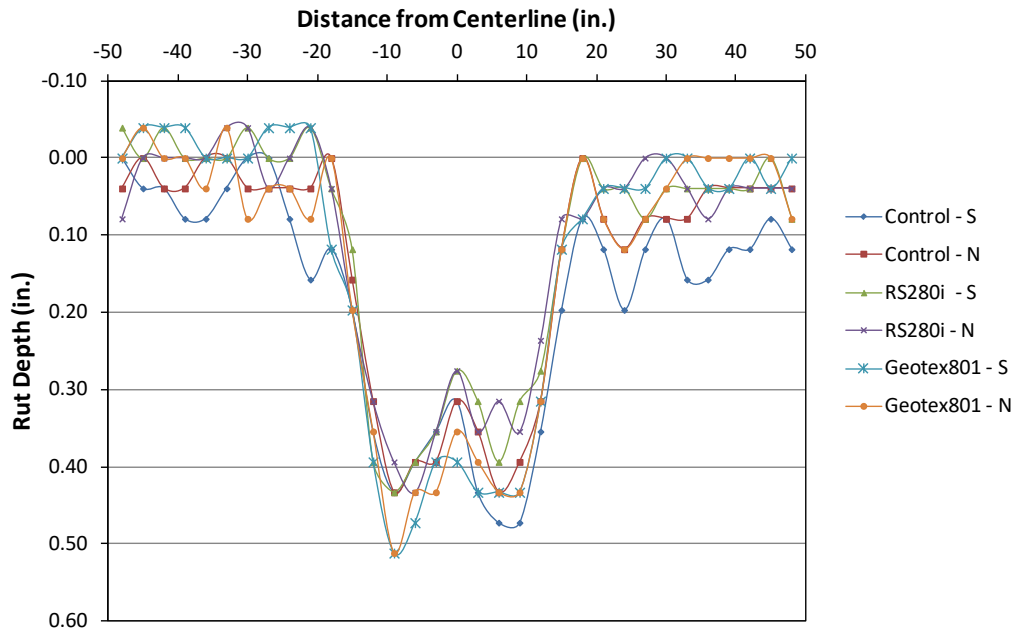


Figure 6-5: Transverse rut profiles of all test sections and measurement lines at 903,438 wheel passes.

6.2 Base Course and Subgrade Deflection Measurement Results

Linear variable differential transducers (LVDTs) were installed to measure the displacement of subgrade and base course surfaces during trafficking. Three sensors were installed in the subgrade and three sensors were installed in the base course within each test section. The position of these measurements was designed to capture vertical movements caused by the load wheels during trafficking. Displacement responses from these measurements are shown below in Figure 6-6 through Figure 6-11. The average of these responses within each test section are shown in Figure 6-12 through Figure 6-14.

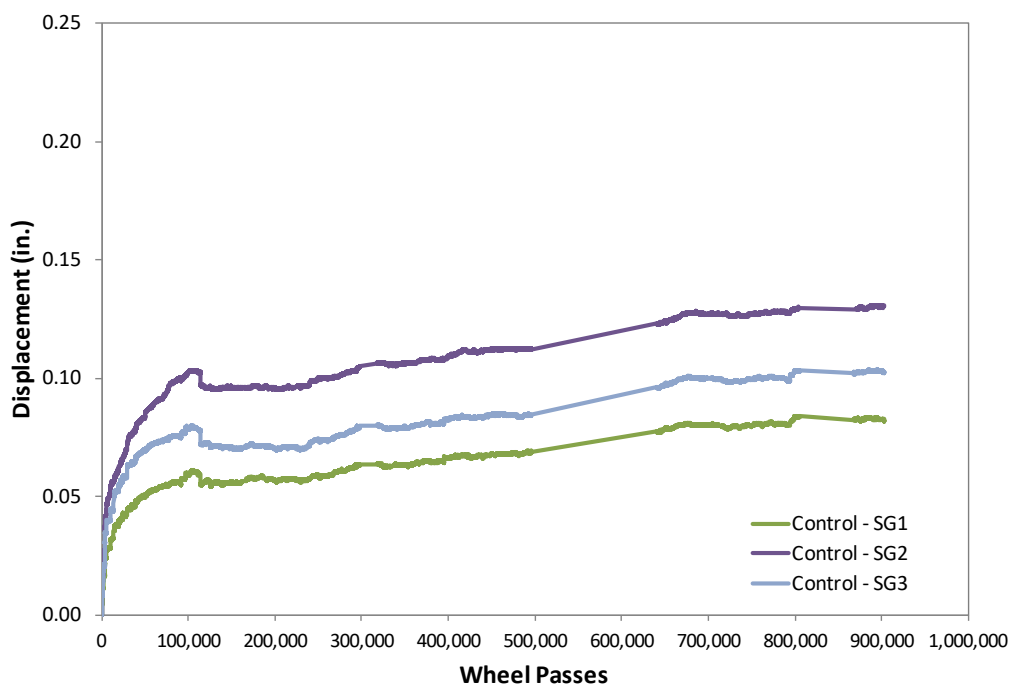


Figure 6-6: Displacement response of Control subgrade sensors.

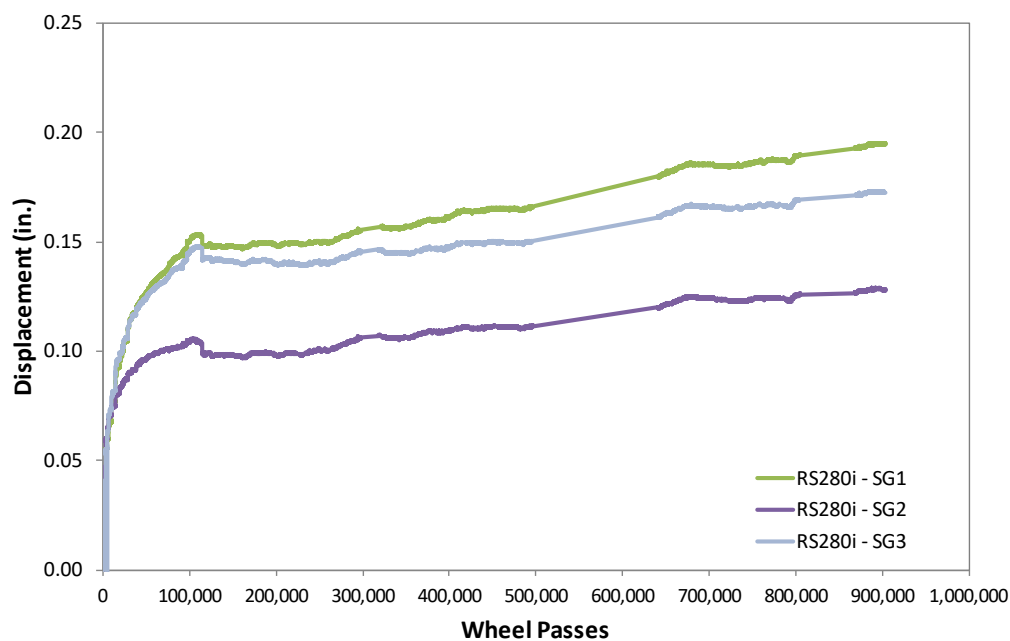


Figure 6-7: Displacement response of RS280i subgrade sensors.

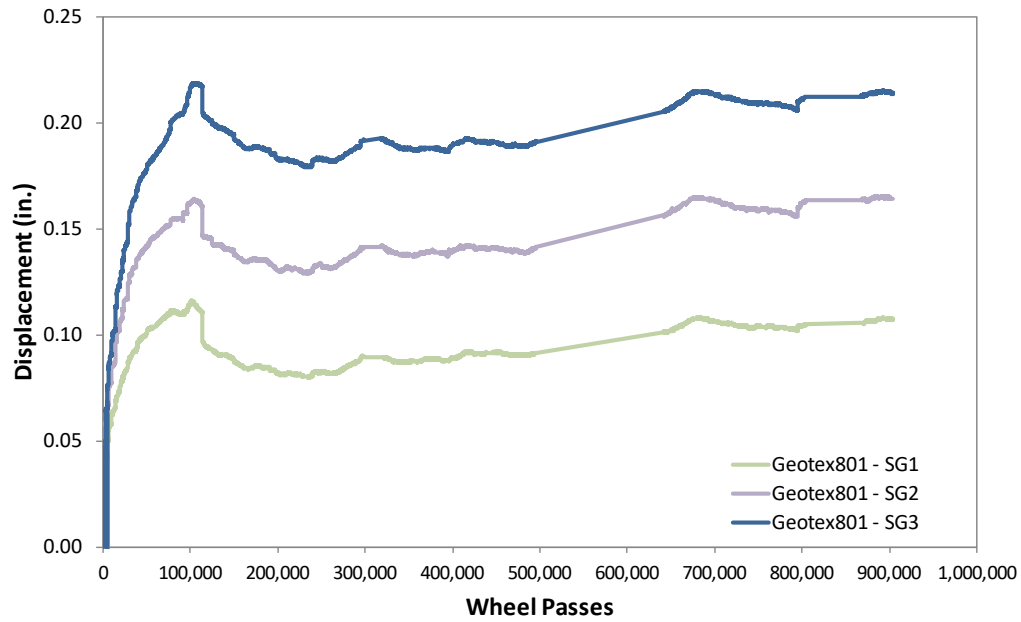


Figure 6-8: Displacement response of Geotex801 subgrade sensors.

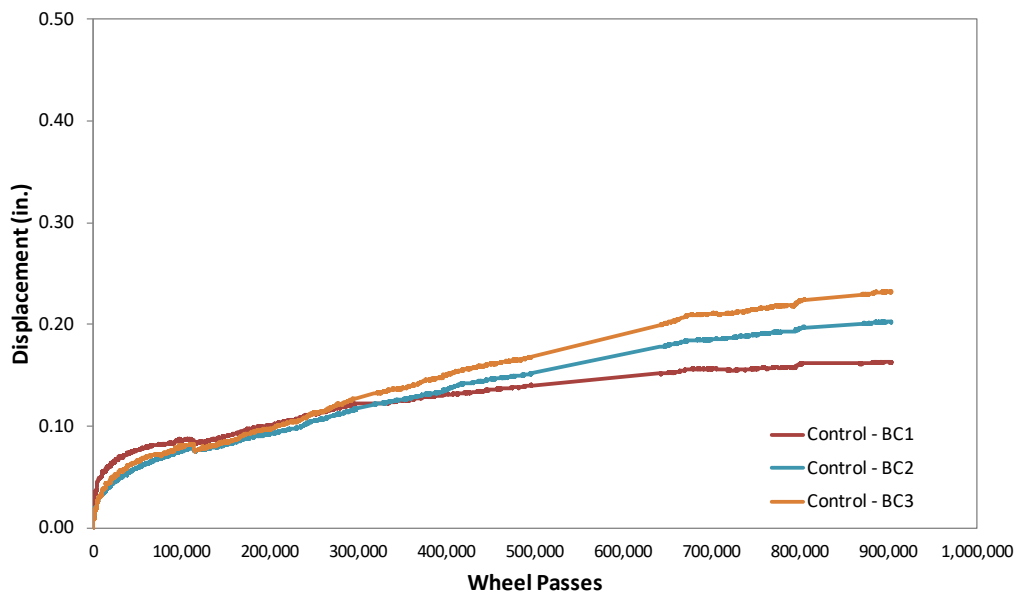


Figure 6-9: Displacement response of Control base course sensors.

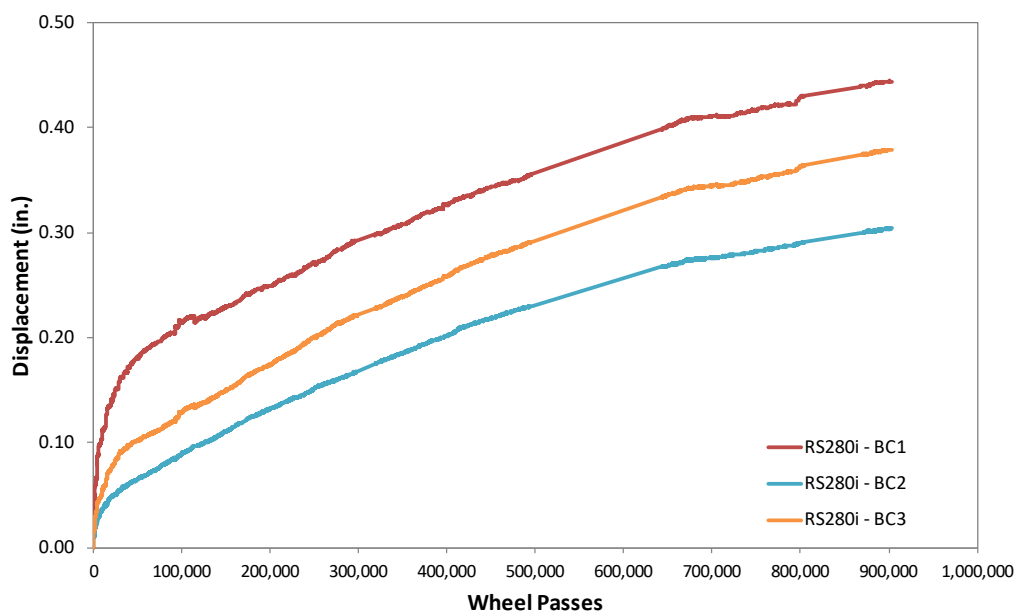


Figure 6-10: Displacement response of RS280i base course sensors.

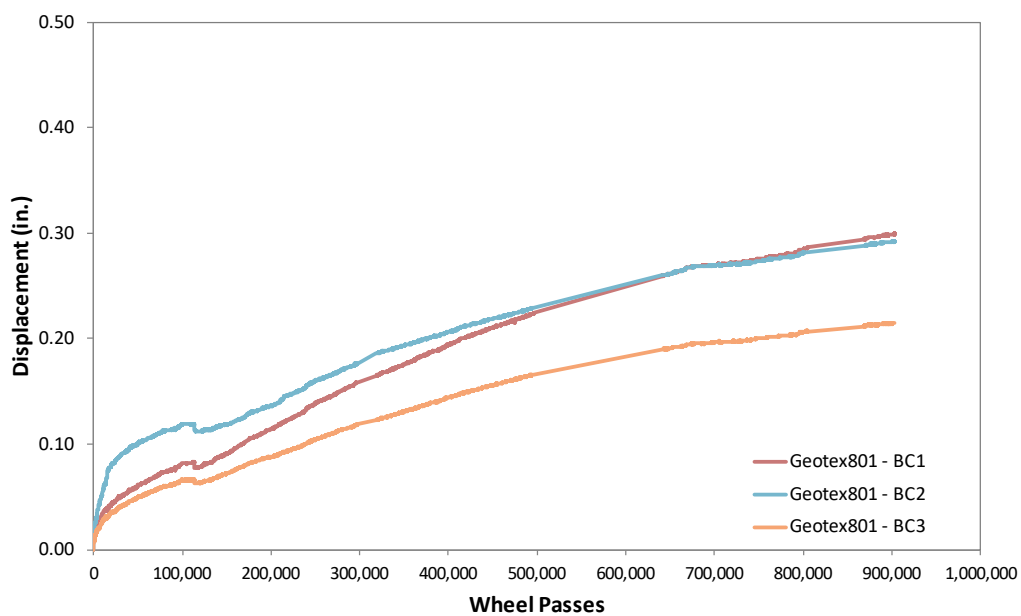


Figure 6-11: Displacement response of Geotex801 base course sensors.

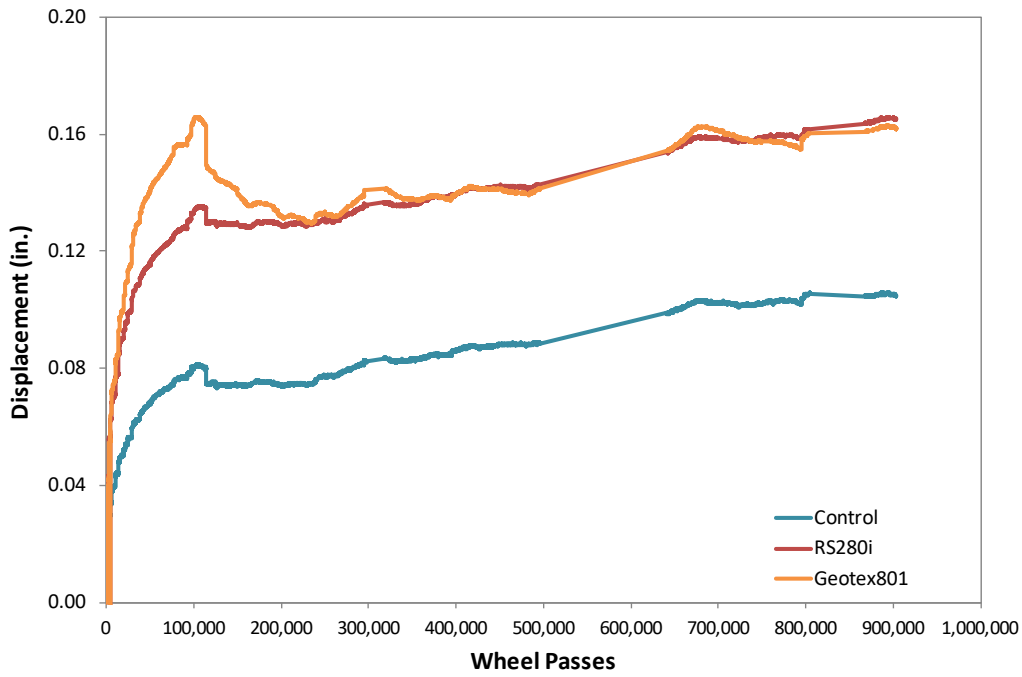


Figure 6-12: Average displacement response of all subgrade sensors.

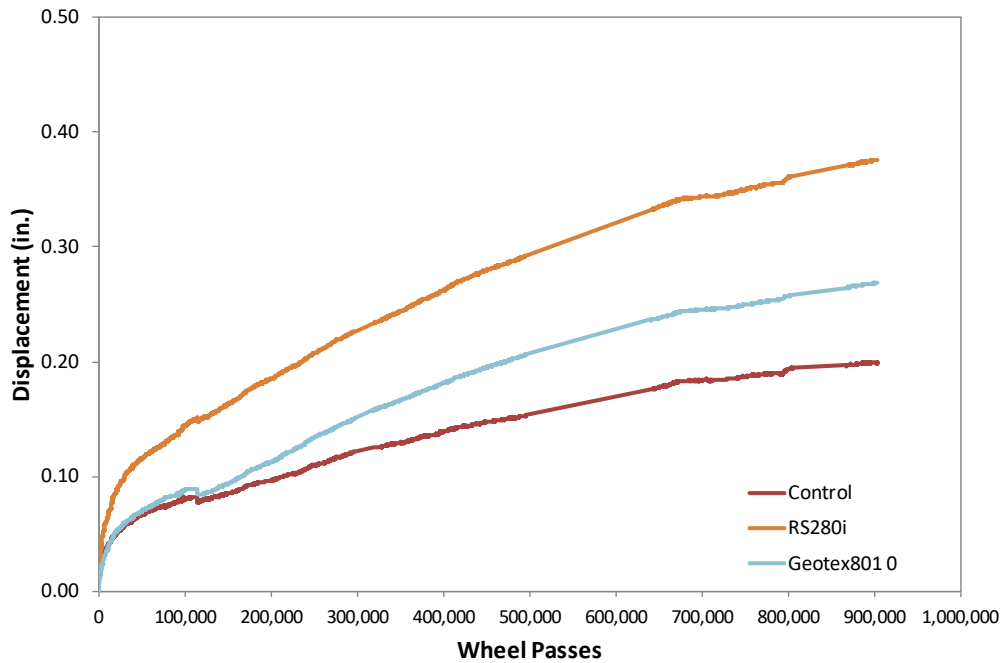


Figure 6-13: Average displacement response of all base course sensors.

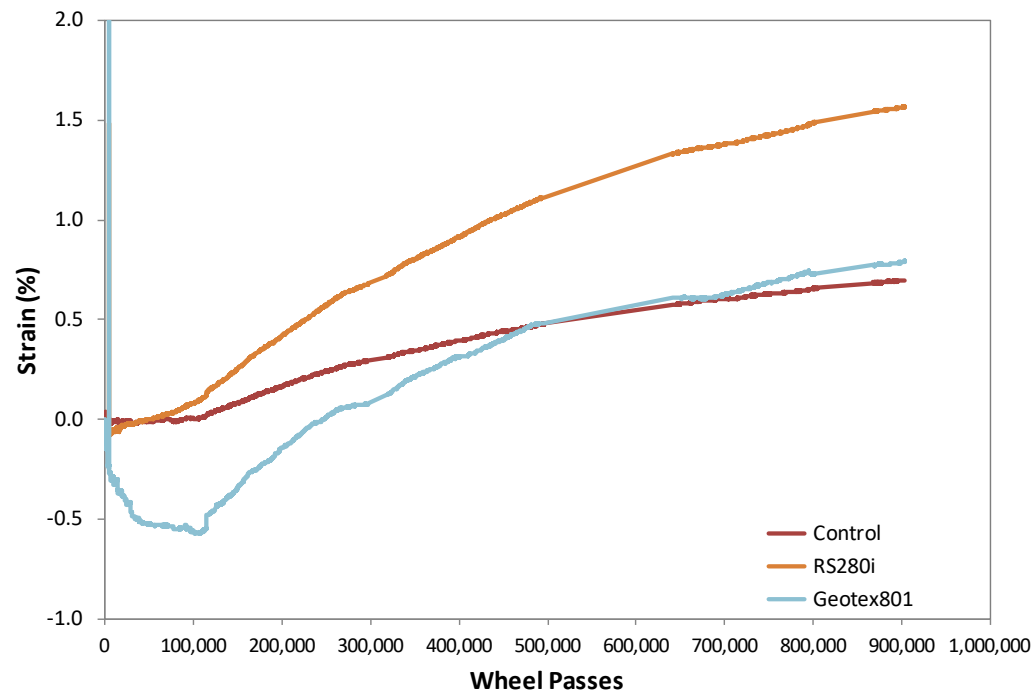


Figure 6-14: Average strain response in the base course for all test sections.

7 Post Trafficking Forensic Evaluation

Forensic investigations were conducted to assess the condition and properties of the asphalt, base course and subgrade in each of the test sections following trafficking. These investigations were done in each of the three test sections by focusing on an area 3 feet long (in the direction of traffic) by the entire width of the test section. The asphalt was cut and removed to expose the base course aggregate and the base course was carefully removed from above the geotextile and subgrade. A fines migration analysis was done near the bottom of the base course layer and the geotextiles were removed to evaluate the moisture content and strength of the subgrade in the reinforced test sections. Detailed topographic surveys were done on each layer. Finally, the geosynthetics were visually inspected to evaluate possible damage from construction or trafficking.

7.1 Asphalt

A single asphalt core from within each test section outside the wheel path was taken to evaluate the dynamic modulus of the asphalt (detailed report is in Appendix K). Additional samples of the asphalt were also taken from the area within and outside the wheel path to determine in-place density after trafficking. One or two samples from each test section were trimmed into rectangular prisms, weighed and measured. Density results are summarized in Table 7-1, along with densities from cores. The target density of the asphalt during construction was 140.7 lb/ft³. Comparison of density values from Table 5-10 and Table 7-1 shows the nuclear gauge measurements were 2 to 4 lb/ft³ less than those from physical samples. Test section 1 (control) had the lowest asphalt density from both nuclear density measurements and cores and does not help explain the better performance seen with this test section. Dynamic modulus tests on the cores taken from the test sections show little variation of modulus between test sections and indicates that the variation in asphalt density between test sections is inconsequential.

Table 7-1: Summary of post-trafficking asphalt density.

Location	Density (lb/ft ³)			Average
	Test Section 1	Test Section 2	Test Section 3	
Prisms Inside Wheel Path	142.7	143.5	142.8 143.6	143.1
Prisms Outside Wheel Path	139.6	142.3	141.7	141.2
Cores Outside Wheel Path	141.6	144.2	142.9	142.9
Average	141.3	143.3	142.8	142.4

7.2 Base Course Aggregate

Once exposed, the base course aggregate was carefully removed to expose the geosynthetic or subgrade surface. An evaluation was made within each test section to determine whether fines from the subgrade had migrated upward into the base during trafficking. This assessment was made by extracting samples from above the geosynthetic (in the reinforced test sections) or subgrade (in the control test section). One sample was taken from directly above the geosynthetic/subgrade level up to an inch above. A second sample was taken directly above the first sample from 1 inch to 5 inches above the geosynthetic/subgrade. Two areas within each test section were evaluated. A washed sieve analysis was done on each sample. The fines content for each sample within each test section are summarized in Table 7-2. The data shows that the fines content was slightly greater for the samples taken at a level of 1 to 5 inches above the geosynthetic/subgrade layer as compared to the level of 1 inch above the layer and indicates that fines did not migrate from the subgrade up into the base course in any of the test sections.

Table 7-2: Results of washed sieve analysis on extracted samples from the base course.

Layer	Average Fines (%)					
	Control		RS280i		Geotex 801	
	Test 1	Test 2	Test 1	Test 2	Test 1	Test 2
1 in. above	5.2	6.6	5.8	5.7	6.0	6.2
1-5 in. above	6.0	6.5	6.6	6.5	6.4	6.2

7.3 Subgrade

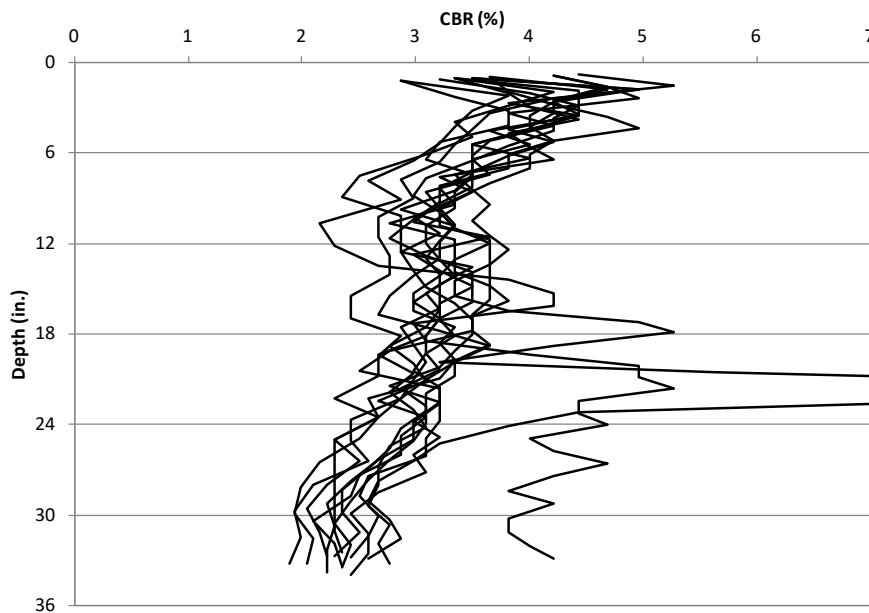
Moisture content, vane shear and DCP tests were performed on the exposed subgrade to evaluate its properties after trafficking. Moisture content samples were taken from the surface, 1 in. below the surface and 2 in. below the surface, as summarized in Table 7-3. The values indicate that the subgrade surface lost a small amount of moisture but that the underlying layers were at a similar moisture content as compared to the values measured prior to the placement of base course aggregate during the second construction (Table 5-4).

Twelve vane shear tests were run in each test section. The average shear strength for each test section was as follows: Control = 221 kPa, RS280i = 205 kPa and Geotex 801 = 216 kPa. These values indicate an approximate 50 % increase in vane shear strength of the upper layer of subgrade over the course of construction and trafficking.

Table 7-3: Post-trafficking subgrade average moisture content.

Measurement Depth	Average Moisture Content (%)		
	Control	RS280i	Geotex 801
Surface	25.0	25.3	24.4
1 in. below	25.5	25.7	25.2
2 in. below	26.3	26.2	25.5

Four DCP measurements were taken within each test section using the dual mass DCP device (drop hammer weight of 10.1 lb.) on the exposed surface of the subgrade. The results from these tests are shown in the plot in Figure 7-1. The bearing strength (in terms of CBR) as a function of depth was calculated using Equation 6 developed by Kleyn (1975). The average post-trafficking strengths were as follows: Control CBR = 3.2%, RS280i CBR = 3.3% and Geotex 801 CBR = 3.2%. These values are approximately 41 to 45 % greater than those measured during the second construction.

**Figure 7-1: Post-trafficking subgrade DCP results as a function of depth.**

7.4 Topographic Profiles and Photos

Transverse surveys were taken of the surface of the asphalt, base course and subgrade to show the surface contours after trafficking. Surveys were taken on both sides of the trench (referred to as south and north in this report). The profiles are shown in Figure 7-2, Figure 7-4 and Figure 7-6 for the Control, RS280i and Geotex 801 test sections, respectively, with accompanying photographs given in Figure 7-3, Figure 7-5 and Figure 7-7, respectively. Each of these plots is followed by profile photos of the north trench walls in each of the test sections. A photo of the entire cross-section in the Geotex 801 test section is shown in Figure 7-8. Several other photos taken during the forensic investigations are provided in Appendix L.

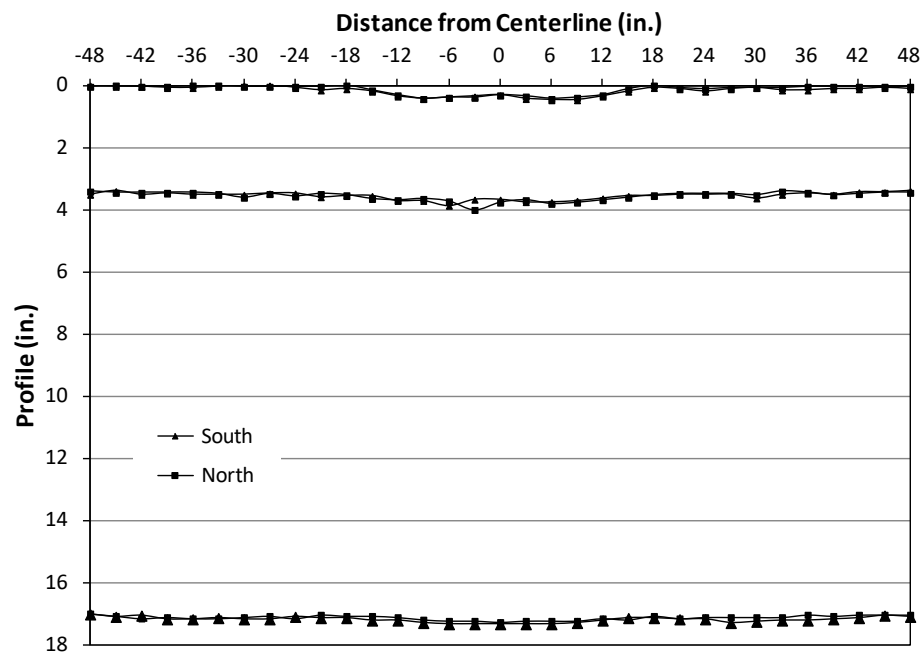


Figure 7-2: Post-trafficking surface profiles of the Control test section.



Figure 7-3: Post-trafficking profile photo of north face of Control trench wall.

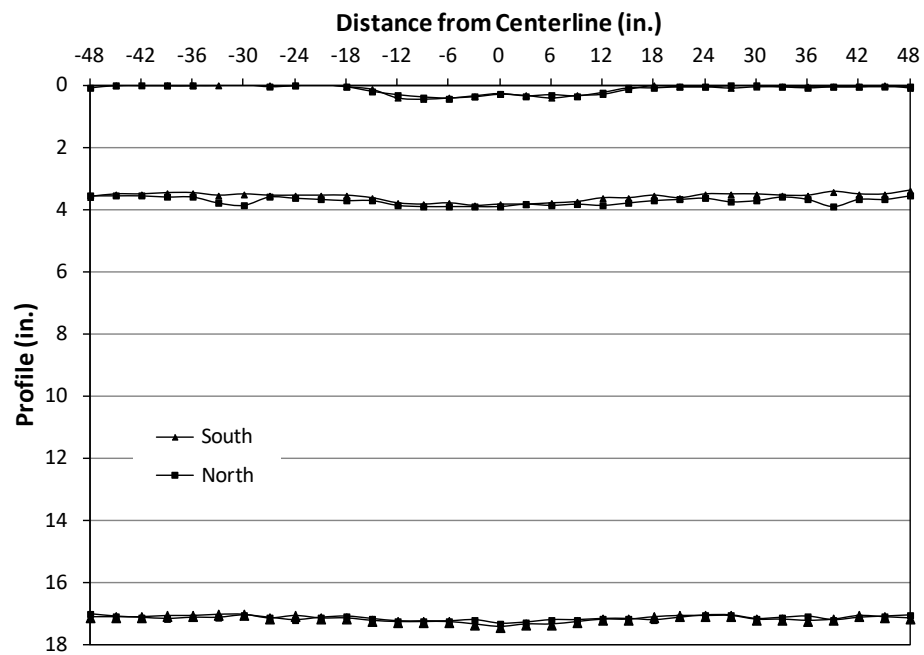


Figure 7-4: Post-trafficking surface profiles of the RS280i test section.



Figure 7-5: Post-trafficking profile photo of north face of RS280i trench wall.

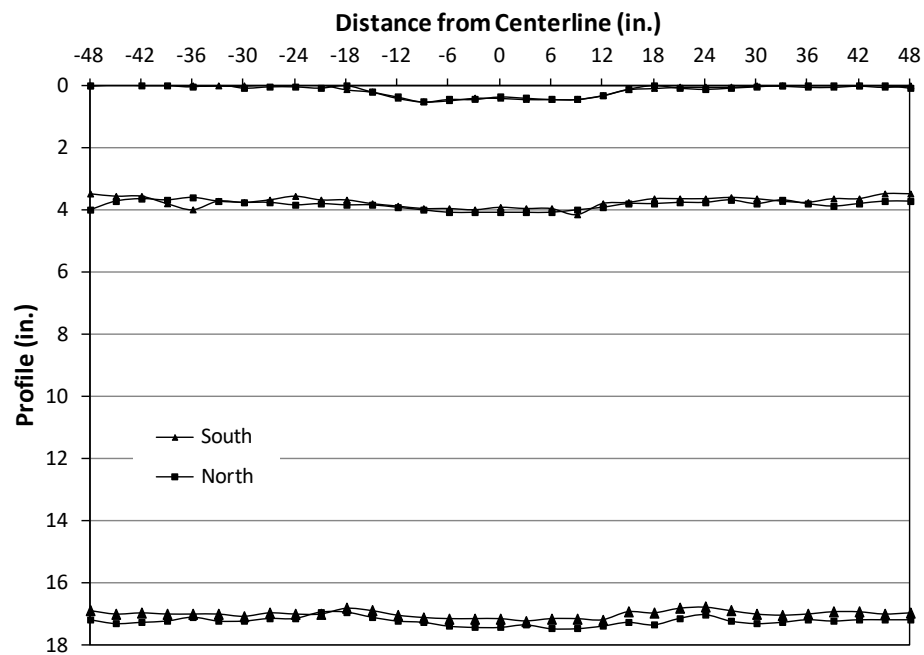


Figure 7-6: Post-trafficking surface profiles of the Geotex 801 test section.



Figure 7-7: Post-trafficking profile photo of north face of Geotex 801 trench wall.



Figure 7-8: Post-trafficking full profile photo of Geotex 801 test section.

7.5 Geosynthetics

The geotextiles removed from the forensic trench were visually evaluated to assess damage. No damage was noticed in either of the textiles from construction or trafficking, other than the holes that were cut to accommodate the base course LVDTs. In the wheel path of the Geotex 801 nonwoven geotextile, small deposits of soil were bonded to the surface due to the applied wheel load; however, there was no visible damage or holes in these areas. Photos of the extracted geotextiles are shown in Figure 7-9 and Figure 7-10 for the RS280i geotextile and Figure 7-11 and Figure 7-12 for the Geotex 801 geotextile.



Figure 7-9: Photo of extracted RS280i geotextile.



Figure 7-10: Close-up photo of extracted RS280i geotextile.



Figure 7-11: Photo of extracted Geotex 801 geotextile.

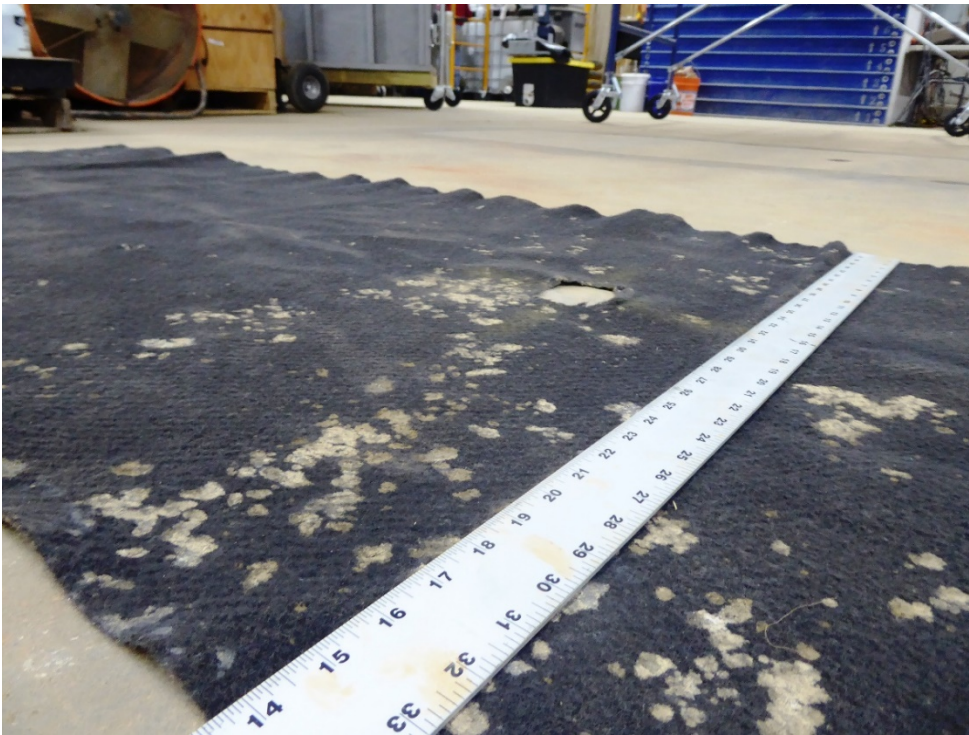


Figure 7-12: Close-up photo of extracted Geotex 801 geotextile.

8 Analysis of Results

Results of this study are used in this section to 1) evaluate a representative subgrade CBR strength for the test sections, 2) compare results of the project to those from other studies, 3) analyze and explain differences in the rutting response curves for the three test sections and 4) evaluate the suitability of the spreadsheet model for predicting reinforcement benefit seen in the sections with a geotextile.

8.1 Evaluation of Representative Subgrade CBR Strength

An evaluation of subgrade CBR strength for each test section representative of the subgrade during the traffic period is complicated by several conditions, including the elapsed time from subgrade placement to trafficking, the strength gain that occurs due to the thixotropic nature of clays, strength gain due to potential moisture loss and the reconstruction of the HMA and base layers. The initial placement of the subgrade during the first construction yielded an average placement moisture content of approximately 28 % and a vane shear strength of approximately 100 kPa. From data presented in Figure 4-2, this should have produced a subgrade with an average CBR of 2.5 %. In-field CBR tests yielded average values of 2.01 to 2.27. DCP measurements yielded average CBR values of 2.09 to 2.16. Vane shear strength measurements on the upper layer prior to placement of base course for the second construction together with previous measurements on lower layers and data from Figure 4-5 suggest that the subgrade may have increased in strength between the first and second constructions to CBR value of approximately 3. DCP measurements taken during the second construction; however, indicate average CBR values ranging from 2.24 to 2.27. Measurements taken following trafficking and during the forensic work show the subgrade to have further increased in strength with DCP measurements yielding an average subgrade CBR of 3.3 %. From initial placement of the subgrade to the end of trafficking, DCP measurements showed the subgrade to have increased by a total of approximately 55 %. If this increase is applied to the initial target CBR of 2.5 %, CBR might be expected to be approximately 3.9 at the end of trafficking. Given the long period between initial placement of the subgrade to the start of trafficking, a representative value of subgrade CBR of 3.5 appears reasonable. Variations of CBR strength between sections is examined more closely in Section 8.3.

8.2 Comparison of Results to Literature

Chapter 2 of this report showed the amount of performance data for test sections using geotextiles is small in comparison to those using geogrids. For the test sections available in the literature containing geotextiles, there are even fewer studies incorporating conditions comparable to those used in this study. This makes it difficult to make a direct comparison of results in this study to those in the literature. The most pertinent study in the literature is from Saghebfar et al. (2016).

Table 2-6 provides information on the conditions used in the test sections and shows the section was more thick than the one in this study and used a stronger subgrade (CBR=5). The geotextile RS280i was used and resulted in a TBR of 1.38. Given the stronger conditions in this test section, this result is seen to show significantly more benefit than that observed in this project for this product.

Results summarized in Berg et al. (2000) tend to show modest values of benefit for pavement conditions weaker than those used in this study. The information available at that time was used to develop guidelines and expected benefit for geotextiles used for reinforcement. Table 4-1 of this document is reproduced as Table 8-14 presented later in this chapter. This table states that both woven and non-woven geotextiles are not usually applicable for reinforcement of roads with a subgrade CBR between 3 and 8 and a base thickness greater than 300 mm. These guidelines match the results from the test sections. Additional examination of the results of this study as compared to the guideline given in Berg et al. (2000) are presented in Section 8.4 when results from the spreadsheet model are evaluated.

8.3 Analysis of Rutting Response

The rutting response given previously in Figure 6-3 showed the control section to out-perform the two reinforced sections containing the geotextiles RS280i and Geotex 801. The section containing RS280i performed slightly better than the section with Geotex 801. The raw result of the control section performing better than the reinforced sections was unexpected and can be explained by several arguments.

The average rutting response curves given in Figure 6-3 show the reinforced sections to develop rut more quickly for the initial portion of trafficking up to approximately 75,000 passes. After 75,000 passes, the average slope of the rutting curve for the three test sections are approximately equal. Small differences in construction may lead to significant differences in the initial seating or shakedown of the pavement layers under trafficking. Statistical differences in constructed properties of the test sections are evaluated later in this section. The absence of construction traffic on the test sections failed to provide seating of the materials as would have occurred in a field application. The inability to incorporate construction traffic and material seating in the test sections may provide justification for comparison of the rutting response once seating due to initial trafficking is completed. Since the average slope of the rutting curves for the three test sections are approximately equal, this argument leads to the conclusion that the three test sections performed similarly.

A second argument is made by plotting the rutting curves showing a statistical measure of data scatter associated with each measurement point. Figure 8-1 shows the average rut response for the three test sections and measurement error bands associated with each measurement point. The error

bands correspond to plus and minus one standard deviation of the measurement points taken along the longitudinal path of each test section at each measurement point and used to calculate the average values shown in Figure 8-1. This plot shows overlap of the error bands and provides further justification for the argument that the three test sections performed similarly within the scatter of rut depth measurement along the test sections.

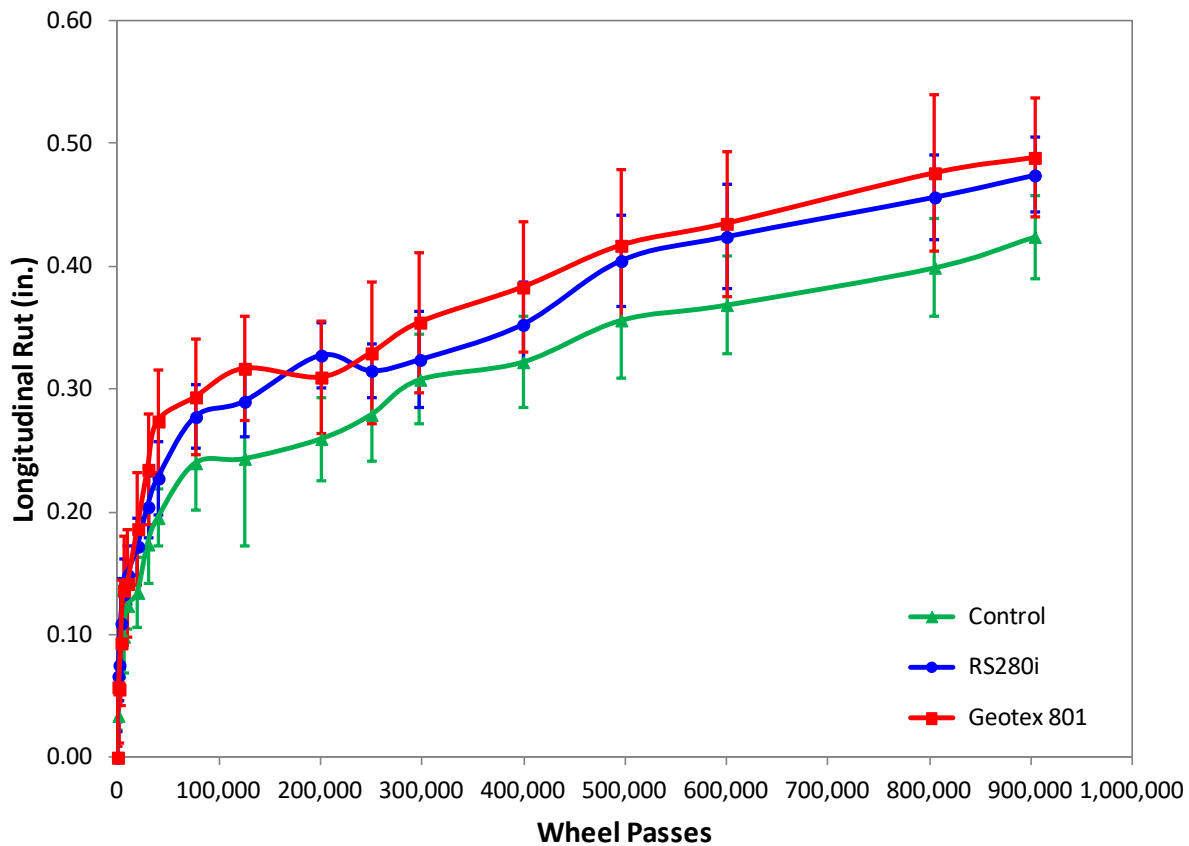


Figure 8-1: Longitudinal rut responses showing data scatter.

A third approach involves evaluating the variability of the constructed properties of the pavement layers, the use of the AASHTO pavement design equation and a statistical analysis to show the probability that variability of constructed properties explains the differences in observed rutting response. This approach involved using the average values of material properties provided in Section 5 measured during construction. The properties of most importance included HMA and base layer thickness, subgrade vane shear strength, subgrade in-field CBR strength, subgrade dynamic stiffness, subgrade DCP, base course dynamic stiffness, base course DCP and HMA dynamic modulus. Standard deviation was calculated for each of these measurement values. Table

8-1 and Table 8-2 provide average thickness and standard deviation of the HMA and base course layers. Table 8-3 through Table 8-6 provide standard deviation of measured properties for the subgrade. Average values of these properties are provided in Section 5, Table 5-3, Table 5-5 and Table 5-6 for the properties of vane shear strength, in-field CBR strength and dynamic stiffness, respectively. Table 8-7 and Table 8-8 provide standard deviation of measured properties for the base course. Average values of dynamic stiffness of the base course are provided in Table 5-8. The dynamic modulus tests performed on HMA cores taken from the test sections (Appendix K) do not show significant differences. These results together with minor differences in asphalt density between test sections indicate that the structural quality of the HMA was consistent between test sections.

Table 8-1: HMA average thickness and standard deviation.

Test Section	Thickness (in)	
	Average	Standard Deviation
1	3.39	0.16
2	3.40	0.13
3	3.31	0.19

Table 8-2: Base course average thickness and standard deviation.

Test Section	Thickness (in)	
	Average	Standard Deviation
1	13.44	0.14
2	13.18	0.19
3	13.26	0.22

Table 8-3: Subgrade vane shear strength standard deviation.

Layer [†]	Vane Shear Strength Standard Deviation (kPa)		
	Test Section 1	Test Section 2	Test Section 3
All	4.7	4.9	5.4
6	4.9	5.1	6.9
5	4.0	3.6	3.7
4	5.2	7.1	4.9
3	5.3	5.0	5.2
2	3.7	4.2	5.8
1	4.6	4.1	3.7

[†] Layer 1 is at the bottom of the subgrade and Layer 6 is at the top.

Table 8-4: Subgrade in-field CBR strength standard deviation.

Layer [†]	In-Field CBR Standard Deviation (%)		
	Test Section 1	Test Section 2	Test Section 3
All	0.29	0.66	0.32
6	0.21	1.41	0.50
5	0.12	0.16	0.18
4	0.37	0.40	0.27
3	0.63	0.06	0.14
2	0.47	0.33	0.21
1	0.39	0.27	0.41

[†] Layer 1 is at the bottom of the subgrade and Layer 6 is at the top.

Table 8-5: Subgrade dynamic stiffness standard deviation.

Layer [†]	Dynamic Stiffness Standard Deviation (MN/mm ²)		
	Test Section 1	Test Section 2	Test Section 3
Composite	0.55	0.35	0.25
6	0.56	0.44	0.29
5	0.34	0.25	0.12
4	0.83	0.30	0.33

[†] Layer 4 is near the center of the subgrade layer and Layer 6 is at the top.

Table 8-6: Subgrade average DCP and standard deviation.

Test Section	CBR (%) From DCP	
	Average	Standard Deviation
1	2.27	0.14
2	2.27	0.10
3	2.24	0.12

Table 8-7: Base course dynamic stiffness standard deviation.

Layer [†]	Dynamic Stiffness Standard Deviation (MN/mm ²)		
	Test Section 1	Test Section 2	Test Section 3
3	9.07	6.93	9.81
2	1.35	2.23	3.53
1	3.09	1.24	1.76

[†] Layer 1 is the bottom base layer and Layer 3 is the top layer.

Table 8-8: Base course average DCP and standard deviation.

Test Section	CBR (%) From DCP	
	Average	Standard Deviation
1	72.4	7.12
2	73.9	3.59
3	73.8	2.65

The measured properties for the subgrade were used to determine an average value and standard deviation of the resilient modulus for each test section. This was accomplished by using the vane shear strength values shown in Table 8-3 for the test section sublayers to compute a composite standard deviation for the test section using the same weighting technique taken in Section 5 to compute composite average values. Average CBR and standard deviation were then computed using the relationship between vane shear strength and CBR presented in Figure 4-2. Average resilient modulus and standard deviation was then computed from Equation 7 where M_R is in units of psi. The in-field CBR strengths were also used to calculate average resilient modulus and standard deviation from Equation 7. Dynamic stiffness measurements were converted directly to units of psi and treated as a resilient modulus. Finally, DCP values converted to CBR were used to calculate average resilient modulus and standard deviation from Equation 7. The four sets of average resilient modulus and standard deviation were then used to calculate composite values for

each test section, which are listed in Table 8-9. The average composite resilient modulus values listed in Table 8-9 were used in Equation 7 to calculate average composite values of subgrade CBR of 3.69, 3.49 and 3.32 for test sections 1, 2 and 3, respectively. These values support the conclusion made in Section 8.1 concerning an average representative value of subgrade CBR of 3.5.

$$M_R = 1500 \text{ CBR} \quad (7)$$

Table 8-9: Subgrade composite average resilient modulus and standard deviation.

Test Section	Resilient Modulus (psi)	
	Average	Standard Deviation
1	5540	455
2	5233	350
3	4985	271

The AASHTO base layer coefficient was determined using dynamic stiffness and DCP measurements. Values of average dynamic stiffness and standard deviation given in Table 5-8 and Table 8-7 were used to calculate composite values for each test section by a straight average of the sublayer values. The base layer coefficient, a_2 , was then assumed to be equal to 0.14 for the control section (section 1). Values of a_2 for test sections 2 and 3 were then scaled according to the composite values for each test section. A similar approach was taken to determine a_2 for each test section from DCP data provided in Table 8-8. The two sets of average a_2 and standard deviation were then used to calculate composite values for each test section, which are listed in Table 8-10.

Table 8-10: Base course composite average a_2 and standard deviation.

Test Section	a_2	
	Average	Standard Deviation
1	0.140	0.013
2	0.135	0.008
3	0.140	0.009

Average values of HMA and base course thickness, subgrade resilient modulus and base layer coefficient (a_2) for each test section were used in the AASHTO pavement design equation to determine the number of predicted ESALs carried, with the parameters used and the predicted ESALs (ESAL-P) shown in Table 8-11. Table 8-11 also lists the ESALs observed (ESAL-O) in

the test sections corresponding to a rut depth of 0.4 inch. This rut depth was chosen to provide a match between ESAL-P and ESAL-O for test section 1. The analysis data in Table 8-11 shows the AASHTO pavement design equation to predict less ESALs for the two sections with a geotextile. The analysis does not show; however, the full degree of underperformance observed in the two sections with a geotextile.

Table 8-11: Parameters used in AASHTO pavement design equation and predicted ESALs.

Parameter	Test Section 1	Test Section 2	Test Section 3
Reliability	85%	85%	85%
Z_R	-0.46	-0.46	-0.46
S_o	0.45	0.45	0.45
ΔPSI	1.7	1.7	1.7
M_R (psi)	5540	5233	4985
a_1	0.41	0.41	0.41
D_1 (in)	3.39	3.40	3.31
a_2	0.140	0.135	0.140
D_2 (in)	13.44	13.18	13.26
SN	3.27	3.24	3.21
ESAL-P	8.05E+05	6.64E+05	5.66E+05
ESAL-O	8.05E+05	4.73E+05	4.34E+05

The AASHTO pavement design equation was also used to examine the impact of the variability of the constructed pavement layer parameters. The statistical analysis performed followed techniques described by Duncan (2000) to examine the probability of the most likely ESAL predicted for the two test sections with geotextile equaling or exceeding the most likely ESAL predicted for the control test section. The AASHTO equation was used to estimate the ESALs for each test section when each parameter known to have variability is increased by one standard deviation and then decreased by one standard deviation from its most likely or average value, with the values of the other parameters equal to their most likely or average values. The parameters varied included HMA and base course thickness, subgrade resilient modulus and base layer coefficient (a_2). The predicted ESAL when the first parameter is increased and then decreased by one standard deviation is termed $ESAL_1^+$ and $ESAL_1^-$, respectively. The difference in predicted ESALs when this first parameter is varied is given by Equation 8. This process is repeated for variation of the next 3 parameters. The standard deviation in predicted ESAL for each test section

is then computed using the Taylor series technique given by Equation 9. Coefficient of variation (COV) of ESALs for each test section is then computed by Equation 10, where $ESAL_{MLV}$ is the most likely ESAL predicted using the average parameters listed in Table 8-11. An ESAL ratio (ER) is then computed for test sections 2 and 3 from Equation 11 and 12. The lognormal reliability index (β_{ln}) is then computed from Equation 13. The standard cumulative normal distribution function found in tables or using the NORMSDIST function in Excel with β_{ln} as the argument of the function returns the reliability. Probability (P) is then one minus the reliability. Table 8-12 provides a summary of the statistical parameters from this analysis.

$$\Delta ESAL_1 = ESAL_1^+ - ESAL_1^- \quad (8)$$

$$\sigma_{ESAL} = \sqrt{\left(\frac{\Delta ESAL_1}{2}\right)^2 + \left(\frac{\Delta ESAL_2}{2}\right)^2 + \left(\frac{\Delta ESAL_3}{2}\right)^2 + \left(\frac{\Delta ESAL_4}{2}\right)^2} \quad (9)$$

$$COV = \frac{\sigma_{ESAL}}{ESAL_{MLV}} \quad (10)$$

$$ER_2 = \frac{ESAL_{MLV-1}}{ESAL_{MLV-2}} \quad (11)$$

$$ER_3 = \frac{ESAL_{MLV-1}}{ESAL_{MLV-3}} \quad (12)$$

$$\beta_{ln} = \frac{\ln\{ER\sqrt{1+COV^2}\}}{\sqrt{\ln(1+COV^2)}} \quad (13)$$

Table 8-12: Parameters from statistical analysis.

Test Section	σ_{ESAL}	COV (%)	P (%)
1	3.21 E 05	39.9	-
2	1.78 E 05	29.6	12.5
3	1.71 E 05	30.3	8.8

The probability values listed in Table 8-12 have the interpretation that the variability in the constructed pavement layer parameters in test section 2 leads to a 12.5 % chance that the ESALs

carried by test section 2 would equal or exceed those of the control test section. Similarly, there is an 8.8 % chance that the ESALs carried by test section 3 would equal or exceed those of the control test section. The low values of probability for test sections 2 and 3 imply that the variation in as-constructed pavement layer properties do not account for the control section outperforming the reinforced test sections. This analysis also implies that the excellent consistency of the constructed pavement layers leads to a low level of uncertainty with the rutting results obtained. Finally, this analysis leads to the most likely explanation for the observation of the control section outperforming the reinforced sections as due to seating or shakedown of the pavement layers during initial trafficking.

8.4 Evaluation of Spreadsheet Model

The spreadsheet model developed previously for MDT and updated to a .xlsm format as part of this project was used to predict Traffic Benefit Ratio (TBR) for the two sections containing a geosynthetic. The average values of HMA and base thickness, HMA and base structural layer coefficient and subgrade resilient modulus provided in Table 8-11 were used in the model. These values along with other input values for the model are listed in Table 8-13. Subgrade CBR was computed from resilient modulus using Equation 7. Geosynthetic modulus and modulus ratio were determined from wide-width tensile tests performed on the materials and reported in Appendix D. The modulus used for the nonwoven geotextile of 26 kN/m is most likely too low due to the lack of confinement in the wide-width tensile test and not representative of in-field stiffness. To produce a TBR equal to 1 for test section 2, it was necessary to turn on the check boxes for reduction for Poisson's ratio and reduction for shear modulus and to set the reduction factor for interface shear to 0.690. For the test section work previously performed for MDT where a lightweight woven geotextile was used, the model was shown to work well for this material when the checkboxes were turned on and the reduction factor for interface shear was set to 0.765, indicating that the values used for test section 2 are reasonable. For test section 3, to produce a TBR equal to 1 when the modulus was set to a value of 26 kN/m, it was necessary to turn off the check boxes and to input a value for reduction factor for interface shear of 0.970. These selections are most likely due to the low value of geosynthetic modulus used. With the check boxes for reduction factors for Poisson's ratio and shear modulus turned on, and the reduction factor for interface shear set to 0.780, a modulus value of 440 kN/m produces a TBR equal to 1. From experience, these values appear to be reasonable for this material.

The model was also used to predict TBR for a subgrade CBR equal to 2.5 while using the other parameters listed in Table 8-13 for test section 2 and the second set of parameters for test section 3. Modest values of TBR equal to 1.35 and 1.19 for test sections 2 and 3 were obtained. These

results suggest that a modest structural benefit can be realized for these materials for a weaker subgrade strength equal to the target in this project.

Table 8-13: Parameters used in spreadsheet model to produce TBR=1.

Parameter	Test Section 2	Test Section 3	Test Section 3
D ₁ (in)	3.40	3.31	3.31
a ₁	0.41	0.41	0.41
D ₂ (in)	13.18	13.26	13.26
a ₂	0.135	0.140	0.140
Subgrade CBR	3.5	3.3	3.3
G _{SM-2%} (kN/m)	775	26	440
G _{MR}	0.897	0.827	0.827
Reduction factor for interface shear	0.690	0.970	0.780
Reduction factor for Poisson's Ratio	checked	unchecked	checked
Reduction factor for shear modulus	checked	unchecked	checked

Results from the test sections and from the spreadsheet model are compared to the guidelines given in Berg et al. (2000). This document serves as the industry standard for guiding when geosynthetic reinforcement in paved roads is beneficial. Table 4-1 of this document is reproduced below as Table 8-14. This table states that both woven and non-woven geotextiles are not usually applicable for reinforcement of roads with a subgrade CBR between 3 and 8 and a base thickness greater than 300 mm. These guidelines match the results from the test sections. This table also states that woven and non-woven geotextiles are usually applicable for reinforcement of paved roads with a subgrade CBR less than 3 and a base thickness greater than 300 mm; however, the geotextile is typically addressed as a subgrade stabilization application. The spreadsheet model together with this guideline suggest that geotextiles should be used for subgrade stabilization for this subgrade condition and may further be relied upon for some modest reinforcement benefit.

Improvements to the spreadsheet model may be made by refinement of the check boxes for reduction factors for Poisson's ratio and in-plane shear modulus and in providing guidance for selecting values for reduction factors for interface shear. Replacement of the check boxes with cells for input of numerical values for reduction factors would allow specific products to be analyzed more accurately. Guidance for selection of numerical values may be derived from recent work performed by the author (Perkins and Haselton, 2019, Perkins et al., 2020) involving biaxial tension tests designed to yield values of Poisson's ratio and in-plane shear modulus.

Table 8-14: Table 4-1 from Berg et al. (2000) providing guidelines for geotextile reinforcement of paved roads.

Roadway Design Conditions		Geosynthetic Type					
Subgrade	Base/Subbase Thickness ¹ (mm)	Geotextile		Geogrid ²		GG-GT Composite	
		Nonwoven	Woven	Extruded	Knitted or Woven	Open-graded Base ³	Well Graded Base
Low (CBR < 3) ($M_R < 30$ MPa)	150 - 300	④	●	●	□	●	⑤
	> 300	④	④	◐	◐	◐	⑤
Firm to Very Stiff ($3 \leq \text{CBR} \leq 8$) ($30 \leq M_R \leq 80$)	150 - 300	⑥	◐	●	□	●	⑤
	> 300	⑥	⑥	◐ ⁷	□	□	⑤
Firmer (CBR > 8) ($M_R > 80$ MPa)	150 - 300	○	○	◐	□	□	⑤
	> 300	○	○	○	○	○	⑤

Key: ● — usually applicable ◐ — applicable for some (various) conditions
 ○ — usually not applicable □ — insufficient information at this time ⑤ — see note

Notes: 1. Total base or subbase thickness with geosynthetic reinforcement. Reinforcement may be placed at bottom of base or subbase, or within base for thicker (usually > 300 mm) thicknesses. Thicknesses less than 150 mm not recommended for construction over soft subgrade. Placement of less than 150 mm over a geosynthetic not recommended.

2. For open-graded base or thin bases over wet, fine-grained subgrades, a separation geotextile should be considered with geogrid reinforcement.

3. Potential assumes base placed directly on subgrade. A subbase also may provide filtration.

④ Reinforcement usually applicable, but typically addressed as a subgrade stabilization application.

⑤ Geotextile component of composite likely is not required for filtration with a well graded base course; therefore, composite reinforcement usually not applicable.

⑥ Separation and filtration application; reinforcement usually not applicable.

7. Usually applicable when placed up in the base course aggregate. Usually not applicable when placed at the bottom of the base course aggregate.

9 Geotextile Costs and Benefits

The Technical Panel for this project provided typical unit costs for the pay items of subgrade excavation/fill, base course material, HMA material and the geotextiles used in this project. These costs are summarized in Table 9-1 for the 5 state districts and are provided to allow for a comparison of geotextile costs to other material costs associated with roadway construction.

Table 9-1: Typical unit pay item costs for typical MDT roadway projects.

District	Subgrade Excavation/Fill (\$/yd ³)	Base Course (\$/yd ³)	HMA (\$/ton)	RS280i (\$/yd ²)	Geotex 801 (\$/yd ²)
1	6.50	25.00	73.05	3.00	1.50
2	7.00	25.00	76.05	3.00	1.50
3	7.50	30.00	79.05	3.00	1.50
4	7.50	37.00	81.05	3.00	1.50
5	7.00	30.00	81.05	3.00	1.50

The benefits associated with the use of a geotextile include its function as a separator, filter and for potential reinforcement. For the conditions associated with the test sections constructed in this project, including a subgrade CBR of 3.5, the two geotextiles were shown to offer no structural reinforcement benefit to increase the amount of traffic carried. Section 8.2 did; however, predict a modest amount of reinforcement benefit in terms of TBR for a subgrade CBR of 2.5. This suggests that the geotextiles provide insurance against more rapid pavement deterioration during seasonally wet periods when the subgrade's strength is reduced and will require fewer pavement rehabilitation treatments over the service life of the pavement.

It is well recognized that geotextiles provide separation and filtration between the relatively clean base course aggregate and the underlying materials containing a higher percentage of fines. This function will reduce the amount of rehabilitation needed at scheduled rehabilitation periods. Alternatively, this function may extend the time-period between rehabilitations and thereby extend the service life of the pavement. Should the geotextile serve a reinforcement function during seasonally wet periods, the above arguments concerning rehabilitation are equally applicable. The use of a geotextile for separation also provides confidence in rehabilitation decision making by knowing the base layer is not contaminated. As a worse case, the use of a geotextile would eliminate the need to replace the base course layer during a scheduled rehabilitation period in the event the base became contaminated with fines due to the absence of a geotextile separator. Comparison of the cost of the geotextile to the cost of more extensive or more frequent rehabilitation operations should be evaluated on a case-by-case basis.

10 Conclusion

The principal objective of this study was to examine whether geotextile materials used by MDT as a separator in flexible pavements provide a structural contribution as a reinforcement material for a typical MDT pavement cross section. The test sections constructed had a target CBR value of the subgrade of 2.5. Measurement of subgrade properties during construction and following trafficking of the test sections showed the average representative CBR for the test sections to be approximately 3.5. The nominal thickness of the HMA and base course layers was 3.4 and 13.3 inch, respectively. The raw rutting results for these conditions showed the unreinforced test section to perform better than the two sections containing a geotextile. An analysis of the data collected involving several different approaches resulted in the conclusion that the three test sections performed similarly in terms of rutting performance for the conditions present in this study.

The spreadsheet design model developed previously for MDT using reasonable input parameters for the geotextiles predicted no reinforcement benefit for these conditions. This model showed moderate reinforcement benefit for a weaker subgrade condition of a CBR of 2.5. This benefit was expressed as a TBR and equaled 1.31 and 1.17 for the woven and non-woven geotextile, respectively. This condition might be present in typical Montana roadways during seasonally wetter periods. Use of geotextiles in a roadway for separation may provide reinforcement during these periods and reduce pavement deterioration during seasonally weak subgrade conditions.

The results of this study are difficult to directly compare to results available in the literature due to the low number of studies involving geotextiles for the conditions present in this project. Comparison of the results from this study to guidelines given in Berg et al. (2000); however, appear to support these guidelines.

It should be noted that this study did not quantify the separation benefit of the geotextiles, which are a recognized benefit applicable to most roadways in the state. Chapter 9 presented typical pay item costs for Montana roadways to compare the cost of typical geotextiles to other pavement material costs. The benefit associated with the cost of the geotextile lies in its primary function as a separator. A geotextile separator will reduce the amount of rehabilitation needed at scheduled rehabilitation periods. Alternatively, this function may extend the time-period between rehabilitations and thereby extend the service life of the pavement. Should the geotextile serve a reinforcement function during seasonally wet periods, the above arguments concerning rehabilitation are equally applicable. The use of a geotextile for separation also provides confidence in rehabilitation decision making by knowing the base layer is not contaminated. As a worse case, the use of a geotextile would eliminate the need to replace the base course layer during a scheduled rehabilitation period in the event the base became contaminated with fines due to the absence of a geotextile separator.

11 References

- AASHTO (1993). *AASHTO Guide for Design of Pavement Structures*. American Association of State Highway and Transportation Officials, Washington, DC.
- AASHTO (2013). *Standard Practice for Geosynthetic Reinforcement of the Aggregate Base Course of Flexible Pavement Structures*. AASHTO Designation R 50-09, Standard Specifications for Transportation Materials and Methods of Sampling and Testing (31st ed.), American Association of State Highway and Transportation Officials, Washington, DC.
- ASTM (2010). *Standard Test Method for Determining Small-Strain Tensile Properties of Geogrids and Geotextiles by In-Air Cyclic Tension Tests*, ASTM D7556, American Society of Testing and Materials.
- ASTM (2014). *Standard Test Method for Measuring Geosynthetic-Soil Resilient Interface Shear Modulus*, ASTM D7499, American Society of Testing and Materials.
- Abu-Farsakh, M., and Nazzal M., (2009). *Evaluation of the Base/Subgrade Soil under Repeated Loading: Phase 1 – Laboratory Testing and Numerical Modeling of Geogrid Reinforced Bases in Flexible Pavement*. Report No. FHWA/LA.04/450, Louisiana Transportation Research Center, Baton Rouge, LA, 121 p.
- Abu-Farsakh, M. Y. and Chen, Q. (2011). “Evaluation of Geogrid Base Reinforcement in Flexible Pavement Using Cyclic Plate Load Testing”, *International Journal of Pavement Engineering*, Vol. 12, No. 3, pp. 275-288.
- Al-Qadi, I.L., Brandon, T.L. and Bhutta, A. (1997). “Geosynthetic Stabilized Flexible Pavements”, *Proceedings of the Conference Geosynthetics '97*, Long Beach, California, USA, March, Vol. 2, pp. 647-662.
- ARA (Applied Research Associates). (2017). *Independent Review and Validation of Tensar's Modified 1993 AASHTO Pavement Design Procedure and Verification of SPECTRAPAVE4-PRO™ Software*, Champaign, IL, 89 p.
- Aran, S. (2006). “Base Reinforcement with Biaxial Geogrid—Long Term Performance”. *Transportation Research Record: Journal of the Transportation Research Board*, No. 1975, pp. 115–123.
- Barksdale, R. D., Brown, S. F. and Chan, F. (1989). *Potential Benefits of Geosynthetics in Flexible Pavement Systems*, National Cooperative Highway Research Program Report No. 315, Transportation Research Board, National Research Council, Washington DC.
- Berg, R.R., Christopher, B.R. and Perkins, S.W. (2000). *Geosynthetic Reinforcement of the Aggregate Base/Subbase Courses of Flexible Pavement Structures - GMA White Paper II*, Geosynthetic Materials Association, Roseville, MN, USA, 176 p.
- Cancelli, A., Montanelli, F., Rimoldi, P. and Zhao, A. (1996). “Full Scale Laboratory Testing on Geosynthetics Reinforced Paved Roads”, *Proceedings of the International Symposium on Earth Reinforcement*, Fukuoka/Kyushu, Japan, November, Balkema, pp. 573-578.

- Cancelli, A. and Montanelli, F. (1999). "In-Ground Test for Geosynthetic Reinforced Flexible Paved Roads", *Proceedings of the Conference Geosynthetics '99*, Boston, MA, USA, Vol. 2, pp. 863-878.
- Clapp, J. (2007). *Analysis of Rutting Development in Flexible Pavements with Geogrid-Reinforced Base Layers Using 3D Finite Element Analysis*. MS Thesis, University of Maine, 232 p.
- Collin, J. G., Kinney, T. C. and Fu, X. (1996). "Full Scale Highway Load Test of Flexible Pavement Systems with Geogrid Reinforced Base Courses", *Geosynthetics International*, Vol. 3, No. 4, pp. 537-549.
- Duncan, M.J. (2000). "Factors of Safety and Reliability in Geotechnical Engineering", *Journal of Geotechnical and Geoenvironmental Engineering*, ASCE, Vol. 125, No. 4, pp. 307-316.
- Ghafoori, N. and Sharbaf, M. (2015). "Evaluation of Triaxial Geogrids for Reduction of Base Thickness in Flexible Pavements", *Proceedings of the 6th International Conference on Bituminous Mixtures and Pavements*, pg. 141.
- Ghafoori, N. and Sharbaf, M. (2016). *Use of Geogrid for Strengthening and Reducing the Roadway Structural Sections*, Report No. 327-12-803, Nevada Department of Transportation, Carson City, NV.
- Haas, R., Wall, J., and Carroll, R.G. (1988). "Geogrid Reinforcement of Granular Bases in Flexible Pavements," In *Transportation Research Record 1188*, TRB, National Research Council, Washington DC, USA, pp. 19 – 27.
- Hanandeh, S., Abu-Farsakh, M., Louay, M., Chen, Q., and Saghebfar, M. (2016). "Full-Scale Accelerated Load Testing of Geosynthetics Reinforced/Stabilized Paved Roads Built Over Native Soft Subgrade", *Proceedings of the 3rd Pan-American Conference on Geosynthetics*, Miami, FL, 10 p.
- Helstrom, C.L., Humphrey, D.N. and Labbe, J.M. (2007). *Performance and Effectiveness of a Thin Pavement Section Using Geogrids and Drainage Composites in a Cold Region*. New England Transportation Consortium, NETCR 60, NETC Project No. 00-8, 265 p.
- Henry, K.S., Clapp, J., Davids, W. Humphrey, D. and Barna, L. (2009). *Structural Improvements of Flexible Pavements Using Geosynthetics for Base Course Reinforcement*, US Army Corps of Engineers Report ERDC\CRREL TR-09-11, 192p.
- Jersey, S.R., Tingle, J.S., Norwood, G.J., Kwon, J. and Wayne, M. (2012). "Full-Scale Evaluation of Geogrid-Reinforced Thin Flexible Pavements", *Transportation Research Record: Journal of the Transportation Research Board*, No. 2310, Washington, D.C., pp. 61-71.
- Kim, M. and Lee, J.H. (2013). "Effects of Geogrid Reinforcement in Low Volume Flexible Pavement", *Journal of Civil Engineering and Management*, Vol. 19, pp. 14-22.
- Kinney, T.C., Abbott, J. and Schuler, J. (1998). "Benefits of Using Geogrids for Base Reinforcement with Regard to Rutting", *Transportation Research Record: Journal of the Transportation Research Board*, No. 1611, Transportation Research Board, Washington, D.C., pp. 86-96.

- Kleyn, E.G. (1975). *The Use of the Dynamic Cone Penetrometer (DCP)*, South Africa, Transvaal Roads Department, Materials Branch.
- Konietzky, H., te Kamp, L., Gröger, T. & Jenner, C. 2004. "Use of DEM to Model the Interlocking Effect of Geogrids Under Static and Cyclic Loading", *Numerical Modeling in Micromechanics via Particle Methods*, A.A. Balkema, Rotterdam, pp. 3-12.
- Kwon, J., Tutumluer, E., and Kim, M. (2005a). "Development of a Mechanistic Model for Geosynthetic-Reinforced Flexible Pavements." *Geosynthetics International*, Vol. 12, No. 6, pp. 310-320.
- Kwon, J., Tutumluer, E. & Kim, M. (2005b). "Interface Modeling for Mechanistic Analysis of Geogrid Reinforced Flexible Pavements." In *Advances in Pavement Engineering, Proceedings of the GeoFrontiers Conference, Geotechnical Special Publication 130*, Schwartz, C. W., Tutumluer, E. & Tashman, L., Editors, ASCE, Austin, TX, CD-ROM.
- Kwon, J. (2007). *Development of a Mechanistic Model for Geogrid Reinforced Flexible Pavements*, Ph.D. Thesis, University of Illinois at Urbana-Champaign, 241 p.
- Kwon, J., Tutumluer, E. and Konietzky, H. (2008). "Aggregate Base Residual Stresses Affecting Geogrid Reinforced Flexible Pavement Response", *International Journal of Pavement Engineering*, Vol. 9, No. 4, pp. 275-285.
- Moayed, H., Kazemian, S., Prasad, A., and Huat, B.B.K. (2009). "Effect of Geogrid Reinforcement Location in Paved Road Improvement". *Electronic Journal of Geotechnical Engineering*, Vol. 14, Bundle P, 11 p.
- Kwon, J., Tutumluer, E. and Al-Qadi, I.L. (2009). "Validated Mechanistic Model for Geogrid Base Reinforced Flexible Pavements", *Journal of Transportation Engineering*, ASCE, Vol. 135, No. 12, pp.915-926.
- Luo, R., Gu, F., Luo, X., Lytton, R.L., Hajj, E.Y., Siddharthan, R.V., Elfass, S., Piratheepan, M., and Pournoman, S. (2017). *Quantifying the Influence of Geosynthetics on Pavement Performance*, National Cooperative Research Project Report 01-50, National Academy of Sciences, Washington, D.C.
- Moayed, H., Kazemian, S., Prasad, A., and Huat, B.B.K. (2009). "Effect of Geogrid Reinforcement Location in Paved Road Improvement", *Electronic Journal of Geotechnical Engineering*, Vol. 14, Bundle P, 11 p.
- Nazzal, M., Abu-Farsakh, M., and Mohammad, L., (2010). "Implementation of a Critical State Two-Surface Model to Evaluate the Response of Geosynthetic Reinforced Pavements," *ASCE International Journal of Geomechanics*, Vol. 10, No. 5, pp. 202-212.
- NCHRP (2004). *NCHRP Project 1-37A Design Guide, Mechanistic-Empirical Design of New and Rehabilitated Pavement Structures*, <http://www.trb.org/mepdg/>.
- Pearce, R. A. (1981). *Guidelines for Design of Flexible Pavements Using Mirafi® Woven Stabilization Fabrics*, Law Engineering, Houston, TX, 35p.
- Perkins, S.W. and Ismeik, M. (1997a). "A Synthesis and Evaluation of Geosynthetic Reinforced Base Course Layers in Flexible Pavements: Part I", *Geosynthetics International*, Vol. 4, No. 6, pp. 549-604.

- Perkins, S.W. and Ismeik, M. (1997b). "A Synthesis and Evaluation of Geosynthetic Reinforced Base Course Layers in Flexible Pavements: Part II", *Geosynthetics International*, Vol. 4, No. 6, pp. 605-621.
- Perkins, S.W. (1999). *Geosynthetic Reinforcement of Flexible Pavements: Laboratory Based Pavement Test Sections*, U.S. Department of Transportation, Federal Highway Administration, Washington, DC, Report No. FHWA/MT-99/8106-1, 140 p.
- Perkins, S.W. (2001a). *Mechanistic-Empirical Modeling and Design Model Development of Geosynthetic Reinforced Flexible Pavements*, U.S. Department of Transportation, Federal Highway Administration, Washington, DC, Report No. FHWA/MT-01-002/99160-1, 170 p.
- Perkins, S.W. (2001b). *Numerical Modeling of Geosynthetic Reinforced Flexible Pavements*, U.S. Department of Transportation, Federal Highway Administration, Washington, DC, Report No. FHWA/MT-01-003/99160-2, 97 p.
- Perkins, S.W. (2002). *Evaluation of Geosynthetic Reinforced Flexible Pavement Systems Using Two Pavement Test Facilities*. U.S. Department of Transportation, Federal Highway Administration, Washington, DC, Report No. FHWA/MT-02-008/20040, 120 p.
- Perkins, S.W. and Edens, M.Q. (2003). "A Design Model for Geosynthetic-Reinforced Pavements", *International Journal of Pavement Engineering*, Vol. 4, No. 1, pp. 37-50.
- Perkins, S.W., Christopher, B.R., Eiksund, G.R., Schwartz, C.W. and Svanø, G. (2004). *Development of Design Methods for Geosynthetic Reinforced Flexible Pavements*, U.S. Department of Transportation, Federal Highway Administration, Washington, DC, FHWA Report Reference Number DTFH61-01-X-00068, 263p
- Perkins, S.W., Christopher, B.R., Eiksund, G.R., Schwartz, C.W. and Svanø, G. (2005). "Modeling Effects of Reinforcement on Lateral Confinement of Roadway Aggregate", *Proceedings of the Conference GeoFrontiers, Geotechnical Special Publication 130, Advances in Pavement Engineering*, ASCE, Austin, Texas.
- Perkins, S.W. and Cortez, E.R. (2005). "Evaluation of Base-Reinforced Pavements Using a Heavy Vehicle Simulator", *Geosynthetics International*, Vol. 12, No. 2, pp. 86-98.
- Perkins, S.W., Eiksund, G.R. (2005). "Geosynthetic Material Properties for Use in 2-D Finite Element Pavement Response Models", *Proceedings of the Seventh International Conference on the Bearing Capacity of Roads, Railways and Airfields*, Trondheim, Norway.
- Perkins, S.W. and Haselton, H.N. (2019). "Resilient Response of Geosynthetics from Cyclic and Sustained In-Air Tensile Loading", *Geosynthetics International*, Vol. 25, No. 4, pp. 428-435.
- Perkins, S.W., Haselton, H.N. and Newman, E.C. (2020). "Orthotropic Elastic Constants of Geosynthetics from Biaxial Tension Tests", Accepted for publication in *Geosynthetics International*, Ahead of Print, pp. 1–44, Published online: December 3, 2020, <https://doi.org/10.1680/jgein.20.00044>
- Robinson, W.J., Tingle, J.S., Norwood, G.J., Wayne, M.H. and Kwon, J. (2018). "Performance of Multi-Axial Geogrid Stabilized Flexible Pavements", *Journal of Ground Improvement*, Ahead of Print, pp. 1–32, Published online: March 28, 2018.

- Saad, B., Mitri, H., and Poorooshab, H. (2006). "3D FE Analysis of Flexible Pavement with Geosynthetic Reinforcement". *Journal of Transportation Engineering*, Vol. 132, No. 5, pp. 402–415.
- Saghebfar, M., Hossain, M. and Lacina, B.A. (2016). "Performance of Geotextile-Reinforced Bases for Paved Roads", *Transportation Research Record: Journal of the Transportation Research Board*, No. 2580, Transportation Research Board, Washington, D.C., pp. 27-33.
- Sharp, J. (2005). *Elk Street North Geogrid Test Section*, Wyoming Department of Transportation Internal Report, 12p.
- Tang, X., Chehab, G.R., Palomino, A.M. (2008). "Accelerated Testing of Geogrid-Reinforced Subgrade in Flexible Pavements", *Proceedings of the Conference GeoCongress 2008*, pp. 1049-1056.
- Tenax (2001). *Design of Flexible Pavements with Tenax Geogrids*. Technical Reference GRID-DE-2, February. 14p.
- TenCate (2010). *Flexible Pavement Design Using TenCate Mirafi Geosynthetics*, TenCate Mirafi, Pendergrass, GA, July, 7 p.
- Tensar (1996). *Design Guideline for Flexible Pavements with Tensar Geogrid Reinforced Base Layers*. Technical Note TTN:BR96, April, 77p.
- Tensar (2014). *SpectraPave4 PRO™ Software for Subgrade Stabilization and Pavement Optimization – Version 4.6.1*, January.
- Thompson, M.R. and Raad, L. (1979). *Fabric Utilization in Transportation Support Systems (Low- Deformation Criteria)*. Civil Engineering Studies, Department of Civil Engineering, University of Illinois, December, 40p.
- Valero, S.N., Sprague, C.J. and Wrigley, N.E. (2014). "Full Scale Trafficking of Geogrid Reinforced Sections Under Realistic Service Conditions", *Proceedings of the 10th International Conference on Geosynthetics*, Berlin, Germany.
- Webster, S. L. (1993). *Geogrid Reinforced Base Courses for Flexible Pavements for Light Aircraft, Test Section Construction, Behavior Under Traffic, Laboratory Tests, and Design Criteria*, Technical Report GL-93-6, USAE Waterways Experiment Station, Vicksburg, Mississippi, USA, 86 p.
- White, D.J., Vennapusa, P.K.R., Gieselman, H.H., Douglas, S.C., Zhang, J. and Wayne, M.H. (2011). "In-Ground Dynamic Stress Measurements for Geosynthetic Reinforced Subgrade/Subbase", *Proceedings of the Conference Geo-Frontiers*, ASCE, pp. 4663-4672.

12 Appendix A: HMA Material Testing Data Sheets

Dynamic modulus tests on Montana mixes



Project: TRI Environmental, Inc
 Date: 11/19/2018
 Sample ID: Dynamic Modulus

Project Notes

Specimens for testing were compacted at NCAT from re-heated plant-produced mix provided by the client
 Three specimens for each mix were prepared and tested in accordance with AASHTO R83-17 to a target of 7.0 +/- 0.5 percent air voids
 Volumetric properties (Gmm, AC%, Gsb) required to calculate the specimen VMA and VFA were provided by the client
 Testing was performed in accordance with AASHTO T378-17 with the testing conditions recommended in AASHTO R84-17
 Dynamic Modulus Testing Temperatures were 4, 20, and 40°C
 Specimens were tested at 10, 1, and 0.1 Hz loading frequencies at all temperatures
 The 0.01 Hz loading frequency was only used at the high temperature
 Analysis was performed using the Mastersolver.exe program
 Dynamic Modulus testing provides a characterization of the stiffness and visco-elastic properties of the mixture across a wide range of temperatures and loading conditions

Results Summary

A summary of the specimens volumetrics is provided in Table 1
 The individual specimen results for the individual mixes are provided in Tables 2, 3, and 4
 The mastercurve coefficients are provided in Table 4 while the mastercurve plots are shown in Figure 1
 Visual inspection of the mastercurves showed the three test mixtures to have very similar Dynamic Modulus results

Table 1: Individual Specimen Volumetrics

Mix ID	Sample ID	Sample Air Voids, %	QC Gsb	QC Pb	Gmm	Gmb	VMA	VFA
Test 20 (Ashland)	5	7.3	2.592	5.1	2.455	2.276	16.7	56.2
Test 20 (Ashland)	6	7.4	2.592	5.1	2.455	2.273	16.8	55.8
Test 20 (Ashland)	7	7.1	2.592	5.1	2.455	2.281	16.5	56.9
Bridger Canyon	4	7.2	2.607	5.3	2.440	2.264	17.7	59.4
Bridger Canyon	5	7.4	2.607	5.3	2.440	2.259	17.9	58.7
Bridger Canyon	6	7.5	2.607	5.3	2.440	2.257	18.0	58.4
Great Falls	9	6.7	2.577	5.4	2.420	2.258	17.1	60.8
Great Falls	10	6.5	2.577	5.4	2.420	2.263	16.9	61.5
Great Falls	11	7.4	2.577	5.4	2.420	2.241	17.7	58.2

Table 2: Individual Specimen Data - Test 20 (Ashland)

Conditions		Specimen 1		Specimen 2		Specimen 3	
Temperature °C	Frequency Hz	E* Ksi	Phase Angle deg	E* Ksi	Phase Angle deg	E* Ksi	Phase Angle deg
4	0.1	729.7	23.4	625.8	24.7	758.8	24.2
4	1	1,180.5	17.0	1,016.3	18.2	1,248.8	17.8
4	10	1,670.7	12.1	1,447.3	13.1	1,821.7	12.7
20	0.1	131.4	34.9	123.9	34.2	149.7	33.7
20	1	335.5	32.3	308.5	32.0	364.8	31.6
20	10	689.7	25.9	629.6	26.2	732.2	25.7
40	0.01	14.5	12.7	15.4	9.1	18.0	10.3
40	0.1	20.0	21.9	19.8	19.3	23.2	19.7
40	1	41.1	32.2	38.9	29.8	43.2	29.9
40	10	120.3	36.7	114.7	34.9	120.1	35.0

Table 3: Individual Specimen Data - Bridger Canyon

Conditions		Specimen 1		Specimen 2		Specimen 3	
Temperature °C	Frequency Hz	E* Ksi	Phase Angle deg	E* Ksi	Phase Angle deg	E* Ksi	Phase Angle deg
4	0.1	759.3	24.0	755.6	23.2	642.7	24.4
4	1	1,211.2	17.2	1,207.9	16.8	1,047.9	17.8
4	10	1,684.2	12.0	1,711.6	12.0	1,485.9	12.8
20	0.1	159.0	33.4	142.4	33.7	123.8	34.2
20	1	390.6	30.8	359.3	31.1	320.7	31.9
20	10	777.8	24.9	726.1	25.1	661.1	25.9
40	0.01	19.8	10.7	17.4	10.8	15.1	10.1
40	0.1	24.3	20.5	21.7	20.8	18.6	20.1
40	1	47.2	31.2	42.8	30.9	35.3	31.8
40	10	137.5	35.5	124.2	35.5	105.5	36.7

Dynamic modulus tests on Montana mixes (continued)

Table 4: Individual Specimen Data - Great Falls

Conditions		Specimen 1		Specimen 2		Specimen 3	
Temperature	Frequency	E*	Phase Angle	E*	Phase Angle	E*	Phase Angle
°C	Hz	Ksi	deg	Ksi	deg	Ksi	deg
4	0.1	701.0	24.2	684.1	24.1	567.2	26.2
4	1	1,163.1	18.0	1,144.9	18.2	937.7	19.6
4	10	1,676.5	13.0	1,661.1	13.3	1,351.5	14.0
20	0.1	122.2	32.0	129.0	32.8	110.9	33.2
20	1	305.0	31.3	315.0	31.7	276.2	32.6
20	10	642.8	26.5	658.3	26.5	583.5	27.3
40	0.01	17.6	14.1	17.4	15.9	14.1	15.3
40	0.1	23.2	20.6	24.0	23.1	17.9	23.6
40	1	42.0	29.0	45.3	30.8	33.7	32.5
40	10	111.7	34.1	118.9	35.3	96.8	36.7

Table 5: Mastercurve Coefficients

Mix ID	Max E* (Ksi)	Min E* (Ksi)	Beta	Gamma	EA	R ²	Se/Sy
Test 20 (Ashland)	3,187.9	6.51	-0.524	-0.579	195,848	0.993	0.06
Bridger Canyon	3,141.9	7.22	-0.528	-0.590	196,118	0.989	0.07
Great Falls	3,181.4	7.28	-0.426	-0.578	194,600	0.994	0.05

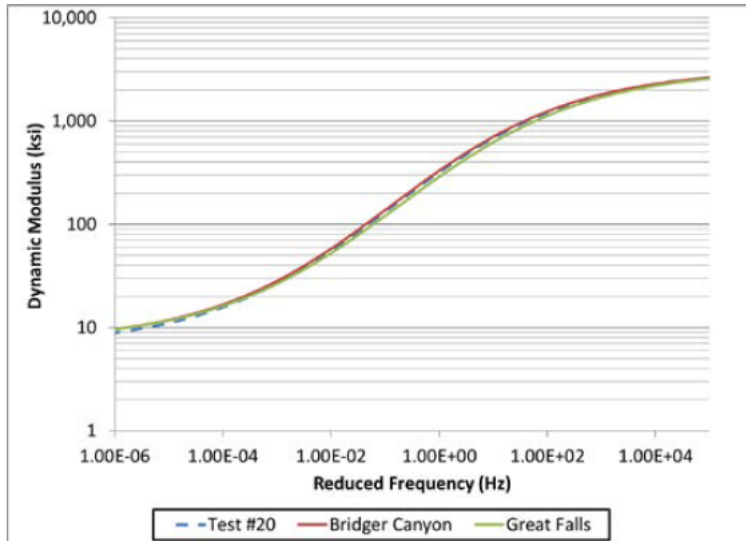


Figure 1: E* Mastercurve Comparison

Appendix A: HMA Material Testing Data Sheets

Batch plant mix test results on SC Surface C mix

ROGERS GROUP GREER - ASPHALT PLANT WORKSHEET NO. 1

File No.:	Project victory	Date:	9/23/19	SC-T-101:	73
Type Mix:	Surface C	Time:	08:30	Tonnage Taken:	80.00
Job Mix No.:	E0130	Sample No.:	8 - 1	Load Weight:	20.30
Temp. Corr. Factor:	0.23	Mix Temp.:	300°	Load No.:	4
Mix Corr. Factor:	0.03	Silo No.:	1		
Oven Type:	NCAT	Tested By:	jordan milford		

Extraction	
Weight of Basket and Sample	4468.4
Weight of Basket	3191.4
Weight of Sample	1277.0
% Asphalt Binder Content (PG 64-22)	5.55
	Tolerance (-/+)
	5.34 6.06

MSG / ESG	Sample 1	Sample 2
(A) Weight of Bowl and Sample in Air	3670.5	3701.2
(B) Weight of Bowl in Air	2154.9	2204.2
(C) Weight of Sample in Air (A-B)	1515.6	1497.0
(D) Weight of Bowl and Sample under water	2258.0	2277.5
(E) Weight of Bowl under Water	1360.3	1391.9
(F) Weight of Sample under water (D-E)	897.7	885.6
Specific Gravity of Binder	1.034	1.034
MSG	2.453	2.448
ESG	2.668	2.662

Average MSG	2.451
Average ESG	2.665

Core Bulk SG Properties	
WEIGHT IN AIR, gms.	4740.6
WEIGHT IN WATER, gms.	2718.4
SSD WEIGHT, gms.	4742.0
VOLUME	2023.6
BSG	2.343
MSG	2.451
% AIR VOIDS	4.41
% VMA	16.99
STABILITY	

AVERAGE BSG	2.345
AVERAGE DENSITY, pcf	146.33
AVERAGE % AIR VOIDS	4.35
AVERAGE % VMA	16.93
AVERAGE STABILITY	

	Tolerance (-/+)
	3.21 - 5.51
	16.26 - 18.56

Mix Gradation	Before Sieve Weight (SC-T-102)									
	37.5mm	25.0mm	19.0mm	12.5mm	9.5mm	4.75mm	2.36mm	0.60mm	0.150mm	0.075mm
SIEVE, mm	1.5"	1"	3/4"	1/2"	3/8"	#4	#8	#30	#100	#200
WEIGHT PASSING	1207.0	1207.0	1207.0	1185.3	1117.3	815.0	585.8	352.0	109.5	53.8
PERCENT PASSING	100.0	100.0	100.0	98.2	92.6	67.5	48.5	29.2	9.1	4.46
JOB MIX TARGET	100.0	100.0	100.0	99.0	94.0	68.0	50.0	30.0	11.0	5.0
JOB MIX USL	100.0	100.0	100.0	100.0	100.0	75.0	56.0	35.0	15.0	7.0
JOB MIX LSL	100.0	100.0	100.0	97.0	87.0	61.0	44.0	25.0	7.0	3.0
(PERCENT PASSING - TARGET)	0.00	0.00	0.00	(0.80)	(1.40)	(0.50)	(1.50)	(0.80)	(1.90)	(0.54)

D/A Ratio	0.80
-----------	------

PAY ITEMS:	% Binder	5.55	3/8 in. Sieve	92.6	No. 8 Sieve	48.5
------------	----------	------	---------------	------	-------------	------

Nuclear density test results on compacted HMA**ASPHALT PLACEMENT
DENSITY**

Client:
TRI/Environmental, Inc.
4915 Clemson Blvd.
Anderson, SC 29621

Report #: BNG-000007
Report Date: 11/21/2019
Test Method: ASTM D2950

Project:
142619038
TRI On-Call Lab Testing
Anderson
Anderson, SC 29621

Test Results															
Test #	Retest Of	Test Date	Test Location	Material	Mix Design	Thickness (in)	Max Density (pcf)	Density Source	In Place Density (pcf)	Probe Depth (in)	Percent Comp.	Min/Max Comp. (%)	Remark	Gauge SN	Technician
55		9/23/19	PAVEMENT: Test Strip 1	Surface	E0130		152.9	Supplied Value	140.6	Backscatter	92	92 / 95		31917	WESLEY EDWARDS
56		9/23/19	PAVEMENT: Test Strip 1	Surface	E0130		152.9	Supplied Value	140.6	Backscatter	92	92 / 95		31917	WESLEY EDWARDS
57		9/23/19	PAVEMENT: Test Strip 1	Surface	E0130		152.9	Supplied Value	136.6	Backscatter	89	92 / 95	FAIL	31917	WESLEY EDWARDS
58		9/23/19	PAVEMENT: Test Strip 1	Surface	E0130		152.9	Supplied Value	138.2	Backscatter	90	92 / 95	FAIL	31917	WESLEY EDWARDS
59		9/23/19	PAVEMENT: Test Strip 1	Surface	E0130		152.9	Supplied Value	137.3	Backscatter	90	92 / 95	FAIL	31917	WESLEY EDWARDS
60		9/23/19	PAVEMENT: Test Strip 1	Surface	E0130		152.9	Supplied Value	137.1	Backscatter	90	92 / 95	FAIL	31917	WESLEY EDWARDS
Remarks								Comments							
FAIL: Tests results DO NOT comply with specifications								Tests are "Direct Transmission" (Method A) unless probe depth is noted as "Backscatter"							
Gauge Information															
Gauge SN	Make	Model	Density Count	Moisture Count	Standard Count Date	Last Calibration Date	Last Calibrated By								
31917	Troxler	3430	1925	510	9/23/19	12/26/18	InstroTek Inc.								

Tests are "Direct Transmission" (Method A) unless probe depth is noted as "Backscatter"

B. E. Hughes

Reviewed/Prepared by:
WILLIAM BRIAN VAUGHAN
Nov 21, 2019

The above tests were performed in general accordance with the applicable test method, except for known deviations noted above.

Page 1 of 18

Nuclear density test results on compacted HMA**ASPHALT PLACEMENT
DENSITY**

Report #: BNG-000026
Report Date: 11/21/2019
Test Method: ASTM D2950

Client:

TRI/Environmental, Inc.
4915 Clemson Blvd.
Anderson, SC 29621

Project:

142619038
TRI On-Call Lab Testing
Anderson
Anderson, SC 29621



Test Results															
Test #	Retest Or	Test Date	Test Location	Material	Mix Design	Thickness (in)	Max Density (pcf)	Max Density Source	In Place Density (pcf)	Probe Depth (in)	Percent Comp.	Min/Max Comp. (%)	Remark	Gauge SN	Technician
61		9/23/19	PAVEMENT: Test Strip 1 B - West (1)	Surface	E0130		152.9	Supplied Value	142.3	Backscatter	93	92 / 95		31917	WESLEY EDWARDS
62		9/23/19	PAVEMENT: Test Strip 1 B - West (2)	Surface	E0130		152.9	Supplied Value	138.1	Backscatter	90	92 / 95	FAIL	31917	WESLEY EDWARDS
63		9/23/19	PAVEMENT: Test Strip 1 B - Center (1)	Surface	E0130		152.9	Supplied Value	138.4	Backscatter	91	92 / 95	FAIL	31917	WESLEY EDWARDS
64		9/23/19	PAVEMENT: Test Strip 1 B - Center (2)	Surface	E0130		152.9	Supplied Value	139.7	Backscatter	91	92 / 95	FAIL	31917	WESLEY EDWARDS
65		9/23/19	PAVEMENT: Test Strip 1 B - East (1)	Surface	E0130		152.9	Supplied Value	139.1	Backscatter	91	92 / 95	FAIL	31917	WESLEY EDWARDS
66		9/23/19	PAVEMENT: Test Strip 1 B - East (2)	Surface	E0130		152.9	Supplied Value	139.2	Backscatter	91	92 / 95	FAIL	31917	WESLEY EDWARDS
Remarks										Comments					
FAIL: Tests results DO NOT comply with specifications										Tests are "Direct Transmission" (Method A) unless probe depth is noted as "Backscatter"					
Gauge Information															
Gauge SN	Make	Model	Density Count	Moisture Count	Standard Count Date	Last Calibration Date	Last Calibrated By								
31917	Troxler	3430	1925	510	9/23/19	12/26/18	InstroTek Inc.								

Reviewed/Prepared by:
WILLIAM BRIAN VAUGHAN
Nov 21, 2019

The above tests were performed in general accordance with the applicable test method, except for known deviations noted above.

Page 2 of 18

Nuclear density test results on compacted HMA**ASPHALT PLACEMENT
DENSITY**

Client: TRI/Environmental, Inc.
4915 Clemson Blvd.
Anderson, SC 29621

Report #: BNG-000010
Report Date: 11/21/2019
Test Method: ASTM D2950

Project: 142619038
TRI On-Call Lab Testing
Anderson
Anderson, SC 29621


Test Results															
Test #	Retest Of	Test Date	Test Location	Material	Mix Design	Thickness (in)	Max Density (pcf)	Max Density Source	In Place Density (pcf)	Probe Depth (in)	Percent Comp.	Min/Max Comp. (%)	Remark	Gauge SN	Technician
67		9/23/19	PAVEMENT: Test Strip 1 C - West (1)	Surface	E0130		152.9	Supplied Value	136.1	Backscatter	89	92 / 95	FAIL	31917	WESLEY EDWARDS
68		9/23/19	PAVEMENT: Test Strip 1 C - West (2)	Surface	E0130		152.9	Supplied Value	137.9	Backscatter	90	92 / 95	FAIL	31917	WESLEY EDWARDS
69		9/23/19	PAVEMENT: Test Strip 1 C - Center (1)	Surface	E0130		152.9	Supplied Value	136.5	Backscatter	89	92 / 95	FAIL	31917	WESLEY EDWARDS
70		9/23/19	PAVEMENT: Test Strip 1 C - Center (2)	Surface	E0130		152.9	Supplied Value	135.1	Backscatter	88	92 / 95	FAIL	31917	WESLEY EDWARDS
71		9/23/19	PAVEMENT: Test Strip 1 C - East (1)	Surface	E0130		152.9	Supplied Value	139.2	Backscatter	91	92 / 95	FAIL	31917	WESLEY EDWARDS
72		9/23/19	PAVEMENT: Test Strip 1 C - East (2)	Surface	E0130		152.9	Supplied Value	137.9	Backscatter	90	92 / 95	FAIL	31917	WESLEY EDWARDS
Remarks										Comments					
FAIL: Tests results DO NOT comply with specifications										Tests are "Direct Transmission" (Method A) unless probe depth is noted as "Backscatter"					
Gauge Information															
Gauge SN	Make	Model	Density Count	Moisture Count	Standard Count Date	Last Calibration Date	Last Calibrated By								
31917	Troxler	3430	1925	510	9/23/19	12/26/18	InstroTek Inc.								

Reviewed/Prepared by:
WILLIAM BRIAN VAUGHAN
Nov 21, 2019

The above tests were performed in general accordance with the applicable test method, except for known deviations noted above.

Page 3 of 18

Nuclear density test results on compacted HMA

 S&M, Inc. 301 Zima Park Drive Spartanburg, SC 29301 Phone: 864-574-2360 Fax: 864-576-8730		Client: TRI/Environmental, Inc. 4915 Clemson Blvd. Anderson, SC 29621		Project: 142619038 TRI On-Call Lab Testing Anderson Anderson, SC 29621	
		ASPHALT PLACEMENT DENSITY Report #: BNG-000011 Report Date: 11/21/2019 Test Method: ASTM D2950			

Test Results															
Test #	Retest Of	Test Date	Test Location	Material	Mix Design	Thickness (in)	Max Density (pcf)	Max Density Source	In Place Density (pcf)	Probe Depth (in)	Percent Comp.	Min/Max Comp. (%)	Remark	Gauge SN	Technician
73		9/23/19	PAVEMENT: Test Strip 1 D - West (1)	Surface	E0130		152.9	Supplied Value	136.8	Backscatter	89	92 / 95	FAIL	31917	WESLEY EDWARDS
74		9/23/19	PAVEMENT: Test Strip 1 D - West (2)	Surface	E0130		152.9	Supplied Value	136.9	Backscatter	90	92 / 95	FAIL	31917	WESLEY EDWARDS
75		9/23/19	PAVEMENT: Test Strip1 D - Center (1)	Surface	E0130		152.9	Supplied Value	137.5	Backscatter	90	92 / 95	FAIL	31917	WESLEY EDWARDS
76		9/23/19	PAVEMENT: Test Strip1 D - Center (2)	Surface	E0130		152.9	Supplied Value	135.8	Backscatter	89	92 / 95	FAIL	31917	WESLEY EDWARDS
77		9/23/19	PAVEMENT: Test Strip 1 D - East (1)	Surface	E0130		152.9	Supplied Value	136.9	Backscatter	90	92 / 95	FAIL	31917	WESLEY EDWARDS
78		9/23/19	PAVEMENT: Test Strip 1 D - East (2)	Surface	E0130		152.9	Supplied Value	137.4	Backscatter	90	92 / 95	FAIL	31917	WESLEY EDWARDS
Remarks							Comments								
FAIL: Tests results DO NOT comply with specifications							Tests are "Direct Transmission" (Method A) unless probe depth is noted as "Backscatter"								
Gauge Information															
Gauge SN	Make	Model	Density Count	Moisture Count	Standard Count Date	Last Calibration Date	Last Calibrated By								
31917	Troxler	3430	1925	510	9/23/19	12/26/18	InstroTek Inc.								



Reviewed/Prepared by:
 WILLIAM BRIAN VAUGHAN
 Nov 21, 2019

The above tests were performed in general accordance with the applicable test method, except for known deviations noted above.

Page 4 of 18

Nuclear density test results on compacted HMA**ASPHALT PLACEMENT
DENSITY**

Client: TRI/Environmental, Inc.
4915 Clemson Blvd.
Anderson, SC 29621

Report #: BNG-000012
Report Date: 11/21/2019
Test Method: ASTM D2950

Project: 142619038
TRI On-Call Lab Testing
Anderson
Anderson, SC 29621


Test Results															
Test #	Retest Of	Test Date	Test Location	Material	Mix Design	Thickness (in)	Max Density (pcf)	Max Density Source	In Place Density (pcf)	Probe Depth (in)	Percent Comp.	Min/Max Comp. (%)	Remark	Gauge SN	Technician
79		9/23/19	PAVEMENT: Test Strip 1	Surface	E0130		152.9	Supplied Value	139.2	Backscatter	91	92 / 95	FAIL	31917	WESLEY EDWARDS
80		9/23/19	PAVEMENT: Test Strip 1	Surface	E0130		152.9	Supplied Value	138.5	Backscatter	91	92 / 95	FAIL	31917	WESLEY EDWARDS
81		9/23/19	PAVEMENT: Test Strip 1	Surface	E0130		152.9	Supplied Value	138.6	Backscatter	91	92 / 95	FAIL	31917	WESLEY EDWARDS
82		9/23/19	PAVEMENT: Test Strip 1	Surface	E0130		152.9	Supplied Value	136.5	Backscatter	89	92 / 95	FAIL	31917	WESLEY EDWARDS
83		9/23/19	PAVEMENT: Test Strip 1	Surface	E0130		152.9	Supplied Value	137.5	Backscatter	90	92 / 95	FAIL	31917	WESLEY EDWARDS
84		9/23/19	PAVEMENT: Test Strip 1	Surface	E0130		152.9	Supplied Value	139.0	Backscatter	91	92 / 95	FAIL	31917	WESLEY EDWARDS
Remarks										Comments					
FAIL: Tests results DO NOT comply with specifications										Tests are "Direct Transmission" (Method A) unless probe depth is noted as "Backscatter"					
Gauge Information															
Gauge SN	Make	Model	Density Count	Moisture Count	Standard Count Date	Last Calibration Date	Last Calibrated By								
31917	Troxler	3430	1925	510	9/23/19	12/26/18	InstroTek Inc.								

Reviewed/Prepared by:
WILLIAM BRIAN VAUGHAN
Nov 21, 2019

The above tests were performed in general accordance with the applicable test method, except for known deviations noted above.

Page 5 of 18

Nuclear density test results on compacted HMA

ASPHALT PLACEMENT DENSITY		Client:	Project:
		TRI/Environmental, Inc. 4915 Clemson Blvd. Anderson, SC 29621	142619038 TRI On-Call Lab Testing Anderson Anderson, SC 29621
Report #: BNG-000013			
Report Date: 11/21/2019			
Test Method: ASTM D2950			

Test Results															
Test #	Retest Of	Test Date	Test Location	Material	Mix Design	Thickness (in)	Max Density (pcf)	Max Density Source	In Place Density (pcf)	Probe Depth (in)	Percent Comp.	Min/Max Comp. (%)	Remark	Gauge SN	Technician
85		9/23/19	PAVEMENT: Test Strip 1	Surface	E0130		152.9	Supplied Value	136.6	Backscatter	89	92 / 95	FAIL	31917	WESLEY EDWARDS
86		9/23/19	PAVEMENT: Test Strip 1	Surface	E0130		152.9	Supplied Value	135.6	Backscatter	89	92 / 95	FAIL	31917	WESLEY EDWARDS
87		9/23/19	PAVEMENT: Test Strip 1	Surface	E0130		152.9	Supplied Value	137.8	Backscatter	90	92 / 95	FAIL	31917	WESLEY EDWARDS
88		9/23/19	PAVEMENT: Test Strip 1	Surface	E0130		152.9	Supplied Value	137.9	Backscatter	90	92 / 95	FAIL	31917	WESLEY EDWARDS
89		9/23/19	PAVEMENT: Test Strip 1	Surface	E0130		152.9	Supplied Value	136.7	Backscatter	89	92 / 95	FAIL	31917	WESLEY EDWARDS
90		9/23/19	PAVEMENT: Test Strip 1	Surface	E0130		152.9	Supplied Value	135.3	Backscatter	88	92 / 95	FAIL	31917	WESLEY EDWARDS
Remarks												Comments			
FAIL: Tests results DO NOT comply with specifications															
Tests are "Direct Transmission" (Method A) unless probe depth is noted as "Backscatter"															
Gauge Information															
Gauge SN	Make	Model	Density Count	Moisture Count	Standard Count Date	Last Calibration Date	Last Calibrated By								
31917	Troxler	3430	1925	510	9/23/19	12/26/18	InstroTek Inc.								




Reviewed/Prepared by:
WILLIAM BRIAN VAUGHAN
Nov 21, 2019

The above tests were performed in general accordance with the applicable test method, except for known deviations noted above.

Page 6 of 18

Nuclear density test results on compacted HMA

		ASPHALT PLACEMENT DENSITY Report #: BNG-000014 Report Date: 11/21/2019 Test Method: ASTM D2950		Client: TRI/Environmental, Inc. 4915 Clemson Blvd. Anderson, SC 29621	Project: 142619038 TRI On-Call Lab Testing Anderson Anderson, SC 29621
SAME, Inc. 301 Zima Park Drive Spartanburg, SC 29301 Phone: 864-574-2360 Fax: 864-576-8730					

Test Results														
Test #	Retest Of	Test Date	Test Location	Material	Mix Design	Thickness (in)	Max Density (pcf)	In Place Density (pcf)	Probe Depth (in)	Percent Comp.	Min/Max Comp. (%)	Remark	Gauge SN	Technician
91		9/23/19	PAVEMENT: Test Strip 2	Surface	E0130		152.9	141.3	Backscatter	92	92 / 95		31917	WESLEY EDWARDS
92		9/23/19	PAVEMENT: Test Strip 2	Surface	E0130		152.9	138.0	Backscatter	90	92 / 95	FAIL	31917	WESLEY EDWARDS
93		9/23/19	PAVEMENT: Test Strip 2	Surface	E0130		152.9	136.3	Backscatter	89	92 / 95	FAIL	31917	WESLEY EDWARDS
94		9/23/19	PAVEMENT: Test Strip 2	Surface	E0130		152.9	136.3	Backscatter	89	92 / 95	FAIL	31917	WESLEY EDWARDS
95		9/23/19	PAVEMENT: Test Strip 2	Surface	E0130		152.9	140.6	Backscatter	92	92 / 95		31917	WESLEY EDWARDS
96		9/23/19	PAVEMENT: Test Strip 2	Surface	E0130		152.9	143.7	Backscatter	94	92 / 95		31917	WESLEY EDWARDS
Remarks												Comments		
FAIL: Tests results DO NOT comply with specifications														
Tests are "Direct Transmission" (Method A) unless probe depth is noted as "Backscatter"														
Gauge Information														
Gauge SN	Make	Model	Density Count	Moisture Count	Standard Count Date	Last Calibration Date	Last Calibrated By							
31917	Troxler	3430	1925	510	9/23/19	12/26/18	InstroTek Inc.							



Reviewed/Prepared by:
WILLIAM BRIAN VAUGHAN
Nov 21, 2019

The above tests were performed in general accordance with the applicable test method, except for known deviations noted above.

Page 7 of 18

Nuclear density test results on compacted HMA

ASPHALT PLACEMENT DENSITY

Report #: BNG-000015
Report Date: 11/21/2019
Test Method: ASTM D2950

Client: TRI/Environmental, Inc.
4915 Clemson Blvd.
Anderson, SC 29621

Project: 142619038
TRI On-Call Lab Testing
Anderson
Anderson, SC 29621

Test Results															
Test #	Retest Or	Test Date	Test Location	Material	Mix Design	Thickness (in)	Max Density (pcf)	Max Density Source	In Place Density (pcf)	Probe Depth (in)	Percent Comp.	Min/Max Comp. (%)	Remark	Gauge SN	Technician
97		9/23/19	PAVEMENT: Test Strip 2 B - West (1)	Surface	E0130		152.9	Supplied Value	139.8	Backscatter	91	92 / 95	FAIL	31917	WESLEY EDWARDS
98		9/23/19	PAVEMENT: Test Strip 2 B - West (2)	Surface	E0130		152.9	Supplied Value	138.8	Backscatter	91	92 / 95	FAIL	31917	WESLEY EDWARDS
99		9/23/19	PAVEMENT: Test Strip 2 B - Center (1)	Surface	E0130		152.9	Supplied Value	143.1	Backscatter	94	92 / 95		31917	WESLEY EDWARDS
100		9/23/19	PAVEMENT: Test Strip 2 B - Center (2)	Surface	E0130		152.9	Supplied Value	140.9	Backscatter	92	92 / 95		31917	WESLEY EDWARDS
101		9/23/19	PAVEMENT: Test Strip 2 B - East (1)	Surface	E0130		152.9	Supplied Value	137.7	Backscatter	90	92 / 95	FAIL	31917	WESLEY EDWARDS
102		9/23/19	PAVEMENT: Test Strip 2 B - East (2)	Surface	E0130		152.9	Supplied Value	136.6	Backscatter	89	92 / 95	FAIL	31917	WESLEY EDWARDS
Remarks								Comments							
FAIL: Tests results DO NOT comply with specifications								Tests are "Direct Transmission" (Method A) unless probe depth is noted as "Backscatter"							
Gauge Information															
Gauge SN	Make	Model	Density Count	Moisture Count	Standard Count Date	Last Calibration Date	Last Calibrated By								
31917	Troxler	3430	1925	510	9/23/19	12/26/18	InstroTek Inc.								

B. E. Vaughan

Reviewed/Prepared by:
WILLIAM BRIAN VAUGHAN
Nov 21, 2019

The above tests were performed in general accordance with the applicable test method, except for known deviations noted above.

Page 8 of 18

Nuclear density test results on compacted HMA

ASPHALT PLACEMENT DENSITY

Report #: BNG-000016
Report Date: 11/21/2019
Test Method: ASTM D2950

Client: TRI/Environmental, Inc.
4915 Clemson Blvd.
Anderson, SC 29621

Project: 142619038
TRI On-Call Lab Testing
Anderson
Anderson, SC 29621

Test Results															
Test #	Retest Of	Test Date	Test Location	Material	Mix Design	Thickness (in)	Max Density (pcf)	Max Density Source	In Place Density (pcf)	Probe Depth (in)	Percent Comp.	Min/Max Comp. (%)	Remark	Gauge SN	Technician
103		9/23/19	PAVEMENT: Test Strip 2	Surface	E0130		152.9	Supplied Value	139.3	Backscatter	91	92 / 95	FAIL	31917	WESLEY EDWARDS
104		9/23/19	PAVEMENT: Test Strip 2	Surface	E0130		152.9	Supplied Value	138.1	Backscatter	90	92 / 95	FAIL	31917	WESLEY EDWARDS
105		9/23/19	PAVEMENT: Test Strip 2	Surface	E0130		152.9	Supplied Value	140.2	Backscatter	92	92 / 95		31917	WESLEY EDWARDS
106		9/23/19	PAVEMENT: Test Strip 2	Surface	E0130		152.9	Supplied Value	143.0	Backscatter	94	92 / 95		31917	WESLEY EDWARDS
107		9/23/19	PAVEMENT: Test Strip 2	Surface	E0130		152.9	Supplied Value	140.5	Backscatter	92	92 / 95		31917	WESLEY EDWARDS
108		9/23/19	PAVEMENT: Test Strip 2	Surface	E0130		152.9	Supplied Value	139.7	Backscatter	91	92 / 95	FAIL	31917	WESLEY EDWARDS
Remarks												Comments			
FAIL: Tests results DO NOT comply with specifications															
Tests are "Direct Transmission" (Method A) unless probe depth is noted as "Backscatter"															
Gauge Information															
Gauge SN	Make	Model	Density Count	Moisture Count	Standard Count Date	Last Calibration Date	Last Calibrated By								
31917	Troxler	3430	1925	510	9/23/19	12/26/18	InsitroTek Inc.								

B. E. Vaughan

Reviewed/Prepared by:
WILLIAM BRIAN VAUGHAN
Nov 21, 2019

The above tests were performed in general accordance with the applicable test method, except for known deviations noted above.

Page 9 of 18

Nuclear density test results on compacted HMA

S&M, Inc.
301 Zina Park Drive
Spartanburg, SC 29301
Phone: 864-574-2360 | Fax: 864-576-8730

ASPHALT PLACEMENT DENSITY

Report #: BNG-000017
Report Date: 11/21/2019
Test Method: ASTM D2950

Client:

TRI/Environmental, Inc.
4915 Clemson Blvd.
Anderson, SC 29621

Project:

142619038
TRI On-Call Lab Testing
Anderson
Anderson, SC 29621

Test Results															
Test #	Retest Of	Test Date	Test Location	Material	Mix Design	Thickness (in)	Max Density (pcf)	Max Density Source	In Place Density (pcf)	Probe Depth (in)	Percent Comp.	Min/Max Comp. (%)	Remark	Gauge SN	Technician
109		9/23/19	PAVEMENT: Test Strip 2 D - West (1)	Surface	E0130		152.9	Supplied Value	137.0	Backscatter	90	92 / 95	FAIL	31917	WESLEY EDWARDS
110		9/23/19	PAVEMENT: Test Strip 2 D - West (2)	Surface	E0130		152.9	Supplied Value	136.7	Backscatter	89	92 / 95	FAIL	31917	WESLEY EDWARDS
111		9/23/19	PAVEMENT: Test Strip 2 D - Center (1)	Surface	E0130		152.9	Supplied Value	138.0	Backscatter	90	92 / 95	FAIL	31917	WESLEY EDWARDS
112		9/23/19	PAVEMENT: Test Strip 2 D - Center (2)	Surface	E0130		152.9	Supplied Value	137.9	Backscatter	90	92 / 95	FAIL	31917	WESLEY EDWARDS
113		9/23/19	PAVEMENT: Test Strip 2 D - East (1)	Surface	E0130		152.9	Supplied Value	142.3	Backscatter	93	92 / 95		31917	WESLEY EDWARDS
114		9/23/19	PAVEMENT: Test Strip 2 D - East (2)	Surface	E0130		152.9	Supplied Value	140.7	Backscatter	92	92 / 95		31917	WESLEY EDWARDS
Remarks										Comments					
FAIL: Tests results DO NOT comply with specifications										Tests are "Direct Transmission" (Method A) unless probe depth is noted as "Backscatter"					
Gauge Information															
Gauge SN	Make	Model	Density Count	Moisture Count	Standard Count Date	Last Calibration Date	Last Calibrated By								
31917	Troxler	3430	1925	510	9/23/19	12/26/18	Instrotek Inc.								

Tests are "Direct Transmission" (Method A) unless probe depth is noted as "Backscatter"


B. E. Hughes

Reviewed/Prepared by:
WILLIAM BRIAN VAUGHAN
Nov 21, 2019

The above tests were performed in general accordance with the applicable test method, except for known deviations noted above.

Page 10 of 18

Nuclear density test results on compacted HMA

		ASPHALT PLACEMENT DENSITY		Client:	Project:
S&E, Inc. 301 Zima Park Drive Spartanburg, SC 29301 Phone: 864-574-2360 Fax: 864-576-8730		Report #: BNG-000018 Report Date: 11/21/2019 Test Method: ASTM D2950		TRI/Environmental, Inc. 4915 Clemson Blvd. Anderson, SC 29621	142619038 TRI On-Call Lab Testing Anderson Anderson, SC 29621

Test Results															
Test #	Retest Of	Test Date	Test Location	Material	Mix Design	Thickness (in)	Max Density (pcf)	Max Density Source	In Place Density (pcf)	Probe Depth (in)	Percent Comp.	Min/Max Comp. (%)	Remark	Gauge SN	Technician
115		9/23/19	PAVEMENT: Test Strip 2	Surface	E0130		152.9	Supplied Value	138.7	Backscatter	91	92 / 95	FAIL	31917	WESLEY EDWARDS
116		9/23/19	PAVEMENT: Test Strip 2	Surface	E0130		152.9	Supplied Value	137.8	Backscatter	90	92 / 95	FAIL	31917	WESLEY EDWARDS
117		9/23/19	PAVEMENT: Test Strip 2	Surface	E0130		152.9	Supplied Value	139.4	Backscatter	91	92 / 95	FAIL	31917	WESLEY EDWARDS
118		9/23/19	PAVEMENT: Test Strip 2	Surface	E0130		152.9	Supplied Value	137.3	Backscatter	90	92 / 95	FAIL	31917	WESLEY EDWARDS
119		9/23/19	PAVEMENT: Test Strip 2	Surface	E0130		152.9	Supplied Value	140.1	Backscatter	92	92 / 95		31917	WESLEY EDWARDS
120		9/23/19	PAVEMENT: Test Strip 2	Surface	E0130		152.9	Supplied Value	142.4	Backscatter	93	92 / 95		31917	WESLEY EDWARDS
Remarks											Comments				
FAIL: Tests results DO NOT comply with specifications											Tests are "Direct Transmission" (Method A) unless probe depth is noted as "Backscatter"				
Gauge Information															
Gauge SN	Make	Model	Density Count	Moisture Count	Standard Count Date		Last Calibration Date		Last Calibrated By						
31917	Troxler	3430	1925	510	9/23/19		12/26/18		InstroTek Inc.						




Reviewed/Prepared by:
WILLIAM BRIAN VAUGHAN
Nov 21, 2019

The above tests were performed in general accordance with the applicable test method, except for known deviations noted above.

Page 11 of 18

Nuclear density test results on compacted HMA

		ASPHALT PLACEMENT DENSITY Report #: BNG-000019 Report Date: 11/21/2019 Test Method: ASTM D2950		Client: TRI/Environmental, Inc. 4915 Clemson Blvd. Anderson, SC 29621	Project: 142619038 TRI On-Call Lab Testing Anderson Anderson, SC 29621
SAME, Inc. 301 Zima Park Drive Spartanburg, SC 29301 Phone: 864-574-2360 Fax: 864-576-8730					

Test Results														
Test #	Retest Of	Test Date	Test Location	Material	Mix Design	Thickness (in)	Max Density (pcf)	In Place Density (pcf)	Probe Depth (in)	Percent Comp.	Min/Max Comp. (%)	Remark	Gauge SN	Technician
121		9/23/19	PAVEMENT: Test Strip 2 F - West (1)	Surface	E0130		152.9	138.3	Backscatter	90	92 / 95	FAIL	31917	WESLEY EDWARDS
122		9/23/19	PAVEMENT: Test Strip 2 F - West (2)	Surface	E0130		152.9	139.0	Backscatter	91	92 / 95	FAIL	31917	WESLEY EDWARDS
123		9/23/19	PAVEMENT: Test Strip 2 F - Center (1)	Surface	E0130		152.9	137.5	Backscatter	90	92 / 95	FAIL	31917	WESLEY EDWARDS
124		9/23/19	PAVEMENT: Test Strip 2 F - Center (2)	Surface	E0130		152.9	139.0	Backscatter	91	92 / 95	FAIL	31917	WESLEY EDWARDS
125		9/23/19	PAVEMENT: Test Strip 2 F - East (1)	Surface	E0130		152.9	143.1	Backscatter	94	92 / 95		31917	WESLEY EDWARDS
126		9/23/19	PAVEMENT: Test Strip 2 F - East (2)	Surface	E0130		152.9	141.2	Backscatter	92	92 / 95		31917	WESLEY EDWARDS
Remarks							Comments							
FAIL: Tests results DO NOT comply with specifications							Tests are "Direct Transmission" (Method A) unless probe depth is noted as "Backscatter"							
Gauge Information														
Gauge SN	Make	Model	Density Count	Moisture Count	Standard Count Date	Last Calibration Date	Last Calibrated By							
31917	Troxler	3430	1925	510	9/23/19	12/26/18	InstroTek Inc.							




Reviewed/Prepared by:
WILLIAM BRIAN VAUGHAN
Nov 21, 2019

The above tests were performed in general accordance with the applicable test method, except for known deviations noted above.

Page 12 of 18

Nuclear density test results on compacted HMA

 S&ME, Inc. 301 Zima Park Drive Spartanburg, SC 29301 Phone: 864-574-2360 Fax: 864-576-8730		ASPHALT PLACEMENT DENSITY Report #: BNG-000020 Report Date: 11/21/2019 Test Method: ASTM D2950		Client: TRI/Environmental, Inc. 4915 Clemson Blvd. Anderson, SC 29621	Project: 142619038 TRI On-Call Lab Testing Anderson Anderson, SC 29621

Test Results														
Test #	Retest Of	Test Date	Test Location	Material	Mix Design	Thickness (in)	Max Density (pcf)	In Place Density (pcf)	Probe Depth (in)	Percent Comp.	Min/Max Comp. (%)	Remark	Gauge SN	Technician
127		9/23/19	PAVEMENT: Test Strip 3	Surface	E0130		152.9	141.2	Backscatter	92	92 / 95		31917	WESLEY EDWARDS
128		9/23/19	PAVEMENT: Test Strip 3	Surface	E0130		152.9	139.7	Backscatter	91	92 / 95	FAIL	31917	WESLEY EDWARDS
129		9/23/19	PAVEMENT: Test Strip 3	Surface	E0130		152.9	141.5	Backscatter	93	92 / 95		31917	WESLEY EDWARDS
130		9/23/19	PAVEMENT: Test Strip 3	Surface	E0130		152.9	142.6	Backscatter	93	92 / 95		31917	WESLEY EDWARDS
131		9/23/19	PAVEMENT: Test Strip 3	Surface	E0130		152.9	142.2	Backscatter	93	92 / 95		31917	WESLEY EDWARDS
132		9/23/19	PAVEMENT: Test Strip 3	Surface	E0130		152.9	143.5	Backscatter	94	92 / 95		31917	WESLEY EDWARDS
Remarks								Comments						
FAIL: Tests results DO NOT comply with specifications								Tests are "Direct Transmission" (Method A) unless probe depth is noted as "Backscatter"						
Gauge Information														
Gauge SN	Make	Model	Density Count	Moisture Count	Standard Count Date	Last Calibration Date	Last Calibrated By							
31917	Troxler	3430	1925	510	9/23/19	12/26/18	InstroTek Inc.							




Reviewed/Prepared by:
 WILLIAM BRIAN VAUGHAN
 Nov 21, 2019

The above tests were performed in general accordance with the applicable test method, except for known deviations noted above.

Page 13 of 18

Nuclear density test results on compacted HMA

		ASPHALT PLACEMENT DENSITY		Client:	Project:
S&ME, Inc. 301 Zina Park Drive Spartanburg, SC 29301 Phone: 864-574-2360 Fax: 864-576-8730		Report #: BNG-000021 Report Date: 11/21/2019 Test Method: ASTM D2950		TRI/Environmental, Inc. 4915 Clemson Blvd. Anderson, SC 29621	142619038 TRI On-Call Lab Testing Anderson Anderson, SC 29621

Test Results										
Test #	Retest Of	Test Date	Test Location	Material	Mix Design	Thickness (in)	Max Density (pcf)	Max Density Source	In Place Density (pcf)	Probe Depth (in)
133		9/23/19	PAVEMENT: Test Strip 3 B - West (1)	Surface	E0130		152.9	Supplied Value	137.7	Backscatter
134		9/23/19	PAVEMENT: Test Strip 3 B - West (2)	Surface	E0130		152.9	Supplied Value	140.1	Backscatter
135		9/23/19	PAVEMENT: Test Strip 3 B - Center (1)	Surface	E0130		152.9	Supplied Value	142.4	Backscatter
136		9/23/19	PAVEMENT: Test Strip 3 B - Center (2)	Surface	E0130		152.9	Supplied Value	140.7	Backscatter
137		9/23/19	PAVEMENT: Test Strip 3 B - East (1)	Surface	E0130		152.9	Supplied Value	145.0	Backscatter
138		9/23/19	PAVEMENT: Test Strip 3 B - East (2)	Surface	E0130		152.9	Supplied Value	144.9	Backscatter
Remarks										
FAIL: Tests results DO NOT comply with specifications										
Gauge Information										
Gauge SN	Make	Model	Density Count	Moisture Count	Standard Count Date	Last Calibration Date	Last Calibrated By			
31917	Troxler	3430	1925	510	9/23/19	12/26/18	InstroTek Inc.			

Comments

Tests are "Direct Transmission" (Method A) unless probe depth is noted as "Backscatter"

B. E. Vaughan

Reviewed/Prepared by:
WILLIAM BRIAN VAUGHAN
Nov 21, 2019

The above tests were performed in general accordance with the applicable test method, except for known deviations noted above.

Page 14 of 18

Nuclear density test results on compacted HMA**ASPHALT PLACEMENT
DENSITY**

Report #: BNG-000022
Report Date: 11/21/2019
Test Method: ASTM D2950

Client:

TRI/Environmental, Inc.
 4915 Clemson Blvd.
 Anderson, SC 29621

Project:

142619038
 TRI On-Call Lab Testing
 Anderson
 Anderson, SC 29621

 **S&ME, Inc.**
 301 Zina Park Drive
 Spartanburg, SC 29301
 Phone: 864-574-2360 | Fax: 864-576-8730

Test Results															
Test #	Retest Of	Test Date	Test Location	Material	Mix Design	Thickness (in)	Max Density (pcf)	Max Density Source	In Place Density (pcf)	Probe Depth (in)	Percent Comp.	Min/Max Comp. (%)	Remark	Gauge SN	Technician
139		9/23/19	PAVEMENT: Test Strip 3	Surface	E0130		152.9	Supplied Value	141.1	Backscatter	92	92 / 95		31917	WESLEY EDWARDS
140		9/23/19	PAVEMENT: Test Strip 3	Surface	E0130		152.9	Supplied Value	138.1	Backscatter	90	92 / 95	FAIL	31917	WESLEY EDWARDS
141		9/23/19	PAVEMENT: Test Strip 3	Surface	E0130		152.9	Supplied Value	138.4	Backscatter	91	92 / 95	FAIL	31917	WESLEY EDWARDS
142		9/23/19	PAVEMENT: Test Strip 3	Surface	E0130		152.9	Supplied Value	142.6	Backscatter	93	92 / 95		31917	WESLEY EDWARDS
143		9/23/19	PAVEMENT: Test Strip 3	Surface	E0130		152.9	Supplied Value	139.1	Backscatter	91	92 / 95	FAIL	31917	WESLEY EDWARDS
144		9/23/19	PAVEMENT: Test Strip3	Surface	E0130		152.9	Supplied Value	138.7	Backscatter	91	92 / 95	FAIL	31917	WESLEY EDWARDS
Remarks						Comments									
FAIL: Tests results DO NOT comply with specifications						Tests are "Direct Transmission" (Method A) unless probe depth is noted as "Backscatter"									
Gauge Information															
Gauge SN	Make	Model	Density Count	Moisture Count	Standard Count Date	Last Calibration Date	Last Calibrated By								
31917	Troxler	3430	1925	510	9/23/19	12/26/18	Instrotek Inc.								




Reviewed/Prepared by:
 WILLIAM BRIAN VAUGHAN
 Nov 21, 2019

The above tests were performed in general accordance with the applicable test method, except for known deviations noted above.

Page 15 of 18

Nuclear density test results on compacted HMA

 S&M, Inc. 301 Zima Park Drive Spartanburg, SC 29301 Phone: 864-574-2360 Fax: 864-576-8730		ASPHALT PLACEMENT DENSITY Report #: BNG-000023 Report Date: 11/21/2019 Test Method: ASTM D2950		Client: TRI/Environmental, Inc. 4915 Clemson Blvd. Anderson, SC 29621	Project: 142619038 TRI On-Call Lab Testing Anderson Anderson, SC 29621
--	--	--	--	---	---

Test Results														
Test #	Retest Of	Test Date	Test Location	Material	Mix Design	Thickness (in)	Max Density (pcf)	In Place Density (pcf)	Probe Depth (in)	Percent Comp.	Min/Max Comp. (%)	Remark	Gauge SN	Technician
145		9/23/19	PAVEMENT: Test Strip3 D - West (1)	Surface	E0130		152.9	143.5	Backscatter	94	92 / 95		31917	WESLEY EDWARDS
146		9/23/19	PAVEMENT: Test Strip 3 D - West (2)	Surface	E0130		152.9	140.1	Backscatter	92	92 / 95		31917	WESLEY EDWARDS
147		9/23/19	PAVEMENT: Test Strip 3 D - Center (1)	Surface	E0130		152.9	136.8	Backscatter	89	92 / 95	FAIL	31917	WESLEY EDWARDS
148		9/23/19	PAVEMENT: Test Strip 3 D - Center (2)	Surface	E0130		152.9	137.4	Backscatter	90	92 / 95	FAIL	31917	WESLEY EDWARDS
149		9/23/19	PAVEMENT: Test Strip 3 D - East (1)	Surface	E0130		152.9	139.5	Backscatter	91	92 / 95	FAIL	31917	WESLEY EDWARDS
150		9/23/19	PAVEMENT: Test Strip 3 D - East (2)	Surface	E0130		152.9	139.1	Backscatter	91	92 / 95	FAIL	31917	WESLEY EDWARDS
Remarks						Comments								
FAIL: Tests results DO NOT comply with specifications						Tests are "Direct Transmission" (Method A) unless probe depth is noted as "Backscatter"								
Gauge Information														
Gauge SN	Make	Model	Density Count	Moisture Count	Standard Count Date	Last Calibration Date	Last Calibrated By							
31917	Troxler	3430	1925	510	9/23/19	12/26/18	InstroTek Inc.							



Reviewed/Prepared by:
WILLIAM BRIAN VAUGHAN
Nov 21, 2019

The above tests were performed in general accordance with the applicable test method, except for known deviations noted above.

Page 16 of 18

Nuclear density test results on compacted HMA

 S&M&E, Inc. 301 Zina Park Drive Spartanburg, SC 29301 Phone: 864-574-2360 Fax: 864-576-8730	ASPHALT PLACEMENT DENSITY		Client:	Project:
	Report #: BNG-000024		TRI/Environmental, Inc.	142619038
	Report Date: 11/21/2019		4915 Clemson Blvd.	TRI On-Call Lab Testing
	Test Method: ASTM D2950		Anderson, SC 29621	Anderson
			Anderson, SC 29621	

Test Results															
Test #	Retest Of	Test Date	Test Location	Material	Mix Design	Thickness (in)	Max Density (pcf)	Max Density Source	In Place Density (pcf)	Probe Depth (in)	Percent Comp.	Min/Max Comp. (%)	Remark	Gauge SN	Technician
151		9/23/19	PAVEMENT: Test Strip 3 E - West (1)	Surface	E0130		152.9	Supplied Value	137.4	Backscatter	90	92 / 95	FAIL	31917	WESLEY EDWARDS
152		9/23/19	PAVEMENT: Test Strip 3 E - West (2)	Surface	E0130		152.9	Supplied Value	139.4	Backscatter	91	92 / 95	FAIL	31917	WESLEY EDWARDS
153		9/23/19	PAVEMENT: Test Strip 3 E - Center (1)	Surface	E0130		152.9	Supplied Value	140.1	Backscatter	92	92 / 95		31917	WESLEY EDWARDS
154		9/23/19	PAVEMENT: Test Strip 3 E - Center (2)	Surface	E0130		152.9	Supplied Value	141.6	Backscatter	93	92 / 95		31917	WESLEY EDWARDS
155		9/23/19	PAVEMENT: Test Strip3 E - East (1)	Surface	E0130		152.9	Supplied Value	142.7	Backscatter	93	92 / 95		31917	WESLEY EDWARDS
156		9/23/19	PAVEMENT: Test Strip 3 E - East (2)	Surface	E0130		152.9	Supplied Value	143.9	Backscatter	94	92 / 95		31917	WESLEY EDWARDS
Remarks									Comments						
FAIL: Tests results DO NOT comply with specifications									Tests are "Direct Transmission" (Method A) unless probe depth is noted as "Backscatter"						
Gauge Information															
Gauge SN	Make	Model	Density Count	Moisture Count	Standard Count Date	Last Calibration Date	Last Calibrated By								
31917	Troxler	3430	1925	510	9/23/19	12/26/18	InstroTek Inc.								



Reviewed/Prepared by:
WILLIAM BRIAN VAUGHAN
Nov 21, 2019

The above tests were performed in general accordance with the applicable test method, except for known deviations noted above.

Page 17 of 18

Nuclear density test results on compacted HMA

ASPHALT PLACEMENT DENSITY		Client:	Project:
 S&ME, Inc. 301 Zima Park Drive Spartanburg, SC 29301 Phone: 864-574-2360 Fax: 864-576-8730		TRI/Environmental, Inc. 4915 Clemson Blvd. Anderson, SC 29621	142619038 TRI On-Call Lab Testing Anderson Anderson, SC 29621
Report #: BNG-000025			
Report Date: 11/21/2019			
Test Method: ASTM D2950			

Test Results															
Test #	Retest Of	Test Date	Test Location	Material	Mix Design	Thickness (in)	Max Density (pcf)	Density Source	In Place Density (pcf)	Probe Depth (in)	Percent Comp.	Min/Max Comp. (%)	Remark	Gauge SN	Technician
157		9/23/19	PAVEMENT: Test Strip 3 F - West (1)	Surface	E0130		152.9	Supplied Value	136.2	Backscatter	89	92 / 95	FAIL	31917	WESLEY EDWARDS
158		9/23/19	PAVEMENT: Test Strip 3 F - West (2)	Surface	E0130		152.9	Supplied Value	138.8	Backscatter	91	92 / 95	FAIL	31917	WESLEY EDWARDS
159		9/23/19	PAVEMENT: Test Strip 3 F - Center (1)	Surface	E0130		152.9	Supplied Value	145.6	Backscatter	95	92 / 95		31917	WESLEY EDWARDS
160		9/23/19	PAVEMENT: Test Strip 3 F - Center (2)	Surface	E0130		152.9	Supplied Value	144.0	Backscatter	94	92 / 95		31917	WESLEY EDWARDS
161		9/23/19	PAVEMENT: Test Strip 3 F - East (1)	Surface	E0130		152.9	Supplied Value	141.0	Backscatter	92	92 / 95		31917	WESLEY EDWARDS
162		9/23/19	PAVEMENT: Test Strip 3 F - East (2)	Surface	E0130		152.9	Supplied Value	141.8	Backscatter	93	92 / 95		31917	WESLEY EDWARDS
Remarks										Comments					
FAIL: Tests results DO NOT comply with specifications										Tests are "Direct Transmission" (Method A) unless probe depth is noted as "Backscatter"					
Gauge Information															
Gauge SN	Make	Model	Density Count	Moisture Count	Standard Count Date	Last Calibration Date	Last Calibrated By								
31917	Troxler	3430	1925	510	9/23/19	12/26/18	InstroTek Inc.								



Reviewed/Prepared by:
WILLIAM BRIAN VAUGHAN
Nov 21, 2019

The above tests were performed in general accordance with the applicable test method, except for known deviations noted above.

Page 18 of 18

13 Appendix B: Base Aggregate Material Testing Data Sheets

Appendix B: Base Aggregate Material Testing Data Sheets

Atterburg limits test on base course aggregate

Form No. TR-D4318-T89-90

Revision No. 1

Revision Date: 7/26/17

LIQUID LIMIT, PLASTIC LIMIT, & PLASTIC INDEX



ASTM D 4318 ☐ AASHTO T 89 ☒ AASHTO T 90 ☒

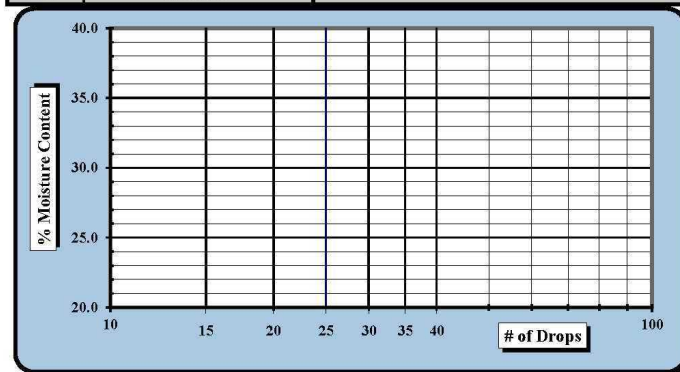
S&ME, Inc. - Greenville 48 Brookfield Oaks Dr., Suite F Greenville, SC 29607

Project #:	1426-16-063 Phase 900	Report Date:	8/07/18
Project Name:	TRI/Environmental - General Laboratory Testing	Test Date(s)	8/07/18
Client Name:	TRI/Environmental, Inc.		
Client Address:	P.O. Box 9192 Greenville, SC 29604		
Location:	Montana 7A	Log #:	77g
		Sample Date:	July 2018

Sample Description: Montana 7A Stone [A-1-a]

Type and Specification	S&ME ID #	Cal Date:	Type and Specification	S&ME ID #	Cal Date:
Balance (0.01 g)	13942	8/18/2017	Grooving tool	23119	10/15/2017
LL Apparatus	23158	2/1/2018			
Oven	13978	10/7/2017			

Pan #	Tare #:	Liquid Limit				Plastic Limit	
A	Tare Weight						
B	Wet Soil Weight + A						
C	Dry Soil Weight + A						
D	Water Weight (B-C)						
E	Dry Soil Weight (C-A)						
F	% Moisture (D/E)*100						
N	# OF DROPS					Moisture Contents determined by AASHTO T 265	
LL	LL = F * FACTOR						
Ave.	Average						



One Point Liquid Limit			
N	Factor	N	Factor
20	0.974	26	1.005
21	0.979	27	1.009
22	0.985	28	1.014
23	0.99	29	1.018
24	0.995	30	1.022
25	1.000		

NP, Non-Plastic ☒

Liquid Limit ---

Plastic Limit **NP**

Plastic Index **NP**

Group Symbol **A-1-a**

Multipoint Method ☒

One-point Method ☐

Wet Preparation ☐ Dry Preparation ☒ Air Dried ☒ % Passing the #200 Sieve: 4.6%

Notes / Deviations / References:

AASHTO T90: Determining the Plastic Limit & Plastic Index of Soils

AASHTO T89: Determining the Liquid Limit of Soils

Benjamin J. Kovaleski
Technician Name

8/07/18
Date

Brian Vaughan
Technical Responsibility

8/07/18
Date

This report shall not be reproduced, except in full, without the written approval of S&ME, Inc.

S&ME, INC. - Corporate

3201 Spring Forest Road
Raleigh, NC. 27616

PI (Montana 7A).xlsx
Page 1 of 1

Appendix B: Base Aggregate Material Testing Data Sheets

CBR test on base course aggregate

Form No. TR-D1883-T193-3
Revision No. 2
Revision Date: 08/11/17

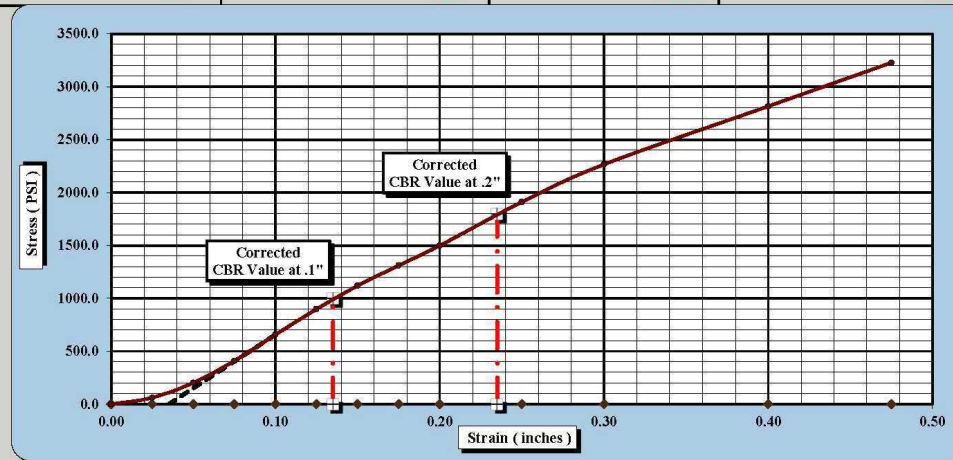
CBR (CALIFORNIA BEARING RATIO) OF LABORATORY COMPACTED SOIL



AASHTO T 193

S&ME, Inc. - Greenville 48 Brookfield Oaks Dr., Suite F Greenville, SC 29607			
Project #:	1426-16-063 Phase 900	Report Date:	8/10/18
Project Name:	TRI/Environmental - General Laboratory Testing	Test Date(s)	8/06 - 8/10/18
Client Name:	TRI/Environmental		
Client Address:	P.O. Box 9192 Greenville, SC 29604		
Boring #:	N/A	Log #:	77g
Location:	Montana 7A	Sample Date:	July 2018
		Type:	Bulk
		Depth:	N/A
Sample Description:	Montana 7A Stone [A-1-a]		
AASHTO T180 Method D	Maximum Dry Density:	136.7 PCF	Optimum Moisture Content: 7.7%
	Compaction Test performed on grading complying with CBR spec.		% Retained on the 3/4" sieve: 0.0%

Uncorrected CBR Values		Corrected CBR Values	
CBR at 0.1 in.	65.7	CBR at 0.2 in.	99.9
		CBR at 0.1 in.	100.0
		CBR at 0.2 in.	120.0



CBR Sample Preparation:

The entire gradation was used and compacted in a 6" CBR mold in accordance with AASHTO T 193, Section 5.1.1

Before Soaking		After Soaking	
Compactive Effort (Blows per Layer)	35	Final Dry Density (PCF)	129.9
Initial Dry Density (PCF)	129.9	Moisture Content (top 1" after soaking)	8.4%
Moisture Content of the Compacted Specimen	7.7%	Percent Swell	0.0%
Percent Compaction	95.0%		

Soak Time:	96 hrs.	Surcharge Weight	10.0	Surcharge Wt. per sq. Ft.	50.9
Liquid Limit	---	Plastic Index	NP	Apparent Relative Density	2.700

Notes/Deviations/References:

Brian Vaughan, P.E.
Technical Responsibility

Brian Vaughan
Signature

Group Leader
Position

8/10/18
Date

This report shall not be reproduced, except in full without the written approval of S&ME, Inc.

S&ME, Inc. - Corporate

3201 Spring Forest Road
Raleigh, NC. 27616

CBR (Montana 7A).xlsx
Page 1 of 1

Fractured faces test on base course aggregate



48 Brookfield Oaks Dr., Suite F
Greenville, SC 29607

Percentage of Fractured Particles in Coarse Aggregate

ASTM D5821

TRI/Environmental - General Laboratory Testing

S&ME Project No. 1426-16-063 Phase 900

Sample ID	Total Sample Mass (grams)	Mass of Aggregate Particles with One or More Fractured Faces (grams)	Mass of Aggregate Particles with No Fractured Faces (grams)	Fractured Face %
Montana 7A Stone	1576.21	1029.90	546.31	65%

$$P = [F/(F+N)] \times 100$$

P = Percentage of particles with the specified number of fractured faces (≥ 1 for this project)

F = Mass of fractured particles with at least the specified number of fractured faces (≥ 1 for this project)

N = Mass of particles in the non-fractured category not meeting the fractured particle criteria

Appendix B: Base Aggregate Material Testing Data Sheets

Compaction test on base course aggregate

Form No. TR-D698-2
Revision No. : 1
Revision Date: 07/25/17

MOISTURE - DENSITY REPORT

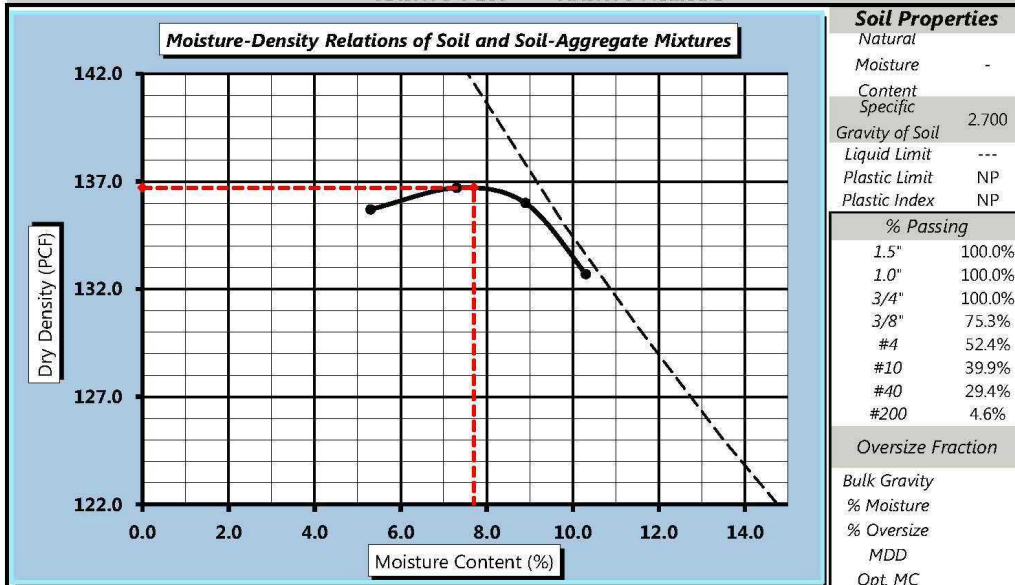


S&ME, Inc. - Spartanburg: 301 Zima Park Drive, Spartanburg, SC 29301			
Project #:	1426-16-063 Phase 900	Report Date:	8/07/18
Project Name:	TRI/Environmental - General Laboratory Testing	Test Date:	7/25/18
Client Name:	TRI/Environmental, Inc.		
Client Address:	P.O. Box 9192 Greenville, SC 29604		
Location:	Montana 7A	Log #:	77g
		Sample Date:	July 2018

Sample Description: Montana 7A Stone [A-1-a]

Maximum Dry Density **136.7** PCF. Optimum Moisture Content **7.7%**

AASHTO T 180 -- AASHTO Method D



Moisture-Density Curve Displayed: Fine Fraction ☒ Corrected for Oversize Fraction (ASTM D 4718) ☐
Sieve Size used to separate the Oversize Fraction: #4 Sieve ☐ 3/8 inch Sieve ☐ 3/4 inch Sieve ☒
Mechanical Rammer ☐ Manual Rammer ☒ Moist Preparation ☐ Dry Preparation ☒

References / Comments / Deviations:

AASHTO T 265: Laboratory Determination of Moisture Content of Soils

AASHTO T 180: Moisture-Density Relations of Soil Using a 10 Lb. Rammer and a 18" Drop

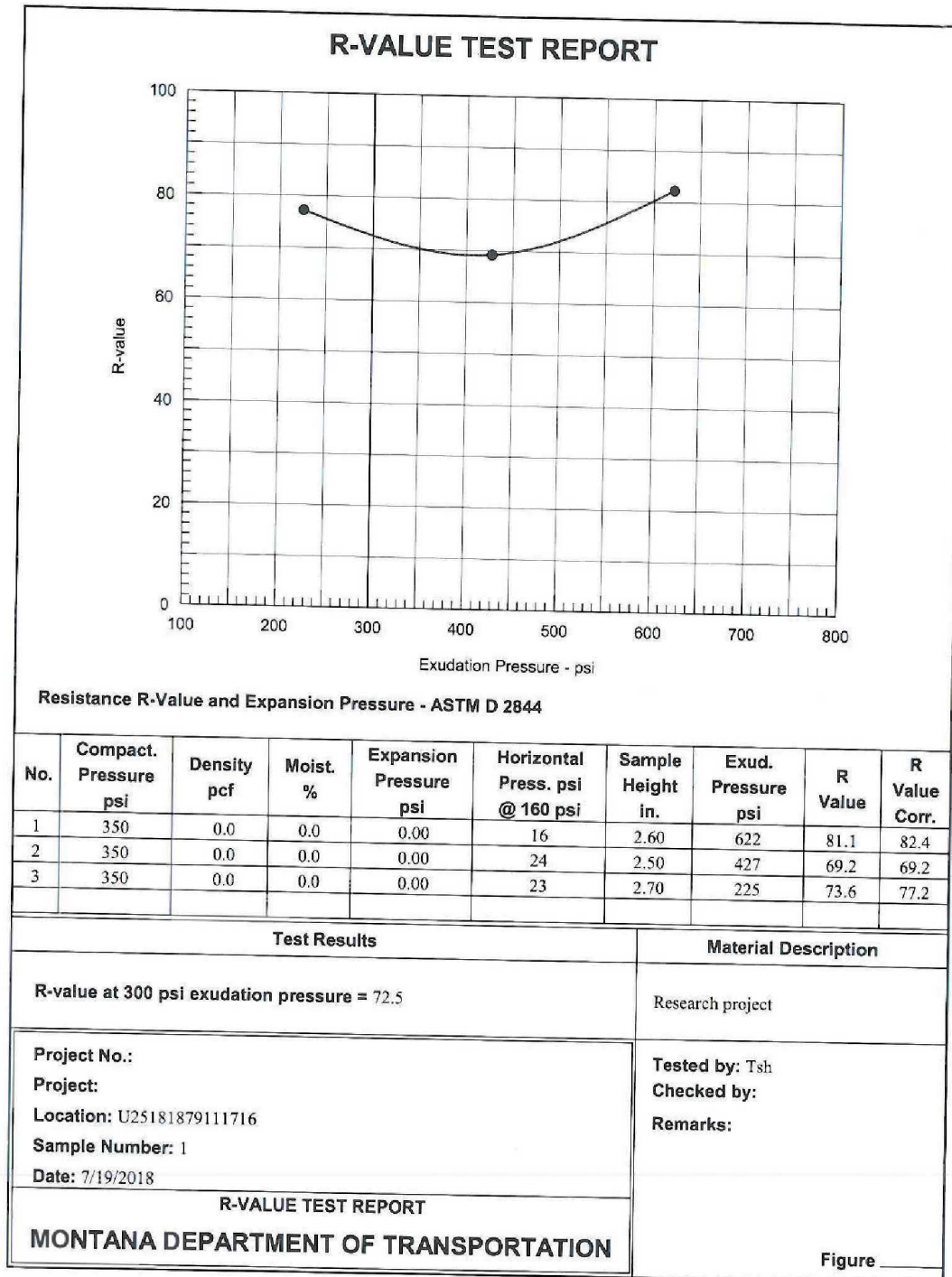
Brian Vaughan, P.E.
Technical Responsibility

Brian Vaughan
Signature

Group Leader
Position

8/07/18
Date

This report shall not be reproduced, except in full, without the written approval of S&ME, Inc.

R-Value test on base course aggregate

Nuclear density test results on base course aggregate

<

The above tests were performed in general accordance with the applicable test method, except for known deviations noted above. The density determined represents the soil density at the test location at the time of the test. The test result relates only to the material tested.

Nuclear density test results on base course aggregate

**DENSITY - NUCLEAR
METHOD**

Report #: SNG-000005
Report Date: 11/20/2019
Test Method: ASTM D 6938

Client:

TRI/Environmental, Inc.
4915 Clemson Blvd.
Anderson, SC 29621

Project:

142619038
TRI On-Call Lab Testing
Anderson
Anderson, SC 29621

 S&ME, Inc.
301 Zima Park Drive
Spartanburg, SC 29301
Phone: 864-574-2360 | Fax: 864-576-8730

Test Results													
Test #	Retest Of	Test Date	Proctor ID	Method	Soil Classification	Optimum Moisture (%)	Maximum Dry Density (pcf)	In Place Moisture (%)	In Place Dry Density (pcf)	Probe Depth (in)	Percent Compaction	Min Comp. (%)	Remark
70		9/13/19	100	D698-C	GW	7.7	136.7	2.9	138.5	8	101	95	PASS
71		9/13/19	100	D698-C	GW	7.7	136.7	2.8	134.7	8	99	95	PASS
72		9/13/19	100	D698-C	GW	7.7	136.7	2.9	135.8	8	99	95	PASS
73		9/13/19	100	D698-C	GW	7.7	136.7	2.6	138.5	8	101	95	PASS
74		9/13/19	100	D698-C	GW	7.7	136.7	3.5	137.3	8	100	95	PASS
75		9/13/19	100	D698-C	GW	7.7	136.7	3.8	133.7	8	98	95	PASS
76		9/13/19	100	D698-C	GW	7.7	136.7	3.6	137.0	8	100	95	PASS
77		9/13/19	100	D698-C	GW	7.7	136.7	3.1	139.7	8	102	95	PASS
Test Information													
Test #	Test Location		Elevation		Reference		Gauge		Make / Model / SN / Calibrated		Field Technician		
70	PAVEMENT - Base: Location 9		0.0		SG		Troxler / 3411-B / 10156 / 11/27/2018		Troxler / 3411-B / 10156 / 11/27/2018		WILLIAM BRIAN VAUGHAN		
71	PAVEMENT - Base: Location 10		0.0		SG		Troxler / 3411-B / 10156 / 11/27/2018		Troxler / 3411-B / 10156 / 11/27/2018		WILLIAM BRIAN VAUGHAN		
72	PAVEMENT - Base: Location 11		0.0		SG		Troxler / 3411-B / 10156 / 11/27/2018		Troxler / 3411-B / 10156 / 11/27/2018		WILLIAM BRIAN VAUGHAN		
73	PAVEMENT - Base: Location 12		0.0		SG		Troxler / 3411-B / 10156 / 11/27/2018		Troxler / 3411-B / 10156 / 11/27/2018		WILLIAM BRIAN VAUGHAN		
74	PAVEMENT - Base: Location 13		0.0		SG		Troxler / 3411-B / 10156 / 11/27/2018		Troxler / 3411-B / 10156 / 11/27/2018		WILLIAM BRIAN VAUGHAN		
75	PAVEMENT - Base: Location 14		0.0		SG		Troxler / 3411-B / 10156 / 11/27/2018		Troxler / 3411-B / 10156 / 11/27/2018		WILLIAM BRIAN VAUGHAN		
76	PAVEMENT - Base: Location 15		0.0		SG		Troxler / 3411-B / 10156 / 11/27/2018		Troxler / 3411-B / 10156 / 11/27/2018		WILLIAM BRIAN VAUGHAN		
77	PAVEMENT - Base: Location 16		0.0		SG		Troxler / 3411-B / 10156 / 11/27/2018		Troxler / 3411-B / 10156 / 11/27/2018		WILLIAM BRIAN VAUGHAN		
Remarks			Comments										
PASS: Density test results comply with specifications. Tests are "Direct Transmission" (Method A) unless probe depth is noted as "Backscatter". Gauge calibration data on file with the testing agency.													

The above tests were performed in general accordance with the applicable test method, except for known deviations noted above. The density determined represents the soil density at the test location at the time of the test. The test result relates only to the material tested.

Nuclear density test results on base course aggregate**DENSITY - NUCLEAR
METHOD**

Report #: SNG-000005
Report Date: 11/20/2019
Test Method: ASTM D 6938

Client:

TRI/Environmental, Inc.
4915 Clemson Blvd.
Anderson, SC 29621

Project:

142619038
TRI On-Call Lab Testing
Anderson
Anderson, SC 29621

 S&M, Inc.
301 Zima Park Drive
Spartanburg, SC 29301
Phone: 864-574-2360 | Fax: 864-576-8730

Test Results													
Test #	Retest Of	Test Date	Proctor ID	Method	Soil Classification	Optimum Moisture (%)	Maximum Dry Density (pcf)	In Place Moisture (%)	In Place Dry Density (pcf)	Probe Depth (in)	Percent Compaction	Min Comp. (%)	Remark
78		9/13/19	100	D698-C	GW	7.7	136.7	2.7	139.3	8	102	95	PASS
79		9/13/19	100	D698-C	GW	7.7	136.7	2.8	136.3	8	100	95	PASS
80		9/13/19	100	D698-C	GW	7.7	136.7	3.0	139.0	8	102	95	PASS
81		9/13/19	100	D698-C	GW	7.7	136.7	2.9	137.5	8	101	95	PASS
82		9/13/19	100	D698-C	GW	7.7	136.7	2.9	139.1	8	102	95	PASS
83		9/13/19	100	D698-C	GW	7.7	136.7	3.1	134.3	8	98	95	PASS
84		9/13/19	100	D698-C	GW	7.7	136.7	2.8	137.1	8	100	95	PASS
85		9/13/19	100	D698-C	GW	7.7	136.7	3.0	138.8	8	102	95	PASS
Test Information													
Test #	Test Location			Elevation		Reference		Gauge		Field Technician			
78	PAVEMENT - Base: Location 17			0.0		SG		Make / Model / SN / Calibrated		Troxler / 3411-B / 10156 / 11/27/2018 WILLIAM BRIAN VAUGHAN			
79	PAVEMENT - Base: Location 18			0.0		SG				Troxler / 3411-B / 10156 / 11/27/2018 WILLIAM BRIAN VAUGHAN			
80	PAVEMENT - Base: Location 19			0.0		SG				Troxler / 3411-B / 10156 / 11/27/2018 WILLIAM BRIAN VAUGHAN			
81	PAVEMENT - Base: Location 20			0.0		SG				Troxler / 3411-B / 10156 / 11/27/2018 WILLIAM BRIAN VAUGHAN			
82	PAVEMENT - Base: Location 21			0.0		SG				Troxler / 3411-B / 10156 / 11/27/2018 WILLIAM BRIAN VAUGHAN			
83	PAVEMENT - Base: Location 22			0.0		SG				Troxler / 3411-B / 10156 / 11/27/2018 WILLIAM BRIAN VAUGHAN			
84	PAVEMENT - Base: Location 23			0.0		SG				Troxler / 3411-B / 10156 / 11/27/2018 WILLIAM BRIAN VAUGHAN			
85	PAVEMENT - Base: Location 24			0.0		SG				Troxler / 3411-B / 10156 / 11/27/2018 WILLIAM BRIAN VAUGHAN			
Remarks				Comments									
PASS: Density test results comply with specifications. Moisture Not Specified.				Tests are "Direct Transmission" (Method A) unless probe depth is noted as "Backscatter". Gauge calibration data on file with the testing agency.									

The above tests were performed in general accordance with the applicable test method, except for known deviations noted above. The density determined represents the soil density at the test location at the time of the test. The test result relates only to the material tested.

14 Appendix C: Subgrade Material Testing Data Sheets

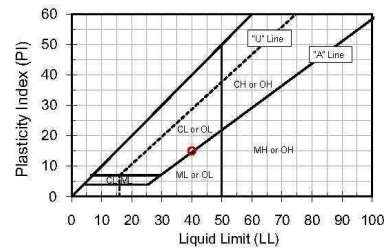
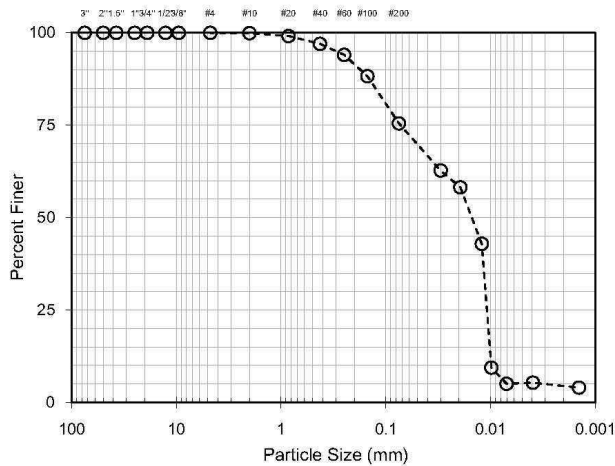
Classification tests on subgrade soil



Particle Size, Atterberg Limit, and USCS Analyses for Soils

Client: DDRF
 Project: CBR Testing Program
 Sample ID: Soil

TRI Log #: 36943.2



Atterberg Limits	
(ASTM D4318, Method A : Multipoint, Air Dried)	
Liquid Limit	40
Plastic Limit	25
Plastic Index	15
(NL = No Liquid Limit, NP = No Plastic Limit)	

Mechanical Sieve		
(ASTM D422)		
Sieve Designation		Percent Passing
-	mm	
3 in.	76.2	100.0
2 in.	50.8	100.0
1.5 in.	38.1	100.0
1 in.	25.4	100.0
3/4 in.	19.0	100.0
1/2 in.	12.7	100.0
3/8 in.	9.51	100.0
No. 4	4.76	100.0
No. 10	2.00	99.9
No. 20	0.841	99.2
No. 40	0.420	97.0
No. 60	0.250	94.0
No. 100	0.149	88.3
No. 200	0.074	75.5

Hydrometer Analysis	
(ASTM D422)	
Particle Size	Percent Passing
mm	
0.0299	62.77
0.0194	58.18
0.0121	42.91
0.0098	9.42
0.0070	5.04
0.0039	5.35
0.0014	4.01

Log-Linear Interpolation	
Particle Size	Percent Passing
mm	
0.005	5.2
0.002	4.5

D _x (mm), Log-Linear Interpolation			
10	30	50	60
0.01	0.01	0.02	0.02
Cu	Cc		
2.34	0.55		

USCS Classification (ASTM D2487)	
Lean clay with sand (CL)	
Moisture Content (%) (ASTM D2216)	
14.2	
Organic Content (%) (ASTM D2974)	
0.9	
Carbonate Content (%) (ASTM D4373)	
<1 (Below Method Detection Limit)	
pH	
ASTM D4972 (method A)	
(H ₂ O)	(CaCl ₂)
4.90	4.10

Jeffrey A. Kuhn, Ph.D., P.E., 6/7/2018

Analysis & Quality Review/Date

The testing herein is based upon accepted industry practice as well as the test method listed. Test results reported herein do not apply to samples other than those tested. TRI neither accepts responsibility for nor makes claim as to the final use and purpose of the material. TRI observes and maintains client confidentiality. TRI limits reproduction of this report, except in full, without prior approval of TRI.

TRI ENVIRONMENTAL, INC.
 9063 BEE CAVES RD. - AUSTIN, TX 78733 - USA | PH: 800.880.TEST OR 512.263.2101

Standard Proctor compaction test on subgrade soil



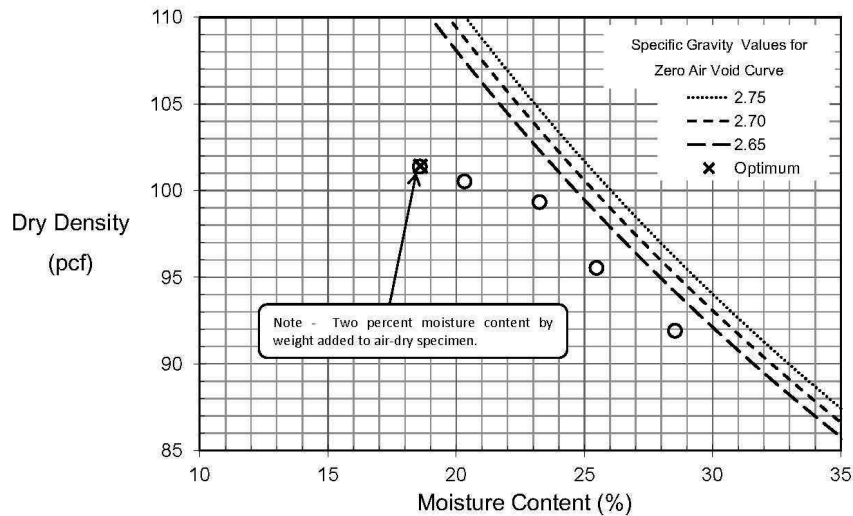
Laboratory Compaction Characteristics of Soil Using Standard Effort (ASTM D698)

Client: DDRF
Project: CBR Testing Program
Sample ID: Soil

TRI Log #: 36943.2

Compaction Effort	-	Standard
Method	-	A
Rammer Type	-	Automatic
Maximum Dry Density	pcf	101.4
Optimum Water Content	%	18.6

Oversize Particle / "Rock" Correction (ASTM D4718)		
Oversized Particles	%	--
Maximum Dry Density	pcf	--
Optimum Water Content	%	--



Jeffrey A. Kuhn, Ph.D., P.E., 6/7/2018
Quality Review / Date

Page 1 of 1

The testing herein is based upon accepted industry practice as well as the test method listed. Test results reported herein do not apply to samples other than those tested. TRI neither accepts responsibility for nor makes claim as to the final use and purpose of the material. TRI observes and maintains client confidentiality. TRI limits reproduction of this report, except in full, without prior approval of TRI.

TRI ENVIRONMENTAL, INC.
9063 BEE CAVES RD. - AUSTIN, TX 78733 - USA | PH: 800.880.TEST OR 512.263.2101

Modified Proctor compaction test on subgrade soil



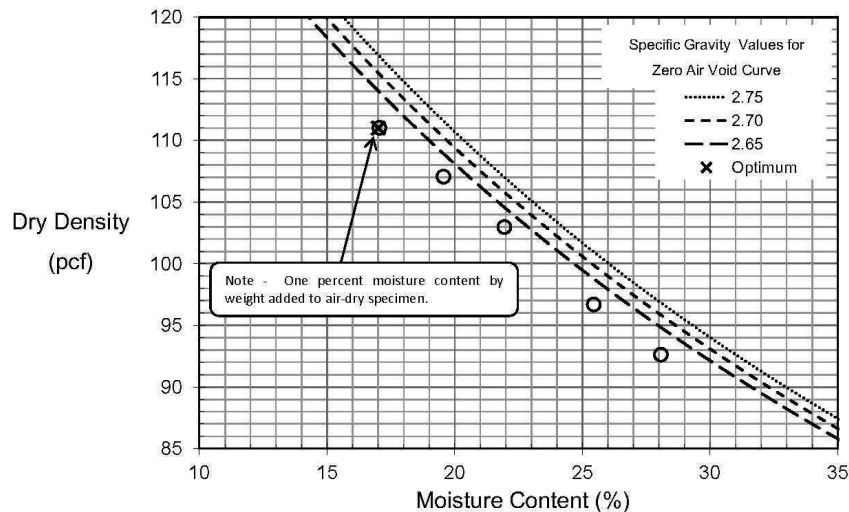
Laboratory Compaction Characteristics of Soil Using Modified Effort (ASTM D1557)

Client: DDRF
Project: CBR Testing Program
Sample ID: Soil

TRI Log #: 36943.2

Compaction Effort	-	Modified
Method	-	A
Rammer Type	-	Automatic
Maximum Dry Density	pcf	111.0
Optimum Water Content	%	17.0

Oversize Particle / "Rock" Correction (ASTM D4718)		
Oversized Particles	%	--
Maximum Dry Density	pcf	--
Optimum Water Content	%	--



Jeffrey A. Kuhn, Ph.D, P.E., 6/7/2018
Quality Review / Date

R-Value test on subgrade soil

R-VALUE TEST REPORT																	
Resistance R-Value and Expansion Pressure - ASTM D 2844																	
No.	Compact. Pressure psi	Density pcf	Moist. %	Expansion Pressure psi	Horizontal Press. psi @ 160 psi	Sample Height in.	Exud. Pressure psi	R Value	R Value Corr.								
1	350	0.0	0.0	0.00	132	2.60	153	13.2	14.0								
2	350	0.0	0.0	0.00	120	2.60	221	19.8	21.1								
3	350	0.0	0.0	0.00	116	2.50	370	22.2	22.2								
<table border="1" style="width: 100%; border-collapse: collapse;"> <thead> <tr> <th style="width: 60%;">Test Results</th> <th style="width: 40%;">Material Description</th> </tr> </thead> <tbody> <tr> <td style="padding: 5px;"> R-value at 300 psi exudation pressure = 23.5 </td> <td style="padding: 5px;"> Subgrade for the South Carolina Geosynthetics Trafficking Study </td> </tr> <tr> <td style="padding: 5px;"> Project No.: Project: MDT Research Location: SubGrade Material Sample Number: 1 Date: 6/19/2018 </td> <td style="padding: 5px;"> Tested by: TSH Checked by: Remarks: </td> </tr> <tr> <td colspan="2" style="text-align: center; padding: 5px;"> R-VALUE TEST REPORT MONTANA DEPARTMENT OF TRANSPORTATION </td> </tr> </tbody> </table>										Test Results	Material Description	R-value at 300 psi exudation pressure = 23.5	Subgrade for the South Carolina Geosynthetics Trafficking Study	Project No.: Project: MDT Research Location: SubGrade Material Sample Number: 1 Date: 6/19/2018	Tested by: TSH Checked by: Remarks:	R-VALUE TEST REPORT MONTANA DEPARTMENT OF TRANSPORTATION	
Test Results	Material Description																
R-value at 300 psi exudation pressure = 23.5	Subgrade for the South Carolina Geosynthetics Trafficking Study																
Project No.: Project: MDT Research Location: SubGrade Material Sample Number: 1 Date: 6/19/2018	Tested by: TSH Checked by: Remarks:																
R-VALUE TEST REPORT MONTANA DEPARTMENT OF TRANSPORTATION																	
Figure _____																	

15 Appendix D: Geotextile Material Testing Data Sheets

Appendix D: Geotextile Material Testing Data Sheets

Test results on RS280i



TESTING, RESEARCH, CONSULTING AND FIELD SERVICES
 Austin, TX - USA | Anaheim, CA - USA | Anderson, SC - USA | Gold Coast - Australia | Suzhou - China

GEOTEXTILE TEST RESULTS
 TRI Client: TRI Environmental
 Project: Geotextile Testing

Material: Tencate RS280i Woven Geotextile
 Sample Identification: Lot: 023181328, Unit: 958718035
 TRI Log #: 43853

PARAMETER	TEST REPLICATE NUMBER										MEAN	STD. DEV.
	1	2	3	4	5	6	7	8	9	10		
Wide Width Tensile Properties (ASTM D 4595)												
MD Specimen Width (inches)	8											
MD Specimen Width (mm)	203											
MD Ultimate Strength (lbs)	3008	3001	3012	3108	2979	2911					3003	63
MD Ultimate Strength (N)	13384	13353	13405	13830	13256	12955					13364	282
MD Ultimate Strength (ppi)	376	375	377	388	372	364					375	8
MD Ultimate Strength (kN/m)	65.9	65.7	66.0	68.1	65.2	63.8					65.8	1.4
MD Strength @ 2% Strain (lbs)	646	640	640	642	618	619					634	12
MD Strength @ 2% Strain (N)	2874	2847	2848	2857	2750	2757					2822	54
MD Strength @ 2% Strain (ppi)	80.7	80.0	80.0	80.3	77.2	77.4					79.3	1.5
MD Strength at 2% Strain (kN/m)	14.1	14.0	14.0	14.1	13.5	13.6					13.9	0.3
MD Strength @ 5% Strain (lbs)	1434	1412	1427	1430	1402	1389					1416	18
MD Strength @ 5% Strain (N)	6382	6283	6349	6364	6239	6182					6300	79
MD Strength @ 5% Strain (ppi)	179	176	178	179	175	174					177	2
MD Strength at 5% Strain (kN/m)	31.4	30.9	31.2	31.3	30.7	30.4					31.0	0.4
MD Strength @ 10% Strain (lbs)	2714	2649	2712	2727	2656	2650					2685	37
MD Strength @ 10% Strain (N)	12079	11788	12067	12135	11819	11791					11947	163
MD Strength @ 10% Strain (ppi)	339	331	339	341	332	331					336	5
MD Strength at 10% Strain (kN/m)	59.4	58.0	59.4	59.7	58.2	58.0					58.8	0.8
MD Break Elongation (%)	11.7	12.2	11.8	11.8	11.6	11.5					11.8	0.2
TD Specimen Width (in)	8											
TD Specimen Width (mm)	203											
TD Ultimate Strength (lbs)	2483	2237	2259	2245	2322	2277					2304	93
TD Ultimate Strength (N)	11048	9954	10051	9990	10335	10133					10252	413
TD Ultimate Strength (ppi)	310	280	282	281	290	285					288	12
TD Ultimate Strength (kN/m)	54.4	49.0	49.5	49.2	50.9	49.9					50.5	2.0
TD Strength @ 2% Strain (lbs)	699	684	686	762	706	697					706	29
TD Strength @ 2% Strain (N)	3111	3045	3054	3393	3141	3101					3141	129
TD Strength @ 2% Strain (ppi)	87.4	85.5	85.8	95.3	88.2	87.1					88.2	3.6
TD Strength at 2% Strain (kN/m)	15.3	15.0	15.0	16.7	15.5	15.3					15.5	0.6
TD Strength @ 5% Strain (lbs)	1458	1423	1434	1523	1466	1465					1461	35
TD Strength @ 5% Strain (N)	6487	6331	6380	6778	6526	6519					6503	156
TD Strength @ 5% Strain (ppi)	182	178	179	190	183	183					183	4
TD Strength at 5% Strain (kN/m)	31.9	31.2	31.4	33.4	32.1	32.1					32.0	0.8
TD Strength @ 10% Strain (lbs)	2398	2209	2226	2148	2271	2223					2246	85
TD Strength @ 10% Strain (N)	10672	9832	9905	9556	10106	9890					9894	377
TD Strength @ 10% Strain (ppi)	300	276	278	268	284	278					281	11
TD Strength at 10% Strain (kN/m)	52.5	48.4	48.7	47.0	49.7	48.7					49.2	1.9
TD Break Elongation (%)	11.4	9.5	9.5	9.2	9.5	9.4					9.75	0.82
MD Machine Direction	TD Transverse Direction											

Page 2 of 2

The testing herein is based upon accepted industry practice as well as the test method listed. Test results reported herein do not apply to samples other than those tested. TRI neither accepts responsibility for nor makes claim as to the final use and purpose of the material. TRI observes and maintains client confidentiality. TRI limits reproduction of this report, except in full, without prior approval of TRI.

TRI Environmental | 9063 Bee Cave Rd., Austin, TX 78733, USA | 512-263-5944 | www.tri-env.com

Appendix D: Geotextile Material Testing Data Sheets

Test results on Geotex 801



TESTING, RESEARCH, CONSULTING AND FIELD SERVICES
Austin, TX - USA | Anaheim, CA - USA | Anderson, SC - USA | Gold Coast - Australia | Suzhou - China

GEOTEXTILE TEST RESULTS

TRI Client: TRI
Project: MDT Study

Material: Nonwoven Geotextile
Sample Identification: Geotex 801
TRI Log #: 42772

PARAMETER	TEST REPLICATE NUMBER										MEAN	STD. DEV.	
	1	2	3	4	5	6	7	8	9	10			
Grab Tensile Properties (ASTM D 4632)													
MD - Tensile Strength (lbs)	233	192	208	356	155	330	260	180	147	130	219	76	
TD - Tensile Strength (lbs)	232	243	238	219	125	212	239	251	217	248	222	37	
MD - Elong. @ Max. Load (%)	79	82	95	64	85	75	98	72	71	90	81	11	
TD - Elong. @ Max. Load (%)	113	114	101	115	84	93	101	101	88	80	99	13	
Wide Width Tensile Properties (ASTM D 4595)													
MD Specimen Width (inches)	8												
MD Specimen Width (mm)	203												
MD Ultimate Strength (lbs)	452	510	1001	600	688	791					674	201	
MD Ultimate Strength (N)	2013	2270	4456	2688	3062	3521					2998	896	
MD Ultimate Strength (ppi)	56.6	63.8	125.2	74.9	86.0	98.9					84.2	25.2	
MD Ultimate Strength (kN/m)	9.9	11.2	21.9	13.1	15.1	17.3					14.8	4.4	
MD Strength @ 2% Strain (lbs)	18.5	17.6	34.6	22.1	22.9	27.9					23.9	6.4	
MD Strength @ 2% Strain (N)	82.2	78.2	154	98.4	102	124					106	28	
MD Strength @ 2% Strain (ppi)	2.31	2.20	4.32	2.76	2.86	3.48					2.99	0.80	
MD Strength at 2% Strain (kN/m)	0.40	0.38	0.76	0.48	0.50	0.61					0.52	0.14	
MD Strength @ 5% Strain (lbs)	40.0	37.5	91.0	50.3	54.7	69.6					57.2	20.2	
MD Strength @ 5% Strain (N)	178	167	405	224	244	310					255	90	
MD Strength @ 5% Strain (ppi)	5.00	4.69	11.4	6.29	6.84	8.70					7.15	2.52	
MD Strength at 5% Strain (kN/m)	0.88	0.82	1.99	1.10	1.20	1.52					1.25	0.44	
MD Strength @ 10% Strain (lbs)	74.1	69.7	175	92.4	103.5	131					108	40	
MD Strength @ 10% Strain (N)	330	310	778	411	460	581					478	176	
MD Strength @ 10% Strain (ppi)	9.28	8.72	21.9	11.6	12.9	16.3					13.4	5.0	
MD Strength at 10% Strain (kN/m)	1.62	1.53	3.83	2.02	2.27	2.86					2.35	0.87	
MD Break Elongation (%)	64.0	77.1	78.8	78.6	70.6	79.2					74.0	5.7	
TD Specimen Width (in)	8												
TD Specimen Width (mm)	203												
TD Ultimate Strength (lbs)	798	751	766	879	1006	768					828	98	
TD Ultimate Strength (N)	3552	3341	3407	3910	4476	3419					3884	438	
TD Ultimate Strength (ppi)	100	93.9	95.7	110	126	96.0					103	12	
TD Ultimate Strength (kN/m)	17.5	16.4	16.8	19.2	22.0	16.8					18.1	2.2	
TD Strength @ 2% Strain (lbs)	18.2	17.7	18.1	22.1	23.6	18.8					19.7	2.5	
TD Strength @ 2% Strain (N)	81.0	78.7	80.5	98.5	105	83.5					87.9	11.0	
TD Strength @ 2% Strain (ppi)	2.28	2.21	2.26	2.77	2.95	2.35					2.47	0.31	
TD Strength at 2% Strain (kN/m)	0.40	0.39	0.40	0.48	0.52	0.41					0.43	0.05	
TD Strength @ 5% Strain (lbs)	40.0	36.7	37.4	53.4	62.1	43.5					45.5	10.1	
TD Strength @ 5% Strain (N)	178	163	166	237	276	193					202	45	
TD Strength @ 5% Strain (ppi)	5.01	4.59	4.67	6.67	7.76	5.44					5.69	1.27	
TD Strength at 5% Strain (kN/m)	0.88	0.80	0.82	1.17	1.36	0.95					1.00	0.22	
TD Strength @ 10% Strain (lbs)	80.9	68.7	71.6	109	131	90.6					91.9	24.0	
TD Strength @ 10% Strain (N)	360	306	319	486	581	403					409	107	
TD Strength @ 10% Strain (ppi)	10.1	8.59	8.95	13.7	16.3	11.3					11.5	3.0	
TD Strength at 10% Strain (kN/m)	1.77	1.50	1.57	2.39	2.86	1.98					2.01	0.52	
TD Break Elongation (%)	111	106	107	100	89.7	85.5					100	10	
MD Machine Direction	TD Transverse Direction												

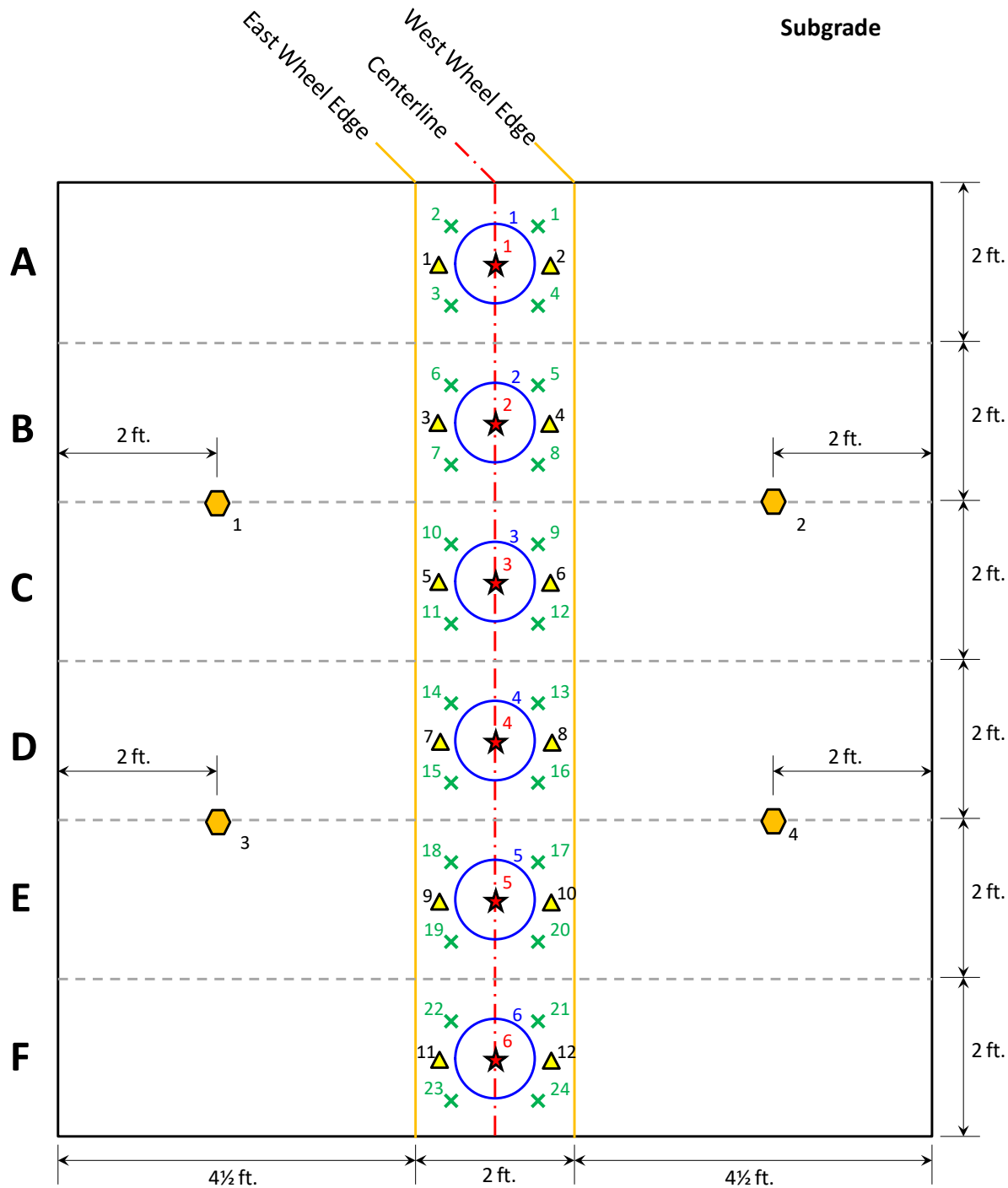
Page 1 of 1

The testing herein is based upon accepted industry practice as well as the test method listed. Test results reported herein do not apply to samples other than those tested. TRI neither accepts responsibility for nor makes claim as to the final use and purpose of the material. TRI observes and maintains client confidentiality. TRI limits reproduction of this report, except in full, without prior approval of TRI.

TRI Environmental | 9063 Bee Cave Rd., Austin, TX 78733, USA | 512-263-5944 | www.tri-env.com

16 Appendix E: Horizontal Layout of Construction QC Measurement Locations

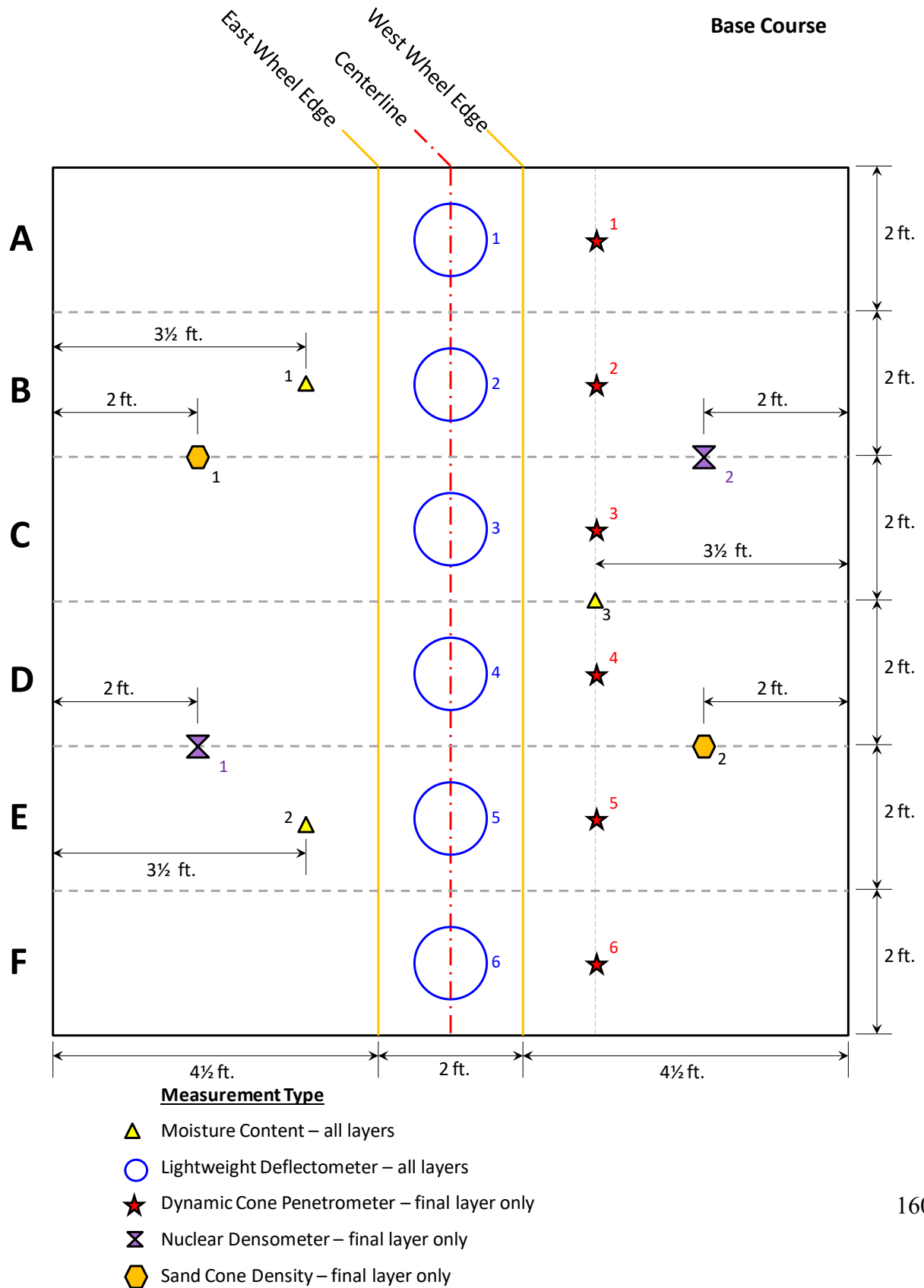
Appendix E: Horizontal Layout of Construction QC Measurement Locations



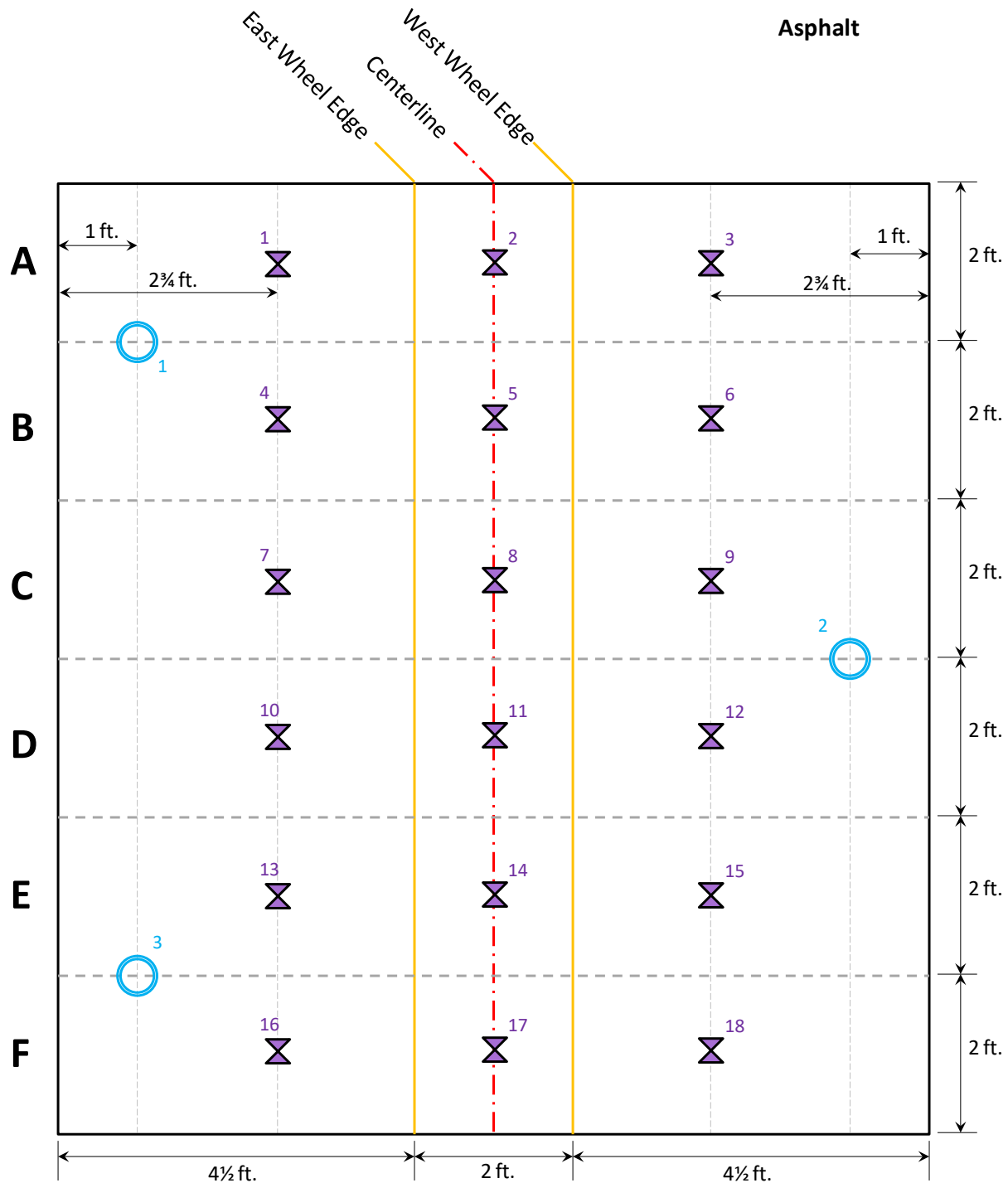
Measurement Type

- ✕ Vane Shear – all layers
- ▲ Moisture Content – all layers
- Lightweight Deflectometer – final 3 layers
- ★ Dynamic Cone Penetrometer – final layer only
- ⬡ Sand Cone Density – final layer only

Appendix E: Horizontal Layout of Construction QC Measurement Locations



Appendix E: Horizontal Layout of Construction QC Measurement Locations



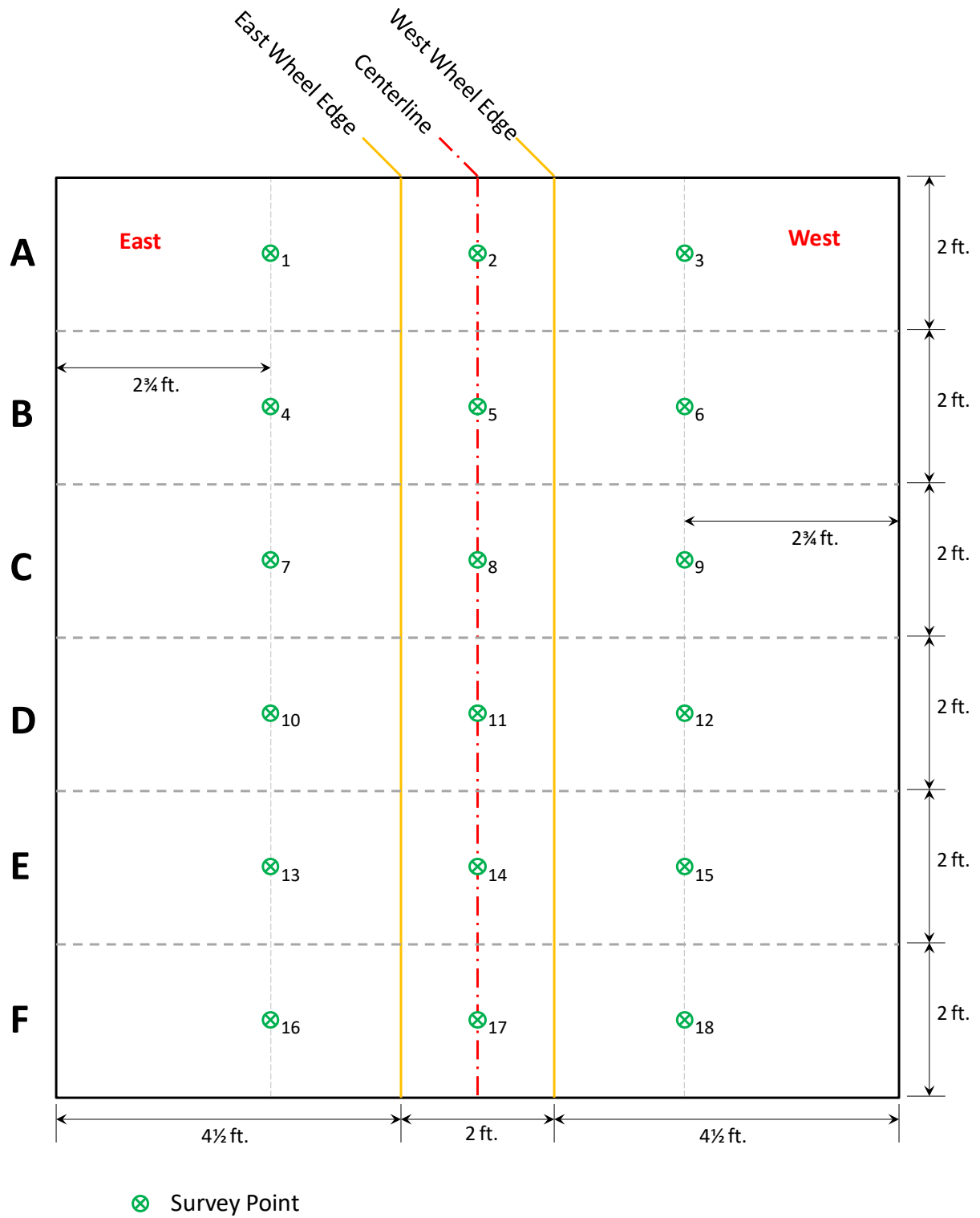
Measurement Type

X Nuclear Densometer

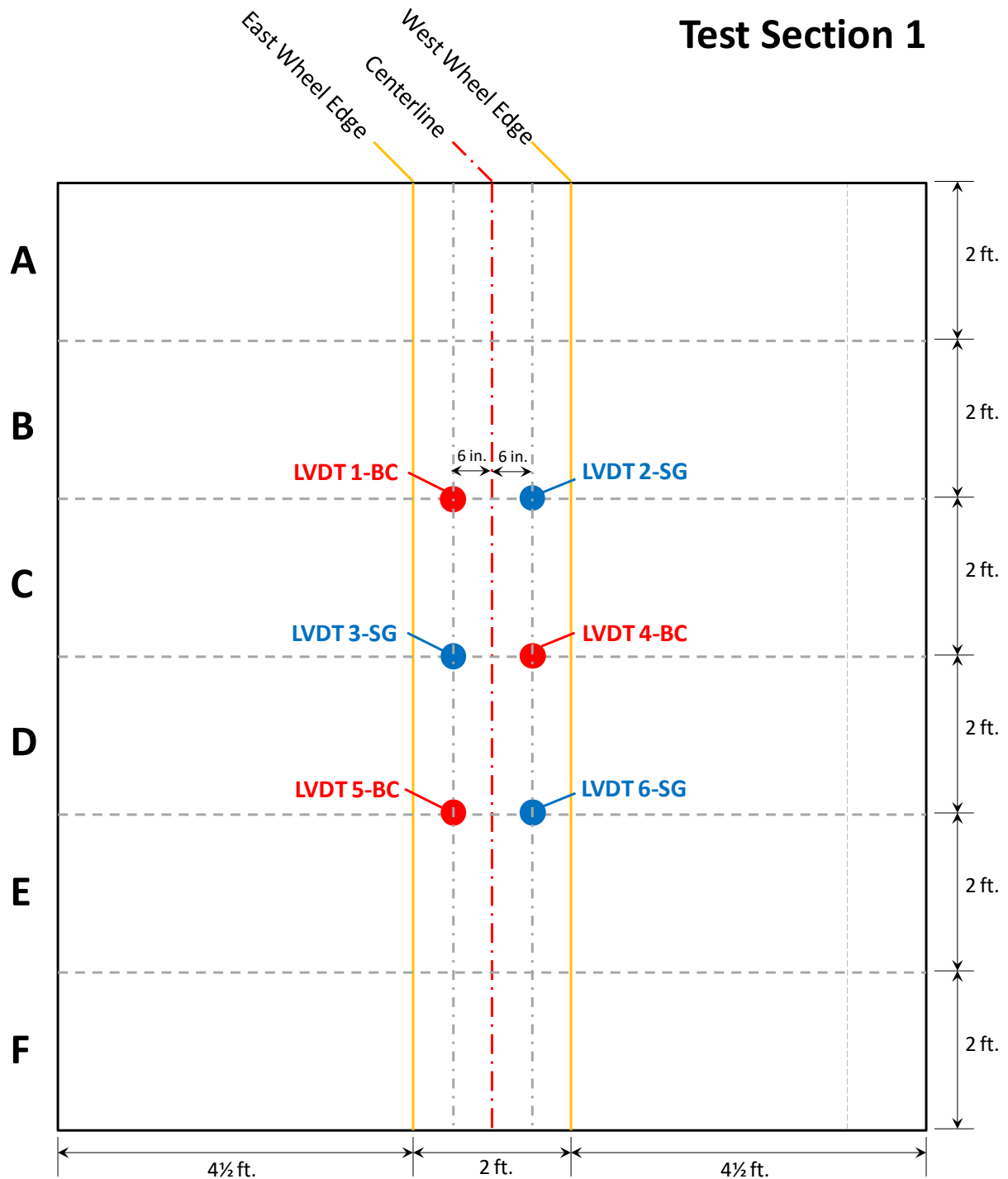
○ 6 in. Asphalt Core

17 Appendix F: Survey Elevation Measurement Layout of Construction QC

Appendix F: Survey Elevation Measurement Layout of Construction QC

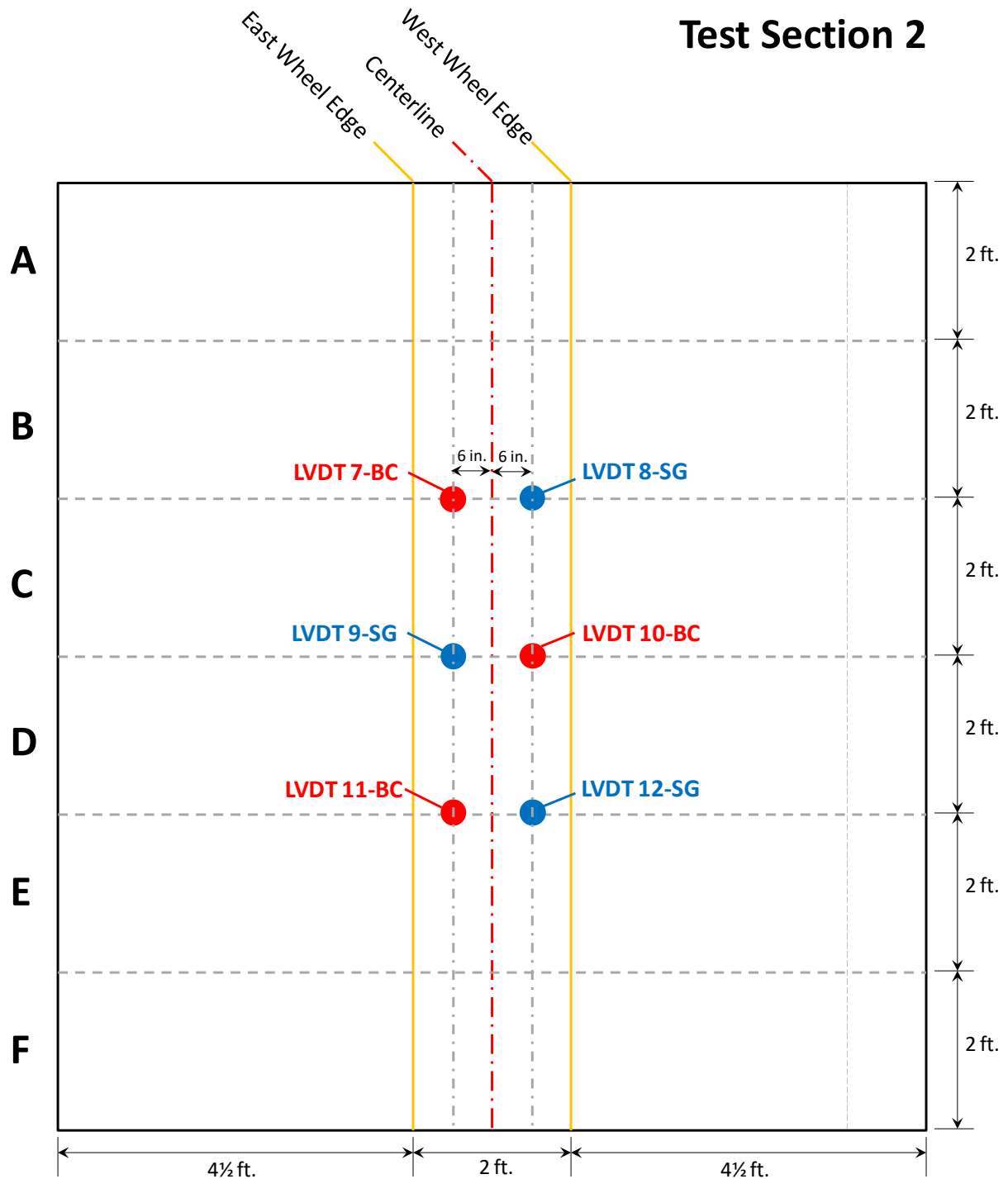


18 Appendix G: Position and Layout of Displacement Sensors within Each Test Section



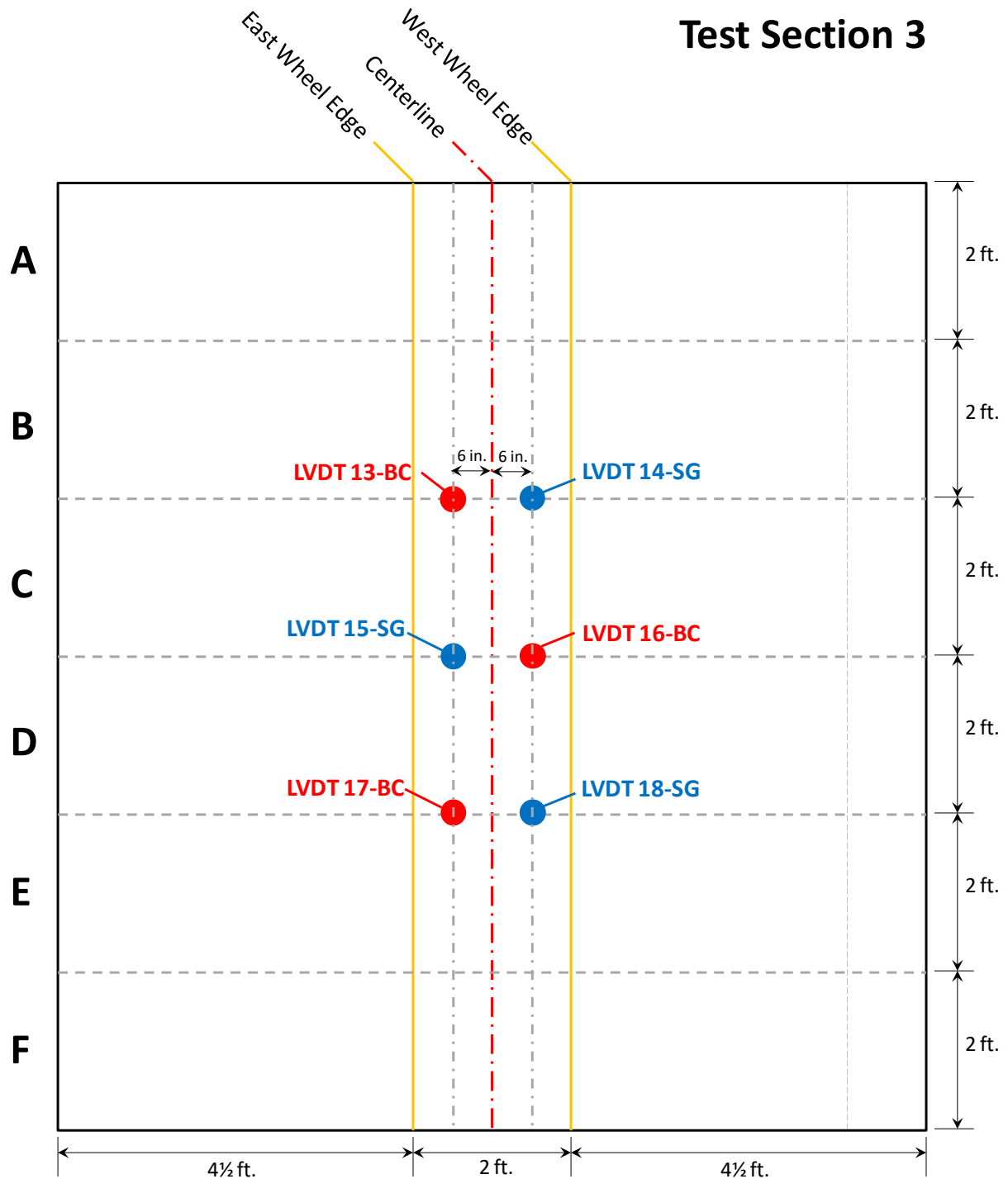
Measurement Type

- Vertical displacement of subgrade surface
- Vertical displacement of base course surface



Measurement Type

- Vertical displacement of subgrade surface
- Vertical displacement of base course surface



Measurement Type

- Vertical displacement of subgrade surface
- Vertical displacement of base course surface

19 Appendix H: Discussion of Base Course Layer Properties During First Construction

The test sections were originally constructed by preparing the base course to a moisture content ranging from 6.4 to 8.2 %. Table 19-1 provides values of moisture content for each test sections and for the two lifts placed. Base aggregate placed during the second construction was placed in three lifts with the moisture content ranging from 5.8 to 7.0 %.

Table 19-1: Average moisture content of the compacted base course for the first construction.

Layer [†]	Average Moisture Content (%)		
	Test Section 1	Test Section 2	Test Section 3
2	5.6	5.1	5.8
1	7.7	7.9	8.2

[†] Layer 1 is the bottom base layer, and Layer 2 is the top layer.

Dynamic stiffness measurements were made with a Light Weight Deflectometer (LWD). Average dynamic stiffnesses for each layer within each test section are summarized in Table 19-2. Average layer values for all test sections during the second construction were 17.7, 22.6 and 120.5 for layers 1, 2 and 3, respectively and are considerably higher than those seen in Table 19-2.

Table 19-2: Average dynamic stiffness of the compacted base course for the first construction.

Layer [†]	Average Dynamic Stiffness (MN/mm ²)		
	Test Section 1	Test Section 2	Test Section 3
2	23.06	24.00	22.13
1	6.34	5.54	5.48

[†] Layer 1 is the bottom base layer and Layer 2 is the top layer.

DCP measurements were taken within each test section using the dual mass DCP device (drop hammer weight of 17.6 lb.) on the finished surface of the base course. The bearing strength (in terms of CBR) as a function of depth was calculated using Equation 6 developed by Kleyn (1975). Average CBR strengths were calculated using values between about 4 and 11 inches of depth to avoid areas near the top and bottom of the compacted layer. The average strengths were as follows: Test Section 1 CBR = 19.0 %, Test Section 2 CBR = 17.8 % and Test Section 3 CBR = 16.3 %.

These values are considerably lower than those reported for the second construction, which were Test Section 1 CBR = 72.4 %, Test Section 2 CBR = 73.9 % and Test Section 3 CBR = 73.8 %.

In-place dry unit weight of the final layer of compacted base course was measured using the sand cone method. A nuclear density gauge was also used to measure the unit weight of the final layer. The average dry unit weights for each test section are summarized in Table 19-3. These values are comparable, if not slightly greater, compared to those reported for the second construction.

Table 19-3: Average dry unit weights of the compacted base course for the first construction.

Layer	Average Dry Unit Weight (lb/ft ³)		
	Test Section 1	Test Section 2	Test Section 3
Nuclear	134.8	137.1	136.0
Sand cone	140.1	139.0	137.4

The higher moisture content values of the first lift during the first construction is believed to be responsible for the significantly lower dynamic stiffness and CBR values of the entire base layer as compared to the second construction.

HMA was placed on the base course layer from the first construction and traffic loading occurred thereafter. The average thickness of the HMA layer was 2.9 inch, which is less than the value of 3.4 inch from the second construction. Figure 19-1 shows the rut response of the test sections, where it is seen that the test sections rutted more rapidly than expected and much more rapidly than from the second construction. At the end of loading at around 4000 passes, the displacement of the top of the base was approximately 0.9 inch for the two sections with geotextile and 0.65 inch for the control section. At this same level of traffic loading, the displacement at the top of the subgrade was approximately 0.35 inch for the two sections with geotextile and 0.25 inch for the control section. This data shows that the base course layer was deforming at a disproportionately high rate as compared to the other layers. Figure 19-2 shows the vertical strain developed in the base layer during the first traffic loading. The strain in the base course layer at the end of traffic loading for the second construction when over 900,000 traffic passes had been applied was between 0.5 and 1.5 % for the three test sections. The values seen in Figure 19-2 are significantly greater at a much lower level of traffic passes.

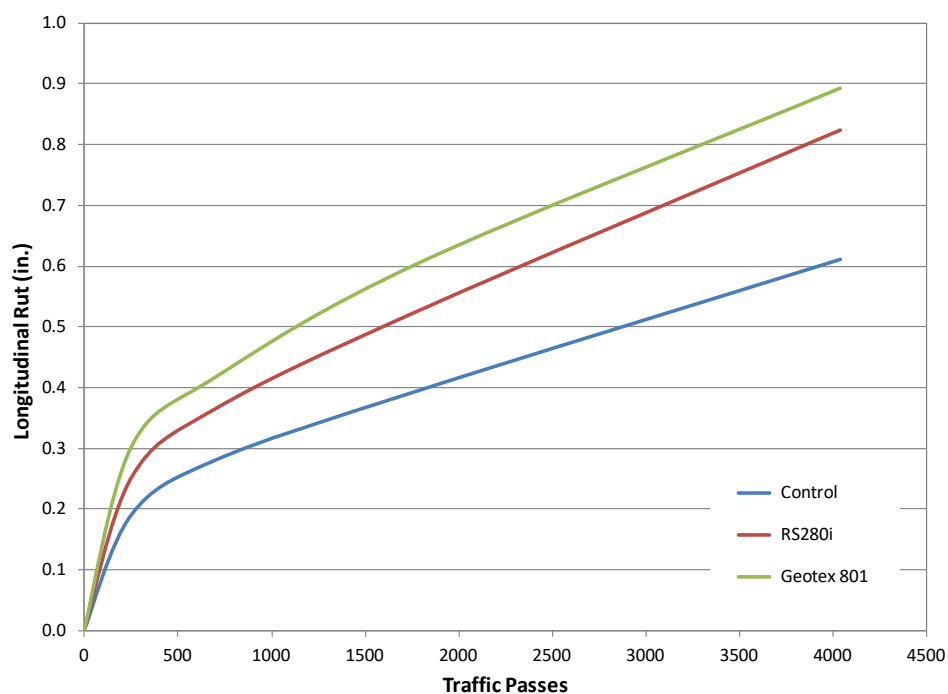


Figure 19-1: Longitudinal rut response from first construction.

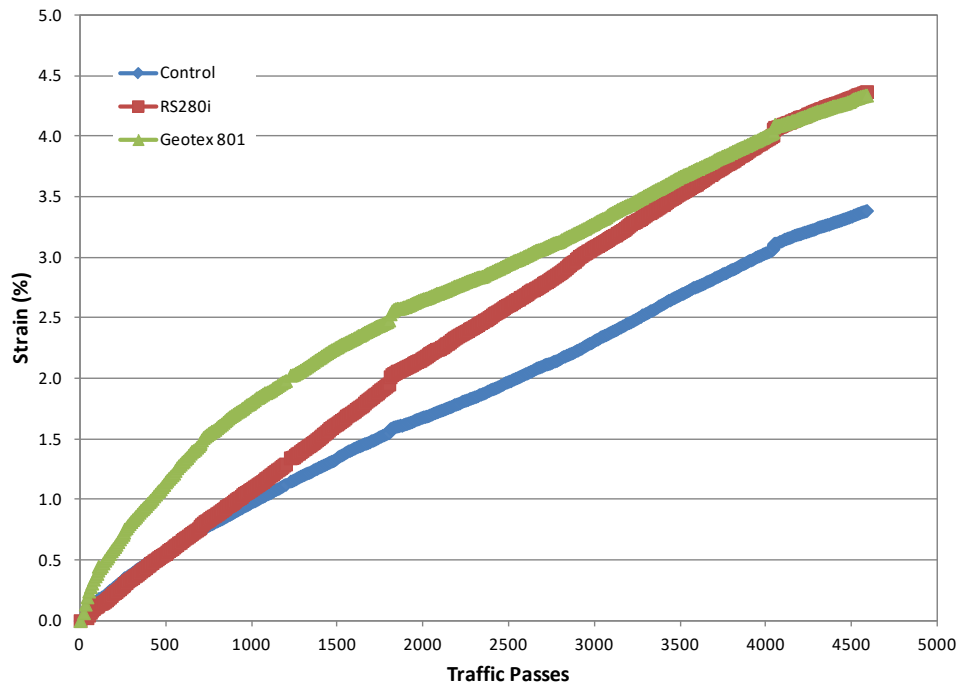
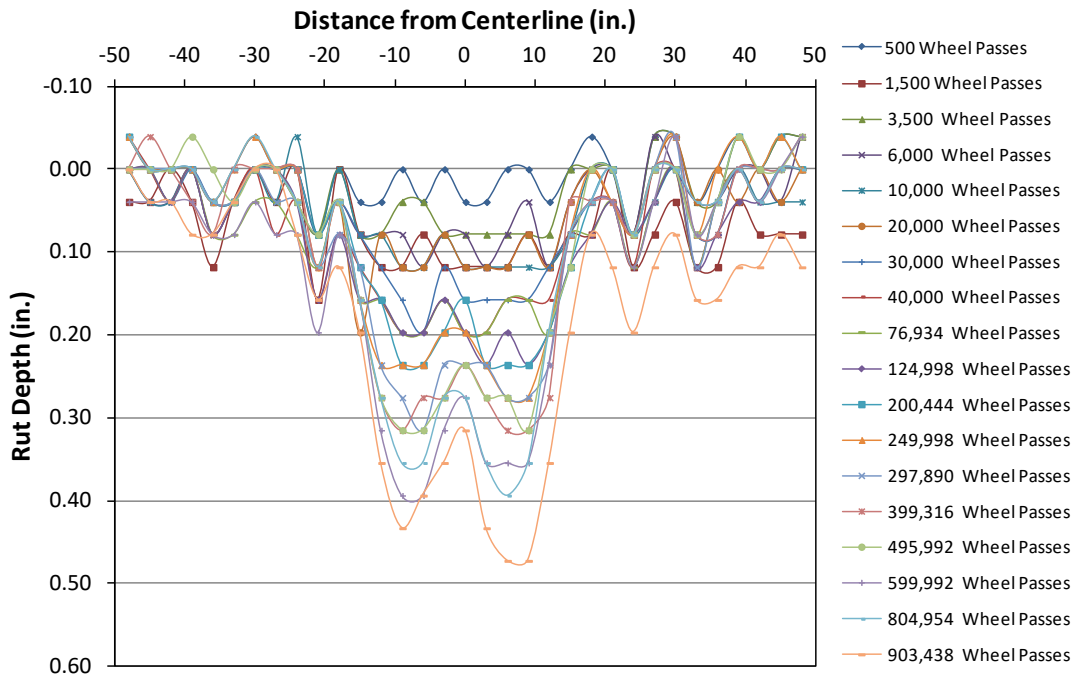


Figure 19-2: Average vertical strain in the base layer from first construction.

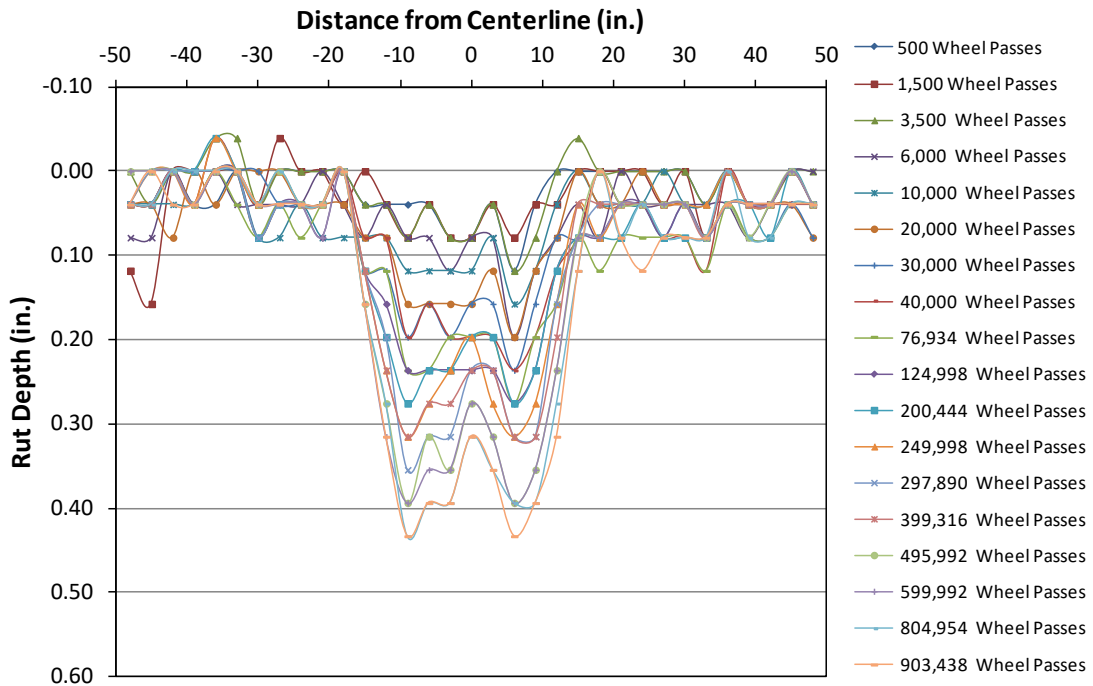
The improved performance of the test sections from the second construction is partly due to the lower moisture content, increased vane shear strength, increased dynamic stiffness and increased CBR of the very upper clay layer and the thicker HMA layer. The data shown above; however, shows that a significant portion of the improved performance of the test sections during the second construction is due to the lower placement moisture content of the base layer and the improved properties that it exhibited. Allowing the base course lift to dry prior to placement of the next lift during the second construction also helped improve the as-constructed base layer properties. This information shows the sensitivity of the base layer to moisture and shows the need to control moisture both during construction and during the service life of the pavement.

20 Appendix I: Transverse rut profiles for each test section as a function of traffic

Appendix I: Transverse rut profiles for each test section as a function of traffic

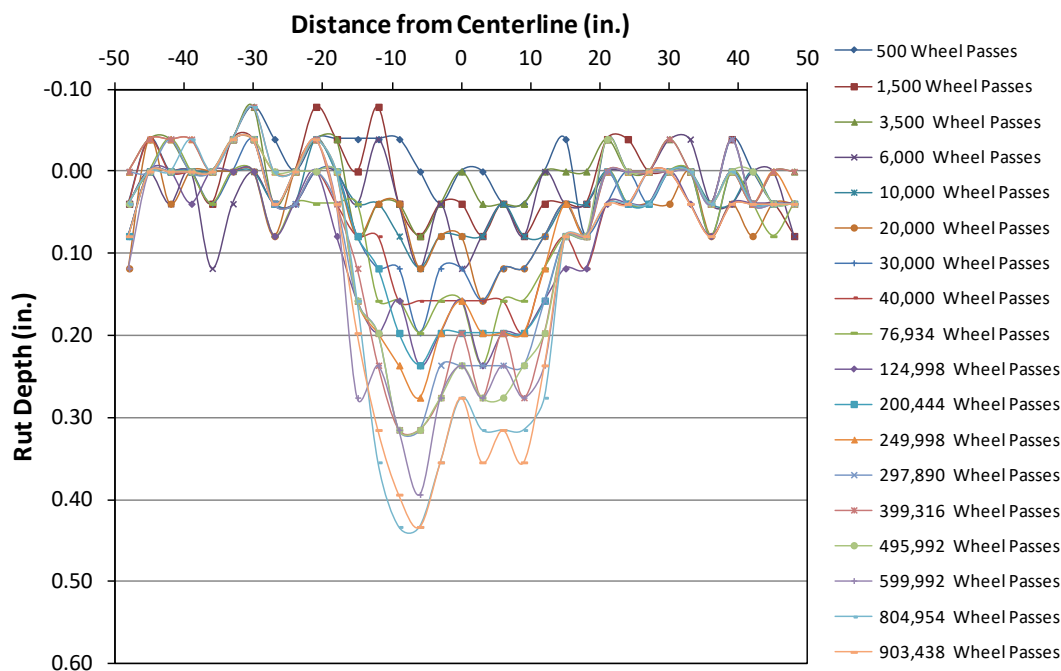


Rut profile progression in the Control test section (south) as a function of increasing traffic.

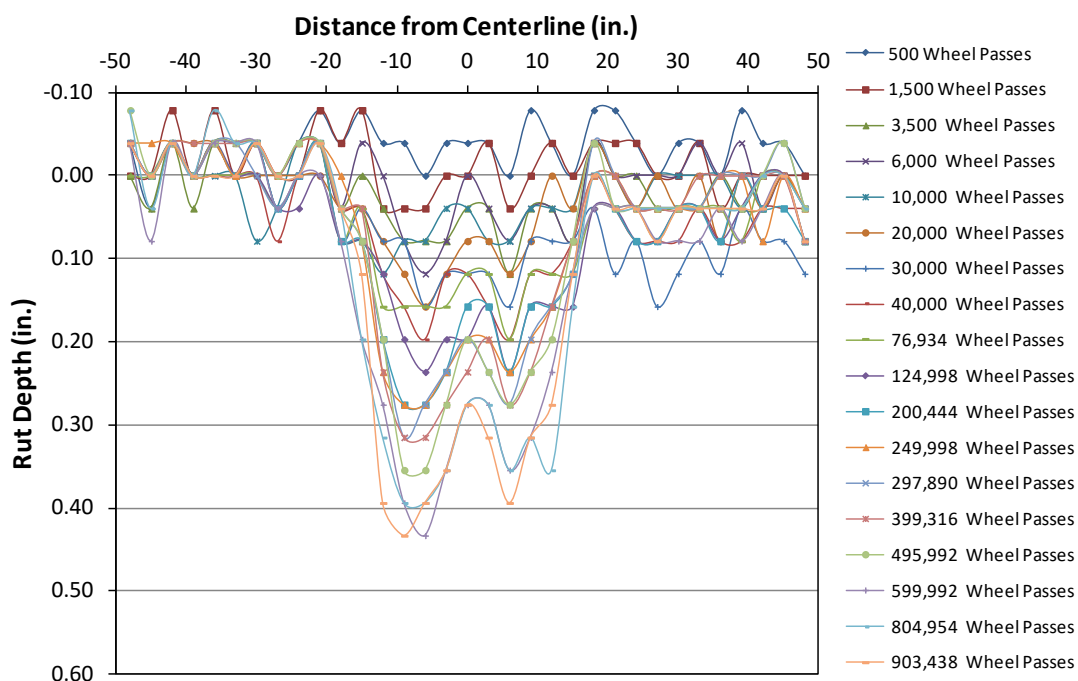


Rut profile progression in the Control test section (north) as a function of increasing traffic.

Appendix I: Transverse rut profiles for each test section as a function of traffic

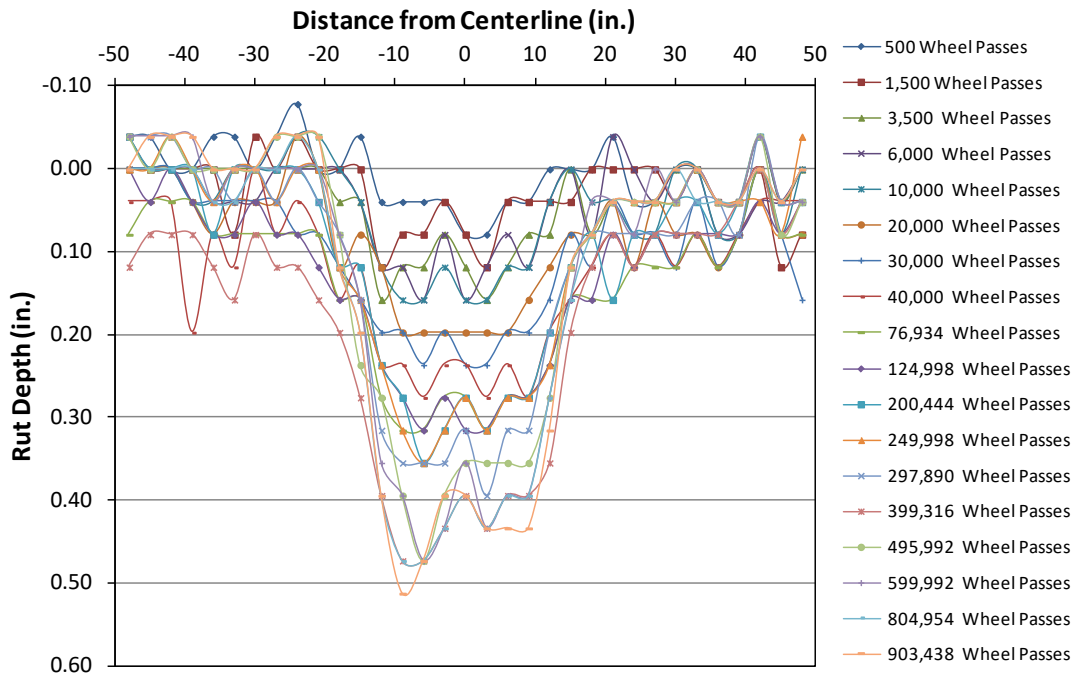


Rut profile progression in the RS280i test section (south) as a function of increasing traffic.

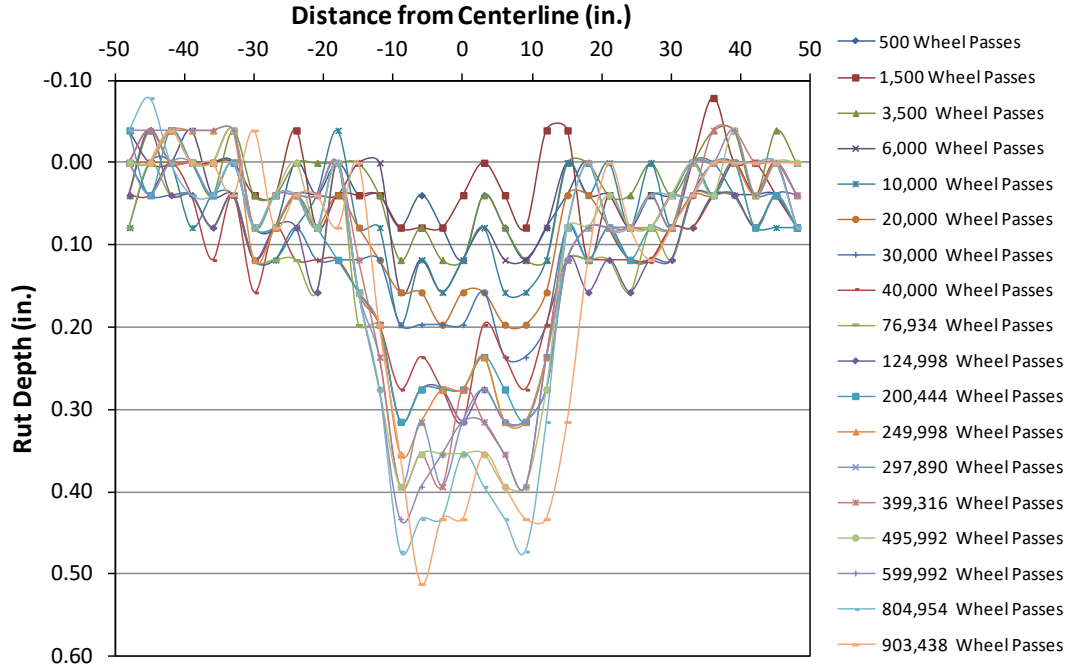


Rut profile progression in the RS280i test section (north) as a function of increasing traffic.

Appendix I: Transverse rut profiles for each test section as a function of traffic

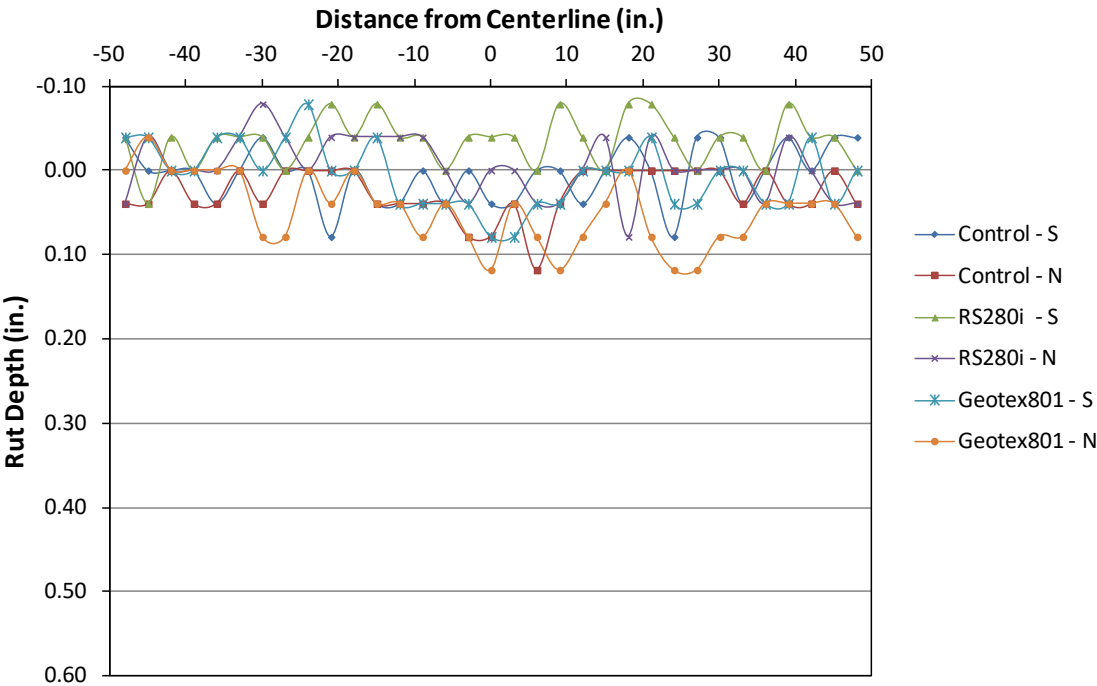


Rut profile progression in the Geotex801 test section (south) as a function of increasing traffic.

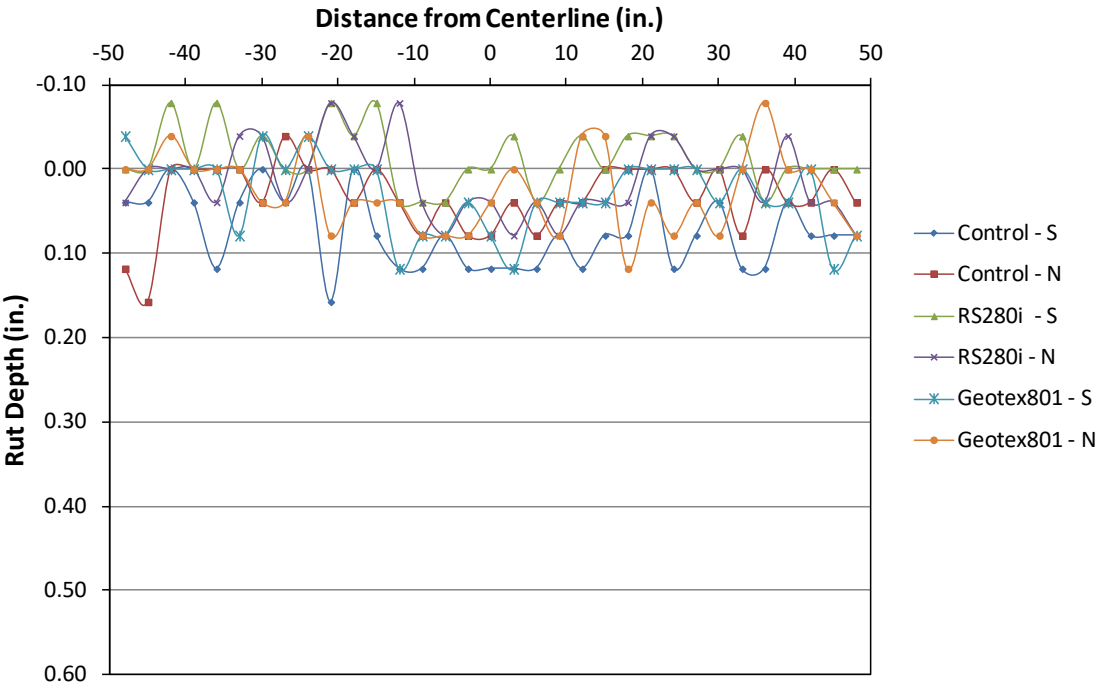


Rut profile progression in the Geotex801 test section (north) as a function of increasing traffic.

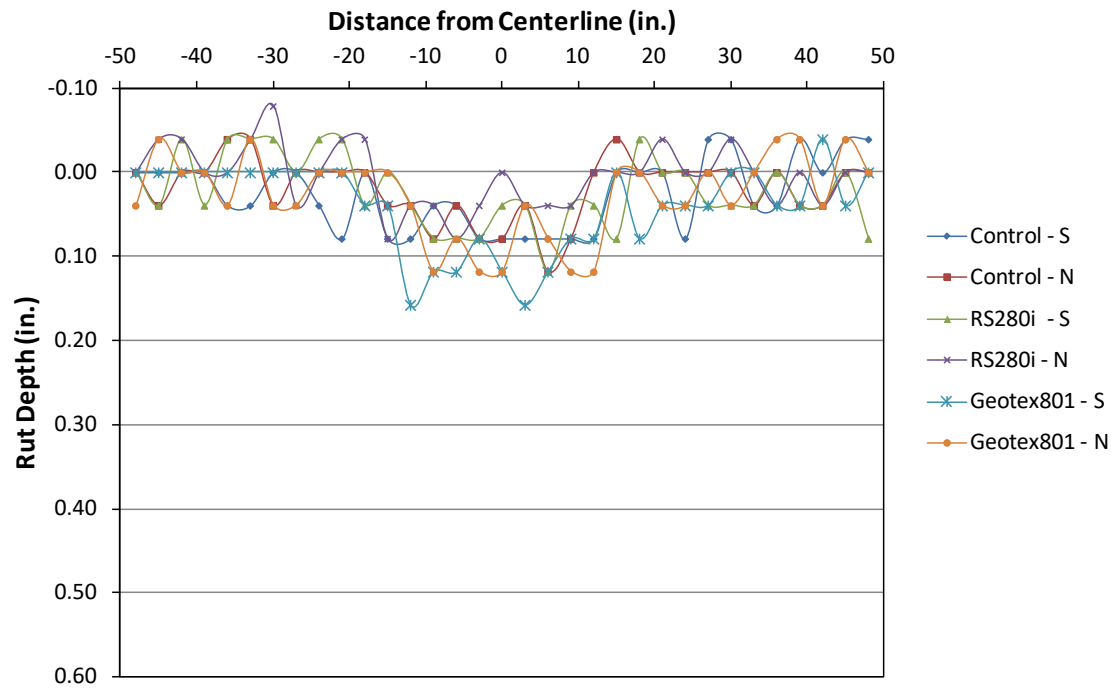
21 Appendix J: Transverse rut profiles of all test sections and measurement lines at all wheel passes



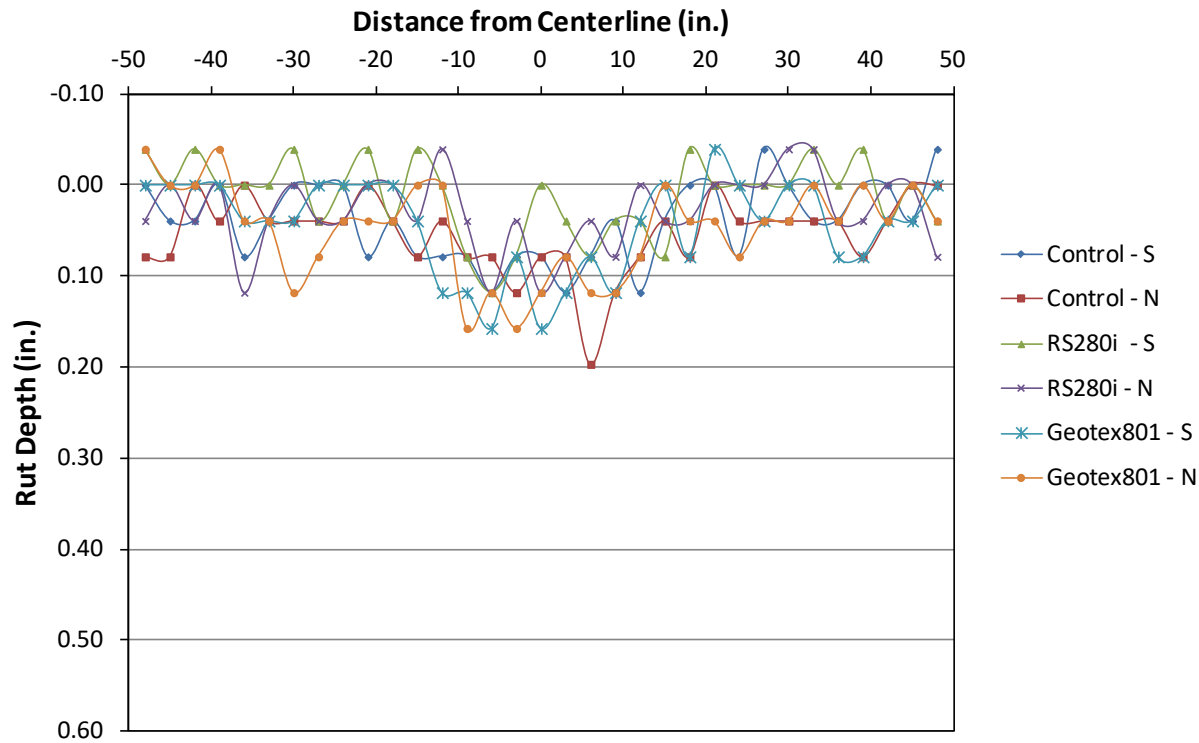
Transverse rut profiles of all test sections at 500 traffic passes.



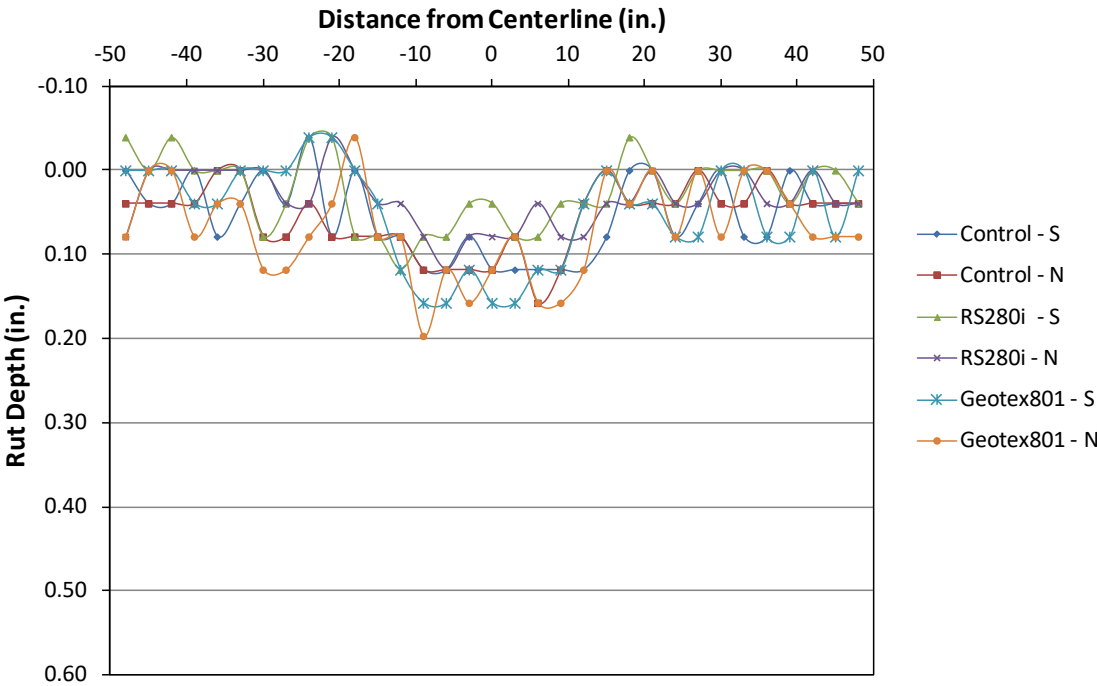
Transverse rut profiles of all test sections at 1,500 traffic passes.



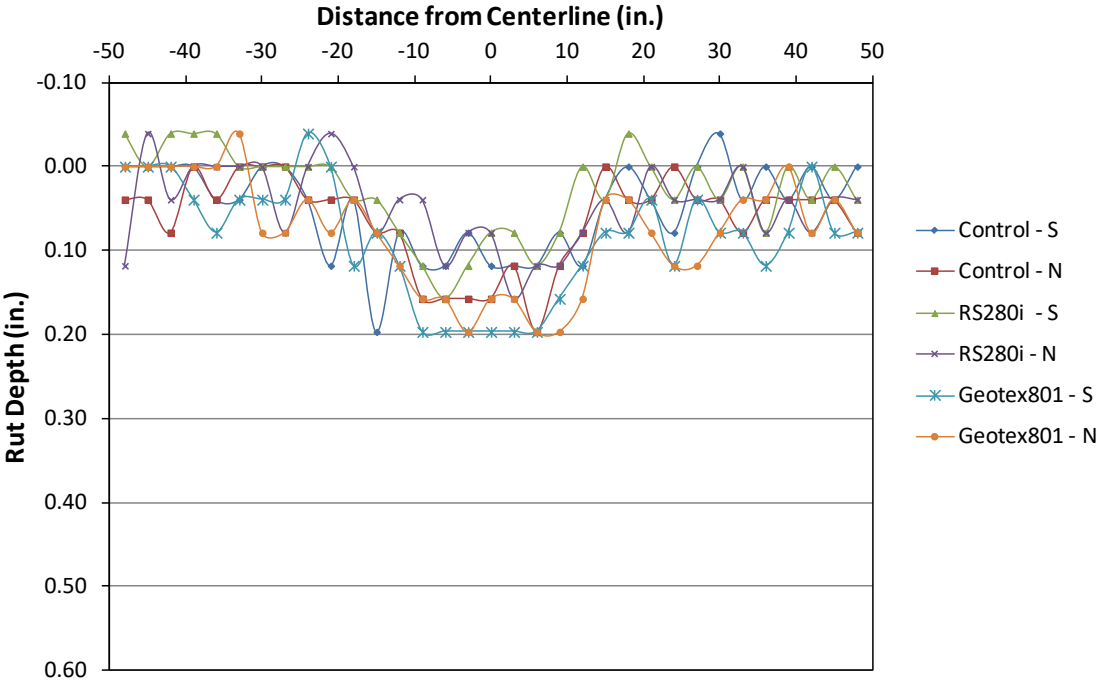
Transverse rut profiles of all test sections at 3,500 traffic passes.



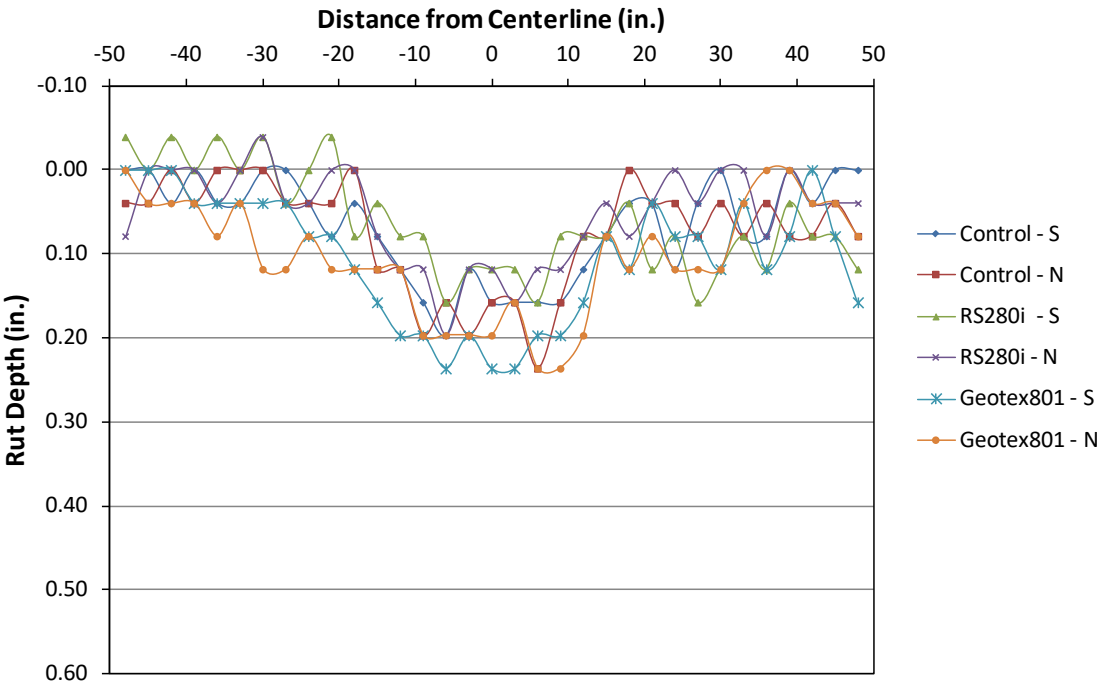
Transverse rut profiles of all test sections at 6,000 traffic passes.



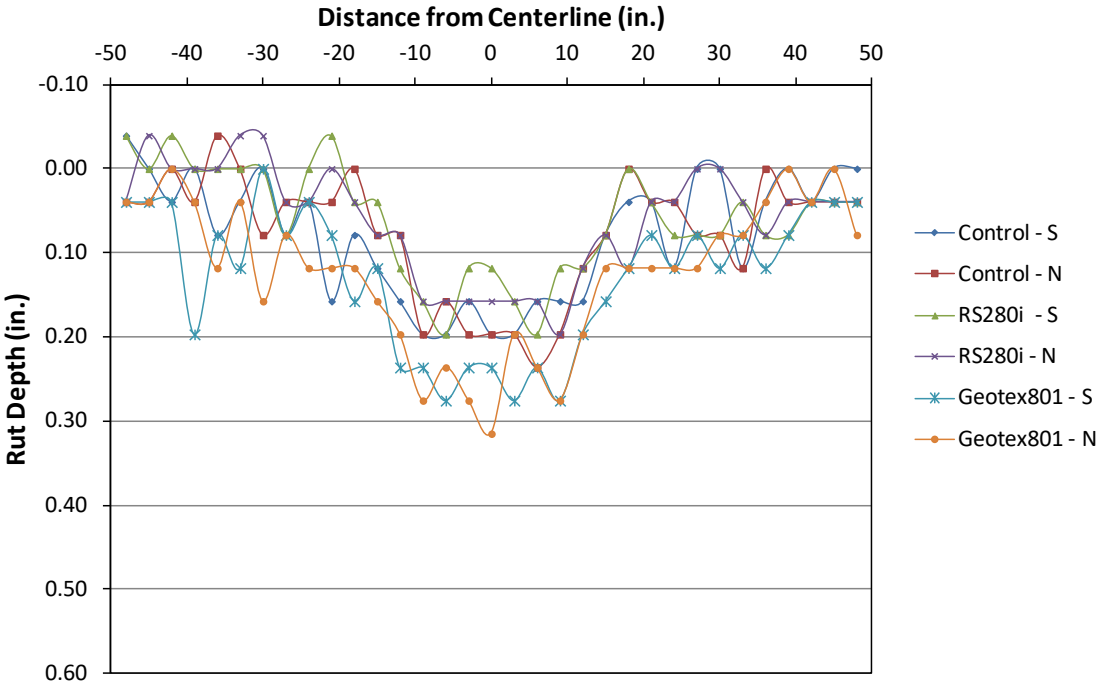
Transverse rut profiles of all test sections at 10,000 traffic passes.



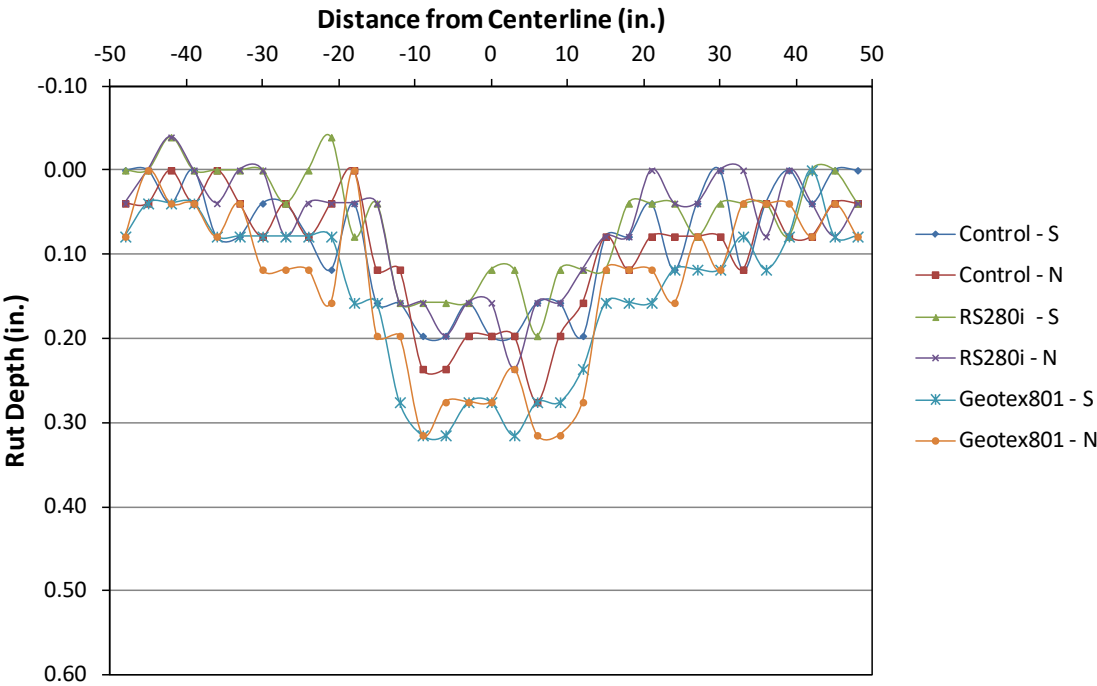
Transverse rut profiles of all test sections at 20,000 traffic passes.



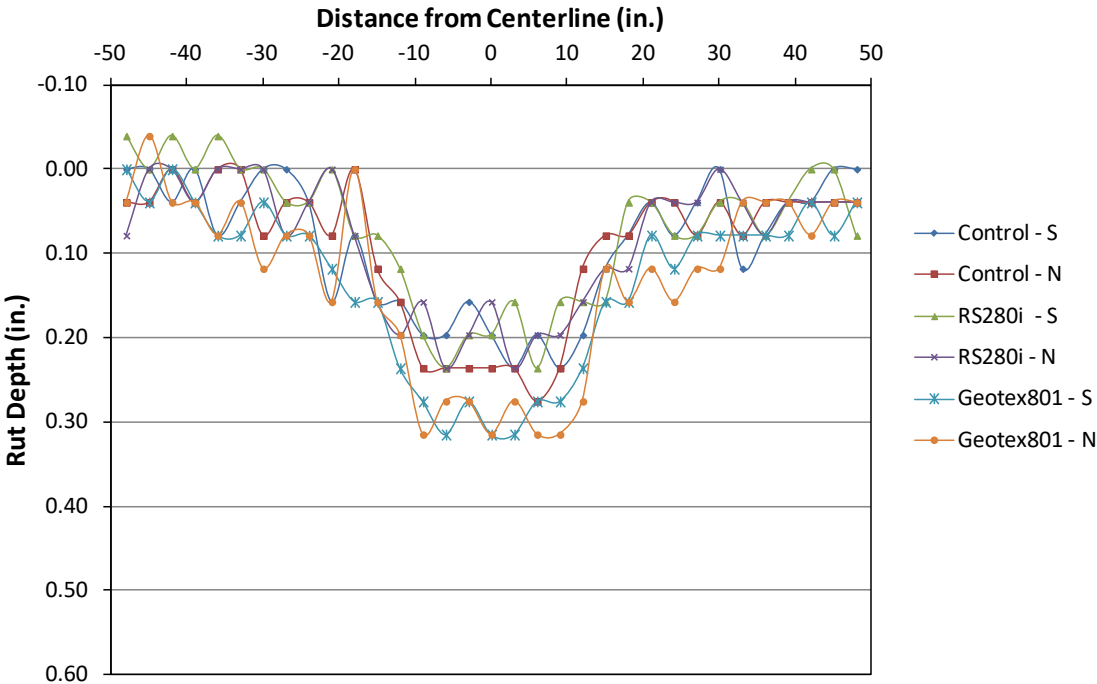
Transverse rut profiles of all test sections at 30,000 traffic passes.



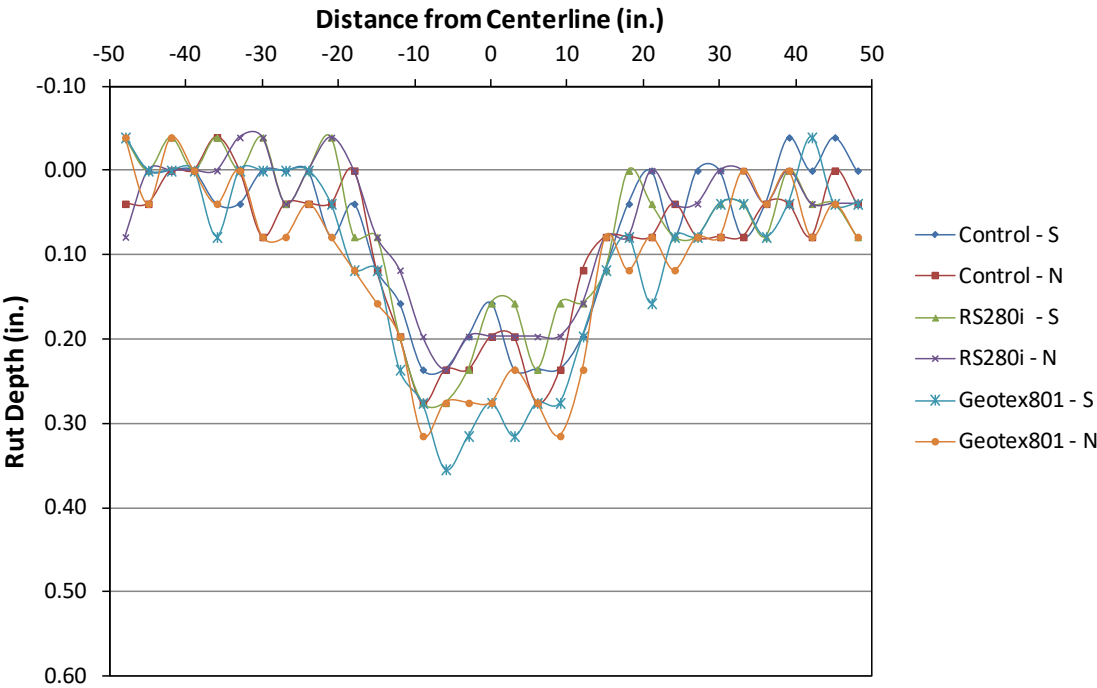
Transverse rut profiles of all test sections at 40,000 traffic passes.



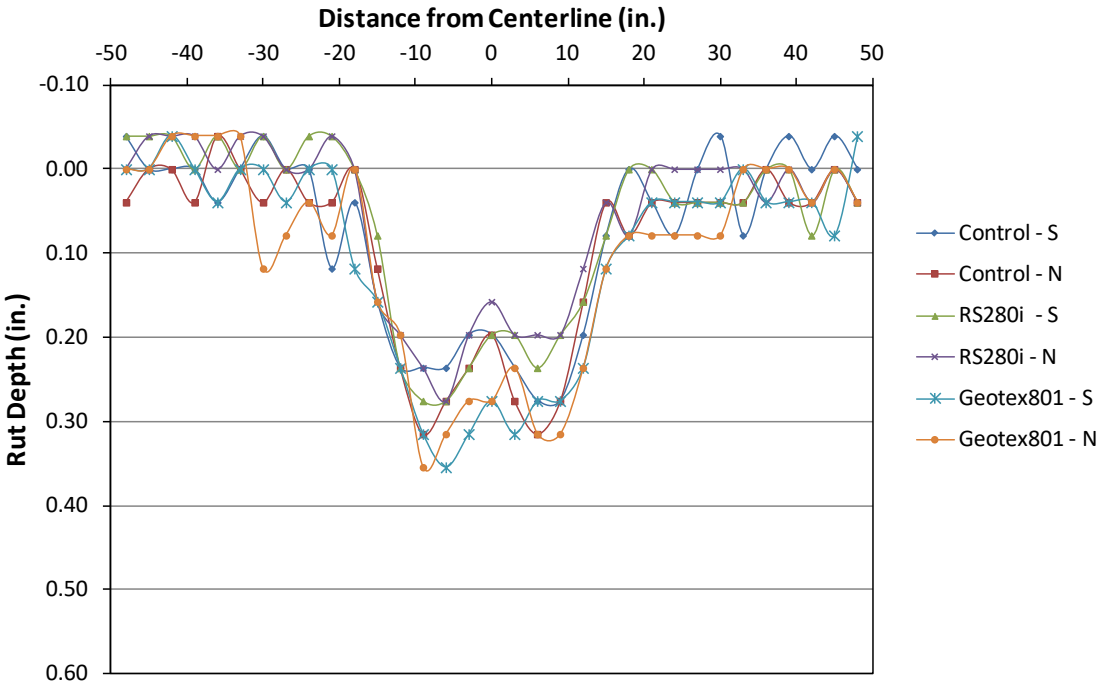
Transverse rut profiles of all test sections at 76,934 traffic passes.



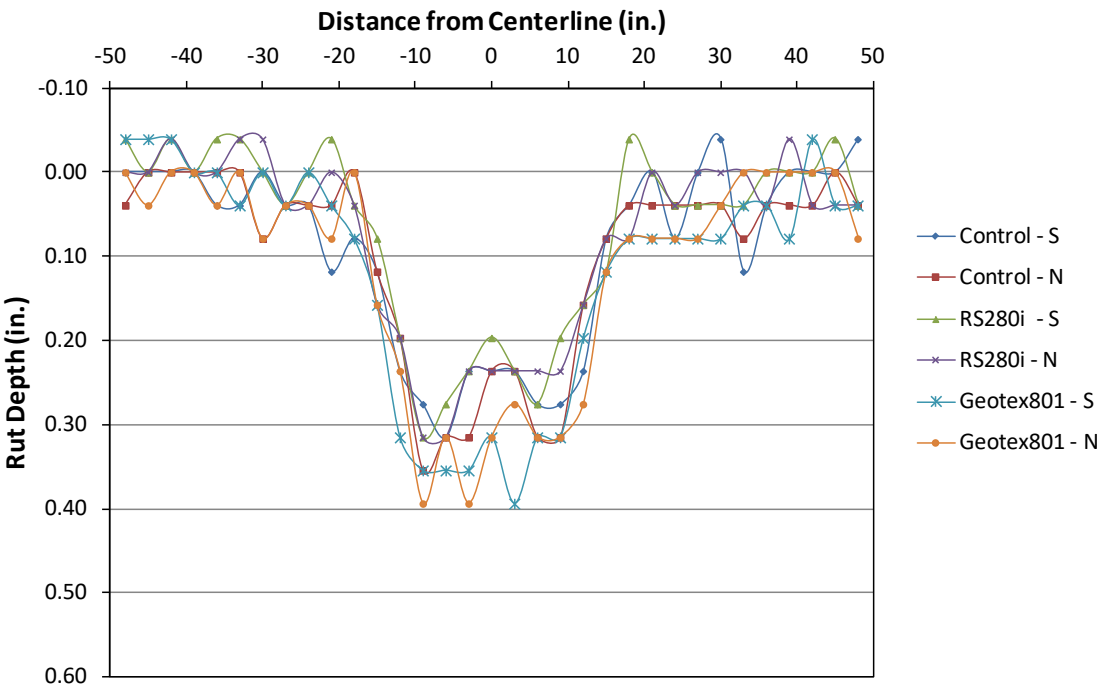
Transverse rut profiles of all test sections at 124,998 traffic passes.



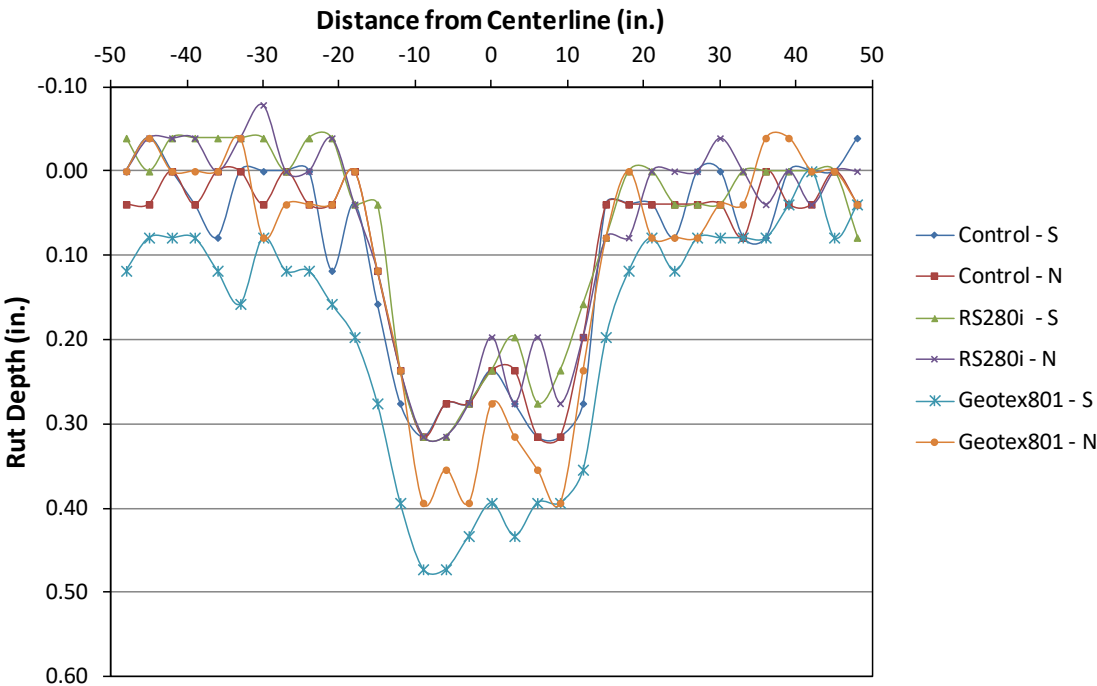
Transverse rut profiles of all test sections at 200,444 traffic passes.



Transverse rut profiles of all test sections at 249,998 traffic passes.

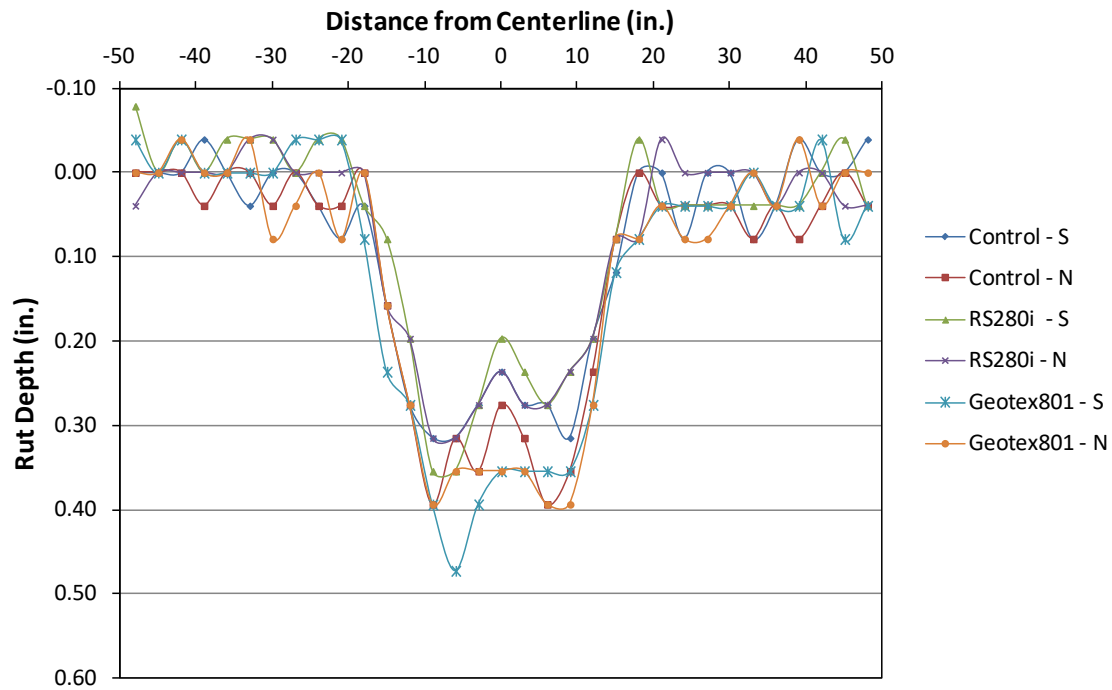


Transverse rut profiles of all test sections at 297,890 traffic passes.

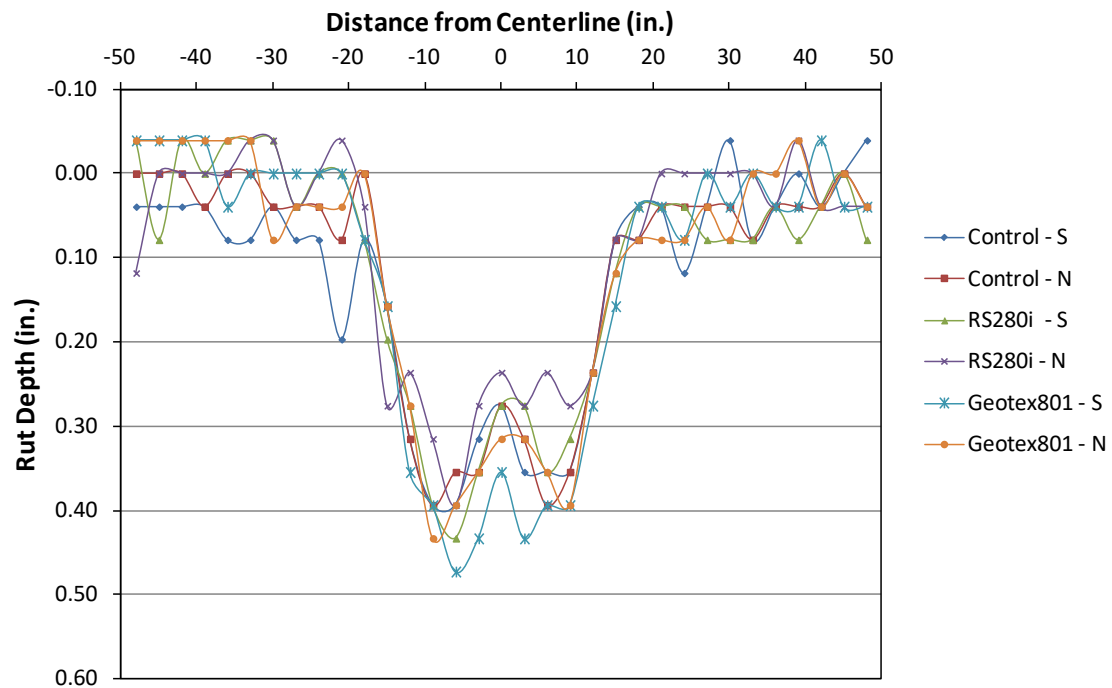


Transverse rut profiles of all test sections at 399,316 traffic passes.

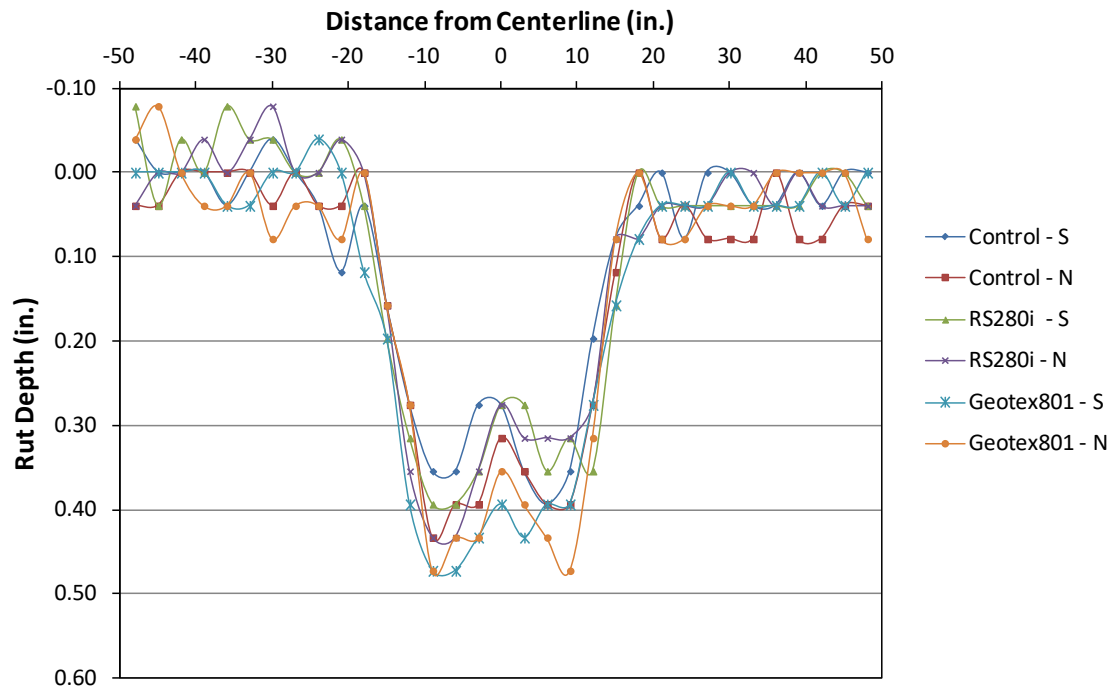
Appendix J: Transverse rut profiles of all test sections and measurement lines at all wheel passes



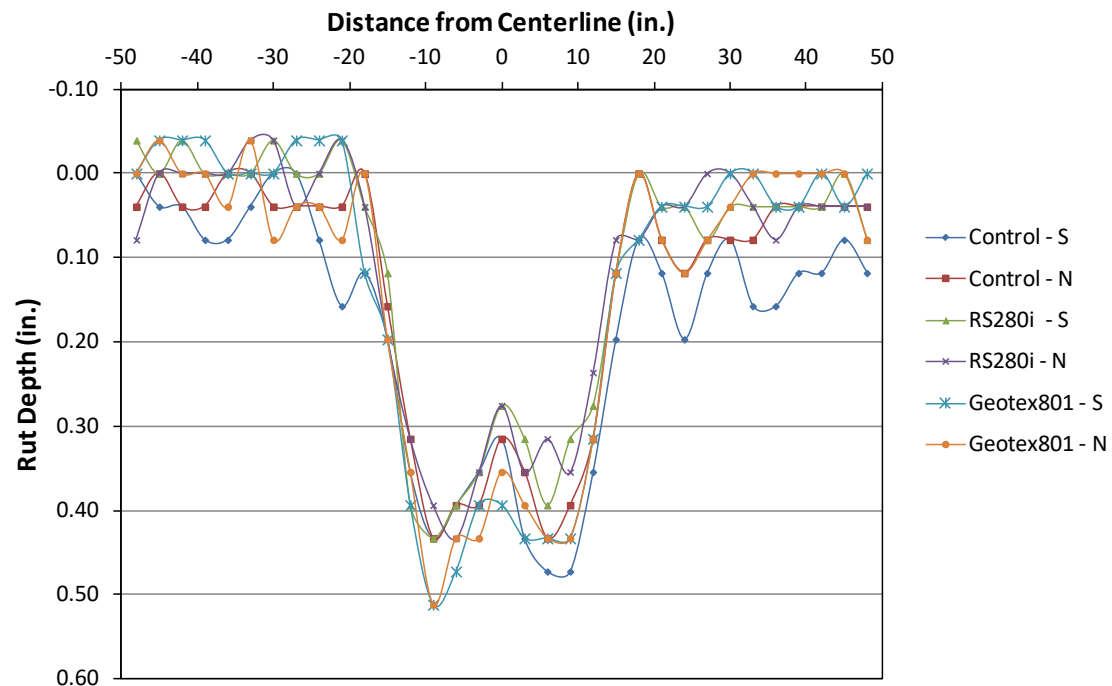
Transverse rut profiles of all test sections at 495,992 traffic passes.



Transverse rut profiles of all test sections at 599,992 traffic passes.



Transverse rut profiles of all test sections at 804,954 traffic passes.



Transverse rut profiles of all test sections at 903,438 traffic passes.

22 Appendix K: Post-Trafficking Dynamic Modulus Test Results for Asphalt Cores

Rowan University – DCM Testing on Field Cores

Rowan University CREATES conducted DCM testing on field cores provided by Eli Cuelho from TRI Environmental, Inc. Three DCM samples were prepared in accordance to Appendix X3 of the AASHTO T378 specification which is applicable for field cores greater than or equal to 2 inches. Each DCM sample was prepared from a 6 inch field core by coring a 1.25 inch diameter from the center of each sample. The samples were then trimmed to the target height of 4.3 inches \pm 0.1 inches. Images of the original field cores and final DCM samples are presented in Figure 1.



Figure 1. DCM field cores and fully prepared small-scale DCM samples.

The bulk specific gravity (G_{mb}) of each final DCM sample was also determined. The bulk specific gravity and air void results are presented in Table 1 using a maximum specific gravity value of 2.451 (provided on the mix design sheet). The DCM test was operated at temperature of 4, 20, and 40°C at frequencies of 10, 1, and 0.1 Hz (0.01 Hz was also included at 40°C). All samples were within the tolerance for data quality (Table 1 of AASHTO T378) have an average Coefficient of Variance (CoV) of 11% for all temperatures and frequencies. A master curve was then developed at 20°C using a polynomial time-temperature shift function and sigmoidal model. The sigmoidal fit is presented in Figure 2 with the original DCM data. An excel sheet of all DCM data and the sigmoidal fit is also provided along with this summary report.

Table 1. Bulk Specific Gravity (G_{mb}) and Air Void Content Measurements for each DCM sample

Label	Dry Weight (g)	Submerged Weight (g)	Saturated Surface Dry Weight (g)	G_{mb}	Air Void Content (%)
Sample 1	255	143	255.4	2.269	7.44
Sample 2	264.6	151	265.5	2.311	5.72
Sample 3	263.3	149	264	2.290	6.59

Table 2. DCM master curve time-temperature shift and sigmoidal fit parameters.

Time-Temperature Shift Parameters		Sigmoidal Fit Parameter	
T_{ref}	20°C	Max E' (kPa)	2.16E7
a_1	1E-9	k	3.969
a_2	-0.1322	δ	-0.289
a_3	4.0068	γ	-0.476

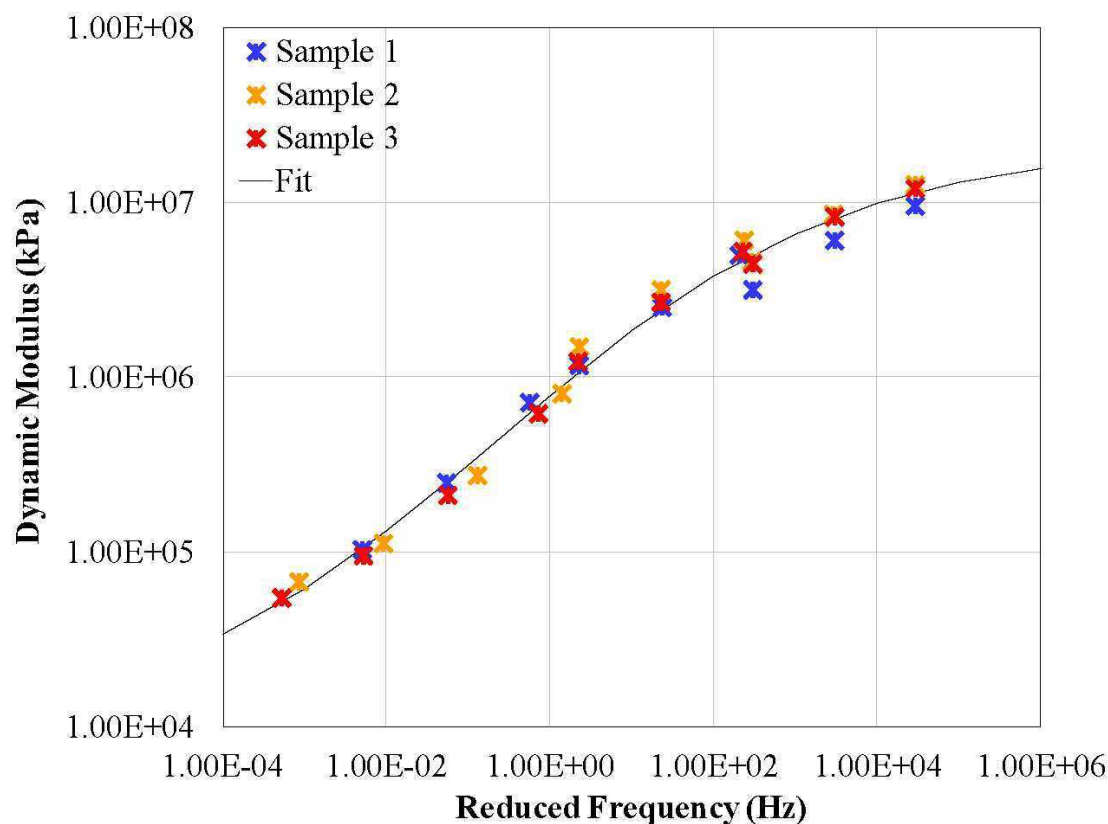


Figure 2. DCM master curve at reference temperature of 20°C

23 Appendix L: Selected Photos of Forensic Investigations



Profile view of north side of forensic trench – Control.



Profile view of south side of forensic trench – Control.



Exposed base course in forensic trench – Control.



Exposed
subgrade in forensic trench – Control.



Profile view of north side of forensic trench – RS280i.



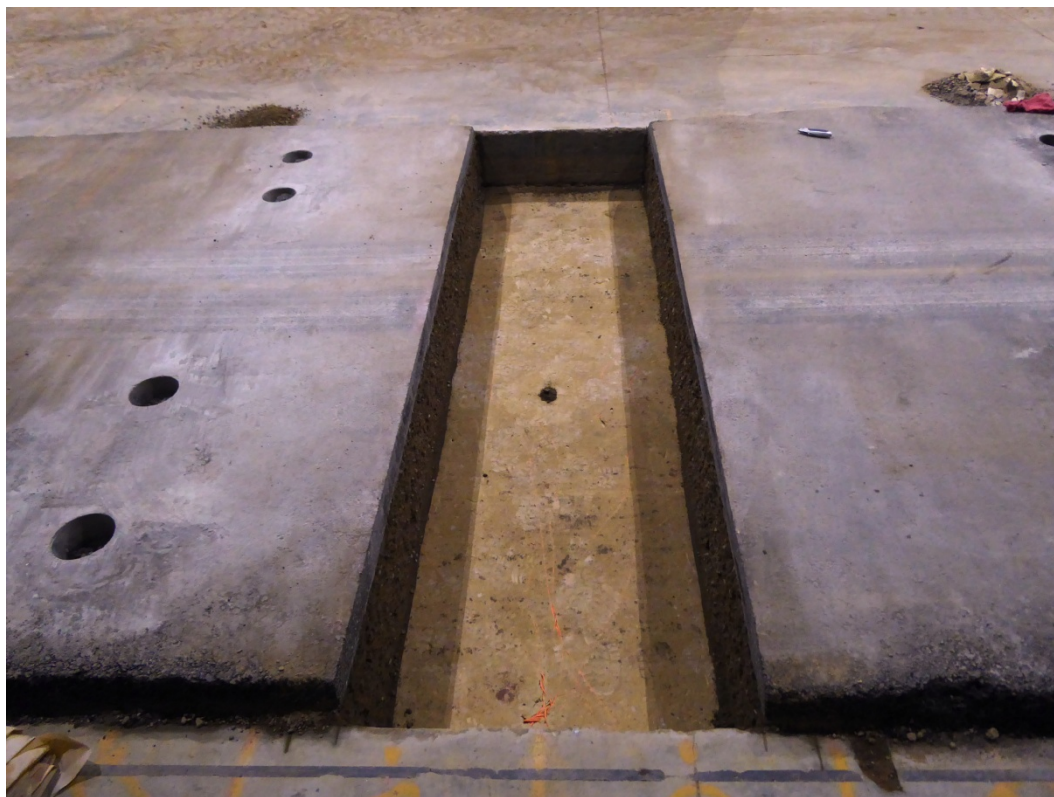
Profile view of south side of forensic trench – RS280i.



Exposed base course in forensic trench – RS280i.



Exposed geotextile in forensic trench – RS280i.



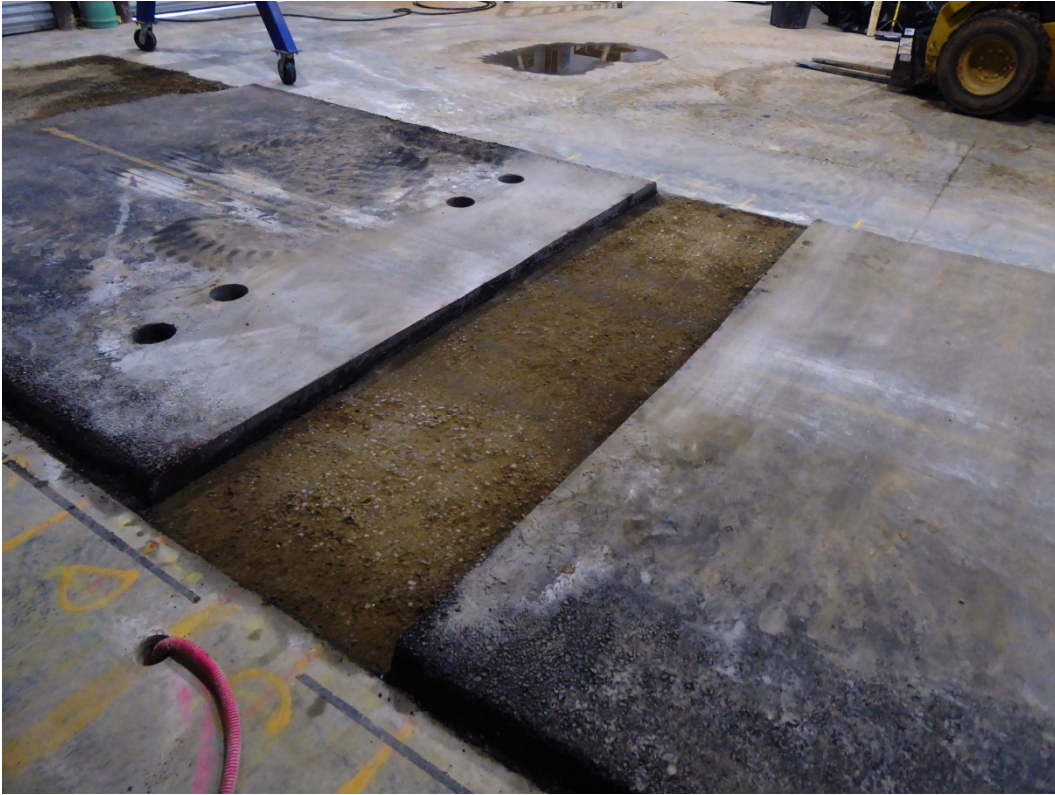
Exposed subgrade in forensic trench – RS280i



Profile view of north side of forensic trench – Geotex 801.



Profile view of south side of forensic trench – Geotex 801.



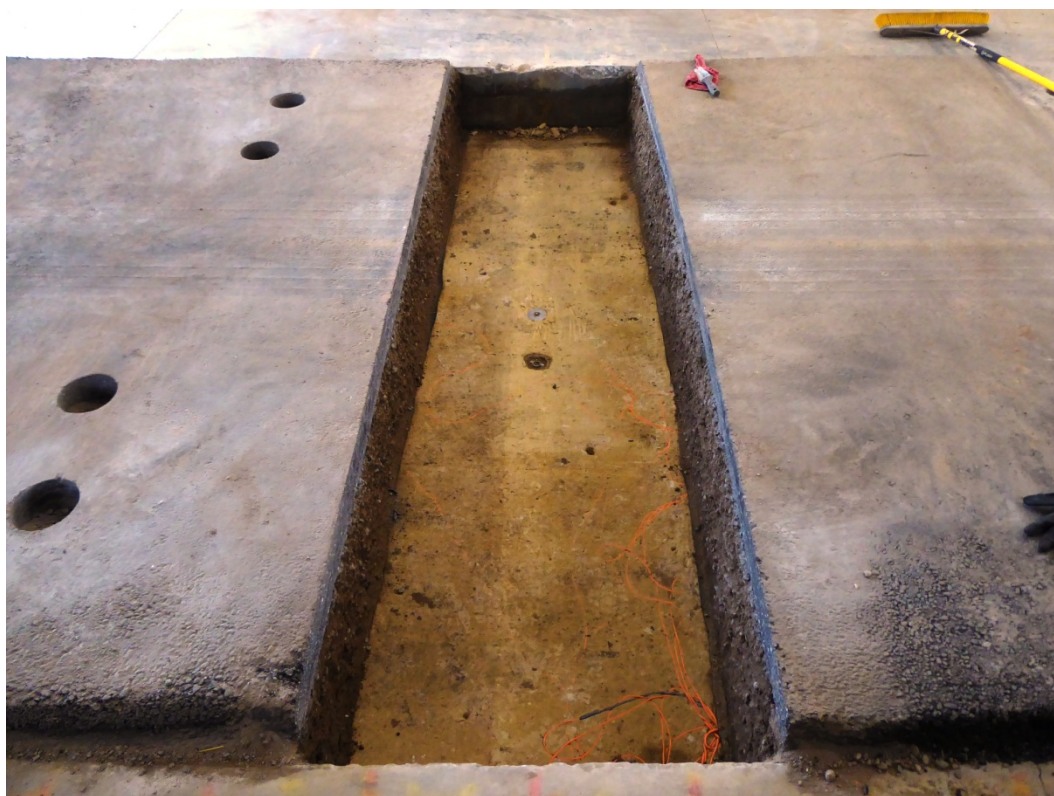
Exposed base course in forensic trench – Geotex 801.



Exposed geotextile in forensic trench – Geotex 801.



Close-up of exposed geotextile in forensic trench – Geotex 801.



Exposed subgrade in forensic trench – Geotex 801.

This public document was published in electronic
format at no cost for printing and distribution.